Redox-active molecules and polymers with photovoltaic applications

Manal Ali Al-Eid

A thesis submitted in part fulfilment of the requirements of the degree of
Doctor of Philosophy

School of Chemistry
University of Glasgow
Glasgow G12 8QQ

August 2013

Abstract

The study presented in this thesis provides details regarding the synthesis and characterization of different redox active molecules which can be applied to form the active layer of photovoltaic devices. For example in chapter two, star-shaped thiophene based molecules are described and their electronic and optical properties have been investigated. In chapter three, oligomers featuring bipyridinium units with different thienyl moieties have been successfully synthesized. Preliminary electropolymerization studies are achieved. In chapter four, two different series of powerful push-pull systems containing dimethyaniline DMA moieties as a strong donating group and TCNE or TCNQ as electron accepting groups have been prepared. These series feature quinone and oligothiophene units as supporting acceptor and donor unit. In chapter five, two different series of powerful organic dyes that could improve the efficiency of DSSCs by modulating the absorption of light towards the near-IR region are achieved. The influence of π-conjugated spacers on the optical and physical properties of synthesized dyes has been investigated. Preliminary DSSCs have been fabricated from some of these systems and their properties have been compared to dye N719.

Dedication

This thesis is dedicated to my beloved family: parents, husband and daughters for their love, support and encouragements.

Acknowledgments

Firstly, I would like to express my honest appreciation to my project's supervisor, Prof. Graeme Cooke, for his guidance, patience and motivation that led to the successful completion of the project. Besides my project's supervisor, I would like to gratefully thank Dr Brian Fitzpatrick, the postdoctoral in our group, for his assistance in developing the experiments.

I would like to thank my second supervisor, Dr. Andrew Sutherland and all other staff at University of Glasgow for their kind assistance especially Dr Deliang Long for X-ray and Dr. David Adam and Jim Tweedie in NMR and mass spectroscopic analysis.

I am also very grateful for Prof. Peter Skabara and Saadeldin Elmasly at University of Strathclyde, for assisting in polymerization studies. I also wish to thank Dr Jong In Hong and his group, from Chung Ang Korean university, for preliminary DSSCs measurement.

A special thank to my parents for their love and support. Most importantly, I would like to express my deep appreciation to my husband and daughters for their unconditioned support. Without their patience and encouragement none of these would be possible to achieve. I would like also to thank all my friends who helped me directly or indirectly for the successful completion of this project.

Finally, I am gratefully acknowledging the Ministry of Higher Education in Saudi Arabia for funding throughout my study.

Manal Al-Eid

Contents

List of tables

List of figures

List of schemes

Abbreviations

Al	……	Aluminum metal
AFM	……	Atomic force microscopy
BHJ	……	Bulk heterojunction device
BLA	……	Bond-length alternation
CV	……...	Cyclic voltammetry
DSSCs	……	Dye sensitized cells
DPP	……	Diketopyrrolopyrroles
DCV	……	Dicyanovinyl
DSC	……	Differential scanning calorimetry
DCE	……	1,1-Dicyanoethene
DCM	……	Dichloromethane
DMSO	……	Dimethyl sulfoxide
DCA	……	Deoxycholic acid
DANS	……	4’-Dimethylamino-4-nitrostilbene
EDOT	……	Ethylenedioxythiophene
EFISH	……	Electric field induced second harmonic
FF	……	Fill factor
PF_6	……	Hexaflourophosphate ions
ICT	……	Intramolecular charge transfer
ITO	……	Indium tin oxide
IPCE	……	Incident photon-to-current conversion efficiency
$LiNbO_3$	……	Lithium niobate
V_{oc}	……	Open circuit voltage
OPV	……	Organic photovoltaic

NLO	……	Non-linear optical
DMA	……	*N*,*N*-dimethyl aniline
PCE	……	Power conversion efficiency
P3HT	……	Poly 3-hexylthiophene
Pc	……	Phthalocyanine
PPVs	……	Polyphenylenevinylenes
PPXs	……	Polyxylylenes
PDIs	……	Perylene diimides
KDP	……	Potassium dihydrogene phosphate
PNA	……	*p*-Nitro aniline
J_{sc}	……	Short circuit current
SubPcs	……	Subphthalocyanines
TCO	……	Transparent conductive oxide
TPA	……	Triphenylamine
THG	……	Third harmonic generation
TCNE	……	Tetracyanoethene
TCNQ	……	7,7,8,8-Tetracyano-*p*-quinodimethane
TCBD	……	1,1,4,4- Tetracyanobuta-1,3-diene
TCAQ	……	Tetracyano-9,10-anthraquinoidimethane
TCV	……	Tricyanovinyl

Declaration

This thesis represents the original work of Manal Ali AL-Eid unless explicitly stated in the text. The research was carried out at the University of Glasgow under the supervision of Prof. Graeme Cooke and I declare that the substance of this thesis has not been submitted for any other degree.

Chapter 1;

General introduction.

1.1. Introduction

The rapid depletion of fossil fuels and their environmental problems associated with flammability have raised the demands for sustainable and renewable energy sources. These factors have motivated scientists to explore clean and effective renewable energy sources. The clean and incredible amount of energy that arrives from solar radiation can be exploited to cover the growing in renewable energy needs. Solar cells offer the most ideal methods to harvest and convert solar energy into electricity without major environmental issues. Although silicon solar cells dominate applications in the global markets due to the stability of the material and the ability to exhibit high power conversion efficiency of 10-20 %, the high cost of silicon materials is the main drawback. Therefore, the cost issue should be considered when choosing photovoltaic materials. The low cost in purification and production of organic materials coupled to the simplicity in modifying and tuning the chemical structure offer an alternative approach in photovoltaic technology. These materials also have other advantages such as; flexibility, processability and producing light weight devices.[1]

1.2. The history of photovoltaics

The discovery of photovoltaic effect was first described in 1839 by E. Bequerel when he observed an electrical current resulted from directing an optical light on a cell consisting of silver coated platinum electrode placed in an electrolyte solution. This was followed by using selenium as a photoconductive element with two platinum contacts for building the first solid state photovoltaic devices in 1876. Improvement in the efficiency was obtained

through forming an asymmetric electronic junction between the metal and the semiconductor element by the way of depositing a layer of metal on top of the semiconductor surface. This led in 1894 to preparation of the first large area of selenium photovoltaic cell.[2,3]

Significant progress in the efficiency of photovoltaic cells was achieved in 1954 by doping silicon as a semiconductor element with boron trichloride gas in order to form p-n electronic junction solar cells.[4] Recently, a number of inorganic semiconducting materials such as CdS, CdTe and GaAs, have been utilized in building solar cells modules. Although the new modules have similar efficiency of traditional silicon modules, the instability and toxicity of the corresponding elements were considered as drawbacks of this approach.[5]

Despite the fact that silicon solar cells dominate the global market, the high cost value of manufacturing the cells and the limited absorption of solar spectrum are disadvantages of this approach.[5] Therefore considerable effort has been directed to utilize organic semiconductors, either conjugated polymers or small molecules, in building less expensive and more efficient solar cells. These materials have posed an alternative way for producing renewable energy with a number of advantages including; the low cost and simple synthesis and manufacturing of the materials, the high absorption coefficients of these materials, the tuneable molecular structure, and the flexibility to fabricate the material either in a large area or small lightweight devices. However, the efficiency of these materials was limited to low values at the beginning of 1980, rising to 0.95 % in 1986 by fabricating bi-layer solar cell devices. Over the years, Sariciftci and Heeger achieved an impressive progress in the efficiency which reached around 5 % for conjugated polymer and 5.7 % for small molecules.[5]

1.3. The solar spectrum

The sun is as an effective and stable source of energy. It has the ability to produce incredible amount of energy around 10^{17} W. This means a small fraction of solar light is capable of covering and exceeding our electricity and heating demands. This amount of solar energy is comparable to the productivity of one hundred million of modern fossil fuel and nuclear stations.[6] The irradiance and the spectral properties of the sun are considered important parameters for solar cells studies. Taking into consideration these parameters, improvement in the performance of solar cells can be achieved. During transmission of solar irradiation from outside the earth's atmosphere to inside, a significant change in the amount of power per unit area has been recorded due to the interaction of the solar spectrum with chemicals in ozone layer before reaching the earth. The amount of light energy outside the earth's atmosphere is determined to be around 1366 W/m^2. However, passing through the atmosphere layer into earth part of the energy is lost. Therefore, on a sunny day the standard amount of power incident per unit area that reaches the earth surface has been calculated of 1000 W/m^2. This value could be ideal to determine the standard solar spectrum. **Figure 1.1** shows the solar spectrum at standard conditions (AM1.5, 1000 W/m^2). Converting the irradiation energy to number of photons per second and unit area gives a better picture about the number of photons that are available for conversion into electrons under ideal conditions and at specific wavelength as the black line in **Figure 1.1** shows. It is clear from the figure that the maximum number of photons is located at the infrared area. However, the energy of photons at this area is low and will reduce the formation of charges and also limit the voltage difference that the photovoltaic devices can generate. Therefore, for maximum photon harvesting in the organic solar cells low band gap materials are required.[3,7]

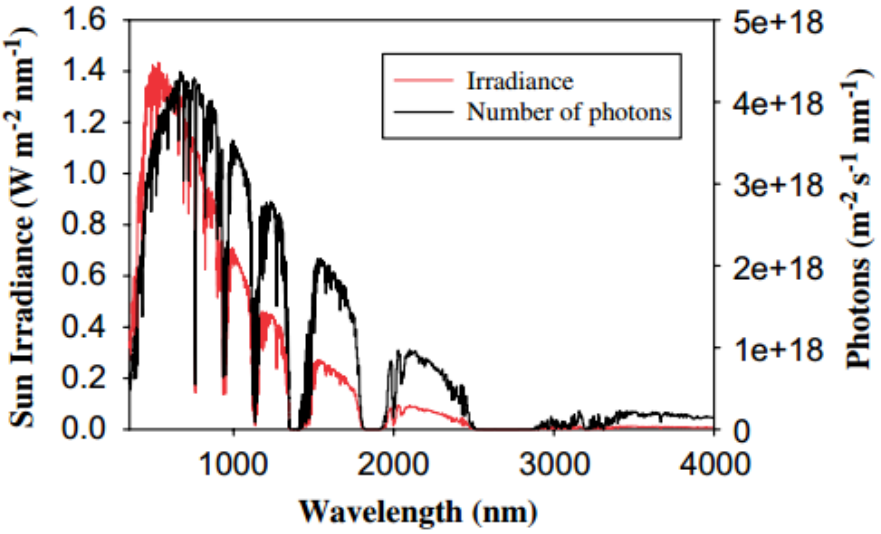

Figure 1.1. The solar spectrum at standard conditions (AM1.5, 1000 W/m^2), and the photon flux (number of photons) for the standard solar spectrum AM1.5.[8]

1.4. Mechanism of converting light into electricity in organic solar cells

The process of converting light into electricity in organic solar cells occurs in four main steps. The first step is photoexcitation of an electron from HOMO to LUMO level leading to formation of a hole in the HOMO level. In this state, a strong Coulombic attraction of around 1-1.4 eV between the formed electron-hole pairs (excitons) develops (**Figure 1.2 (a)**). Therefore, during this step the strongly bound excitons will be produced in high quantities compared with the possibility of producing free charges. However, in order to improve the harvesting ability of the largest number of photons two issues should be considered; the thickness of the active layer and the band gap of the molecules. Because the organic materials have high absorption coefficients, a thin layer of the material enough to harvest sufficient amount of photons. In addition, considering that the maximum number of photons in the solar spectrum is located at wavelength approximately 700 nm and longer (**Figure 1.1**), a small band gap material (around 1.1 eV) has the ability to absorb the maximum solar irradiation and show significant improvement in the characteristic of solar cells.[9,10]

The second step in the mechanism is diffusion and separation of the formed exciton into free charge carries in order to generate electricity (**Figure 1.2 (b)** and **(c)**). This stage requires the presence of two different organic materials (donor and acceptor) that have appropriate HOMO and LUMO energy levels. At the interface between the donor and acceptor, the exciton diffusion occurs where the electron transfer to the LUMO of the acceptor and the hole remains in the HOMO of the donor. However, due to the presence of Coulombic attraction between the newly formed electron-hole charge pairs, an internal strong electrical field should be applied in order to separate these charges. For effective charge dissociation, it is important that excitons reach the interface area within their life time (called exciton diffusion length). However, due to the exciton diffusion length in organic materials being short; this requires paying more attention to the thickness of the active layer. However, choosing the active layer thinner than 10 nm will lead to a reduction in the absorption of the required amount of photons. Increasing the thickness will also result in increasing the distance in the interface between the donor and acceptor. Thus, the exciton might be exposed to decay or recombination before reaching the interface area. To solve this problem an interpenetrating network of donor and acceptor materials should be used to increase the interface area and insure efficient dissociation of the charges.

The third step in the process is the transportation of the charges within their life time to the respective electrodes (**Figure 1.2 (e)**). The electrons travel to the cathode and the holes to the anode. However, because of the mobility of charges in organic molecules is generally low, the active layer should be adjusted to allow the charge carriers to reach the prospective electrode within their life time.

In order to achieve high efficiency in charge collection, which is the final step in the conversion process, the matching between the work function of the electrodes and the organic layer should be considered (**Figure 1.2 (f)**). Therefore, indium tin oxide (ITO) is used as a contact material between the electrode and the organic active layer to assist in matching the high work function of the anode with the HOMO level of the most donors. Using aluminum metal (Al) as a surface of the cathode assists in matching the LUMO level of the PCBM which is the most common acceptor in organic solar cells.[9]

Through the process of converting energy into electricity, the loss in energy could result from three different reasons. One of them is the poor absorption of photons either due to the limitation of the band gap or the thickness of the active layer. The second reason is the possible decay of the produced excitons when they are created too far from the donor-acceptor interface. The third reason is the recombination of charge carriers during the transport process to the respective electrode. In addition, the unfavourable energy alignment of the donor and acceptor assist in losing energy and reducing in the power conversion efficiency through the process.[11]

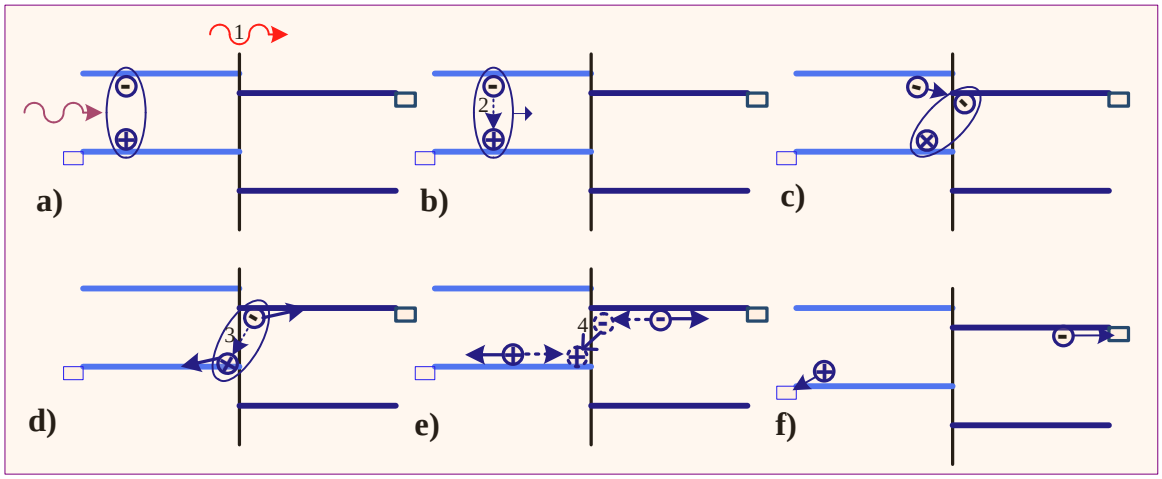

Figure 1.2. Mechanism of converting light into electricity in heterojunction devices.

1.5. Device architectures of organic solar cells

There are three main types of organic photovoltaic architectures; bilayer heterojunction device, bulk heterojunction device (BHJ) and dye sensitized cells (DSSCs). The last two mentioned methods are the most successful types, due to the large interface area between the two components. For example, the nanoscale interpenetrating network resulting from BHJ assists in reducing the distance between both components to be less than the exciton diffusion length.

1.5.1. Bilayer heterojunction device

The device architecture of bilayer solar cells consists of a photoactive layer composed of donor-acceptor material and C_{60} loaded on top of each other to form an interface layer (**Figure 1.3)**. The formed active layer is sandwiched between high function electrode (typically transparent ITO layer) and low function cathode. Interface layers are used

between the active layer and respective electrode to modify the work function of both anode and cathode, respectively. The vacuum deposition technique is used to build the bilayer heterojunction device using small molecules as donor materials of the active layer. A maximum efficiency of 4 % has been recorded for a bilayer device consisting of copper phthalocyanine and C_{60}.[12]

However, the major drawback of this device architecture is the short exciton diffusion length associated with organic materials. For this reason the thickness of the double layer should be adjusted to ensure the exciton reaches the interface area within their lifetime. However, reducing the thickness of the layer will obstruct the harvesting of enough photons from the solar radiation and reflect negatively on the efficiency of the device. At the same time, increasing the thickness of the active layer will result in recombination of the excitons before reaching the interface area.[13]

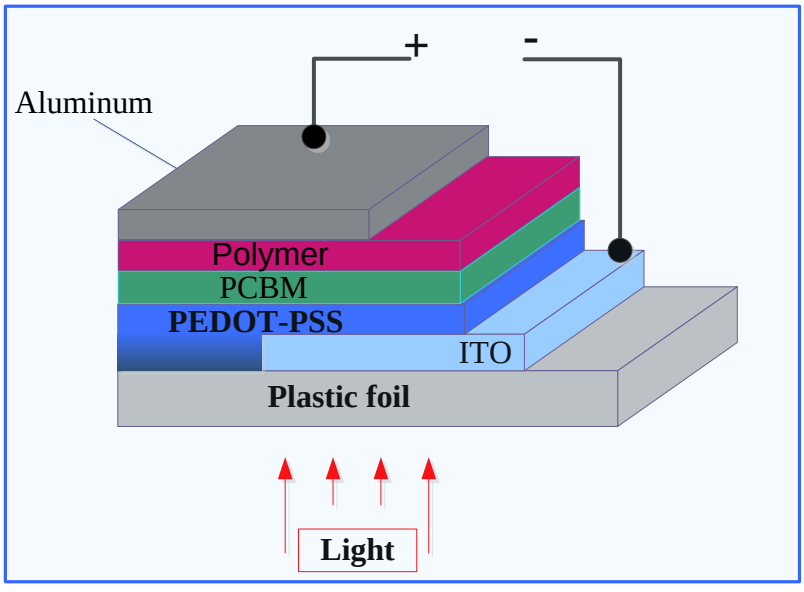

Figure 1.3. Configuration of a bilayer organic solar cell.

1.5.2. Bulk heterojunction device

The active layer of the bulk heterojunction device (BHJ) consists of a blend of a *p*-type polymeric material or small organic molecule, and *n*-type component typically soluble fullerene derivatives. The device architecture is completed by positioning the active layer between a transparent ITO anode and Al metal employed as a cathode electrode.[9] The configuration of a typical BHJ is shown in **Figure 1.4**.

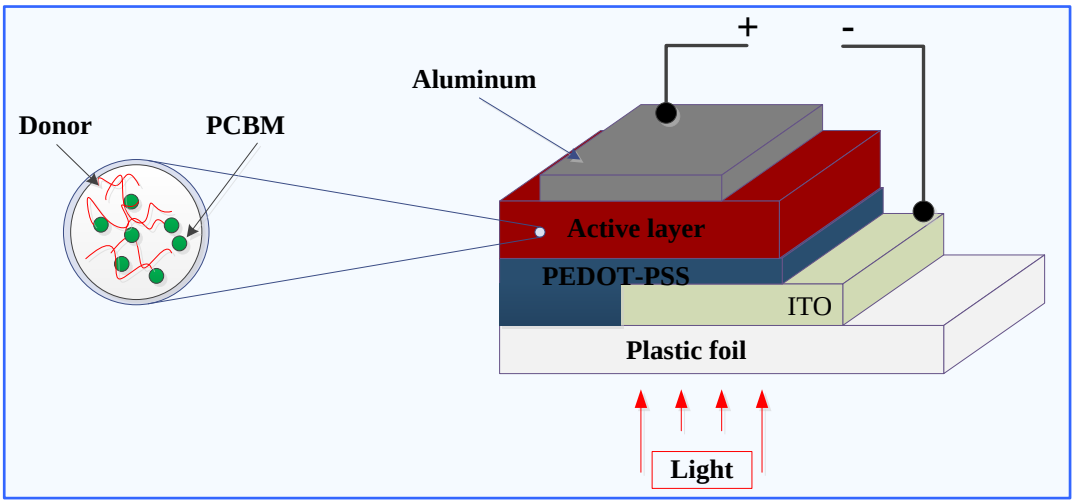

Figure 1.4. Diagram of a bulk heterojunction organic solar cell.[1]

The resulting thin film forms an interpenetrating network of the donor and acceptor materials. This network formation is responsible for absorption the solar photons and assist in reducing the distance between both components to be less than the exciton diffusion length. The active layer of BHJ device can be fabricated by vacuum deposition or solution processing techniques. Although the thickness of the film is not a major problem in BHJ devices compared with the bilayer device, the morphology and the conditions of deposition film have a significant effect on improving the performance of the device. Therefore, a lot of effort has been focused on modifying the donor structure and the conditions of the

annealing process in order to increase the regioregularity and the stacking between the chemical structures, during the manufacturing process.[14]

Most of BHJ devices have been built using conjugated polymers. The high charge mobility of these materials is dependent on good film quality. Mixing conjugated polymers with fullerene derivatives in a bulk volume can enhance the performance of the device due to the fullerene derivatives forming an electron transportation channel in the phase separated materials. An improvement in the efficiency of a blend of MDMO-PPV as a donor and $PC_{60}BM$ as an acceptor reached around 2.5 % in a BHJ device (**Figure 1.5**). This improvement in the performance resulted from modifying the nano-morphology of the blend by changing the spin casting conditions.[15]

The limit in performance of this device has been related to the low charge mobility of the polymer, and poor matching between the solar spectrum and the absorption spectrum of the applied polymer in the active layer. Improvement in the performance was followed by achieving an efficiency of 5 % from an annealed blend of P3HT/$PC_{60}BM$. Due to the high charge carrier mobility and the highly crystalline morphology feature of P3HT, the P3HT/$PC_{60}BM$ heterojunction solar cells has been used as the yardstick for organic solar cells.[9,15]

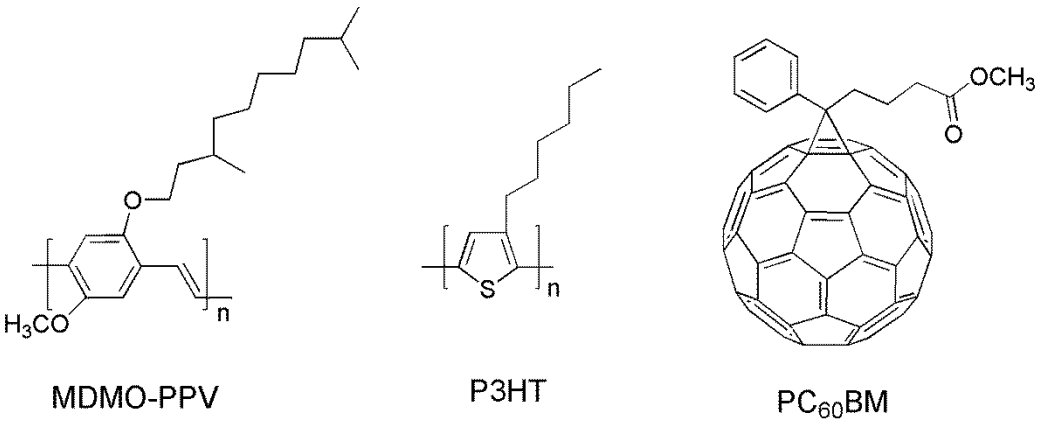

Figure1.5. Molecular structures of materials used in bulk heterojunction devices.

1.5.3. Dye-sensitized Solar Cells

Dye-Sensitized Solar Cells are widely known as Grätzel cells. The device architecture and working mechanism of DSSCs is extremely different from conventional semiconductor solar cells. The device architecture of DSSCs consists of a noncrystalline mesoporous titanium dioxide film as the working electrode. This film deposited on a glass substrate covered with transparent conductive oxide (TCO) substrate (usually fluorine doped with SnO_2). The mesoporous structure of TiO_2 forms an internal contact surface with the dye. The dye is responsible for absorbing the incident light and starting the conversion process. The device architecture is completed with an activated conducting glass substrate and an electrolyte featuring a redox couple. The device architecture and working principle are explained in more detail in chapter 5.[16]

1.6. Determination of power conversion efficiency of photovoltaic devices

Characterization of photovoltaic devices can be carried out by identifying the power conversion efficiency (η) as well as other different parameters. These parameters include; the incident photon-to-current conversion efficiency (IPCE), the short circuit current (J_{sc}), the open circuit voltage (V_{oc}), and the fill factor (FF). These parameters can be collected from two different tools i.e. the spectrum photocurrent response system and the solar simulator.

The resulting photocurrent spectrum of organic solar cells is shown in **Figure 1.6** and gives information about the ability of the applied materials under standard solar radiation to convert photons into electrons at different wavelengths. The performance of these

materials can be tracked by calculation of IPCE from equation **(1-1)**, which represents as a percentage number of electrons flowing through the external circuit divided by the number of incident photons at specific wavelength.

$$\mathrm{IPCE} = \frac{\text{Number of electrons}}{\text{Number of incident photons}} = \frac{\mathrm{I}/e}{\mathrm{P}/h\upsilon} \qquad (1\text{-}1)$$

Where I, represents the photocurrent (A/m^2) and P, represents the incident light power (W/m^2).

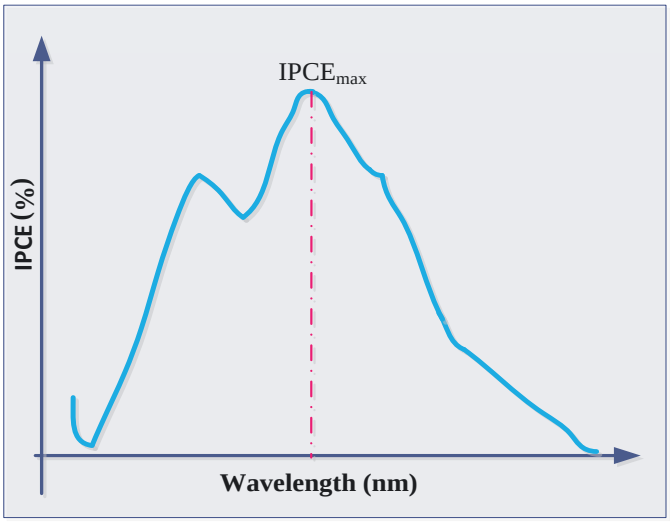

Figure 1.6. Photocurrent spectrum of organic solar cells.

A solar simulator can be used to generate voltage and current plots during the illumination of solar cells with an artificial light that matches the standard solar spectrum radiation. The resulting I-V curve is used to estimate the overall performance of the solar cell (**Figure 1.7**). From the resulting curve number of electrical parameters i.e. J_{sc}, V_{oc}, FF, maximum power, I_{mp} and V_{mp} can be calculated. Applying these parameters in the equation **(1-2)**, the power conversion efficiency can be calculated:

$$\eta = \frac{P_{out}}{P_{in}} = \frac{FF.V_{oc}.J_{sc}}{P_{in}} \qquad (1\text{-}2)$$

Where, P_{out} is the maximum output power (W/m^2), P_{in} is the incident power on the device (W/m^2), V_{oc} is the open circuit voltage when current in the cell equals zero (V), and J_{sc} the short circuit current when the voltage in the cell equals zero (A/m^2). FF is the fill factor and it can be estimated from equation **(1-3)** which represents the ratio between the maximum power to the external short and open circuit values;

$$FF = \frac{V_{mp} . I_{mp}}{V_{oc} . I_{sc}} \qquad (1\text{-}3)$$

Where, V_{mp} and I_{mp} are the voltage and current at the maximum power point in the I-V curve, respectively.[17]

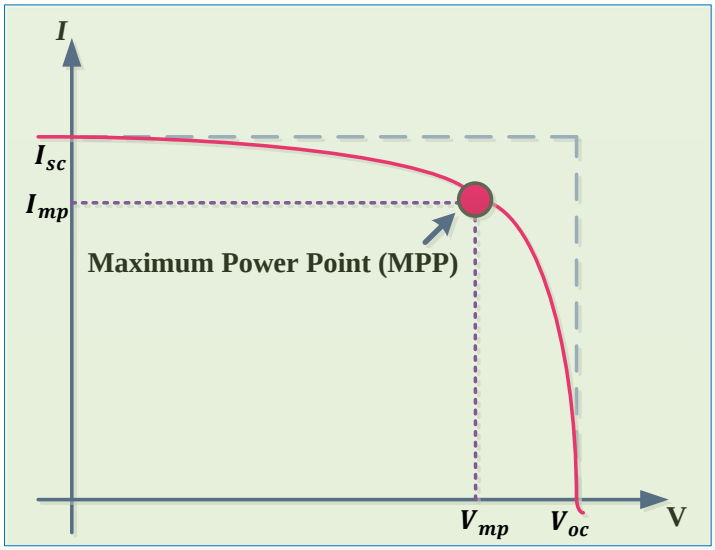

Figure 1.7. Typical I-V curve of solar cells.

1.7. Organic semiconductors for solar cells

1.7.1. *p*-type organic semiconductors

Depending on the molecular structure and the processing techniques used, *p*-type organic materials can be divided into three main sections; conjugated polymers, dendrimers and small molecules. However, for designing ideal *p*-type materials that can be used in organic solar cells, a number of issues should be considered. These issues include: the solubility in organic solvents, the film-forming properties, the HOMO and LUMO energy levels, and the mobility of the hole during the process.[7]

1.7.1.1. Conjugated polymers

Conjugated polymers have been widely used as an active component in organic solar cells. They are made of a large number of repeating units linked together by covalent bonds to form a one dimensional (1D) polymer chain. These polymers can be processed effectively from solution by a number of cheap processing techniques such as spin casting and roll to roll printing techniques.[10]

Poly 3-hexylthiophene (P3HT), and its derivatives are the most important electron donor materials commonly used in organic solar cells. Polymerization of 3-hexylthiophene resulted in three different polymer structures; a regular one where all units couple in a head to tail (HT) or irregular structures where the units couples either head to head (HH) or tail to tail (TT) (**Figure 1.8**). Among the three structures, regioregularity of the substituted poly-thiophene is an important characteristic in enhancing the performance of the molecular device (**Figure 1.9**). The optical properties of regioregular P3HT differs from

random P3HT in terms of its UV-vis spectra. The regioregular material shows a red shift for the maximum absorption band of about 25 nm relative to the random material. In addition, the absorption is longer for the regioregular P3HT in solid state spectra, due to the close intermolecular interactions. Regioregular P3HT in a blended mixture with PCBM has been widely used as a model device for BHJ devices.[18] The good efficiency has been explained in terms of the highly crystalline microstructure of P3HT films which reflects positively on the hole carrier mobility (around 0.1 $cm^2/V.s$).[19] In addition, regioregular P3HT shows a highly planar conformation which improves the structural organization and π-π stacking ability between the molecules. Furthermore, the planarity of regioregular P3HT enhances the electronic connections between the molecules and assists in reducing the band gap by forming an efficient packing of the polymer chains.[20]

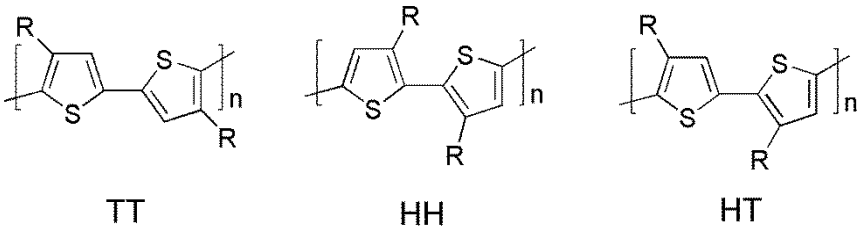

Figure 1.8. Polymers of 3-hexylthiophene.

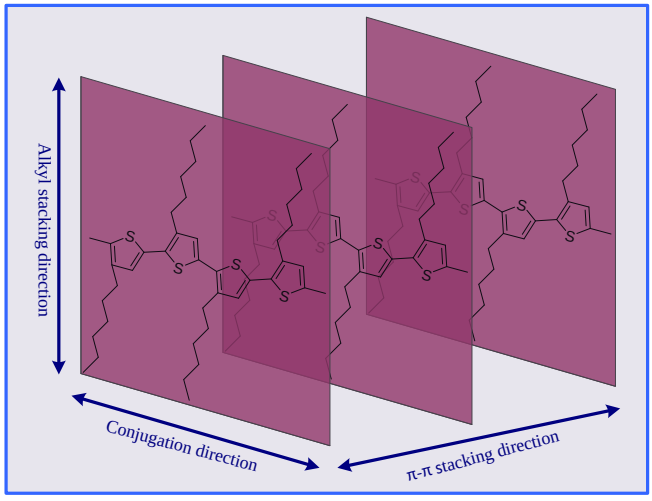

Figure1.9. Schematic structure showing the preferred arrangement of adjacent chains of regioregular P3HT.

The significant drawbacks of P3HT materials as donors in organic solar cells are the large band gap and the narrow absorption band which limits harvesting of low energy photons which reduces the performance of photovoltaic devices. Therefore, further development of power conversion efficiency is essential to meet the requirements of building effective large scale organic solar cells. To harvest the maximum amount of low energy photons, the absorption of conjugated polymers should cover the area that has the maximum photon flux density of the solar spectrum which is the near infrared of the solar spectrum. From this point of view it is of great interest to decrease the band gap of the active material to harvest a larger amount of the solar photons and increase the power conversion efficiency.[21]

Therefore, different strategies have been applied to narrow the band gap of conjugated polymers. One of these strategies involves improving electron delocalization along the polymer chain by formation of quinoid resonance structures.[22] The other strategy is using alternating donor–acceptor units to build the polymer backbone (**Figure 1.10**). Both strategies allow formation of a partial charge separation, facilitate charge carrier mobility along the polymer chain, and manipulate the HOMO and LUMO energy levels. The difference between the new hybridized orbitals narrows the band gap (**Figure 1.11**).[23, 24]

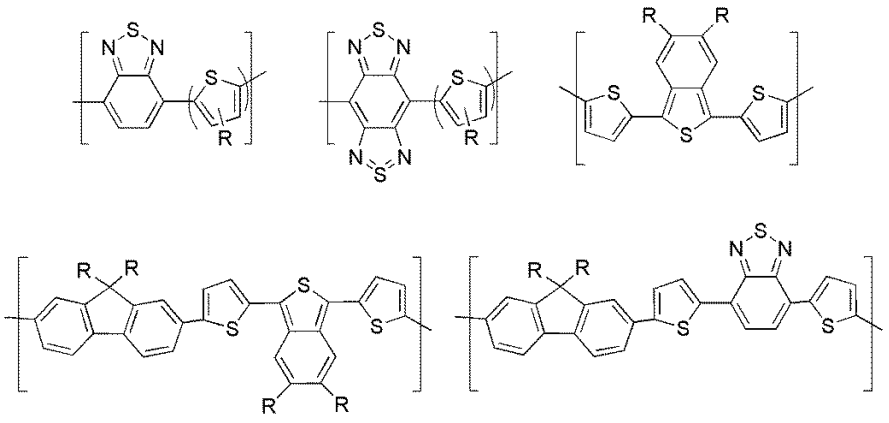

Figure 1.10. Examples of low band gap polymers.

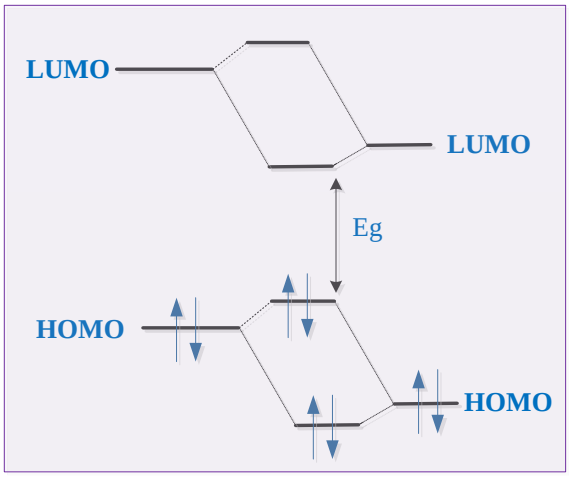

Figure 1.11. Orbital interactions of donor and acceptor units to form a small band gap in a D-A conjugated polymers.

1.7.1.2. Conjugated dendrimers

Dendritic molecules are type of branched conjugated polymer characterized by the unique and distinctive organization of long chain branched units around the multifunctional central part. These branches are covalently attached to the polymer main chain and gathered at one central unit. Due to the assembly of functional groups around the molecular core, the electronic properties of the dendritic structures often differ from those of the isolated and independent linear branched molecules. Also the synthesis of dendritic molecules can be achieved by iterative polymerization procedures, which allows the synthesis of a well-defined molecular structure in each of polymerization step. Also each of the polymarization steps involves addition of a new monomer layer to the branches and leads to formation of a new dendrimer generation. Therefore, the structure of dendrimers can be divided into three different parts: a core, regular branched of repeating units emerging from the core which assist in forming different dimensional structure shapes, and the end functional groups on the outer layer of repeating units as shown in **Figure 1.12**.[25]

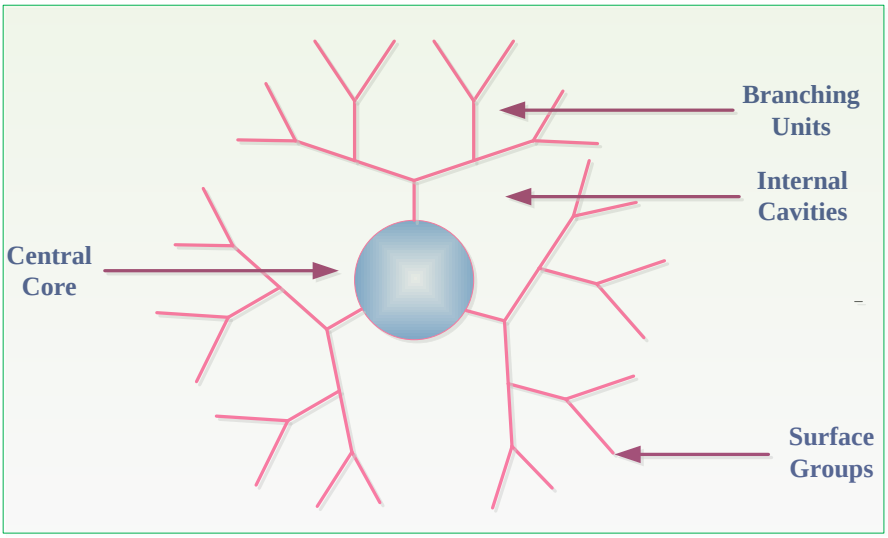

Figure1.12. Structure of dendrimers.

In contrast to linear conjugated polymers, dendritic molecules show a number of distinctive features. The iterative polymerization procedure that is used to prepare the dendritic molecules facilitates the synthesis of a well-defined high molecular weight molecules compared with linear ones. In addition, solubility, which is a major problem associated with increasing the molecular weight of linear polymers, is significantly improved in dendritic molecules by controlling the nature of the end groups. Furthermore, the growth of the dendrimer has a physical limitation which allows significant increase in the number of monomers while the volume of the dendrimer increases proportionally during the polymerization steps giving rise to a globular shape.[26]

The dendritic systems are comparable with the small molecules in terms of forming a well defined structure; however, their synthesis is different from small molecules. Two methods have been developed to synthesize dendritic molecules: the divergent and the convergent methods. In the divergent approach the first layer is built by coupling a simple building block monomer into the core. Then the process can be followed by forming a new generation through activating the peripheral groups to allow coupling to additional monomers. In the convergent approach, a higher generation dendrons are initially prepared

then activated to couple with a multifunctional core to form globular dendrimers. The divergent approach requires the presence of large amounts of reagents before starting the coupling and activating steps, whereas the convergent approach requires a smaller number of components in the reaction mixture to start the process. This causes difficulties in purifying the target dendritic molecules in the divergent approach due to the increased formation of side reactions during the coupling step.[27]

Power conversion efficiencies of 0.32 % have been recorded using dendrimer as donor in BHJ device with fullerene C_{60} as an acceptor. The blend of porphyrin-based dendrimers, which is represented in **Figure 1.13**, and fullerene exhibited a supramolecular complex. A strong and broad absorption band in the near IR region was observed for the blend resulting from π-π interactions and the strong absorbing ability of the porphyrin units. The performance of the device resulted from the efficient electron transfer from porphyrin dendrimers and through the resulting complex.[28]

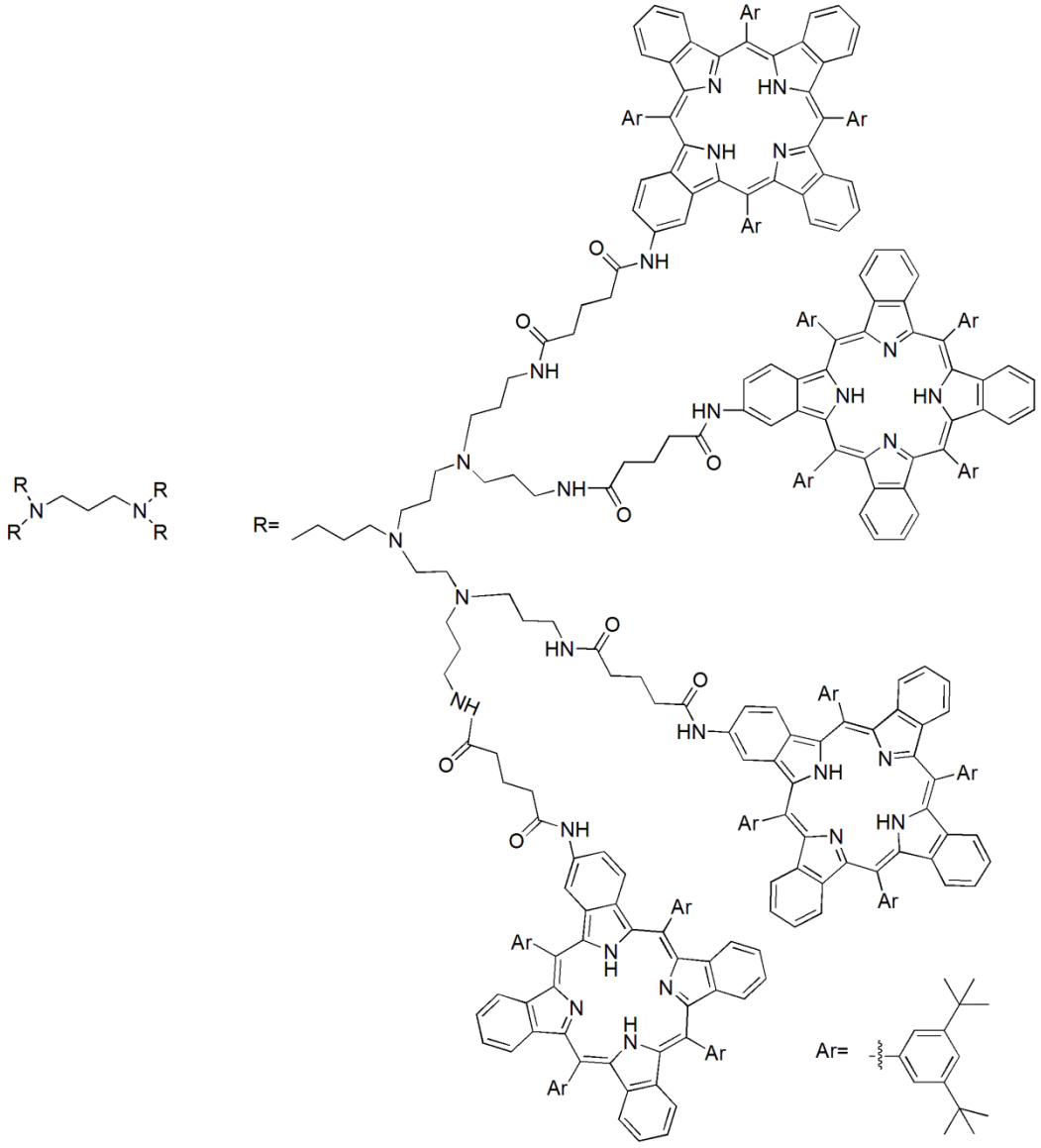

Figure 1.13. Structure of porphyrin dendrimers.

For fabrication of optoelectronic devices, the performance of the device depends not only on the molecular structure of the active layer but also on the organization of dendritic molecules. Due to the fact that self organization of these materials occurs through intermolecular interactions such as; hydrogen bonds, hydrophobic interactions, and π-π stacking interaction, these molecules assist in forming new materials with new properties for nanotechnology application. The structure of the cores, branches and surface groups, the dendron generations and molecule shape play important roles in modifying the surface.

For example; macrocyclic organic molecules which consist of disk shaped cores, tend to form one dimensional self assembled thin films through π-π interactions. These type of molecules and their derivatives form highly ordered columnar structures and exhibit hole mobility of $5\times10^{-3}cm^2/(V.s)$ in organic field effect transistors (OFET).[29] Combining the self assembling properties of macrocyclic molecules with the significant optical and electronic properties of thiophene units in dendrimers structure (**Figure 1.14**) leads to significant improvement in the performance of BHJ device. For example the solubility and self organization of the dendrimers in the solution and solid state of 9,9-dioctylfluorenyl hexaperi-hexabenzocoronene moieties has been shown to enhance the absorption band gap toward IR region upon varying the generation of the dendrimers. Power conversion efficiency of 2.5% have been recorded for BHJ devices containing an interpenetrating network of the second generation dendrimers as donor and $PC_{71}BM$ as an acceptor unit. This improvement in the efficiency resulted from the efficient ordering of the materials in the solid state which leads to high charge transport and efficient photoexciton dissociation.[30]

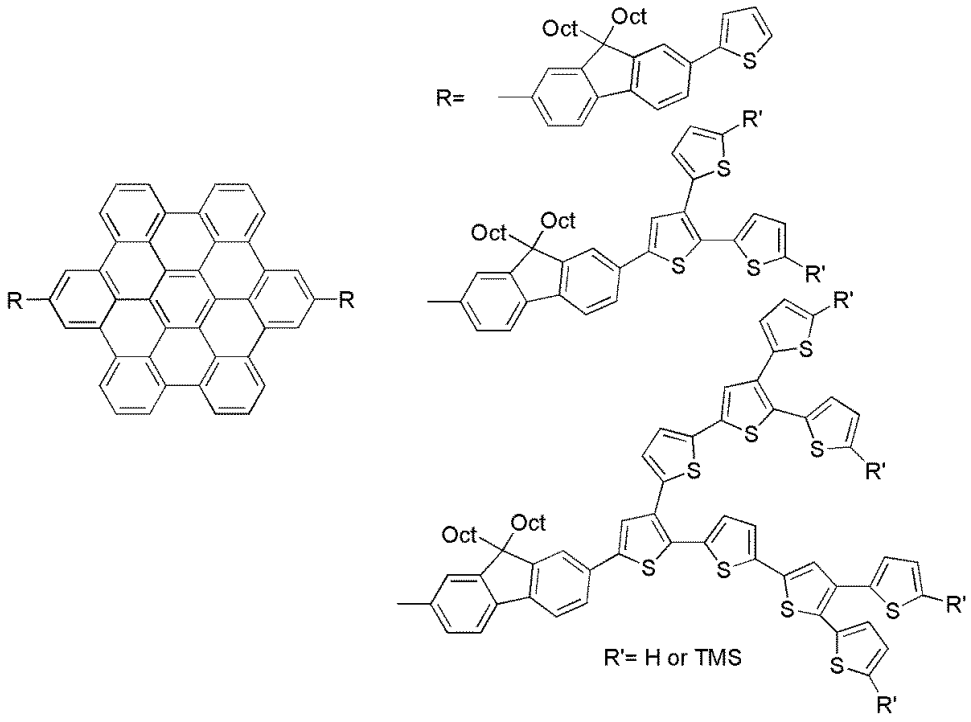

Figure 1.14. Thiophene based dendrimers with a polycyclic organic core.

Polyphenylene dendrimers with their rigid moleular structure can be an ideal examples for improving the morophology of the active layer (**Figure 1.15**). These rigid molecules have the ability to stack to each other by π-π interactions and form highly ordered supramolecular building blocks. Electropolymerization of the resulting dendrimers show a three dimensional network within the film. Also significant charge carrier mobility and improvement in the conductivity was observed for the resulting films due to the small distances between the planar wings of different dendritic cores.[31]

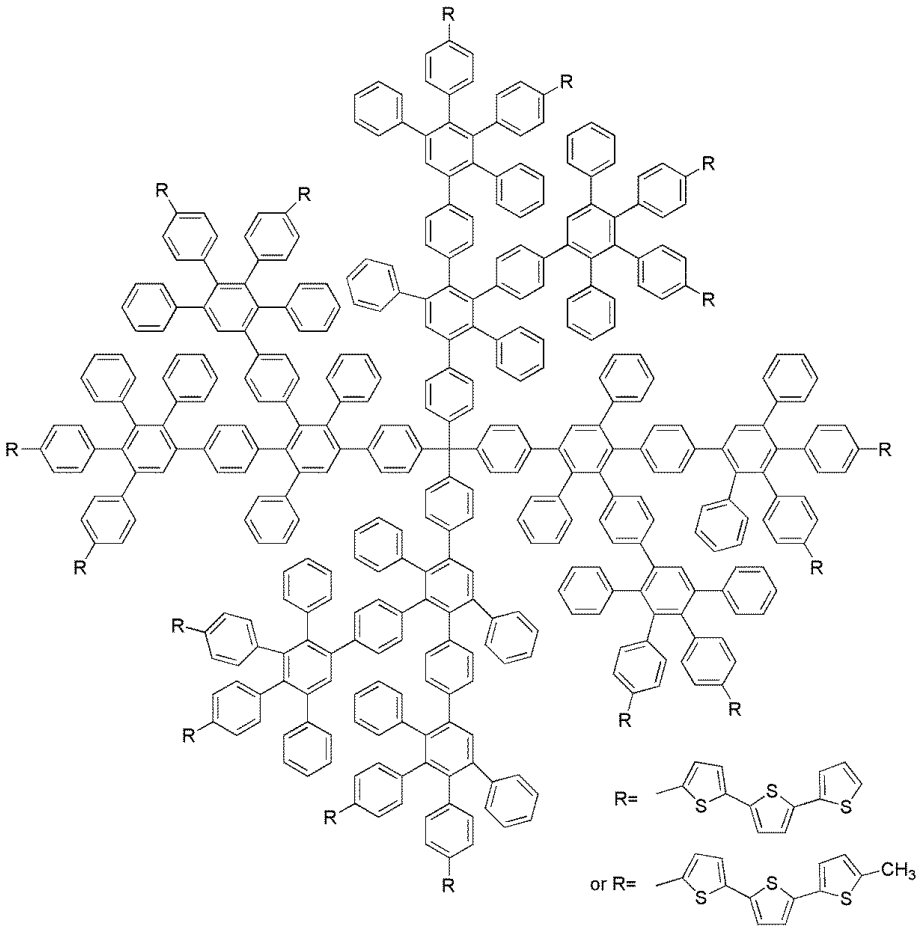

Figure 1.15. Example of polyphenylene dendrimers.

1.7.1.3. Small molecules

Although the linear regioregular conjugated polymers mostly show effective charge transport ability along the stacking direction of the conjugated chains, for some other one-dimensional π-conjugated polymers, the random crystalline microstructure might reflect negatively on the improvement of the hole carrier mobility in BHJ cells. Therefore, replacement conjugated polymers with small conjugated molecules assist in many cases in modifying the performance of solar cells by presenting a number of advantages. One of these advantages is the possibility of controlling the chemical structure of these molecules such as regioregularity, molecular weight and poly-disparity which assist in improving the morphology and the high level of ordering in the device. The second advantage is the charge carrier mobility of the small conjugated molecules is normally higher than conjugated polymers. Also these molecules have the ability of minimizing the problems associated with charge transport, due to their high molecular extinction coefficient. This feature also promotes limiting the thickness of the active layer. Furthermore, simplicity in purification and determination the electronic properties of the small molecules is also an important feature.[25]

A number of small donor molecules and oligomers have been synthesized to be used in the active layer of organic photovoltaic applications. However, considering the factors that affects the performance of the device, such as: the morphology, hole mobility, and the band gap, only a few of these molecules have achieved successful progress in the field. These molecules can be divided depending on the chemical structure into two main sections: organic dyes and small dipolar molecules.[32]

Phthalocyanine (Pc), subphthalocyanines (SubPcs), and diketopyrrolopyrroles (DPP) and their derivatives are the most common organic dyes used in the planar and bulk heterojunction devices (**Figure 1.16**). All these dyes exhibit a number of attractive features for photovoltaic applications such as: strong absorption in the low energy region, good thermal stability and flexibility of modifying the optical and electronic properties. For example the simplicity of modifying the chemical structure of diketopyrrolopyrroles unit by attaching solubilising groups such as neutral long alkyl chains in position 2 and 5, has demonstrated improvement in the charge carrier mobility and enhanced the solid state packing of the molecules by increasing their tendency to self assemble resulting in thin films with highly ordered structure.[33]

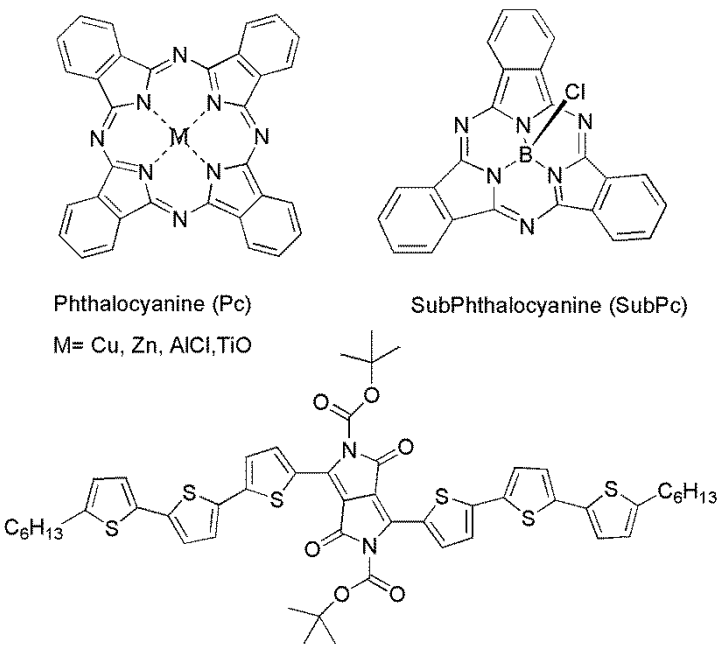

Figure 1.16. Molecular structure of dye-based donors.

Oligothiophene derivatives are also good candidates for photovoltaic applications, due to their high charge carrier mobility and flexibility in tuning their HOMO and LUMO energy levels. The synthesis of star-shaped oligothiophene in 2006 presents the first example of a solution processable small molecule BHJ device (**Figure 1.17**). This example has provided impetus for the further development of small molecules based BHJ devices. The work was

further extended by using different lengths of linear oligothiophene chains surrounding the thiophene core. Investigation revealed that the molecules with the longest linear oligothiophene chains exhibited an improved performance which indicates the formation of good quality films and an efficient band gap.[34]

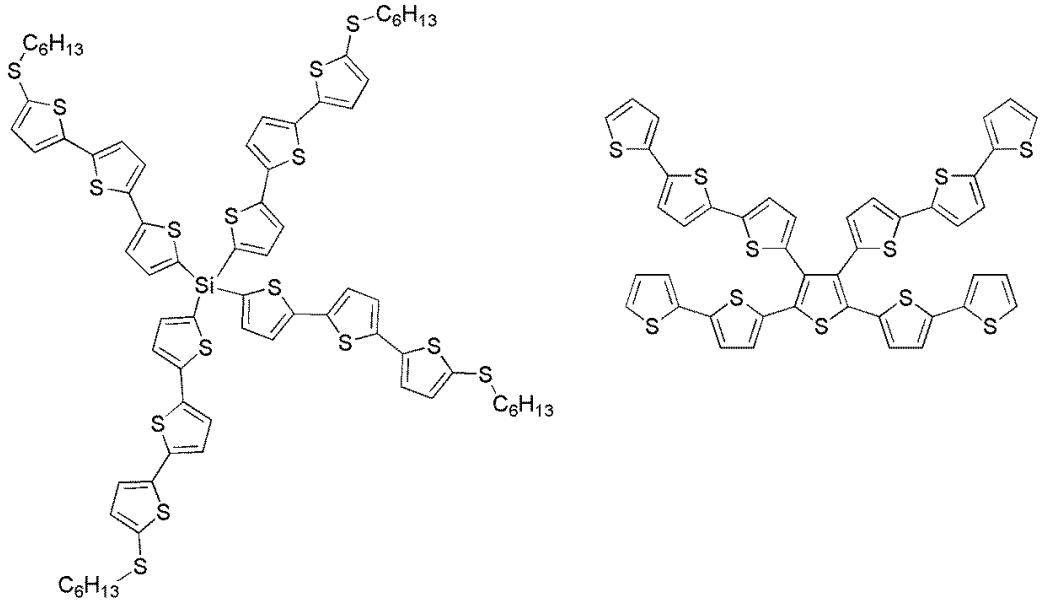

Figure1.17. Molecular structure of star-shaped oligothiophene donors.

In addition, the performance of oligothiophene derivatives can be modified by forming highly polarisable systems through introducing electron withdrawing units such as dicyanovinyl (DCV).[35] or cyanoacetic groups[36] into the π-conjugated oligothiophene structure (**Figure 1.18**). The new molecules showed a good matching property with the solar spectrum due to intermolecular charge transfer between donor and acceptor units, which increases the absorption in the visible region. These materials can be fabricated either by vacuum-deposition or solution-processing techniques especially upon increasing the solubility of the material by attaching alkyl side groups.[37] In addition, precise control of the positions of these side chains on oligothiophene derivatives assists in supporting their miscibility with fullerene and enhancing their packing structure.[38] Changing DCV units to

cyanoacetic groups showed significant improvement in the performance of BHJ device from 3.7 % to 5.08 %, respectively, due to the formation of good quality films.

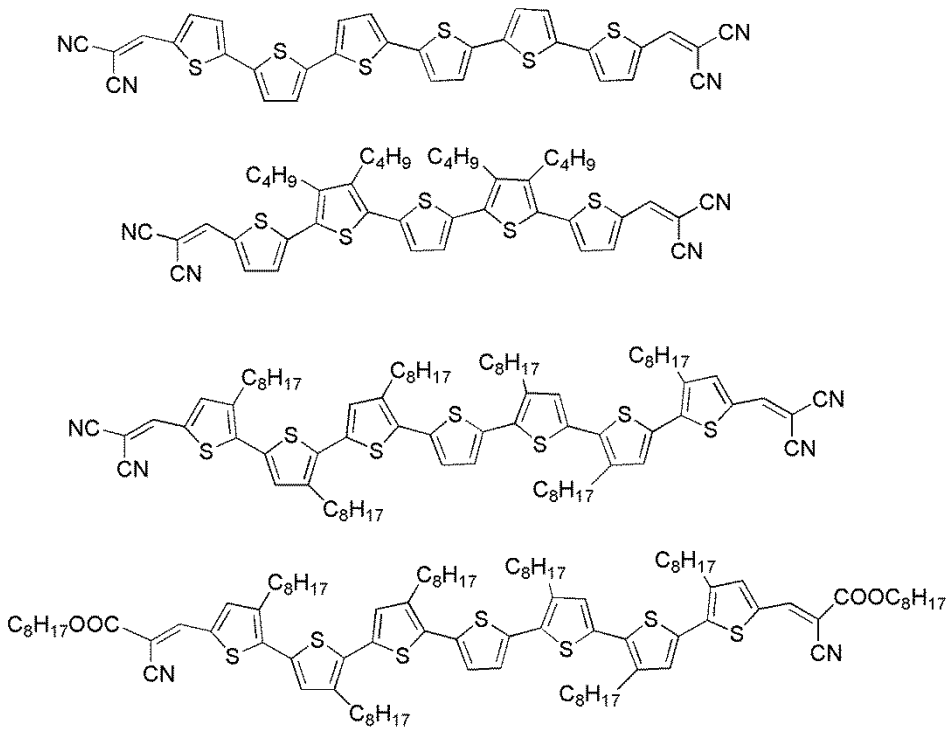

Figure 1.18. Chemical structure of linear oligothiophene donors.

The triphenylamine (TPA) unit due to its features such as: strong donating ability, hole transporting capability, and enhanced non-linear optical (NLO) behaviour of organic materials has been considered as a promising unit for building the active layer in BHJ devices. An improvement in the light harvesting ability and matching with the solar spectrum of this material could be achieved by reducing the band gap. In general, designing a low band gap donor to be used in heterojunction device requires decreasing the LUMO and increasing the HOMO simultaneously. However, applying this approach could negatively affect on the open circuit voltage of the cell. Therefore, a new approach for decreasing the band gap can be done by decreasing both HOMO and LUMO levels with

the most significant change in the LUMO level (**Figure 1.19**).[39,40] This approach will promote the properties of these materials by shifting the absorption toward the infrared region, increasing the V_{oc}, and stabilizing the material chemically against interactions with oxygen. This approach can be done by introducing number of acceptor groups such as dicyanovinylene[41,42] or cyanoacetic acid[43] to build push-pull systems which leads to reduced the π-π* interaction and increase intermolecular charge transfer between the donor and acceptor units (**Figure 1.20**).

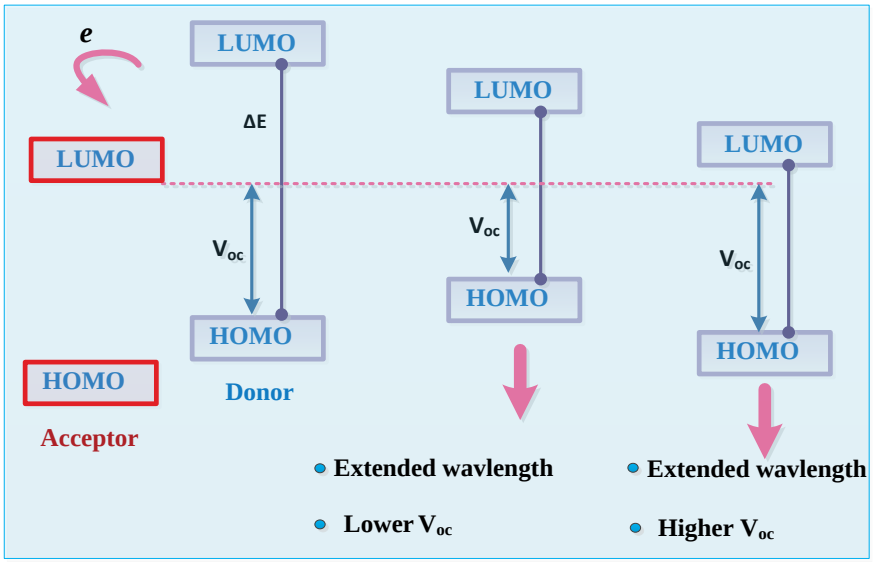

Figure 1.19. Engineering the band gap of conjugated donors.[40]

In addition, the TPA unit can present a central unit of star-shaped molecules containing linear π-conjugated arms with different electron withdrawing groups. These star-shaped materials show a better performance compared with the performance of linear conjugated ones especially by attaching cyano groups at the end of the arms. However, due to the negative effect of cyano groups on the solubility of these materials at the same time taking into account that BHJ cells are in general much more efficient than bilayers based on the same active materials, an improvement in the processability of these materials could be achieved by enhancing the solubility of these materials by attaching solubilising side chain

units. Applying these star-shaped materials in solution processed BHJ device has provided organic photovoltaic (OPV) systems with efficiency up to 4.3 %.[44]

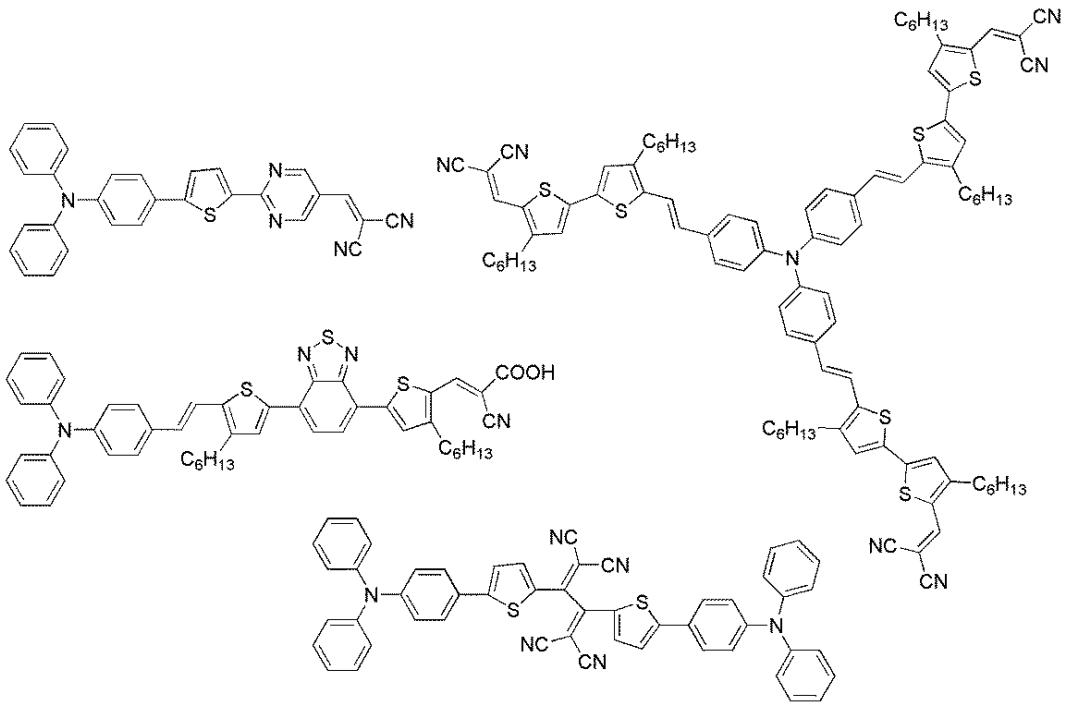

Figure 1.20. Chemical structure of triphenylamine-based donors.

1.7.2. *n*-type organic semiconductors

The improvement in the performance of the heterojunction devices relys not only on the efficiency and the performance of the donor components of polymers and small molecules, the acceptor unit also plays an important role in the progress of these devices. Fullerene and their derivatives are the most important acceptor units used in building OPV devices. However, the challenge of synthesizing and developing new non-fullerene organic system is an important target.

1.7.2.1. Fullerenes and their derivatives

Fullerenes are molecules that contain fused carbon rings, all linked together in a spherical closed cage structure. The family of fullerenes contains a number of allotropes such as; C_{60}, C_{70}, C_{76}, C_{78}, C_{84}. Among these allotropes C_{60}, C_{70} are the most abundant structures and they formed in a higher percentage compared with other fullerene structures. C_{60} in the gas phase was first discovered in 1985 by collecting carbon species from heated graphitic carbon soot using a focused laser.[45] However, the yield of the resulting fullerene material was not enough to measure the physical properties. In 1990, a pure C_{60} was synthesized in gram quantities by Krätschmer and co-workers.[46] Since then a number of investigations have been focused on synthesizing a new fullerene derivatives featuring novel photophysical and electrochemical properties.[47]

C_{60} is the most common type of fullerene contains of 20 hexagons and 12 pentagon rings. These rings are fused and all double bonds are highly conjugated together forming super conjugated aromatic molecule (**Figure 1.21**). The conjugation of the 60 π-electrons causes a rise to the HOMO level and deep decrease in the LUMO level forming a band gap of 2.3 eV. The low level of the LUMO enhances the ability of fullerene and their derivatives to act as ideal electron acceptors. Also the spherical geometry of C_{60} allows transportation of the charges in disordered media by the formation of a three dimensional system leading to high electron mobility reaching around 10^{-2}-10^{-1} cm^2/V.s. Electrochemical studies have revealed up to six reversible reduction waves. The absorption spectrum of C_{60} shows two main bands; an intense broad one in the UV region and a weak absorption band in the visible region.[46]

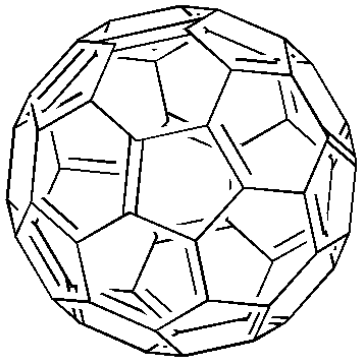

Figure1.21. Chemical structure of fullerene C_{60}.

The discovery of ultrafast electron transfer between conjugated polymer MEH-PPV and C_{60} was first observed in 1992 by Sariciftci and co-workers, since then several studies have focused on investigating this feature by using a blend of different size and structure of π-conjugated oligomers with C_{60} moieties. The study was aimed to find the effect of the chemical structure of the polymer on both the electron transfer process and the morphology of the blend (**Figure 1.22**). However, the most obvious drawback of the resulting blends is the tendency of pristine C_{60} to crystallize.[48, 49]

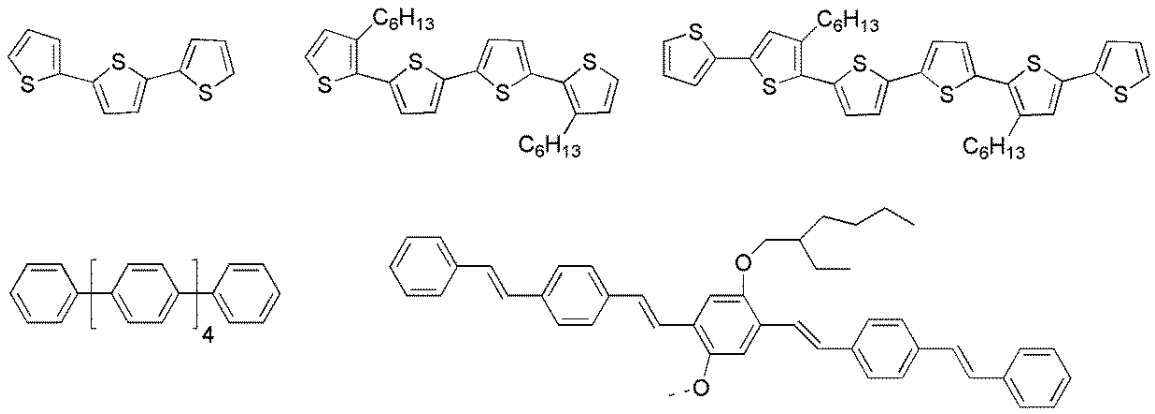

Figure 1.22. Selected examples of π-conjugated oligomers used in blends with C_{60}.

In addition to considering the factors that affect the performance of the organic solar cells such as the thickness of the active layer and the appropriate choice of solvent and temperature conditions for preparing this layer, several efforts have been focused on improving the solubility of the pristine C_{60} in order to enhance the morphology of the thin films and also the interaction between the interpenetrating networks. Therefore, improving the performance of organic solar cells can be made by either replacement the C_{60} with other soluble analogues or the attachement of C_{60} to conjugated polymer structures.[50]

In regard to soluble C_{60} derivatives, $PC_{60}BM$ has been widely used as an electroactive material in BHJ solar cells. The intrinsic advantages of $PC_{60}BM$ and their derivatives make them excellent candidates for BHJ device. These advantages can be concluded in four main features; the excellent ability to form a morphological network with donor polymers, strong tendency to accept up to six electrons from the excited polymer due to the low lying energy level of the lowest unoccupied molecular orbital, and high electron mobility reach around 2×10^{-3} $cm^2/(V.s)$.[42] Also $PC_{60}BM$ shows high thermal stability under both processing and operational conditions which supports its features to be used as an acceptor in organic solar cells. [51,52]

The effectiveness of the BHJ devices depends entirely on the nature of the components of the blend. $PC_{60}BM$ presents 75 % of this blend and it has low absorption coefficient in the visible region resulting from the symmetrical structure of C_{60} which hindrers the lowest energy transitions to occur. Therefore, replacement $PC_{60}BM$ with less symmetrical structure such as $PC_{70}BM$ improves the absorption in the visible region and allows matching between its absorption spectrum and the solar emission spectrum. Therefore $PC_{70}BM$ has been considered another attrative soluble acceptor for organic photovoltaic applications.[51,53]

Functionalizing C_{60} moieties is another alternative way to improve the morphology and reduce the phase separation in BHJ devices. This can be done by replacing the phenyl unit on $PC_{60}BM$ by thiophene.[54] fluorene, or triphenylamine units (**Figure 1.23**).[55] This approach results in another promising fullerene derivatives with power conversion efficiency reach around 4 % using solution processed BHJ devices of the new fullerene derivatives and regioregular P3HT blends.

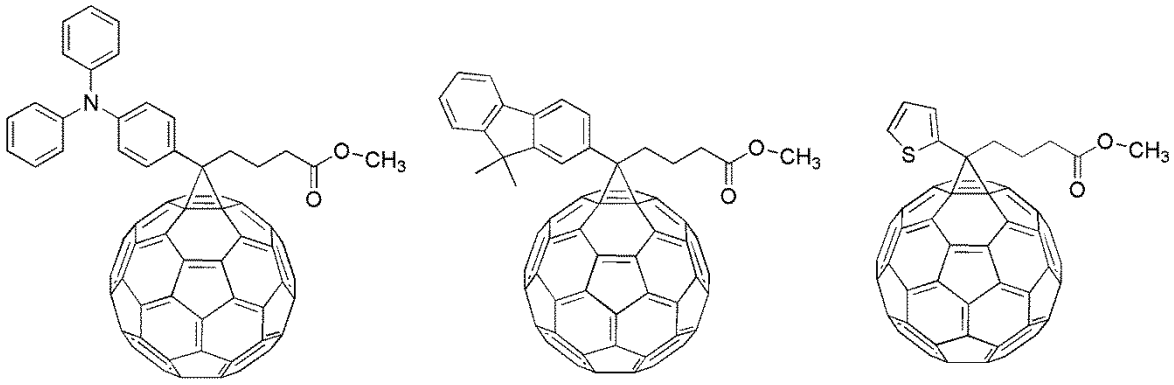

Figure 1.23. Molecular structures of some functionalized $PC_{60}BM$ derivatives.

Studies have also varied the length of ester alkyl chains on $PC_{60}BM$ with the aim of improving the solubility and morphology of the new fullerene derivatives. The length of the alkyl group does not influence the optical and electrochemical properties of fullerene, however the morphology of the thin film changed with increasing the alkyl chain length (**Figure 1.24**).[56]

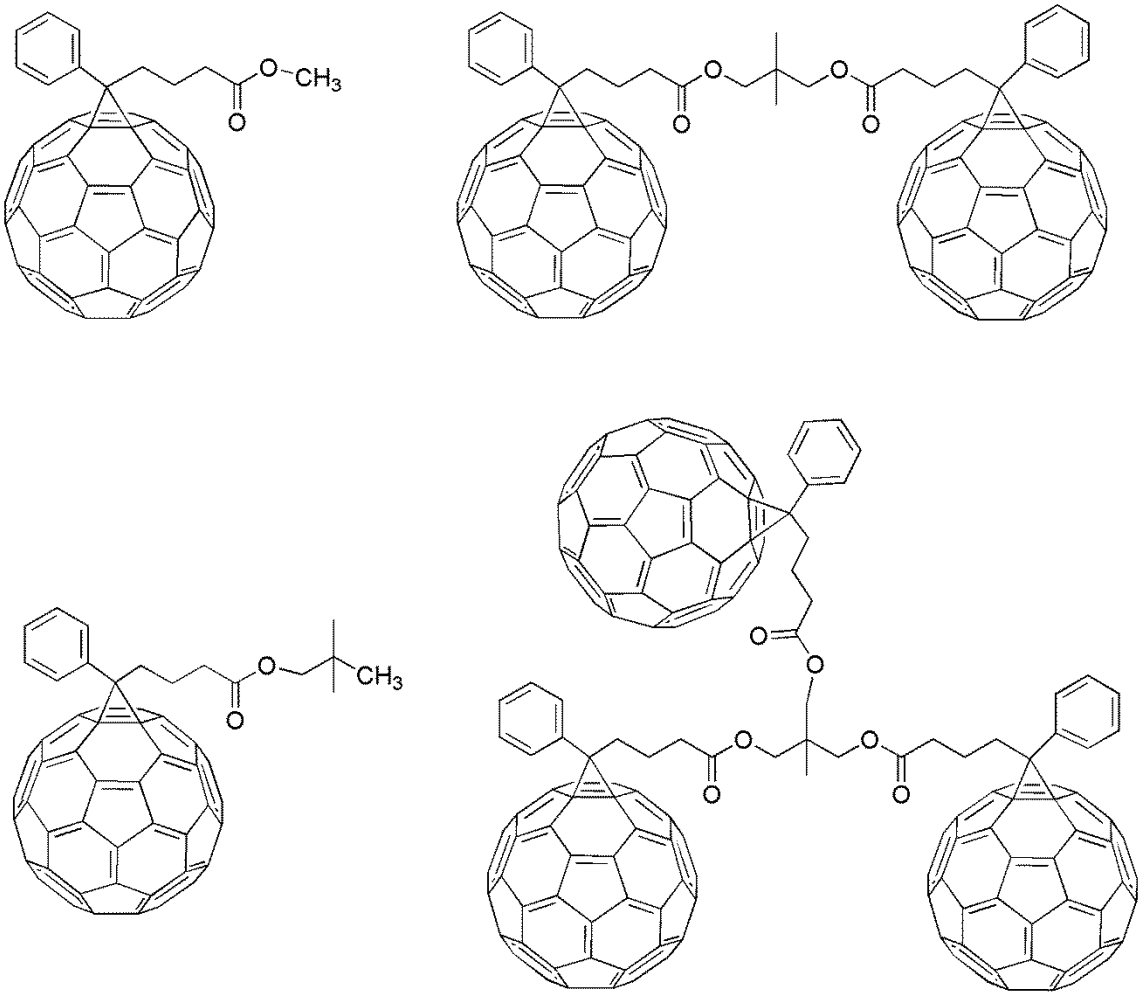

Figure 1.24. Molecular structre of $PC_{60}BM$ with different ester alkyl chains.

Another strategy to functionalize C_{60} moieties was done by linking conjugated polymer structures covalently with fullerene moieties to form donor–acceptor systems. Formation of these derivatives assists in developing the performance of the device by forming a well-organized morphology, reorganization of the energy levels between the donor and acceptor moieties, as well as enhancing the physical and chemical properties of the new materials such as fast charge separation and slow charge recombination (**Figure 1.25**).[49] The attachment of donor moiety to the fullerene can be achieved by cycloaddition reaction of C_{60} with either oligomers featuring either cyclic sulfone unit[56] or hydrazone units.[57] Also nucleophilic addition of oligomers featuring functionalized lithium acetylide units can be used to form donor–fullerene dyad molecules.[58]

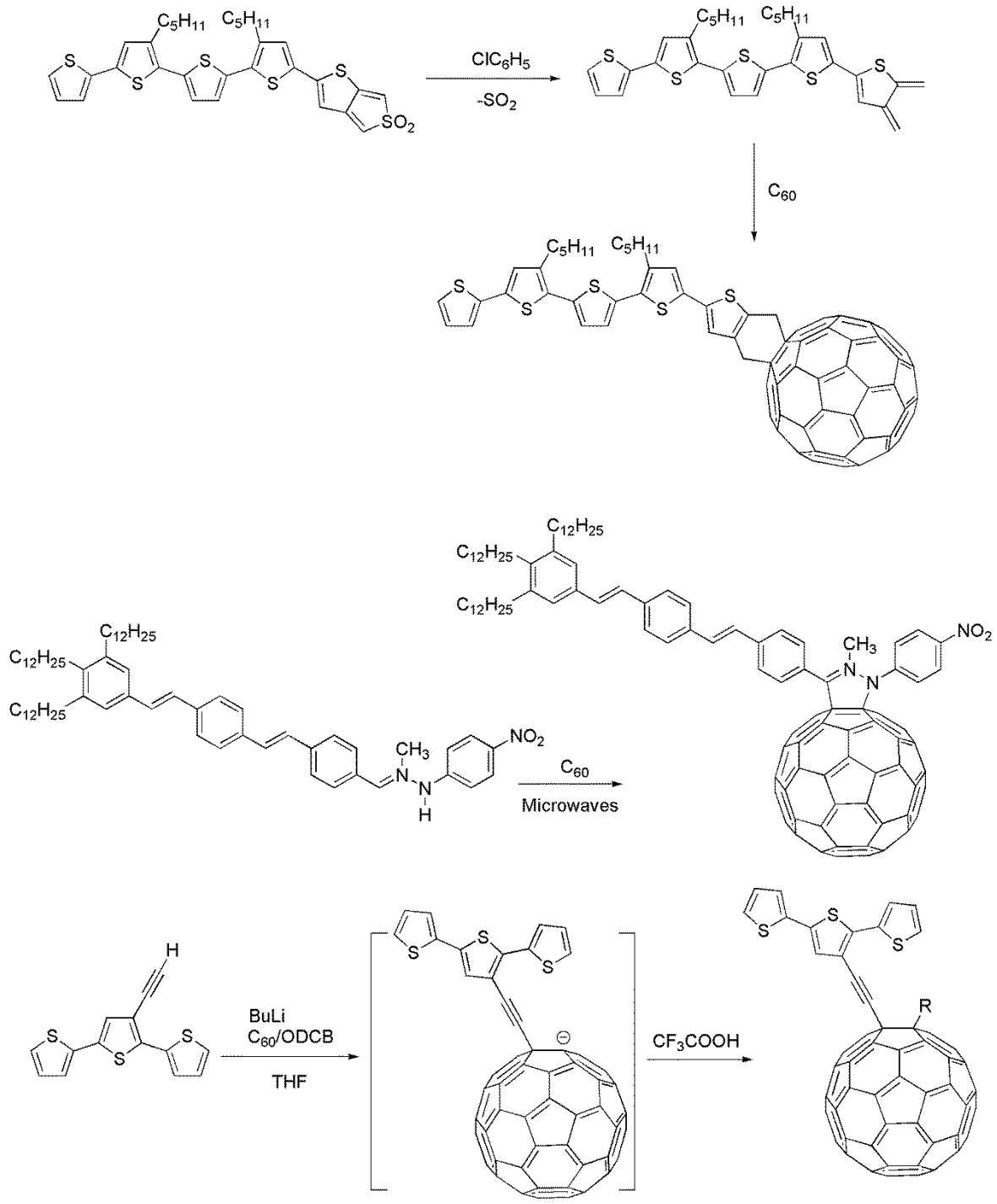

Figure 1.25. Synthetic approaches towards π-conjugated oligomers.

1.7.2.2. Non-fullerene based acceptors

An active layer consisting of a blend of conjugated polymers with high electron affinity molecules such as fullerene derivatives has proved to be an efficient way for improving the performance of BHJ devices. However, the high cost, the poor absorption in the visible and near IR regions, and the mismatching between the LUMO energy levels of fullerene derivatives and some of the commonly used donors, have encouraged researchers to develop new non-fullerene acceptors that have the similar properties of fullerene derivatives at the same time improve their shortcomings in photovoltaic performance.

Rylene diimides have been used as alternative acceptors for organic photovoltaic devices, due to their distinctive features. They exhibit strong accepting ability because of the conjugation mode between imide groups and rylene aromatic core. Also the chemical structure of these materials can be modified easily by attaching different substituent groups on either the imide nitrogen atoms or on the rylene aromatic core. As a result of these modifications, enhancement in the physical properties such as; alteration of HOMO and LUMO energy levels and improvement in the absorption coefficients can be achieved. In addition, their thermal and photochemical stability as well as high electron motilities have supported their use in a variety of organic electronic devices.[59]

Among rylene diimides assembly, perylene diimides (PDIs) are the most common acceptor materials used. The first fabrication of a heterjunction device was done by vacuum deposition techniques of *trans*- isomer of perylene diimides along with CuPc as donor material (**Figure 1.26**). Efficiency of 0.95% was achieved from the fabricated bilayer device. This result was followed by deposition of *cis*-isomer of PDIs with CuPc material. However, the resulting efficiency of *cis*-isomer material was found to be slightly less

efficient compared with *trans*-isomer material. The lower efficiency is attributed to less efficient π-π packing of the *cis*-material during fabrication of the device which leads to shorter exciton diffusion lengths.[60]

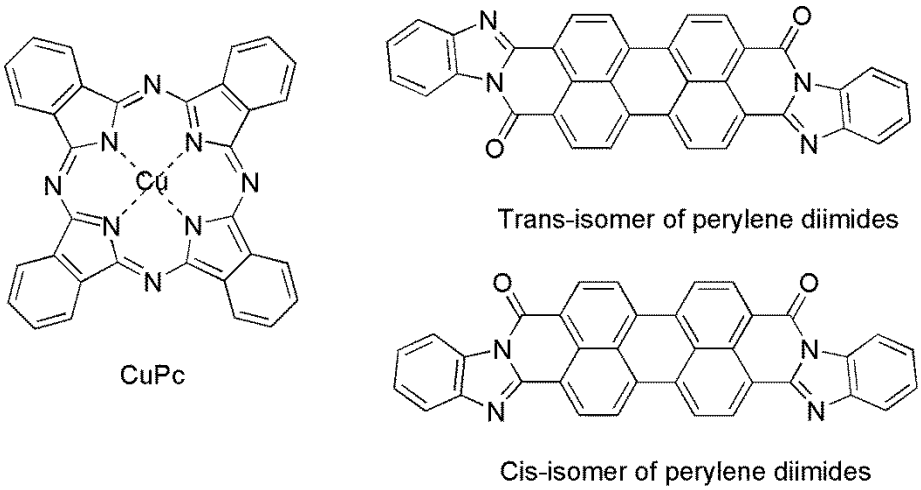

Figure 1.26. Molecular structures of phthalocyanines and perylene derivatives.

Attaching solubilising groups on the imide nitrogen atoms of PDI units facilitated their use with different donor units in BHJ devices. Applying a blend of P3HT and PDIs, which have different alkyl substituents on the imide nitrogen atoms compound **1.1**[61] and **1.2**[62], has resulted in poor device efficiency for both cases even under controlled fabrication conditions. The poor efficiency of these materials resulted from their affinity toward forming crystalline thin film which causes trapping of the transferred electrons and decreases in the resulting photocurrents. Significant improvement in the efficiency of the BHJ device was observed using a blend of a core-alkylated PDI derivative and P3HT. The alkyl groups on the core of PDI unit of compound **1.3** assists in improving the solid state packing of the material as well as increasing the solubility in higher boiling solvents which lead to a better interpenetrating network between the donor and acceptor units.[63]

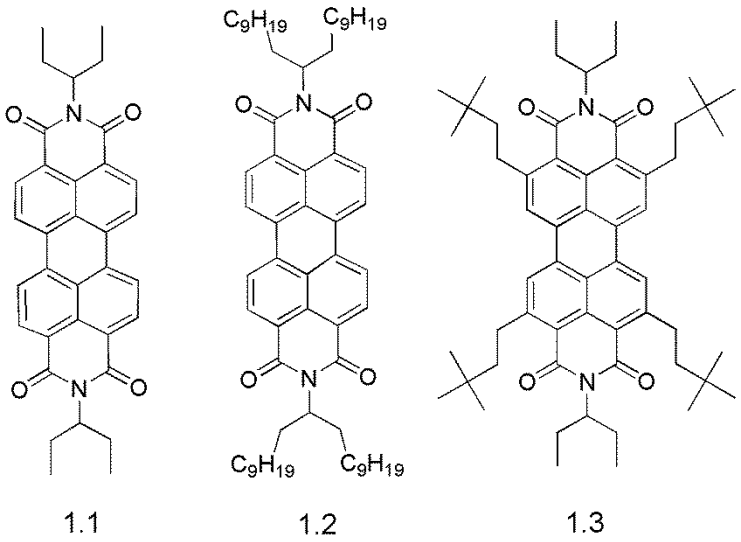

Figure 1.27. Molecular structures of substituted PDIs.

Significant progress was achieved by introducing bulky side chains on the PDI unit. Blends of the new bulky PDI material **1.5** with small donating unit **1.4**[64] exhibited an increase in the electron mobility and improvement in the performance of the device efficiency to 3.88 %. Until now, the best recorded performance of photovoltaic devices using rylene diimides as acceptor units has not exceeded the performance of fullerene derivatives. However, the improvement that has been done by reducing the planarity of the PDI acceptors through introducing bulky side-chains has assisted in increasing the multidimensional electron transport and enhancing the performance of the BHJ devices.[32]

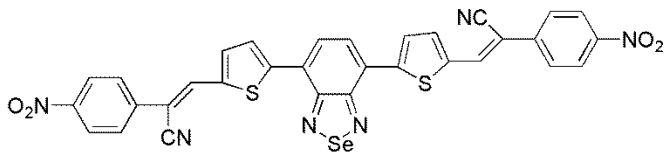

1.4

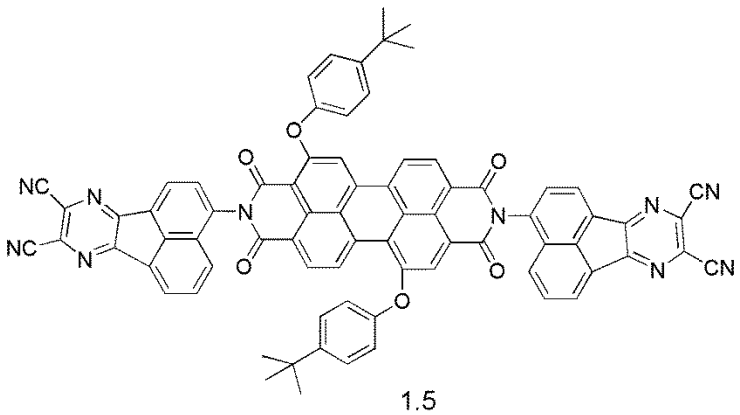

1.5

Other strategies to build *n*-type non-fullerene units are introducing withdrawing groups such as: fluorine, chlorine or cyano groups into the small molecular structures. An improvement in the efficiency and increasing in the V_{oc} was achieved for applying compound **1.6** as an acceptor unit along with compound **1.7** as donor unit in a BHJ device. This result was attributed to the interfacial gap between the HOMO and LUMO leading to efficient exciton dissociation of the charges.[65]

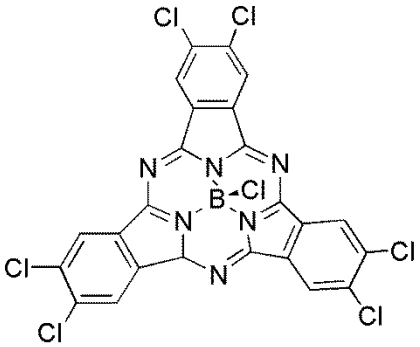

1.6

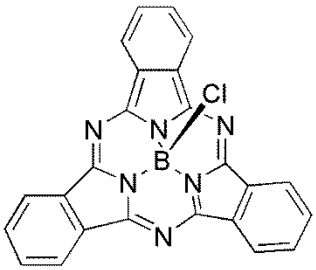

1.7

Cyano units are excellent electron accepting groups which may reduce the electron affinity and improve mobility. A number of substituted 2-vinyl-4,5-dicyanoimidazole units (vinazene units) have been studied as acceptor units in BHJ devices. The simplicity of modifying the chemical structures of vinazene units assist in improving the optical properties and energy levels. Therefore, vinazene-based molecules provide a platform for new non-fullerene acceptors to be investigated in BHJ devices with different donor units. A blend of compound **1.8** or **1.9** with P3HT as an active layer displayed a PCE of 0.45 % [66] and 1.1 % [67], respectively.

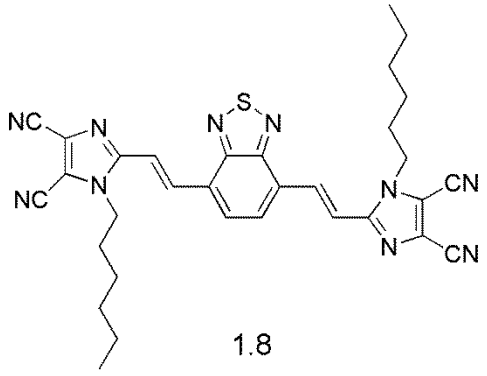

1.8

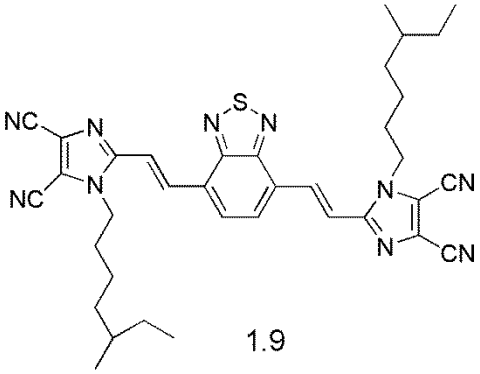

1.9

DCV substituted quinacridone derivatives have been introduced as acceptor units for BHJ devices, due to the strong absorption coefficients in the most effective area of the solar spectrum. For example, compound **1.10** exhibited a strong absorption coefficient in the visible and near-IR region (650-700 nm), and appropriate LUMO energy level (- 4.1 eV) and moderate electron mobility 10^{-4} $cm^2.V^{-1}.s^{-1}$ make it a good candidate acceptor for BHJ devices. Using a blends of compound **1.10** with **P3HT** for the active layer a PCE of 1.57 % and a FF of 57% was achieved indicating that efficient solar cells can be achieved by matching the absorption properties of the acceptor with solar spectrum properties.[67] Furthermore, small molecule compound **1.11** containing fluorene, BT and DCV units can

be annealed carefully at 56°C for 20 min with P3HT to produce a good quality thin film and improve the efficiency of the device from 0.04% to 0.73%. This improvement can be attributed to increasing the electron mobility of the acceptor unit and improvement in charge transport between the donor and acceptor units.[69]

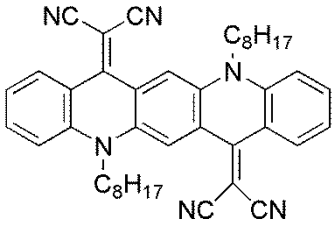

1.10

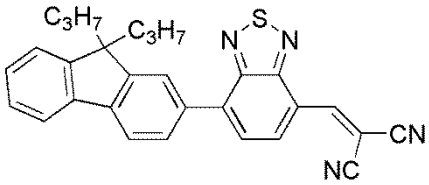

1.11

However, although small non-fullerene molecules can be modified to display good optical properties and electron mobility, the performance of these molecules has not yet exceeded the performance of fullerenes and their derivatives. The poor performance can be explained by poor morphology of the active layer which may decrease long-range mobility and charge transport ability of these systems.[32]

Chapter 2;

Synthesis and characterization of new star-shaped thiophene derivatives.

2.1. Introduction

The inherent features of semiconducting conjugated polymers resulting from the delocalization of π-electrons along the polymer chain as well as their intermolecular interactions have played important roles in choosing the materials for the active layer of electronic and optoelectronic devices. Although the deposition methods used for the manufacture of polymer-based devices are cheap, the stability and solubility of the materials constitute frequently encountered problems. Therefore, small molecules with their remarkable advantages can be considered as alternative systems to conjugated polymers in devices. These types of molecules have the ability to form a high level of ordering through their crystallinity which may result in increased charge carrier mobility and improvements the performance of organic devices. In addition these molecules have well defined structures which facilitates the precise determination of HOMO and LUMO energy levels.[25]

2.1.1. Linear π-conjugated oligothiophene derivatives

Interest of using thiophene as a conducting material started in 1980 after Kuhn and co-workers used α-quinquethiophene on top of an aluminum layer to measure the photo-current resulting from applying different voltages.[70] This discovery led in 1995 to the implementation of α-quinquethiophene **1.1** and α-octathiophene **1.3** as model materials to be used in organic solar cells. [71]

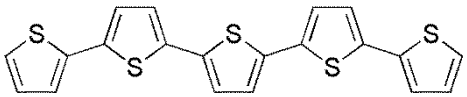

1.1

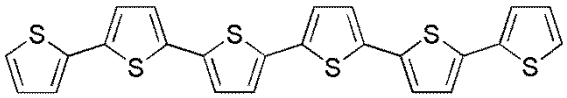

1.2

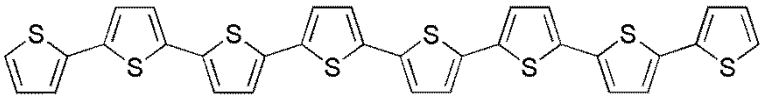

1.3

Since their early discovery, the growth in oligothiophene derivatives as conducting materials has been rapid due to their advantages. Oligothiophene derivatives are characterized by the unique combination of chemical stability and simplicity in modification of their optical and electronic properties. Also, the high polarizability of electron pairs of sulfur atoms can contribute to supporting the conjugation along the polymer chains. These features have classified functionalized oligothiophenes as the most promising conducting materials for organic electronic applications.[72]

Improvement in the conductivity of oligothiophene materials has been enhanced by attaching thiol, disulfides, or phosphines as anchoring groups, in order to form monolayer films onto surfaces (**Figure 2.1**). This property has led to highly organized structures by forming strong covalent bonds between the attached sulfur or phosphorous atoms and the Au surface, while the rest of the compound is organized in perpendicularly from the surface.[73]

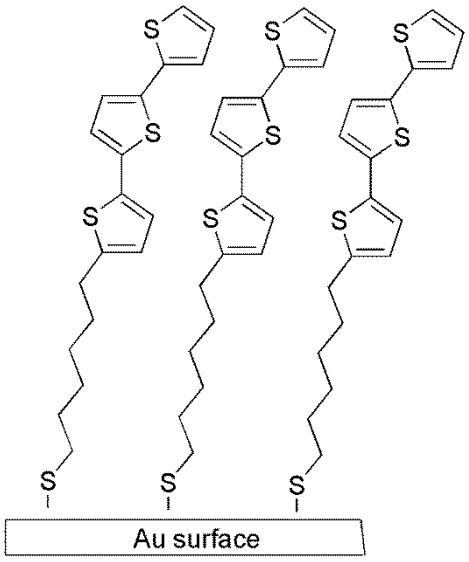

Figure 2.1. Self assembled monolayer of terthiophene with active group surface.

In addition to the careful selection of the chemical structure of organic device architectures, the overall performance of these devices also depends on the purity and the organization properties of these materials on the active layer surface. Combining these factors will effectively support the charge carrier mobility and decrease the trapping or quenching of the charges. Also, the morphology of the active material controls the optical and electrical properties of the materials in the solid state.[73] A well-ordered two-dimensional monolayer was achieved for oligothiophene derivatives using vacuum evaporation techniques which guarantee defect-free films with high charge carrier mobility. However, the vacuum evaporation technique is quite an expensive processing technique.[74] Therefore, the challenge is processing these materials by using a less expensive technique. In this context, the remarkable superamolecular organization of oligothiophene derivatives, including their ability of forming a good quality thin film through π-electron overlap and stacking ability have supported their application in optoelectronic devices. For unsubstituted linear sexithiophenes the mobility up to 0.03 $cm^2/(V.s)$ was found for crystalline films. These unsubstituted linear oligothiophenes with their planar structures formed polycrystalline films in which the molecules are orientated vertically to the substrate.

The performance of BHJ device based on a blend of unsubstituted linear sexithiophenes **1.2** and $PC_{70}BM$ was improved by 2.38 % by increasing the percentage of fullerene derivative in the blend mixture. Increasing the percentage of fullerene was undertaken to reduce the crystallinaty of the sexithiophene and increase the homogeneity of the charge transfer interpenetrating network of the blend.[75] Also, increasing the number of unsubstituted thiophene units show improvement in the active material by reducing the band gap and increasing in the charge carrier mobility of the thin film. Enhancing the mobility of oligothiophene derivatives was achieved by functionalizing oligothiophenes in the α-position as it retrains the planarity of the structure and supports the properties of liquid crystalline films. These properties influence the ordering of the molecules in the solid state which leads to increased charge carrier mobility between the molecules. Although substitution of oligothiophene at the β-position significantly increases the solubility of the molecules, this causes a decrease in the mobility due to the distortion of planarity and molecular stacking.[76]

The formation of homogeneous thin films with high charge carrier mobilities of 10^{-3} cm^2/(V.s) has been identified for liquid crystalline (LC) assemblies. The self assembly of the oligomers in the liquid crystalline phase is supported by combining the mobility of the liquid and the order of the crystal. The improvement of LC orientation can be obtained by tuning the nature, the size and the position of side chain on the oligthiophene. Thus, a highly order smectic phase with high mobility up to 0.1 cm^2/(V.s) was achieved for asymmetrical substituted tetra- and quarter thiophene derivatives **1.4** and **1.5**.[77]

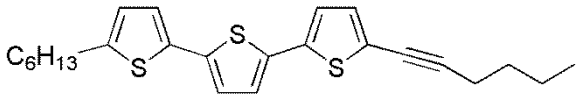

1.4

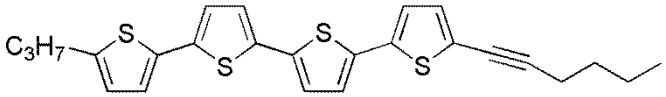

1.5

The supramolecular ordering of oligothiophene semiconductor components through noncovalent bonds such as hydrogen bonding and π-π interactions is considered to be another approach for organizing the material and increasing the charge carrier mobility for reaching optimized device performance. Therefore, in order to support the formation of non-covalent assembly, amphiphilic character can be introduced to the scaffold to get a reliable self assembling system. Mei and co-workers synthesized amphiphilic diketopyrrolo-pyrrole based oligthiophene **1.6** to achieve desirable solution processability and long range order via self-assembly. In this study, atomic force microscopy (AFM) was used to track the aggregation of the molecule on the surface by using different solvents. The results showed that both solvophobic affects and π-π interactions assist in forming strong and highly ordered self-assembled systems. However, the device fabrication of compound **1.6** as donor and $PC_{60}BM$ as an acceptor showed low PCE of 0.45 % and 0.65 % before and after annealing the active layer, respectively.[78]

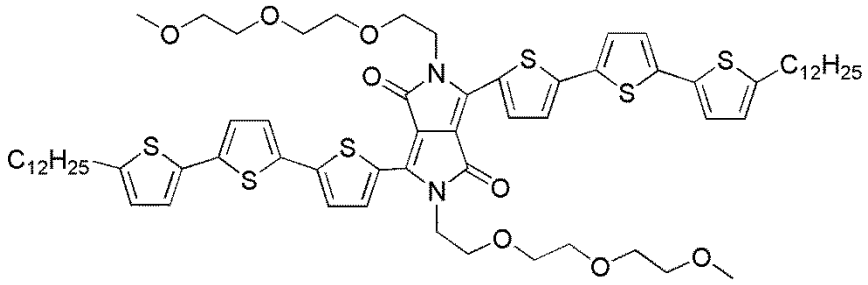

1.6

The best PCE of 2.33 % has been reported for diketopyrrolopyrrole based oligothiophene molecule **1.7**. This significant progress in the performance resulted from the formation of a good quality thin film, high charge mobility and extending the absoption to 800 nm.[33]

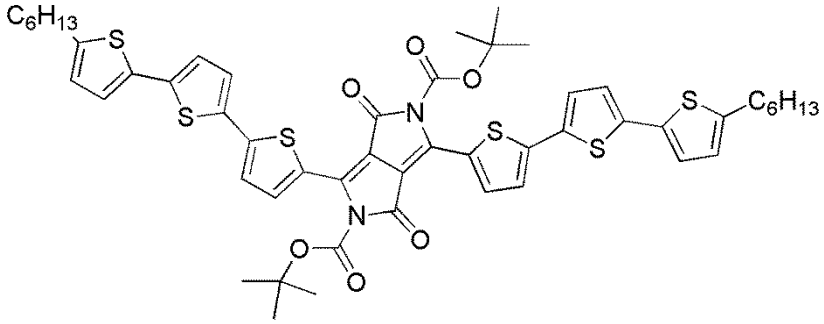

1.7

Yasuda and co-workers prepared new π-conjugated oligthiophenes (5T) **1.8** and (6T) **1.9** with alkoxy-substituted benzene groups attached to both sides of the system by carbonyl groups. The presence of alkoxy groups together with π-π interactions between oligo-thiophene units facilitates self-organization of the molecules into one dimensional columnar structure. However, the formation of columnar phases from these molecules required the number of thiophene units to be greater than four units. This columnar phase organization also encourages applications of these molecules in optoelectronic devices due to the red shifting of the UV absorption in resulting films.[79]

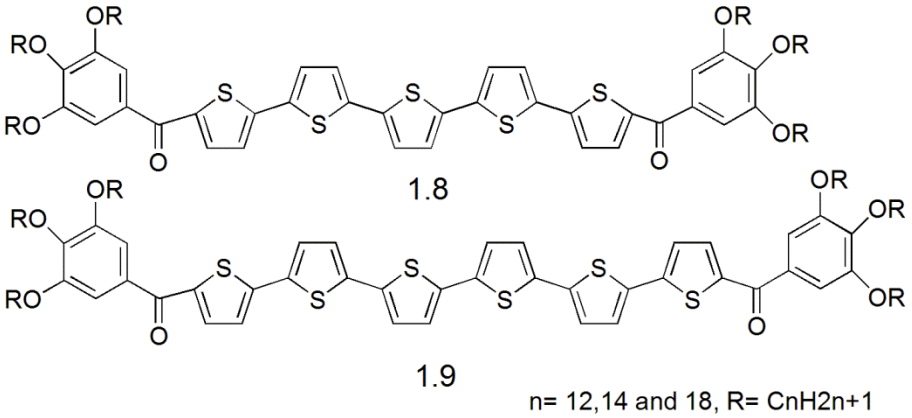

Other rod like quaterthiophenes combining both hydrophilic end groups and lipophilic alkyl chains have been prepared to investigate the effect of the nature and size of these building blocks have on the self-assembly of π-conjugated nanostructures. Changing the size of peripheral groups from hydrogen, methyl to longer alkyl chains has a great effect on inhibiting the formation of liquid crystal phases which could result from disturbing hydrogen bonding between the polar groups. The X-ray powder diffraction pattern for compound **1.10** indicates the formation of a honeycomb-like network with a square cross section of the combined cells as shown in **Figure 2.2**.[80]

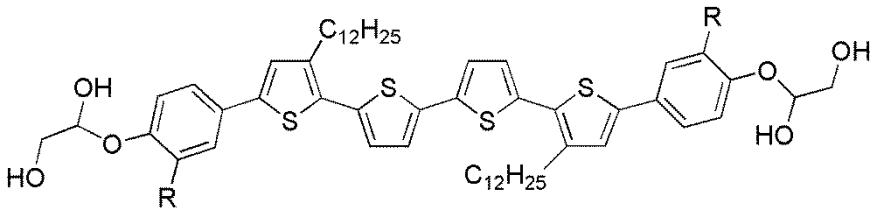

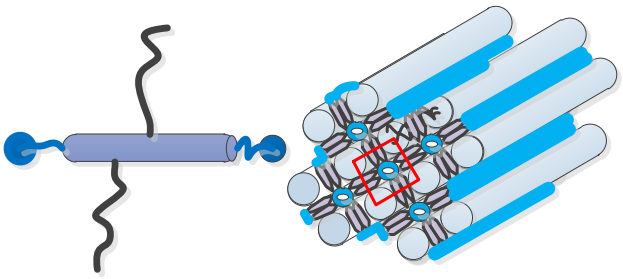

Figure 2.2. Organization of compound **1.10**. Light blue represents cylinders of the alkyl chains, blue represents the hydrogen bonding network and grey represents the aromatic core.

2.1.2. Star-shaped oligothiophene derivatives

Although one-dimensional oligomers with highly π-delocalized systems could facilitate the movement of charge carriers and show improvement in the performance, the PCE of these materials is not high enough for commercial applications. The drawbacks in the performance can be explained in term of; (i) inability to quantity identifies the relation between the molecular modification and the electronic properties of the polymer due to the variation in the molecular weight and conjugation length, (ii) the disorder of packing in these materials which could create inequality in the migration of the charges, and (iii) the tendency of these materials to aggregate in the solid state.[34,81] Therefore, increasing the dimensionality of the oligomers could assist in controlling the materials organization and enhance the charge carriers in multidirectional modes along the active layers.[82]

Conjugated dendrimer systems that consist of several regular branches emerging from the central structure (core), can be used in variety of applications ranging from biological sensors, medicine and nano-technological applications.[83] For example, the nano-star

molecule **1.13** with its fully π-delocalized systems resulting from significant orbital overlap improved the optical properties and increased the emission intensity of this compound up to 400 times compared with 1-ethnylphenylene units. [84]

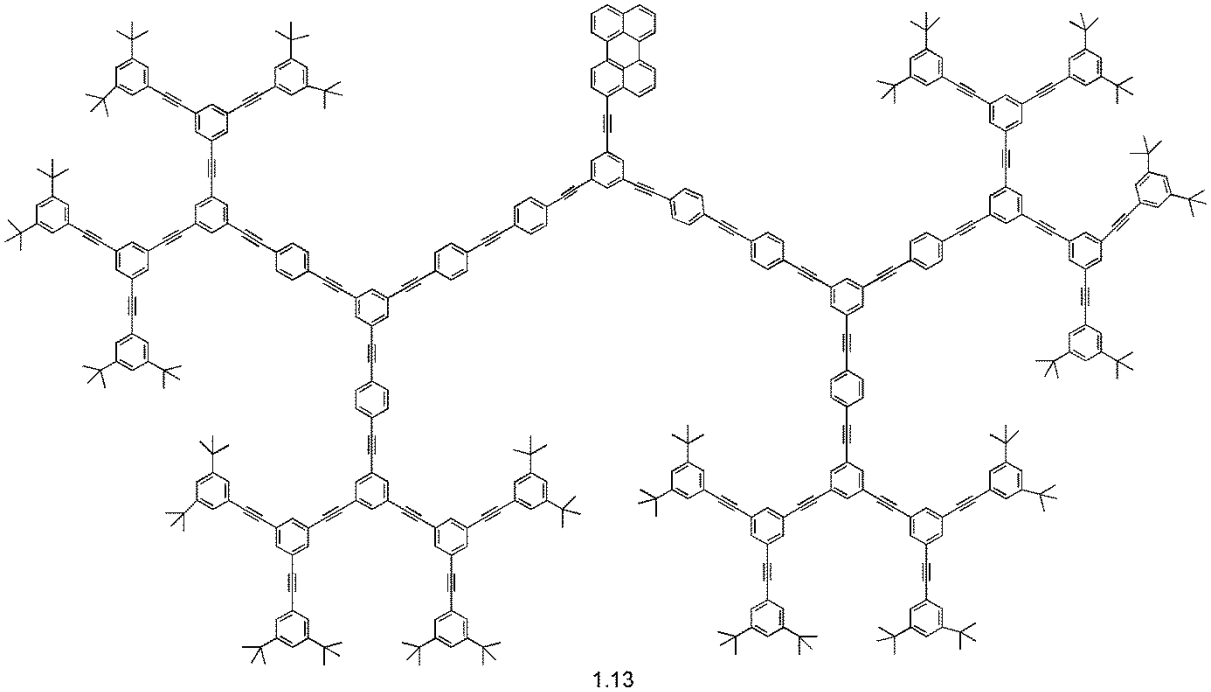

1.13

Divergent and convergent approaches are two basic synthetic strategies for synthesizing dendrimers. In the divergent approach shown in **Figure 2.3.**, the dendrimers can be built from coupling a single monomer on to the central structure unit and repeating the coupling procedure by adding a new layer of monomers to the main core. This approach has the advantage of using a single monomer building block at every coupling stage. However, it can be difficult to separate the target star shaped oligomers from un-reacted products.[85]

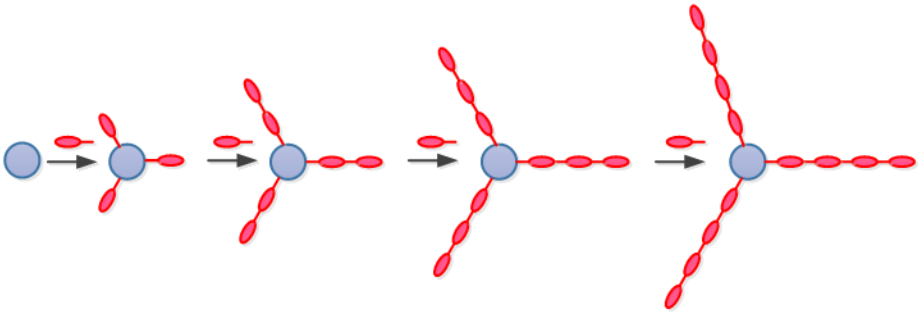

Figure 2.3. Divergent approach for synthesizing star-shaped oligomers.

In contrast, the convergent approach, shown in **Figure 2.4.**, produces more homogenous star shaped oligomers. They can be obtained by either coupling linear functionalized oligomers on to the central structure unit or creating the central structure unit at the final step by a trimerization reaction.[86]

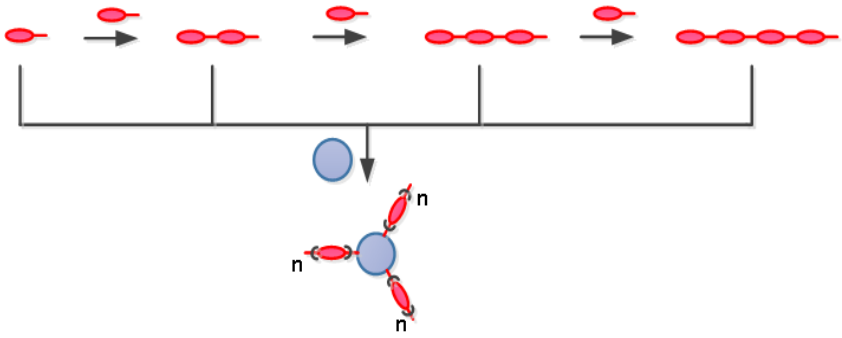

Figure 2.4. Convergent approach for synthesizing star-shaped oligomers.

When compared to linear functional oligomers, π-conjugated multi-branched molecules have raised the possibility of creating promising materials with a number of advantages. These advantages include; multi-functionality in a single molecule, possibility of increasing the product yield by using a convergent route; and enhancing the solubility by increasing the number of branches in the molecule. In addition, these molecules can improve the properties of the device by controlling the morphology through selecting the

nature and the length of the branches. In term of organization of material and film forming properties, these types of materials show a decrease in charge carrier mobility compared with linear molecules. However, modifying the ordering of the side chains and controlling inter chain interactions could assist in improving the properties of the film.[87] For example, the star shaped functionalized truxene unit **1.14** had a charge mobility of 10^{-3} $cm^2/(V.s)$. However, increasing the number of thiophene units on truxene core to form compounds **1.15** and **1.16** affected negatively on the mobility due to forming amorphous films instead of polycrystalline films.[88, 89]

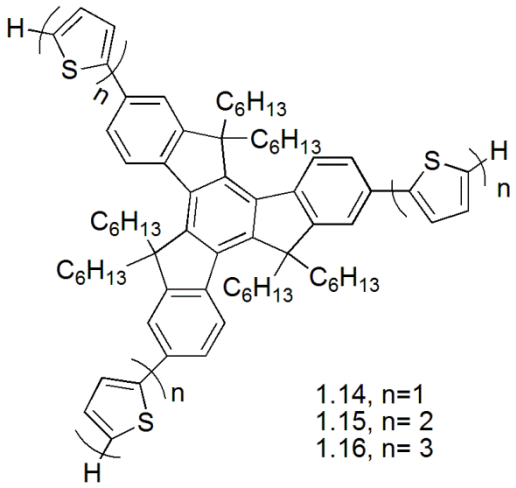

Research on the isotruxene core has been carried on by synthesizing a new class of star shaped molecules containing up to four-hexylthiophene units surrounding a isotruxene central core **1.17**. The photophysical and electrochemical properties of these molecules showed effective conjugation between the arms and the central core. Increasing the thiophene units poses a negative effect on the electronic properties by decreasing the fluorescence quantum yields. The morphology of both the electrodeposited film and the thin film resulting from spin coating technique showed that increasing the number of thiophene rings increases the dimensional structure of the polymer.[90]

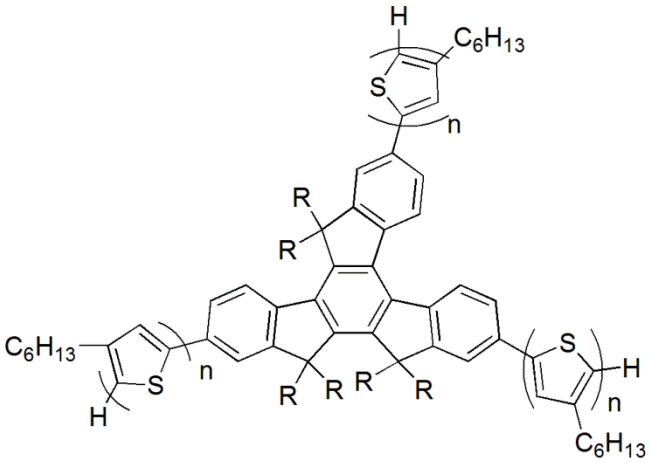

1.17, R=C_2H_5 or C_6H_{13}
n=1, 2, 3 and 4

The study of benzene core dendrimers has attracted much attention due to their ability of forming liquid crystalline and other self assembled supramolecular architectures. Combining the properties of both the benzene core and oligothiophenes derivatives could assist in improving the overall physical and optoelectronic properties of the resulting molecules through increasing the number of hole transporting units and at the same time improving the morphology. Taking into account the limited conjugation resulting from the steric interactions associated with the attaching thiophene unit directly on benzene central core, different numbers of substituted oligothiophene arms surrounding a benzene core and linked through acetylene linkage (**1.18, 1.19** and **1.20**) have been studied. The study shows that the correlation between acetylene linkage and benzene core enhance the π-conjugation through the benzene core by increasing planarity. Changing the benzene core to thiophene **1.21** has also showed an increase in the delocalization of the π-system through the core.[91] The theoretical calculation of these materials in combined with the FT-Raman spectroscopy and electrochemical data revealed that the acetylene linkages have supported the conjugation through the central core by increasing the coplanarity between each arms and the central core, while α-phenyl terthienyl units, which are responsible for hole transportation and absorbing the light, hardly contribute to the conjugation.[92]

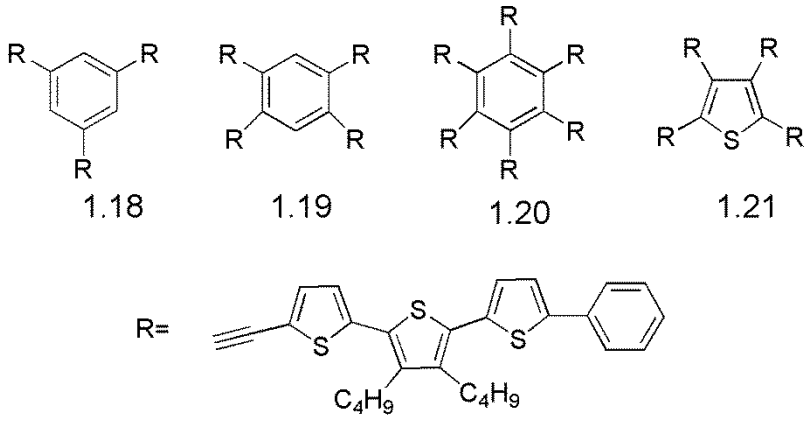

Furthermore, an increase in the solubility and modulation of properties were observed for compounds **1.22**, **1.23** and **1.24** by introducing extra butyl groups to the terthiophene arms. The study shows that compound **1.22** with six arms has amphiphilic properties in organic solvents, due to formation of nanostructured systems from interactions between sulfur and hydrogen atoms which causes twisting of the overall structure between the arms and the central core.[93]

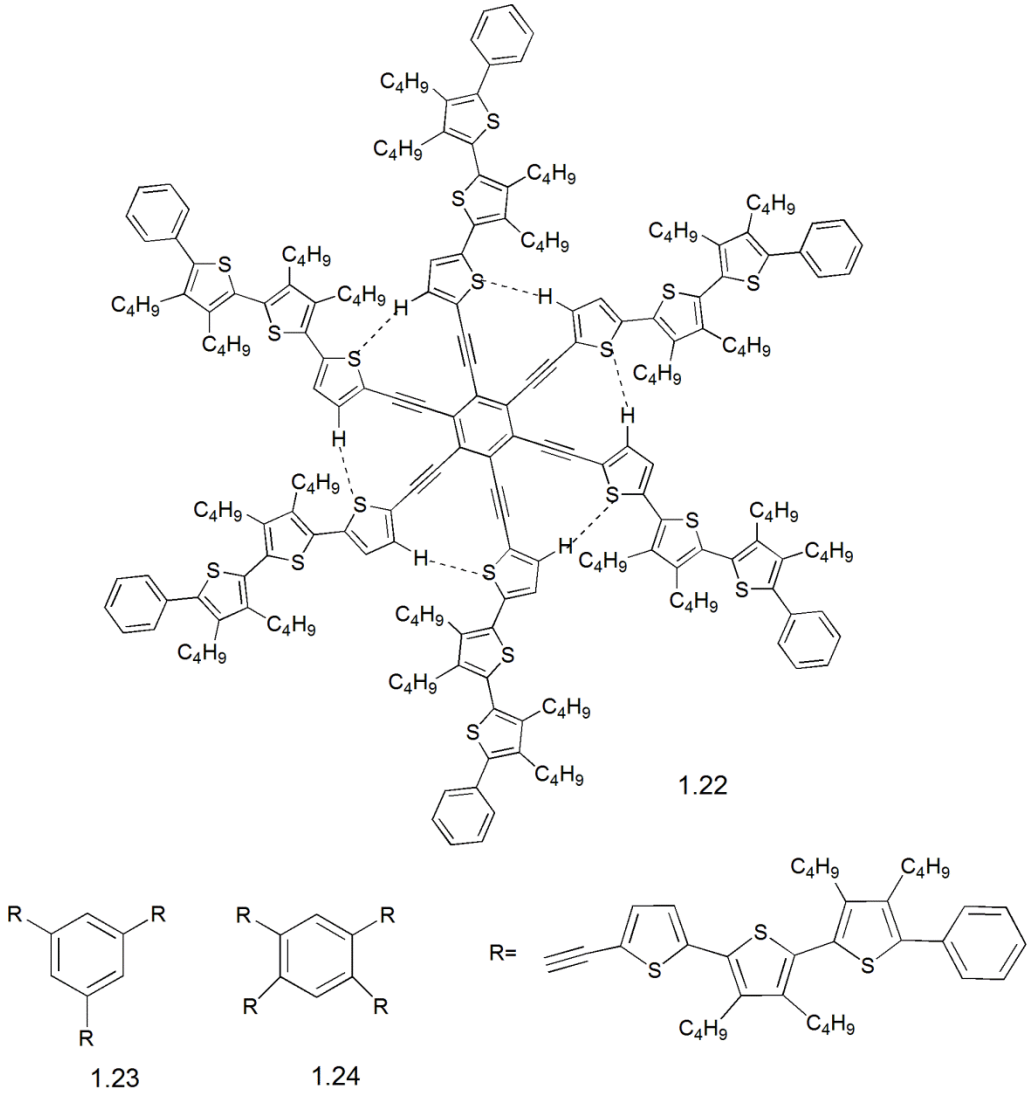

With the aim of building planar conjugated molecules, new molecules have been synthesized by attaching 5-hexyl 5-propenyl and 5-propenyl oligthiophene units, respectively, to a benzene core. Crystallinity studies showed that terminal hexyl chains played an important role in controlling the arrangement of dendritic molecules by providing a high degree of ordering in the vertical direction by intermolecular π–π stacking as shown in **Figure 2.5**. However, the molecules without hexyl groups are randomly ordered in the longitudinal direction which gives several different inter-lamella spacings.[94]

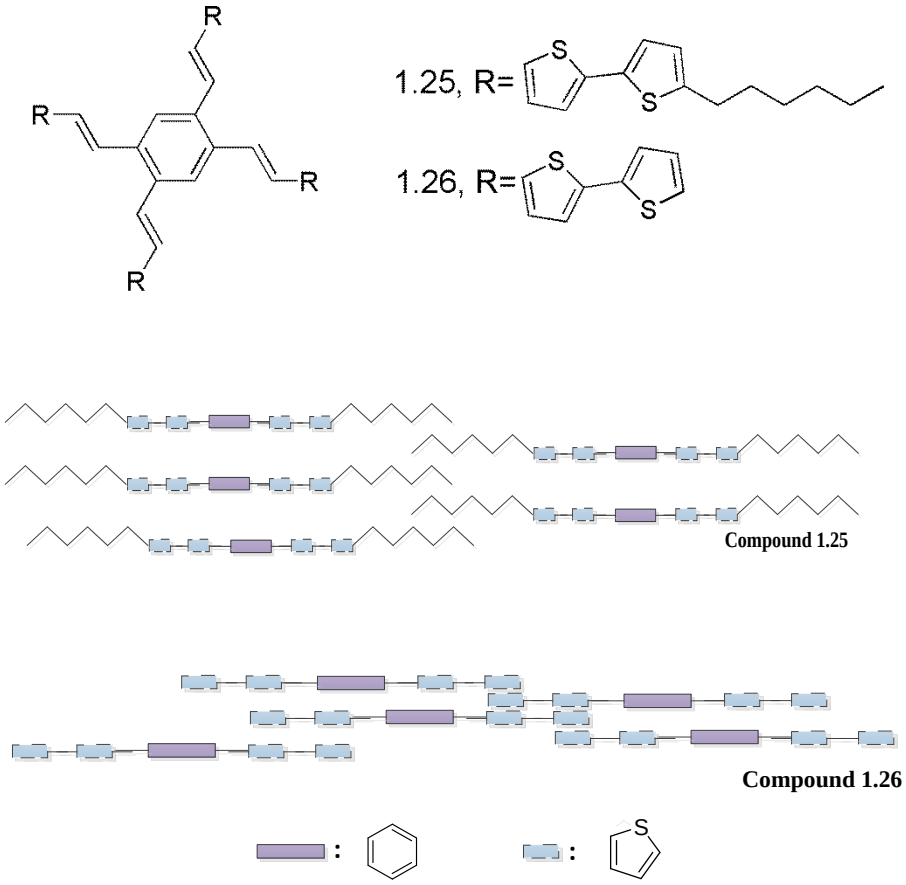

Figure 2.5. Schematic diagram of molecular arrangement for compounds **1.25** and **1.26**.

In order to increase the planarity and conjugation between the oligthiohene arms and the central core in star-shaped molecules, a new star-shaped oligthiophene derivative was synthesized by attaching short hexyl oligthiophene units onto a benzene core through three fused thiophene linkages **1.27**. Decreasing the dihedral angle between the central core and the first thiophene ring was observed from theoretical calculations which was in agreement of X-ray data, resulting in an increase in the planarity and π-delocalization of the system.[95]

Additionally, a study was carried out on the same core upon attaching thiophene **1.28** or 3,4-ethylenedioxythiophene (EDOT) **1.29** as end groups from the three arms. The electro-polymerization results showed that both compounds-(especially EDOT functionalized dendrimer) can be used as monomers to prepare high dimensional conjugated polymers. The spectral and electrochemical results indicate a stable transition between neutral and polaron states on the EDOT arms.[82]

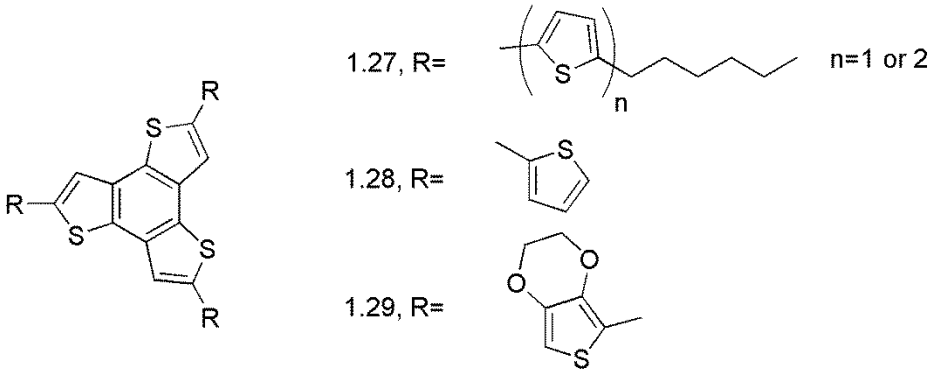

Controlling the thermal state of the dendimer during π-π molecular stacking enhances molecular ordering in columnar phases. In this type of ordering, the molecules adopt a face-on arrangement to the substrate surface and grow vertically to build the columnar phases.[96] The formation of homo-tropic alignment of the columnar phase improves charge carrier mobility through the formation of a highly stacked and an unidirectional charge transport system. The self organization of aromatic cores through the packing process of the molecules is shown in **Figure 2.6**.[97]

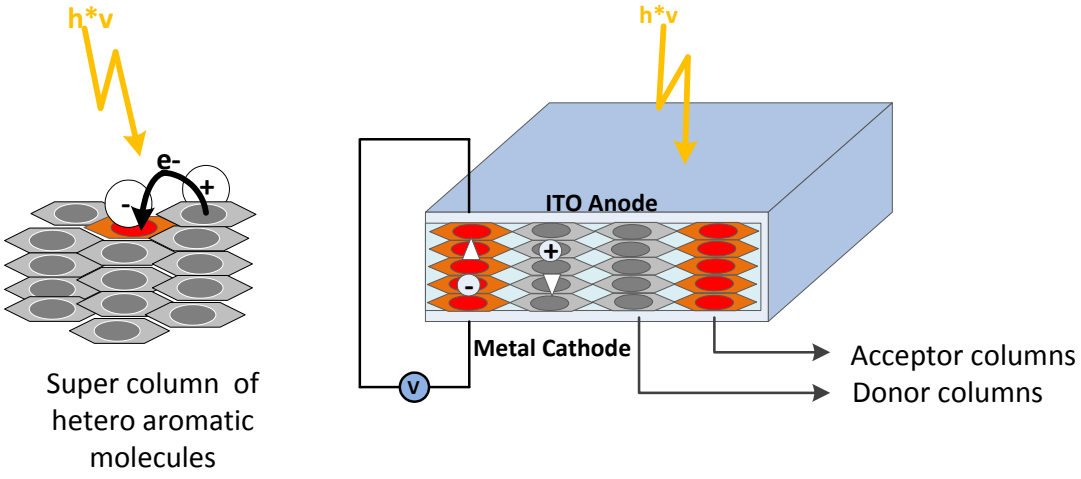

Figure 2.6. Structure of photovoltaic device.[31]

The formation of discotic columnar mesophases during melting of hexasubstituted star-shaped materials increased the charge transport channels of these conjugated molecules in one direction. For example, the formation of more stable and highly ordered crystalline phases for compound **1.32** resulted from π-π interactions in addition to dipole-dipole interaction between sulfur atoms of thiophene units. In contrast, changing the phenyl inner core to thienyl in compounds **1.33**-1.**35** influenced negatively on the order of the packing material due to a resulting low transition temperature.[86]

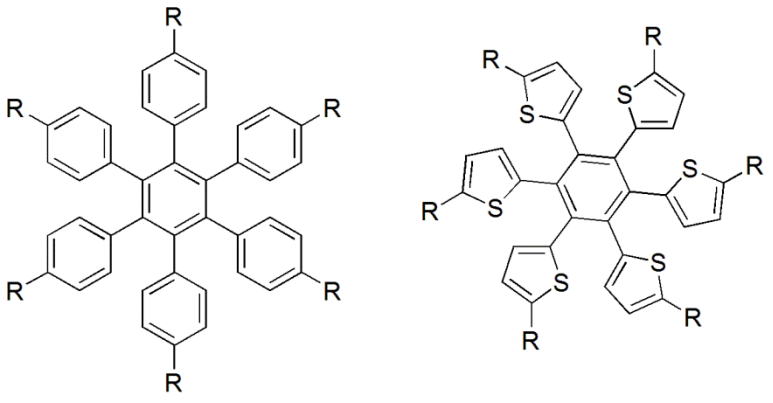

1.30, R= $C_{12}H_{25}$

1.31, R= 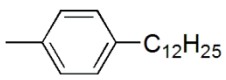

1.32, R= 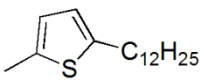

1.33, R= $C_{12}H_{25}$

1.34, R= 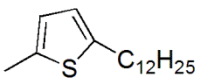

1.35, R= 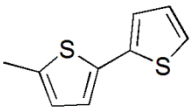

Ponomarenko and co-workers synthesized three new star-shaped oligothiophenes consisting of terthienyl arms surrounding benzene central core. The UV-vis and fluorescence spectra of these compounds indicated a twist between the arms and the central core which prevented π-electron overlap. However, compound **1.37** shows high mobility in the field effect transistor (FET). This result arose from the ability of compound **1.37** to form two dimensional lamellar ordering in a thin film. The two dimensional lamellar ordering resulted from stacking of oligthiophene arms parallel to the surface as shown in **Figure 2.7.** However, compound **1.38** tended to form columnar mesophase morphology during the cooling process which could be the reason for the low mobility value observed for this compound compared with compound **1.37**.[98]

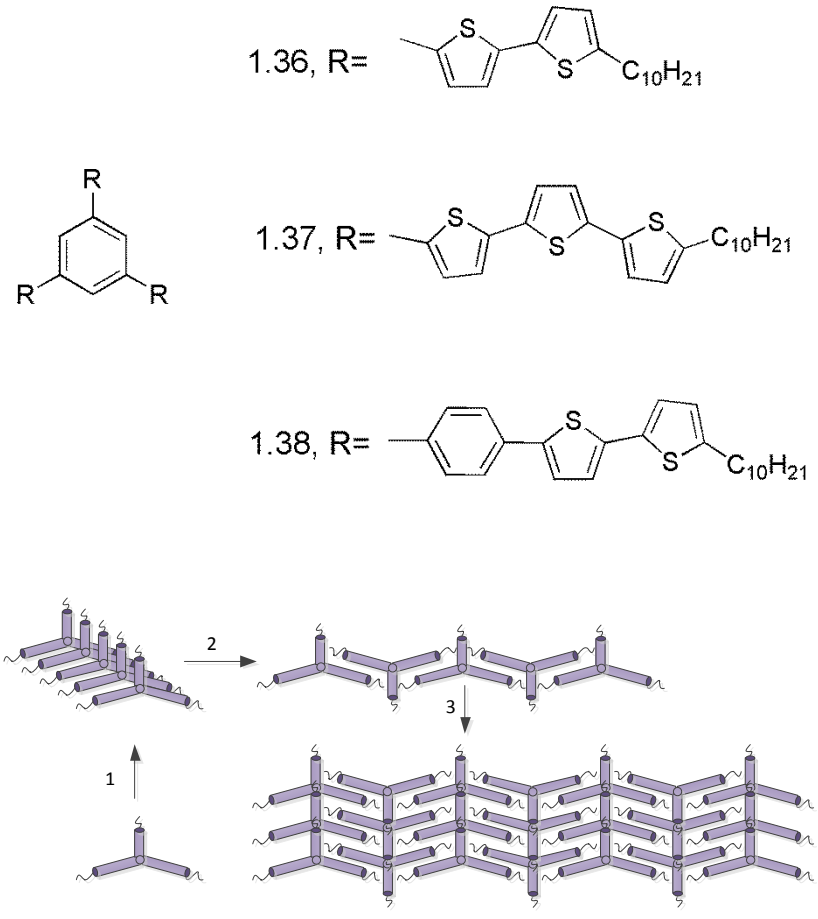

Figure 2.7. Structure of possible molecular packing of star-shaped oligthiophenes.

The morphology of the prepared star shaped compounds has been studied using differential scanning calorimetry (DSC) measurements. The prepared star shaped molecules contain of thioether linkage between the six arms of different numbers of oligothiophene units. The results showed that both compounds **1.39** and **1.40** produce isotropic liquid phases whereas compound **1.41** produced crystalline phases.[99]

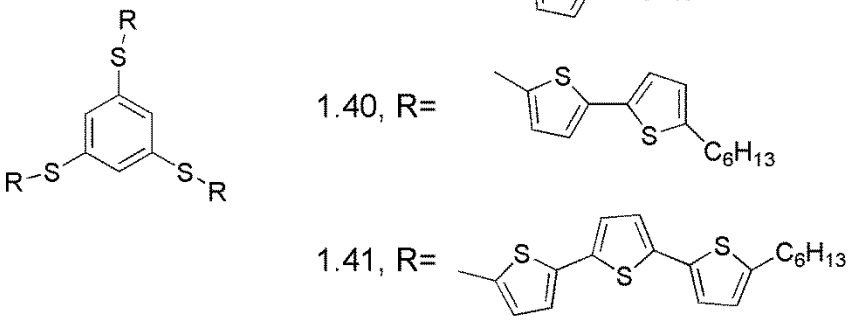

A good PCE of 2.6 % was obtained for photovoltaic cells fabricated by using disk shaped oligothiophene molecules **1.42** and **1.43**. The highly organized donor molecules gave rise to intermolecular π-π interactions (**Figure 2.8**). The blend of these disk-shaped oligothiophene molecules exhibited bicontinuous network with fullerene derivatives. This network performs as channels for collecting the charges within the active layer. The LUMO energy levels of these molecules were ideal for facilitating the electron transfer process to the LUMO energy level of fullerene derivatives.[100]

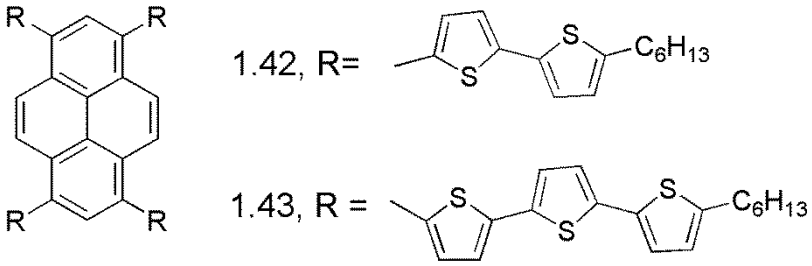

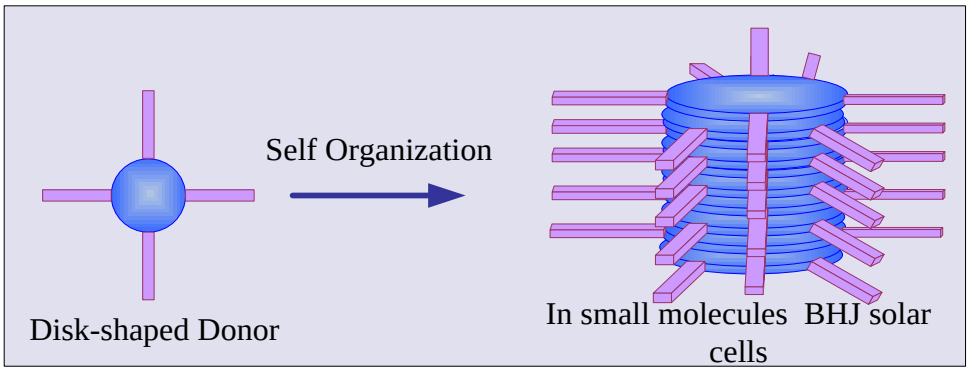

Figure 2.8. Self organization of compounds **1.42** and **1.43**.

Further improvement in the efficiency of small molecule BHJ devices has been achieved by combining the properties of the star-shaped triphenylamine units with oligothiophene derivatives. A blend of compound **1.44** with $PC_{71}BM$ provided good quality nanoscale films. Solution processable molecule **1.44** showed power conversion of 4.3 % without any thermal or solvent treatments.[101]

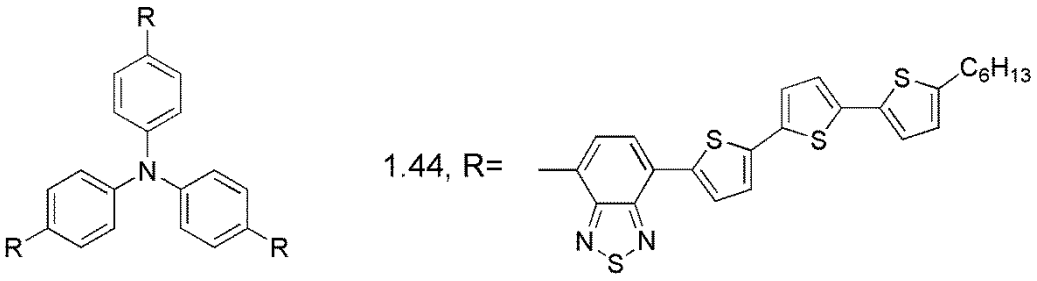

2.2. Aims and objectives

One of the major problems facing the fabrication of organic devices is their solution processability. The uncontrolled behavior of these materials, which results from poor solubility and stability, has opened the field for star-shaped organic molecules to be an alternative choice for device fabrication. The well-defined molecular structures and remarkable solution processability have made them ideal materials for organic solar cells. Combining the properties of both benzene core and oligothiophenes derivatives in a target molecule could assist in improving the optoelectronic properties through increasing the number of hole transporting units and at the same time improving amorphous morphologies of devices.

Therefore, the first aim of the work described in this chapter was to synthesize functionalized star-shaped molecules. These molecules contain thiophene units surrounded and attached to a benzene unit through acetylene linkages as shown in **Figure 2.9.** The second aim was to investigate the diversity of the electronic and optical properties of the resulting target star-shaped molecules.

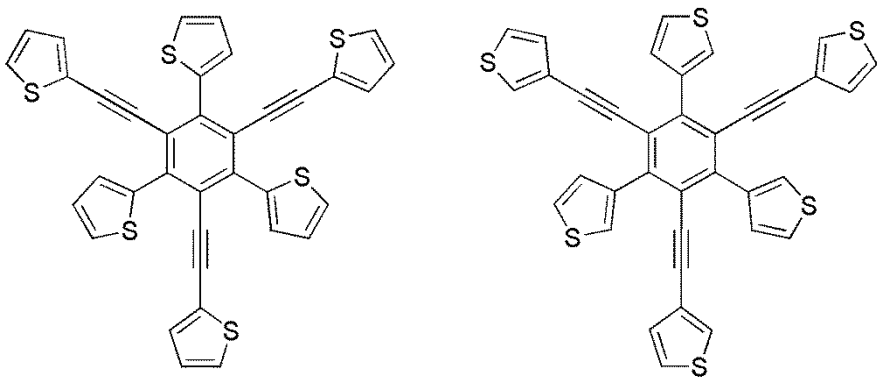

Figure 2.9. Hexasubstituted star thiophene architectures.

2.3. Results and discussion

2.3.1. Synthesis of compounds 3 and 6

The synthetic approach of the star-shaped thiophene compounds **3** and **6** is outlined in **Scheme 2.1**. The synthesis started from homocoupling reaction of 2-ethnyl thiophene and 3-ethnyl thiophene compounds, respectively, to give symmetrical diacetylene substituted thiophene compounds **2** and **5**, respectively.

The homocoupling reaction was carried out in the presence of $CuCl_2$ as a catalyst and triethyamine as a base in dry toluene. Due to the poor thermal stability of these compounds, the best yields of 41% and 25% for compounds **2** and **5**, respectively, were obtained by heating the reaction mixture at 60°C. To synthesize star-shaped hexa-substituted thiophene **3** and **6,** the prepared diacetylene compounds **2** and **5** underwent cyclotrimerization reactions under inert condition and in the presence of cobalt octacarbonyl as a catalyst. The star-shaped thiophene compounds **3** and **6** were obtained in 10% yield by refluxing compounds **2** and **5,** respectively, in 1,4-dioxane. The reaction mixture contained also three other products, however, purification was difficult due to the similar polarity of these products.

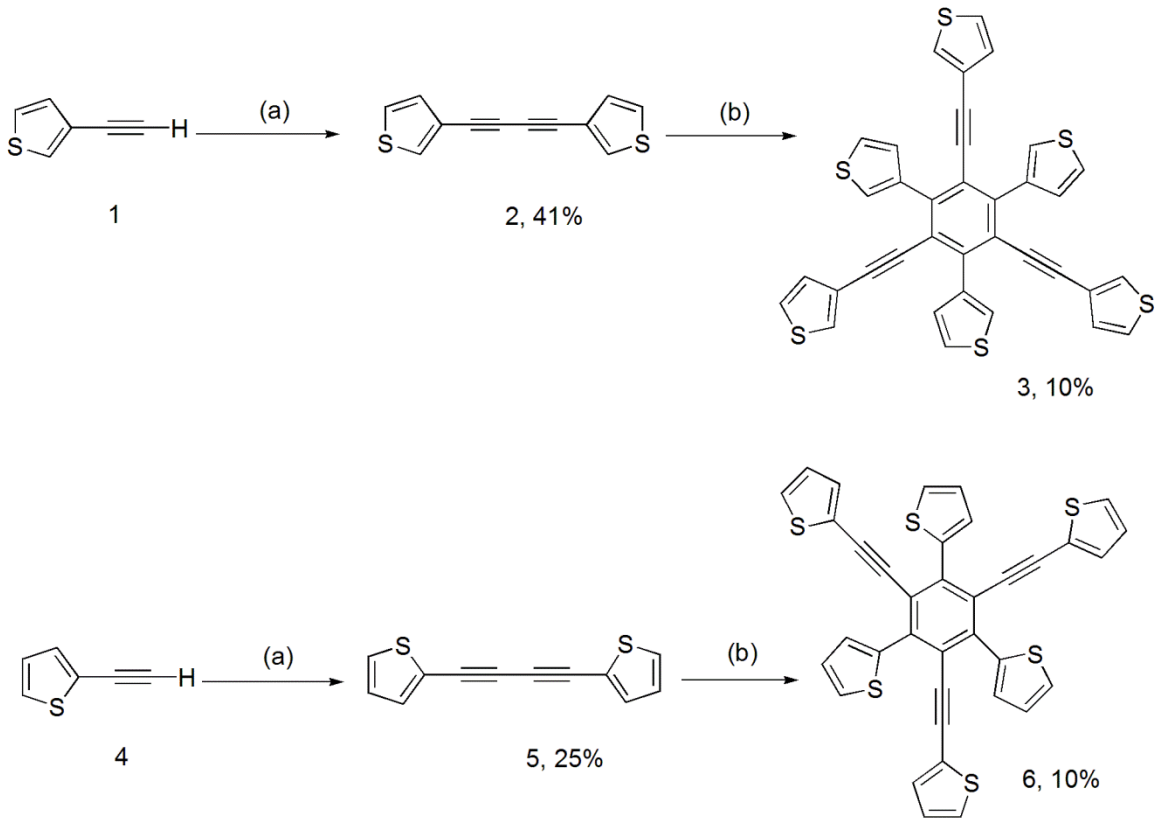

Scheme 2.1. Reagents and conditions: (a); copper (II) chloride, triethylamine, dry toluene, Δ 60°C, 6 hours, (b); cobalt octacarbonyl, 1,4-dioxane, Δ110°C, overnight.

2.3.2. ^{1}H NMR spectroscopic studies

^{1}H NMR spectra for both star shaped thiophene derivatives **3** and **6** were recorded in deuterated chloroform ($CDCl_3$). The positions of the key protons are shown in **Figure 2.10**. Attaching thiophene units to the central benzene core through acetylene linkages at the 2-position, resulted in shifting of protons a' and b' to a lower frequency (7.56 and 7.43 ppm, respectively) compared to the protons at the 3-position (7.65 and 7.47 ppm). The shift indicates an increased conjugation length between the lone pair on the sulfur atoms with π-electrons on benzene unit through the acetylene linkage. The nearest proton (a) to the

sulfur atom of the thiophene unit, which is attached directly to the benzene core for compound **3**, became shielded and shifted significantly to lower frequency (7.10 ppm) compared with the same proton in compound **6** (7.22 ppm). The two doublets at 7.18 ppm and 6.76 ppm (b and c) on the same ring for compound **3** become more separated from each other compared with the protons of compound **6** which became closer to each other and give one multiplet at 6.92 ppm.

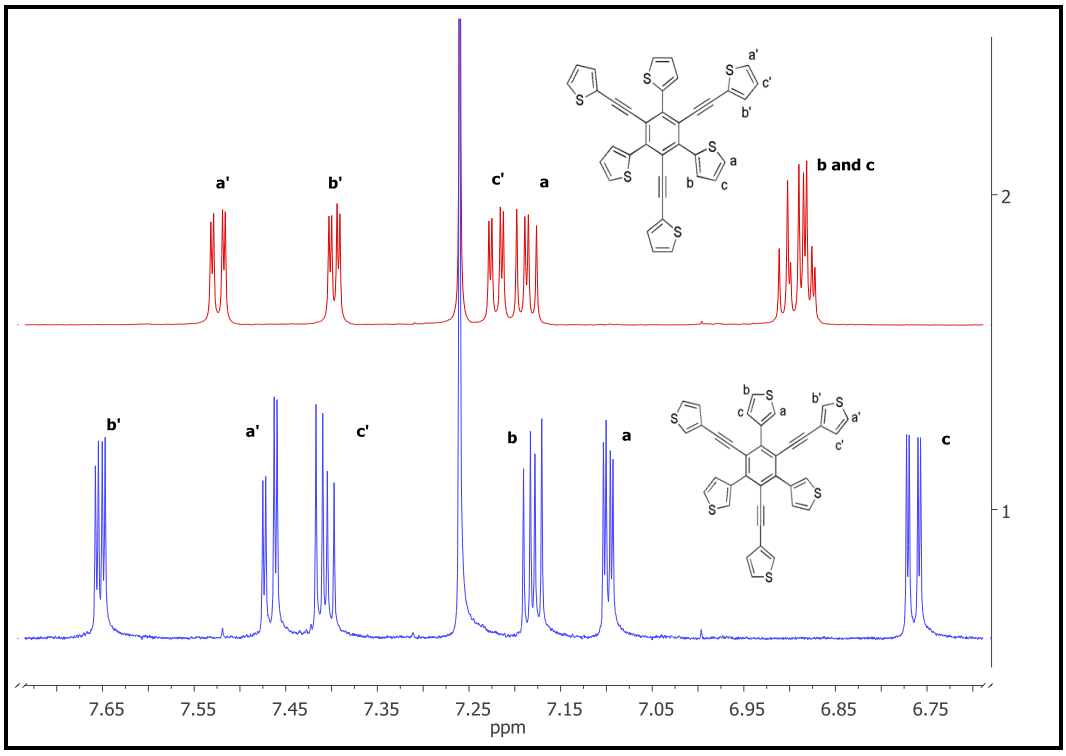

Figure 2.10. Partial ^{1}H NMR spectra for compound **3** (blue spectra) and **6** (red spectra).

2.3.3. UV-vis and fluorescence spectroscopies

UV-Vis absorption spectra of the star-shaped hexasubstituted thiophene compounds **3** and **6** were recorded in CH_2Cl_2 (1×10^{-5}M). The UV-vis spectra are shown in **Figure 2.11.** These star-shaped thiophene compounds displayed an intense and broad absorption bands in the UV-vis regions with maximum around 270-420 nm. The onset of the absorption band provided an optically determined band gap of around 3.5 and 3.2 eV for compound **3** and **6**, respectively. The absorption spectra showed a bathochromic shift from 316 nm for compound **3** to 343 nm for compound **6** which indicates formation of higher energy π–π* transition through the conjugated backbone by attaching acetylene groups in 2-position of the thiophene moiety.

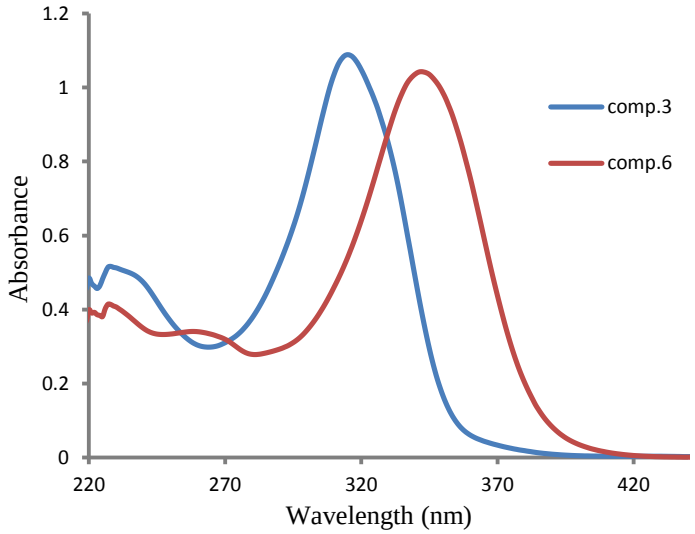

Figure 2.11. UV-vis absorption spectra of compounds **3** and **6** (1×10^{-5}M) recorded in CH_2Cl_2.

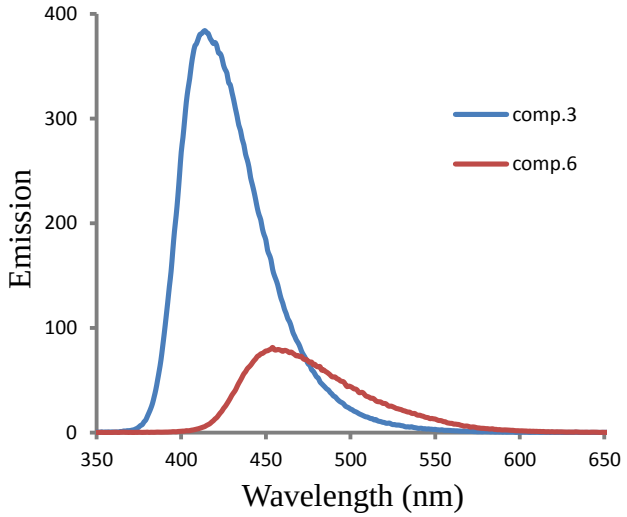

Figure 2.12. Fluorescence emission spectra of compounds **3** and **6** ($1x10^{-5}$M) recorded at an excitation wavelength of λ = 329 nm in CH_2Cl_2.

Figure 2.12 shows the fluorescence emission spectra of compound **3** and **6** in CH_2Cl_2. A maximum emission peak at 420 nm was observed for compound **3** under excitation wavelength of λ= 329 nm, however, under same excitation wavelength compound **6** exhibited red shift and quenching in the emission peak with the maximum emission wavelength occuring at λ= 456 nm.

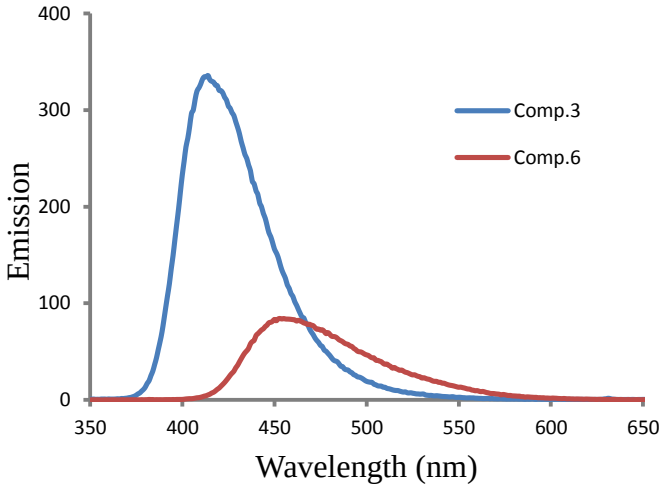

Figure 2.13. Fluorescence emission spectra of compounds **3** and **6** ($1x10^{-5}$M) recorded at excitation wavelengths of λ = 319 and 339 nm, respectively, in CH_2Cl_2.

Similar quenching and shifting toward higher wavelength were observed for the emission peak at 456 nm after excitation of compound **6** with a wavelength of λ= 339 nm. This could be assigned to less conjugation resulting from steric hindrance between the core and the arms. Whereas, emission peak at 420 nm, which resulted from excitation of compound **3** at a excitation wavelength of λ= 319 nm, showed slightly a decreased emission intensity value as shown in **Figure 2.13**.

2.3.4. Square wave voltammetry

The oxidation potential for the prepared star-shaped thiophene derivative **3** and **6** were studied using square wave voltammetry. The electrochemical data are summarised in **Table 2.1**. the experiments were measured at room temperature in (1×10^{-4}M) CH_2CI_2 solution with 0.1 M of $TBAPF_6$ as supporting electrolyte, a working electrode, silver wire as a pseudo reference electrode and a platinum wire counter electrode. The measurements were referenced to Fc/Fc^+ redox couple as an internal reference. The square wave voltammetry data of compounds **3** and **6** showed one oxidation peak on the oxidation scan as shown in **Figure 2.14**. The oxidation potential of compound **3** and **6** were determined to be +1.38V and +1.29V *vs.* Fc/Fc^+= 0.0V, respectively. It is worth mentioning that increasing the conjugation length of compound **6** effects positively on the HOMO energy level by increasing the energy level to -6.09 eV compared with compound **3** which the HOMO energy level appears at -6.18 eV.

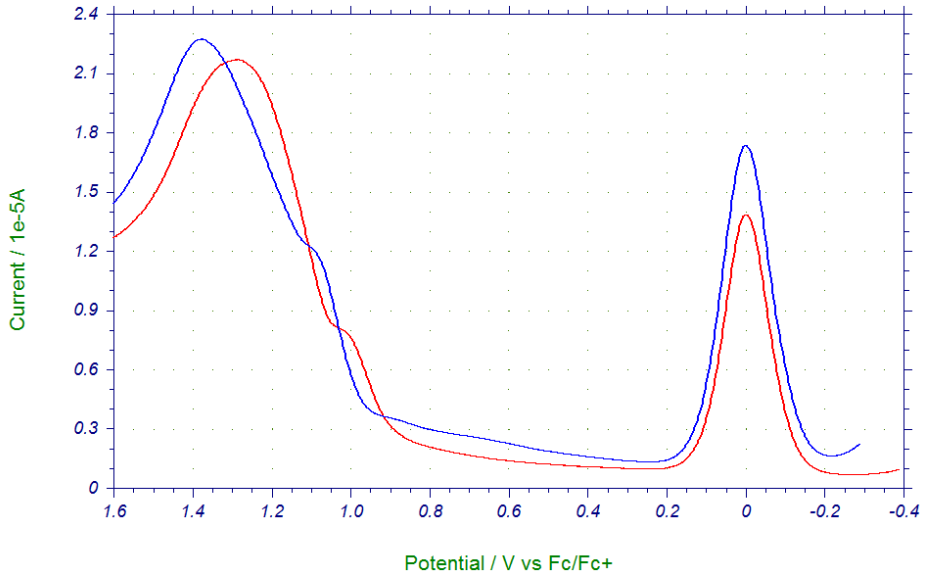

Figure 2.14. Square wave voltammogram of compound **3** (blue line) and **6** (red line) (1×10^{-4}M) recorded in CH_2Cl_2, with $TBAPF_6$ (0.1M) as supporting electrolyte and at $E_{Incr} = 2\ mV$, $E_{Amp} = 25\ mV$ and $SW_{freq} = 25\ Hz$.

Table 2.1. Optical and electrochemical data of star-shaped thiophene derivatives **3** and **6** (1×10^{-4} M) observed by square wave voltammetry in CH_2Cl_2, with $TBAPF_6$ (0.1 M), all potentials are given *vs.* Fc/Fc^+ redox couple used as internal standard.

Compounds	*UV results* λ_{max} / λ_{onset} *(nm)*	*Optically determined band gap (eV)*	*SW results (Volts)* E_{diff}*(ox)*	E_{HOMO} *(eV)*	E_{LUMO} *(eV)*
3	319 / 354	3.51	1.38	- 6.18	-2.67
6	339 / 391	3.18	1.29	- 6.09	-2.91

2.3.5. Electrochemical studies of the monomers 3 and 6

Attempts were made to polymerize both monomers **3** and **6** in solution. The attempts were carried out using a working electrode with a silver wire reference electrode and a platinum counter electrode using a potential-dynamic mode. The potentials were referenced to the Fc/Fc^{+}= 0.0 V. However, evidence for electro-polymerization for both compounds was not observed even with replacement of the working electrode and reference electrode with a glassy carbon working and AgCl electrode, respectively.

2.3.6. X-ray structure

Crystals of compound **3** and **6** which were suitable for X-ray structure determination were obtained by slow evaporation of a 1:1 mixture of CH_2Cl_2 and petroleum ether. It is noteworthy that significant distortion from planarity occurred for a number of the thiophene units. **Figure 2.15** shows the crystal structure of compound **3** and **6**.

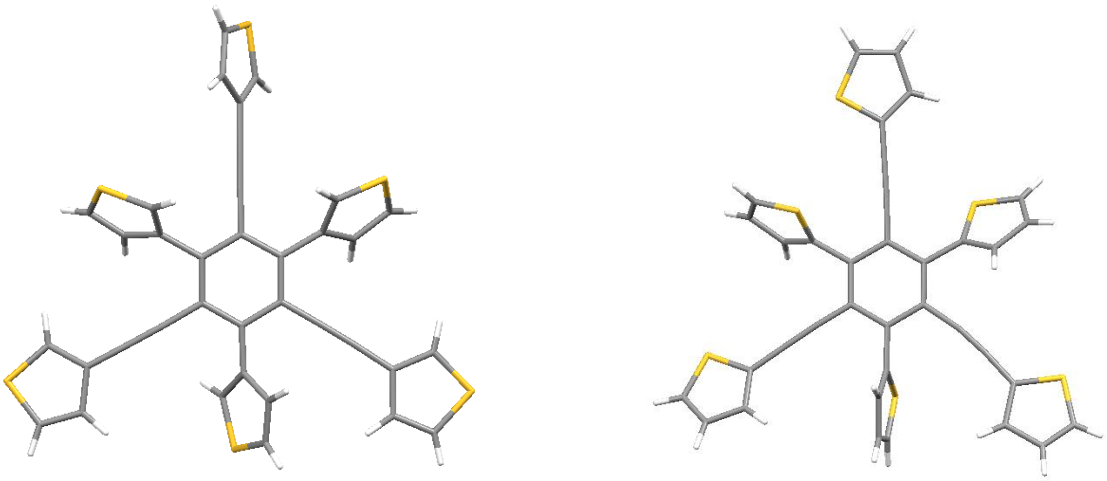

Figure 2.15. Crystal structure of **3** and **6** obtained by slow evaporation of a 1:1 mixture of CH_2Cl_2 and petroleum ether.

Figure 2.16 shows the existence of sulfur-sulfur interactions between the molecules of compound **6**. The calculated intermolecular contacts between the sulfur atoms in compound **6** were shorter than those observed in compound **3**, which were found to be larger than 3.7 Angstroms**.** The intermolecular distance between different sulfur atoms are shown in **Table 2.2**.

Table 2.2. Intermolecular distance between sulfur atoms in compound **6**.

Sulfur atoms	*Intermolecular distance*	*Symmetry operations*
S2 - S3	3.547(4)	x, y+1, z
S4 - S6	3.536(7)	x, -y-1, z+1/2
S5 - S6	3.281(6)	-x, y, -z+1/2

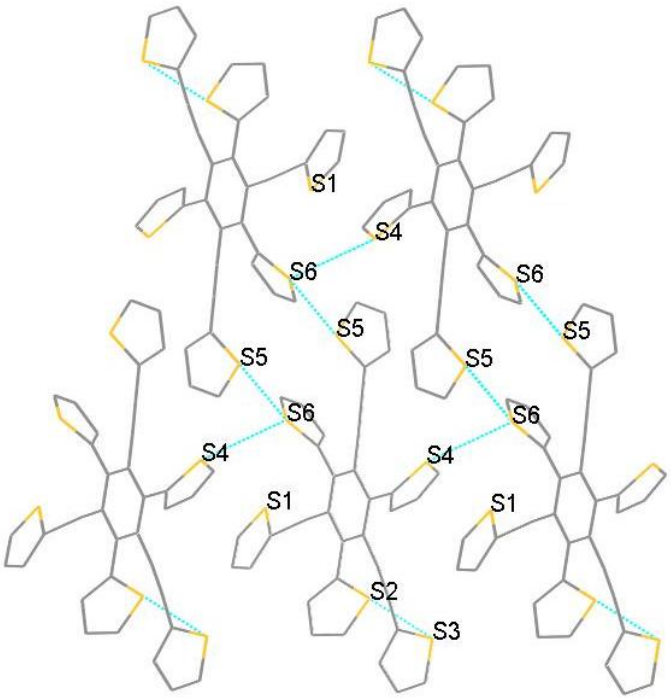

Figure 2.16. Crystal structure of compound **6** showing the close intermolecular contact between sulfur atoms.

2.3.7. Molecular modelling

The molecular orbitals for compounds **3** and **6** were calculated using Spartan 08 software using DFT B3LYP 6-31G level of theory and the results are shown in **Figure 2.17**. For compound **3**, it is clear that the HOMO orbital is delocalized over the benzene ring, two of the side thiophene arms, and the acetylene linkages. In contrast, the HOMO of compound **6** is delocalized over the central part and only four of thiophene side arm units. Whereas, the LUMO orbital is delocalized over the benzene ring and two of the acetylene linkages in compound **3**, the LUMO orbital in compound **6** is delocalized also on one of the thiophene ring.

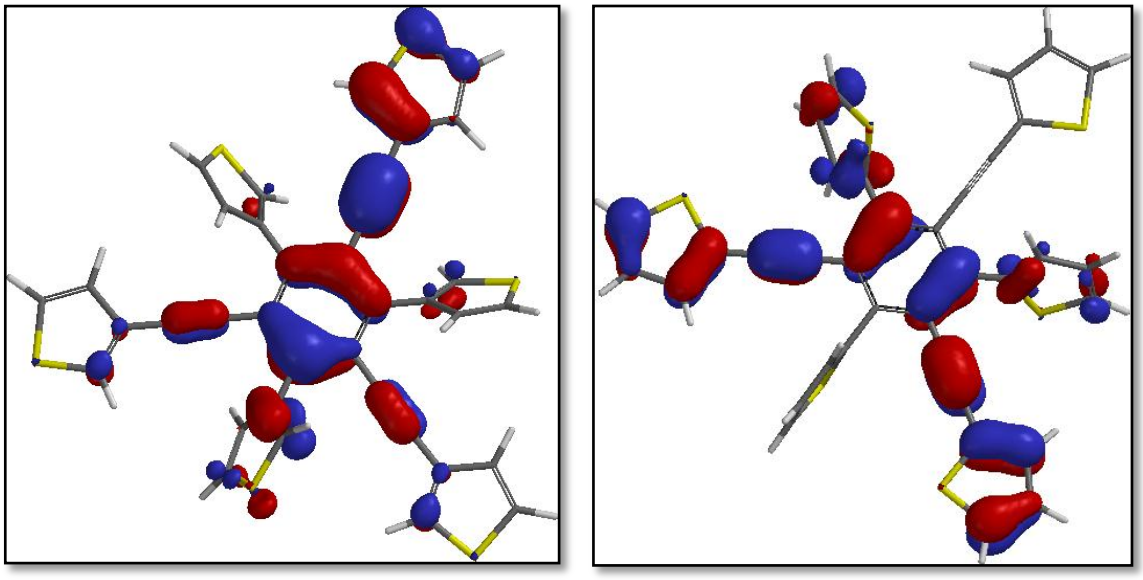

HOMO = -5.46 eV HOMO = -5.39 eV

Figure 2.17. HOMO orbital plots of compound **3** and **6** performed on Spartan 08 program using DFT B3LYP/6-31G calculations.

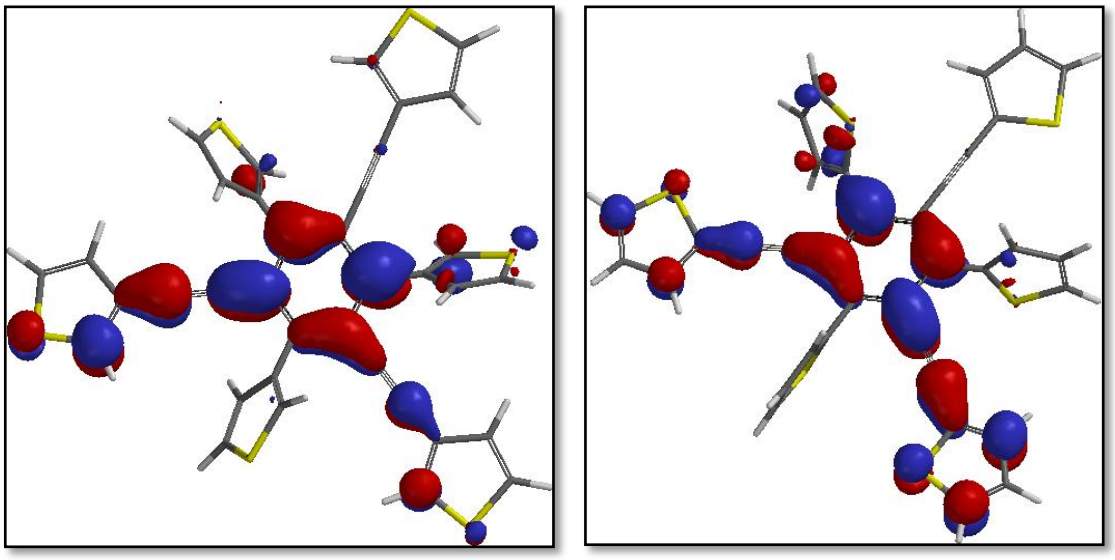

LUMO = -1.61 eV LUMO = -1.79 eV

Figure 2.18. LUMO orbital plots of compound **3** and **6** performed on Spartan 08 program using DFT B3LYP/6-31G calculations.

The calculated energy levels of compound **3** and **6** showed that the LUMO energy of compound **3** occurs at a less negative value (-1.79 eV) and the HOMO energy at a more negative value (-5.39 eV) compared with compound **3**. This resulted in a lower band gap for the more conjugated compound **6**. These results are roughly compatible with the obtained electrochemical data.

2.4. Conclusions and future work

2.4.1. Conclusions

To summarize, we have successfully synthesized two hexasubstituted star-shaped architectures consisting of benzene core as a central unit surrounded by six thiophene units functionalized in their 2- and 3-positions through an acetylene linker. The physical properties of the resulting compounds were studied in solution and the absorption spectra of these compounds displayed an intense band in the UV-vis region indicating the

formation of π–π* transitions through the conjugated backbone. The emission spectra of compound **6** displays obvious quenching and shifting toward higher wavelength compared with compound **3.** The electrochemical studies of the resulting star-shaped compounds showed an increase in the HOMO energy for compound **6.**

2.4.2. Future work

If there had been more time available, further investigations would have been carried out to synthesize and analyse of hexasubstituted star-shaped systems featuring oligothiophene units. More rigorous investigations of the electro-polymerization of these compounds may be an interesting extension to this work. Also the investigation of the ordering and crystallinity of deposited these compounds onto the surfaces would be another key extension to this work.

Chapter 3;

Electropolymerization studies of viologen containing monomers.

3.1. Introduction

The discovery of unusual metallic properties and high conductivity of polyacetylene was reported in 1977 by Shirakawa, Heeger, MacDiarmid and co-workers. These properties result from doping the polyacetylene material with iodine vapour and forming copper coloured films of the *cis* isomer and silver film of the *trans* isomer using the Zeigler catalyst. The materials show thermodynamically stable films and high conductivity up to 4.4 x 10^{-5} $\Omega^{-1}cm^{-1}$ for the *trans* isomer and 1.7×10^{-9} $\Omega^{-1}cm^{-1}$ for the *cis* isomer.[102] The ability of acetylene to undergo rapid doping and forming conducting polymers results from two main reasons: (i) The natural acetylene morphology with associated high surface area allows the doping ions to diffuse in between the weak interchain binding and reach any chain of the polymer. (ii) The strong interachain bonding by the polymer insures preservation of the polymer chain during the diffusion process and reversibility of the doping process.[103]

However, the unstable properties of the resulting polyacetylene film and poor resistance toward oxygen has limited their application and led to synthesise other conducting polymers having similar properties of polyacetylene films at the same time showing better stability features. Therefore, the concept of conductivity in conjugated materials was followed by preparing highly conductive and stable film resulting from electropolymerization of pyrrole monomer on an anodic platinum surface. The electropolymerization study has been applied to other heterocyclic compounds and has resulted in significant enhancement in the conductivity of conjugated polymers. Examples of such polymers are: polyphenylene (pp), polyphenylenevinylene (ppv), polypyrrole (ppy) polythiophene (pth) and polyaniline (pani) as shown in **Figure 3.1**. Further improvement on these polymers has been also carried out by incorporating different substituent into the

heterocyclic systems to assist in improving the physical properties of such classic conducting polymers.[104]

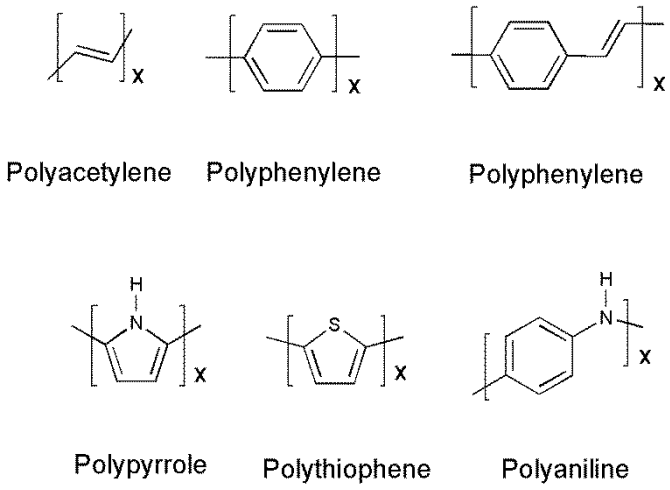

Figure 3.1. Some of the most important conducting polymers.

Controlling the band gap as well as conductivity of the conjugated polymers can be achieved through; firstly selecting appropriate molecular structures, which typically contain alternating double bonds along the chemical structure, Secondly, modifying their semiconductor properties by doping the resulting conjugated materials using either a chemical polymerization method or an electrochemical polymerization method. For conduction to occur in the conjugated materials, the band gap, which is the difference between valence band and conduction band, must be adjusted to allow the electron to be excited from the valence band to the conduction band. However, doping these materials will create impurities through the system by introducing charge defects such as polaron, dipolaron and soliton into the oligomer's backbone (**Figure 3.2**). Formation of these charges assists in tuning the physical properties by changing the band gap structure. Also, movement of these charges along the alternating double bonds in the polymer backbone will assist in enhancing the conductivity of the polymer.[105] Variation in band structure of π -conjugated system through doping process is shown in **Figure 3.3**.

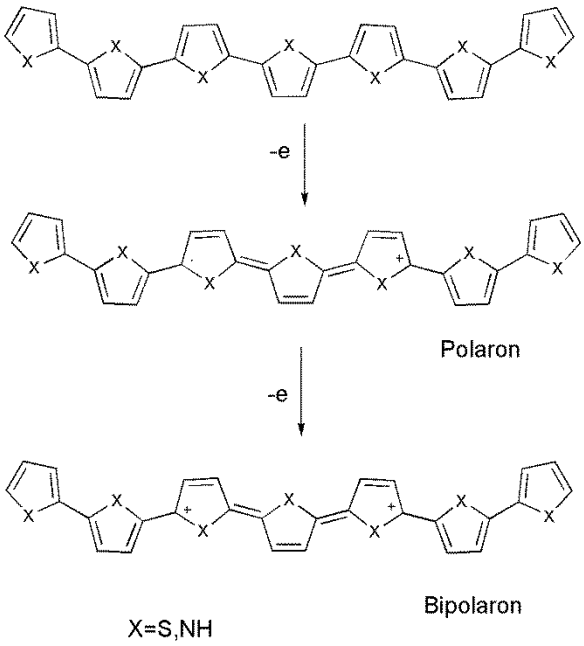

Figure 3.2. Formation of the charge defects in polythiophene and polypyrrole upon oxidation.

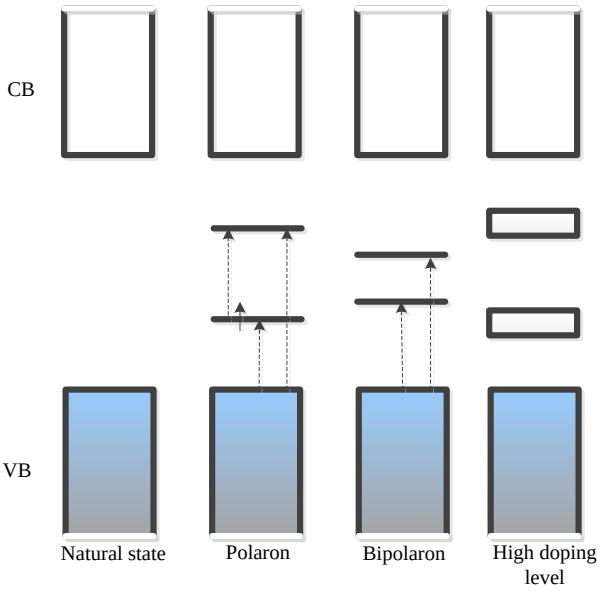

Figure 3.3. Variation in band structure of π -conjugated systems through doping.

Conducting polymers can be prepared by the chemical oxidation method using oxidizing reagent such as $FeCl_3$ or the electrochemical polymerization method using a conventional electrochemical system. The latter method is the most widely used method of controlled morpholgy due to the ability of providing a clean and tuneable thickness. The Electrochemical doping of the materials can occur at the anodic surface (*p*-doping) by withdrawing electrons from the conjugated oligomer or at cathodic surface (*n*-doping) by introducing electrons into the conjugated system. However, due to the huge number of aromatic conjugated monomers that have the ability to be oxidized on the anodic surface (**Figure 3.1**), few of these systems show ability to produce conducting polymer through the reduction process at the cathode surface. The limitation in producing reductively doped polymers is related to the formation of an insulating material instead of conductive polymer on the electrode surface or limited growth in film thickness to 100 nm. The best known conductive polymers produced by reductive process are polyphenylenevinylenes (PPVs) and polyxylylenes (PPXs) shown in **Figure 3.4**.[106]

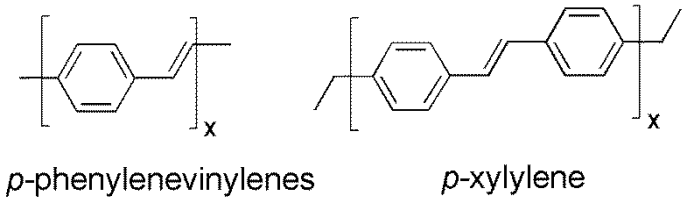

Figure 3.4. Example of conducting polymers formed on cathode surface.

The mechanism of the electrochemical process was first suggested by Diaz in 1983 through studying the formation of polypyrrole films on the anodic surface.[107] He proposed that two molecules at the electrode surface are oxidized and form a dihydro dimer dication species. This step is followed by elimination of two protons from the binary charged dimer to form the aromatic neutral dimer species which represent the driving force of this step as shown in **Scheme 3.1.** The continued formation of these highly reactive species depends

on the experimental conditions such as the nature of the electrode surface, temperature and the change in the applied potential. In addition, due to the readily oxidisable nature of the resulting conjugated dimer, the length of the polymer increases by forming longer radical cations and coupling with monomeric radical cations to form trimer species after eliminating two protons. This process continues until the oligomer becomes insoluble in the medium and precipitates onto the electrode surface.[108]

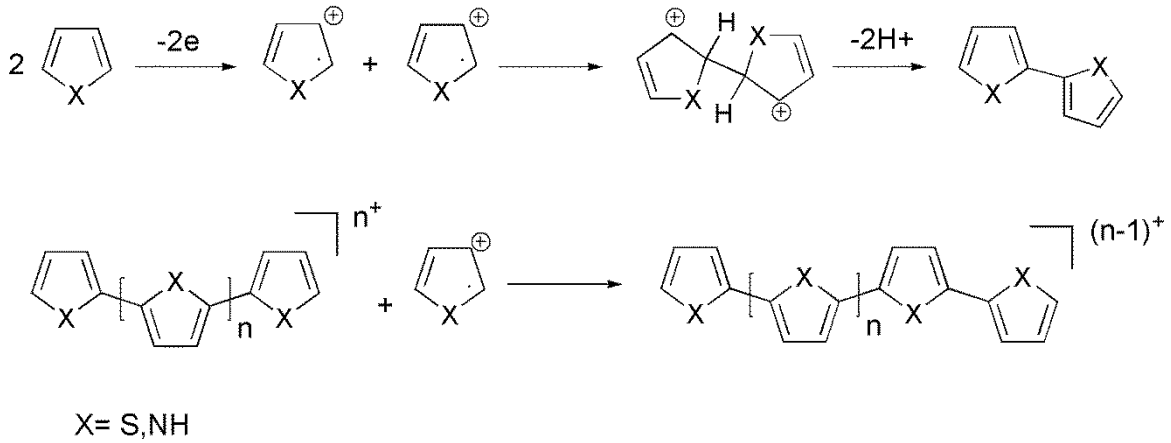

Scheme 3.1. Proposed mechanism of electrochemically formed conducting polymers.

The electropolymerization method provides a number of advantages compared with chemical polymerization, such as the absence of catalysts during the polymarization process, improvement in electrochemical applications through deposition of the conducting film directly on the surface of the electrode without the need to prepare soluble polymers with bulky solubilising side chains. Also, the electropolymerization methods yield the benefit of producing thin-film materials with better electronic characteristics due to more monodisperse polymer chains. Lastly, the electropolymerization methods promotes the ability to characterize the growing film by both electrochemical and spectroscopic techniques.[107]

A number of experimental conditions influence the electropolymerization efficiency and the amount of oligomers deposited on the electrode surface such as: potential scan, nature of the monomer and experiment time scale. Applying high oxidation potential increases the charge and reactivity of the intermediates and leads to the formation of cross-linked materials. However, lowering the oxidation potential can result in weakly charged intermediates and shorter chain oligomers. In addition to these parameters the nature of starting materials has a kinetic effect on the electropolymerization process. For example, through the process of growing different sizes of oligothiophenes on the electrode surface, less reactivity was observed in the oxidation of tetrathiophene and bithiophene compared with thiophene due to a decrease in the reaction rates and increase in the stability of the coupling products associated with increasing the number of thiophene units. However, increasing the reactivity was achieved by introducing accepting group into the system. Therefore, adjusting these parameters will result in enhancing the reactivity and increasing the defect free electropolymerization products.[105]

3.1.1. Alternating donor-acceptor conjugated polymers

The synthesis of π-conjugated systems has progressed due to advances in electropolymerization, as increasing the conjugation length through electrochemical synthesis will assist in lowering oxidation potentials which will limit the possibility of forming side reactions and prevent over-oxidation of the deposited film. Also, if the starting monomer contains α-α′ linkages, the possibility of obtaining cross-coupled products will be reduced. With these improvements in the conditions, the electropolymerization field opens the opportunity to use new building blocks with different electronic properties.[109]

In order to modify and tune the electronic properties of thin film materials, attempts have been focused on preparing well-defined oligomers via incorporating functional units into the oligomer backbone which allows control of the produced film.[110] Therefore, mixed monomers containing poly (isothianaphthene) (PTTN) and thiophene in their building blocks (e.g. **3.1**) represents an early example for electrochemical conjugated polymer synthesis. The cyclic voltammetry of the resulting polymer exhibited a lower oxidation potential value compared with the monomeric precursors. Also, the band gap value of the polymer lies between the bandgap of the monomeric precursors. However, poor conductivity of around 5 $\times 10^{-3}$-10^{-2} S cm^{-1} was recorded for the polymer.[111]

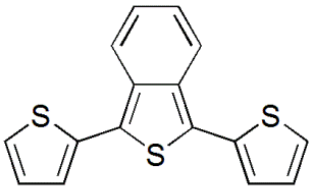

3.1

Vibration properties of neutral and doped thienopyrazine unit with different alkyl groups were measured and compared using Raman spectra and theoretical quantum calculations. The results showed that the low band gap was derived from the bond length alternation along the polymeric backbone with the assistance of π-electron delocalization along the polymer chain. These results suggested that the thienopyrazine polymer has quinoid ground state geometry in the neutral state and an aromatic one in the doped state (**Figure 3.5**).[112]

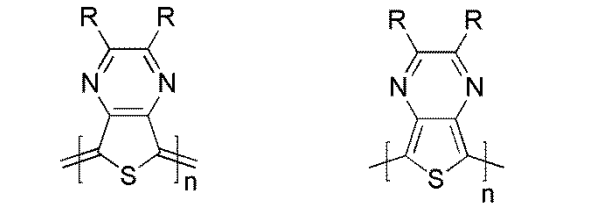

Quinonoid structure Aromatic structure

Figure 3.5. Chemical structures of poly (2, 3-R,R-thieno[3,4-b]-pyrazine).

Another attempt to achieve a low band gap polymer by electropolymerization was carried out by Kitamura and co-workers in 1994. The new low band gap polymer consisted of thiophene aromatic donor units and (thieno- [3,4-b]-pyrazine) acceptor unit featuring different alkyl groups. Compound **3.2** reduced the steric hindrance between the fused benzene ring and the adjacent thiophene rings and increased the conjugation along the polymer backbone. In addition, all polymers resulting from compound **3.2** showed stable films on the electrode surface with a lower oxidation potential and band gap compared with compound **3.1**.[113]

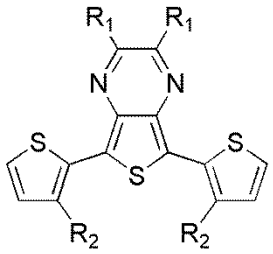

$R_1=R_2=H$
$R_1=CH_3$, $R_2=H$
$R_1=C_6H_{13}$, $R_2=H$
$R_1=C_{13}H_{27}$, $R_2=H$
$R_1=R_2=C_6H_{13}$

3.2

In order to synthesis stable green conducting polymers that could find a commercial electrochromic applications, a new monomer was synthesized by incorporating two different conjugated chains into a building block compound **3.3**. An electropolymerization study of the resulting monomer displayed a green stable polymer with a low oxidation potential. Electrochemical studies of resulting film was achieved by switching the potential values many times between oxidized and neutral states and resulted in a stable conducting film without any significant loss in charge or current. The electrochromic stability and fast switching properties make this polymer a promising material for electrochromic applications.[114]

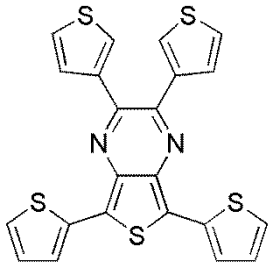

3.3

Due to the ability of thienopyrazine units to tune the polymer's band gap resulting from formation of a quinoid character, Tarkuc and co-workers prepared new organic monomers containing thienyl and ethylenedioxybenzene functionalized thienopyrazine units in order to investigate the effect of these groups on the properties of resulting polymers. The cyclic voltammetry of resulting deposited polymers showed a decrease in the oxidation potential value for polymer **3.5** compared with **3.4**. This result indicates the effect of ethylenedioxybenzene as donating units on decreasing the withdrawing ability of thienopyrazine unit. In addition, the spectral behavior of the resulting deposited polymers were red shifted and had a low band gap for the neutral films.[115]

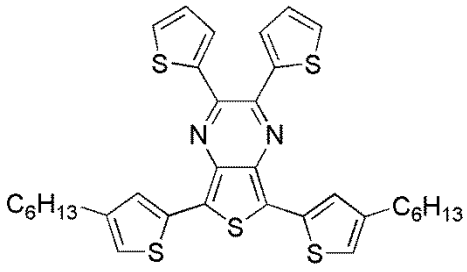

3.4

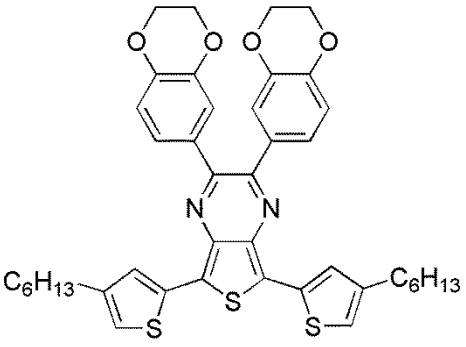

3.5

3.1.2. Viologen incorporating conjugated polymers

Much effort has been made to enhance the properties of conjugated polymers through enhancing the electron affinity features of their building blocks. Viologen has been extensively used as an electron acceptor unit with different *p*-conjugated systems. Viologens which also called *N,N′*-disubstituted bipyridinium salts prepared from diquarternizing of *4,4`*-bipyridine using an excess of alkyl halide to form colorless stable dications. The formed dication can be reduced electrochemically by one electron reduction and form a colored second stable redox state (radical cation). The color depends on the substituent group at the nitrogen atoms. The stability of the radical cation is influenced by the delocalization of the radical electron through π-electron system of bipyridinium rings. The neutral species is formed from one-electron reduction of the radical cation species or two-electron reduction of dication species (**Scheme 3.2**).[116]

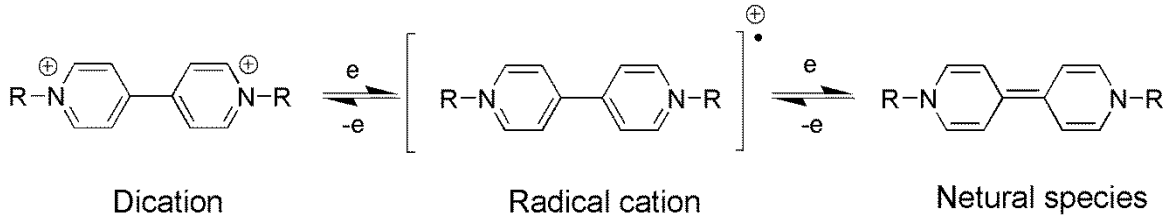

Scheme 3.2. Three common redox states of *N,N′*-disubstituted bipyridinium salts.

Viologen salts with their distinctive redox and photochromic features have found a number of applications. Besides being effective herbicides, they can also be used as redox indicators in biological sensors and redox mediators resulting from their ability to participate in electron transfer to electroactive centers of biological species. In addition due to their marked color change following generation of their different redox states, this type

of material can be used as electrochromic material in many applications such as light emitting diodes LEDs and liquid crystal display LCDs.[117]

The low conductivity of bipyridinium dication salts can be enhanced through the addition of a suitable electron donor due to the formation of charge transfer interactions between the two components. Significant efforts have been focused on the photophysical and photochemical processes of viologen materials to study the electron transfer (ET) reactions in multi-component systems and have led to the concept of building donor- acceptor π-conjugated polymers. The construction of these systems could be a solution to the phase separation problem in donor–acceptor BHJ blends due to the existence of both *p* and *n* doping units. [118]

As an example of this concept, a new diquat salt **3.6** was synthesized from 5,5'-bis(2,2'-bithiophene-5-yl)-2,2'-bipyridine and 1,2-dibromoethane. The conductivity of these materials can be altered by either *p*-doping of thiophene or reducing the bipyridinium unit. Also this building block could increase the effectiveness of the electrode surface as bipyridinium unit adsorbs on the electrode surface and acts as electrocatalystic species. The cyclic voltammetry of compound **3.6** exhibited two reversible reduction peaks typical for the two reduction steps of diquat salt to form the neutral fully reduced species. The electropolymerization of the resulting monomer showed deposition of dark stable polymer film on the electrode surface with a slightly lower oxidation potential value compared with compound **3.6** indicating the formation of conjugated polymer. The CV of the resulting polymer exihibited a reversible oxidation wave assigned to the quaterthiophene unit and reversible reducation wave assigned for the diquat units.[118]

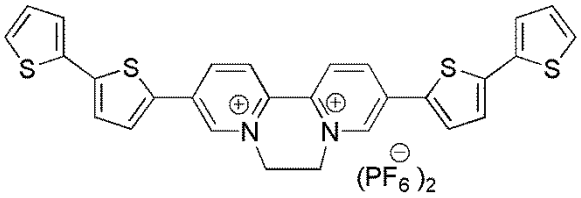

3.6

Kijima and co-workers synthesized a soluble polythiophene derivative **3.7** having viologen moieties as a side chain. The experiments showed that the presence of thiophene in the viologen structure altered the redox function of the viologen moiety and promoted liquid crystalline behavior due to intermolecular forces.[119]

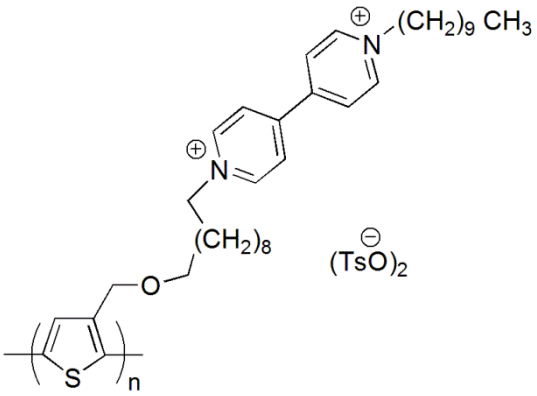

3.7

In order to enhance the electron accepting feature of viologen compounds, different π-conjugated spacers including polyethenylene units and heterocyclic units such as phenyl, furan and thiophene have been incorporated between the pyridylium rings which allows the formation of stable radical cations to occur.[120] Alberto and co-workers synthesized a new extended viologen molecule **3.8** featuring bithiophene unit in between the two pyridylium rings. In contract to traditional viologen compounds that have pyridylium rings connected directly together, this extended viologen compound **3.8** exhibited single stage two-electron reduction waves in the CVs indicating the formation of unstable radical cation resulting from increasing the separation between pyridylium rings.[121]

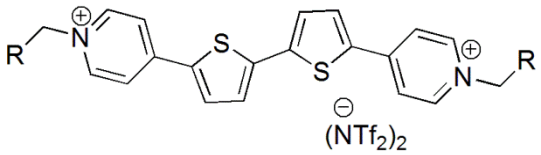

3.8, R = $(CH_2)_9CH_3$

New compounds **3.9, 3.10** and **3.11** were synthesized by introducing sulfur unit between the pyridylium units. The two one-electron reversible peaks in the CVs indicated the presence of pyridylium rings. In comparison with methyl viologen, the potential of first reduction peaks, assigned to the formation of radical cation, was more negative and the ones assigned to the formation of natural species were more positive. This shifting in the potential resulted from a coplanarity in the structure which is induced by the five-membered sulfur heterocycle and an increase in π-conjugation.[122]

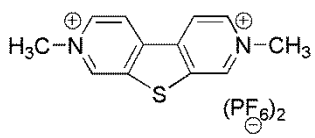

3.9

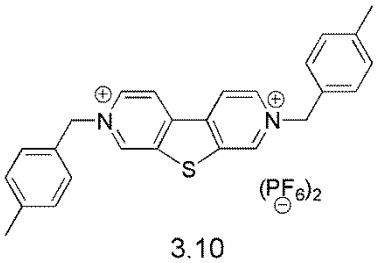

3.10

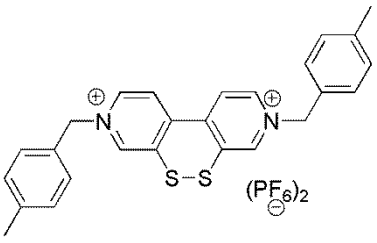

3.11

Electrochromic applications can be achieved by combining the redox electrochromic effects of viologen unit with the unique electronic properties of poly (3,4-ethylenedioxythiophene) PEDOT, in which the EDOT unit shows a number of important properties such as high stability, low electro-polymerization potentials and high reactivity of the resulting radical cations. The cyclic voltammetry of the electropolymerized polymer **3.12** showed two well-defined redox waves corresponding to the viologen unit and one redox peak corresponding to the EDOT unit. These results were also confirmed by spectroelectrochemical measurements of a deposited polymer film. The resulting polymer

showed a maximum electrochromic effect in the visible region due to the presence of viologen and EDOT unit in the polymer chain.[123]

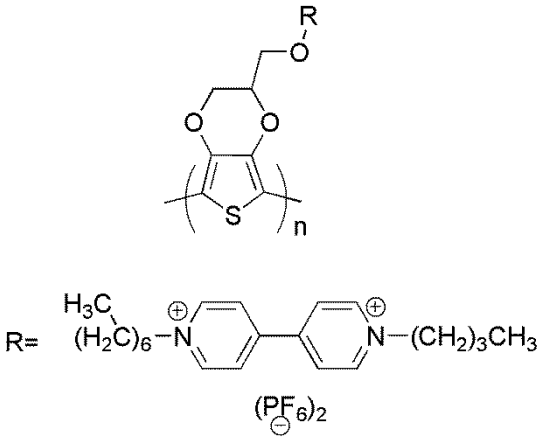

3.12

Materials having thiophene units incorporated into the *N*-atom of viologen unit have been studied to facilitate immobilizing viologens units onto an electrode surface through electrochemical polymerization of thiophene unit (e.g. **3.13**). However, the electroactivity of deposited polymer depends on the nature of thiophene unit. Thus the polymer was deposited on the electrode surface over several redox cycles and the electroactivity of the resulting film was examined in free monomer solution at wide range of potential scan rates. The results show that the polythiophene unit degrades much faster than the viologen moiety, which indicates better stability of viologen moiety compared with thiophene unit. The results suggested that an unstable polymer could result from the irreversible side reactions at the 4-position of thiophene unit during over oxidation.[124]

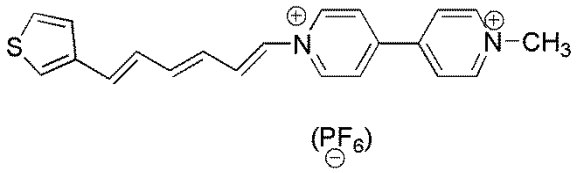

3.13

To overcome the instability of polymer **3.13**, Ko and co-workers synthesized a new polymer from compound **3.14** combining oligothiophene and viologen units in order to increase the delocalization of the radical cation through the oligomer chain. The cyclic voltammetry of resulting electropolymerized film displayed, in addition to the two redox peaks of viologen unit and the reversible oxidation peak of oligthiophene unit, a new reduction peak between 0 and -0.4 V. It was suggested that this peak originated from electron transfer between oligthiophene units to the reduced viologen unit. Also, the resulting polymer showed that the oligthiophene units were stable over a wide range of potential scans, while the viologen units peak current decreased significantly.[125]

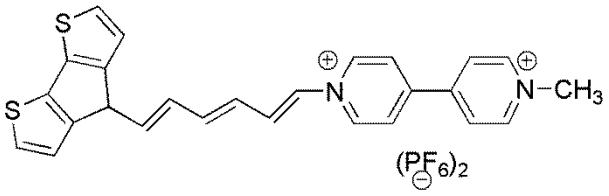

3.14

Combining a viologen with monomer **3.15** assisted in producing mild electropoly-merization conditions by lowering the oxidation potential of the monomer due to the delocalization of the resulting radical cation through the oligomer chain. The cyclic voltammetry showed two redox peaks corresponding to the redox states of viologen unit. The newly prepared unit lowered the oxidation potential and increased the delocalization of the radical cation along the polymer chain. Examination of the resulting polymer was

carried out using CV which indicating that a stable polymer with no significant degradation occurred. Also the resulting polymer showed five multicolored species during switching between oxidation and reduction cycles thereby giving rise to an electrochomic polymer.[126]

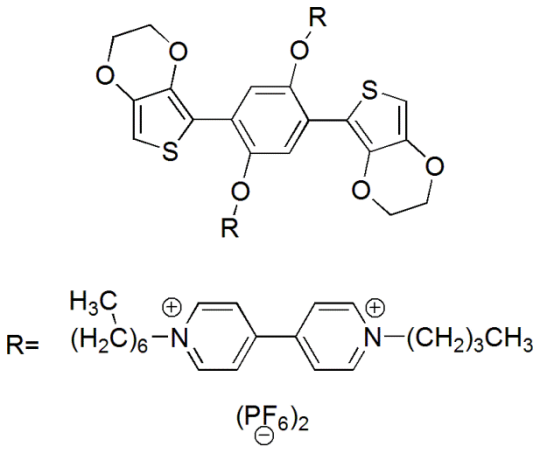

3.15

The study of photophysical and electrochemical properties of viologen derivatives was investigated by combining a number of viologen subunits and building first and second generation dendrimers. Constantin and co-workers synthesized star-shaped triply branched viologen molecules consisting of regularly alternating arrangement of dibenzyl and diphenyl viologen units surrounding a phenyl or a 2,4,6-trimethylphenyl central cores. The CV shows typical two reversible reduction peaks indicating the presence of viologen unit. However, a positive shift of the first benzyl viologen reduction peak was observed for compounds **3.16, 3.17** and **3.18,** which have similar size and carry different peripheral groups, indicating the influence of the surrounding groups, i.e. Br, OH, and CH_3 on redox potential values. Additionally, only the star-shaped viologen monomer with benzyl and bromine end groups formed stable polymer films on the electrode surface. High conductivity in the solid-state was observed if doped with electrons.[127]

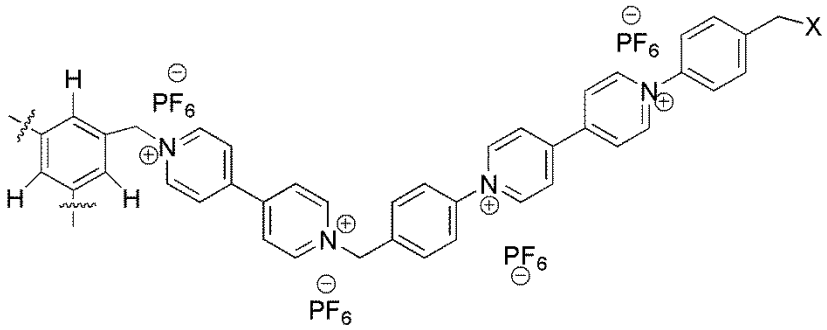

3.16, Y=H, X=Br
3.17, Y=H, X=OH
3.18, Y=H, X=CH_3
3.19, Y=CH_3, X=CH_3

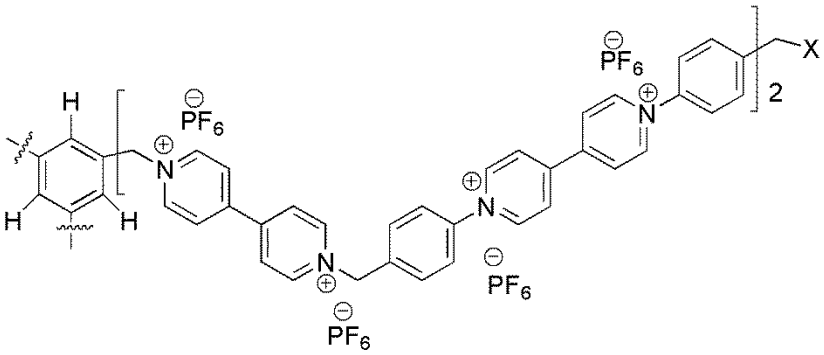

3.20, X=Br

3.2. Aim and objectives

One of the motivations of this project was to synthesise new acceptor units incorporating bipyridinium derivatives and different donor moieties featuring thienyl units for investigating the effect of alternating donor-acceptor architectures has on the physical properties of the resulting polymers. The second motivation was to electropolymerise the monomers onto an electrode surface. The physical properties and electropolymarization investigations were first carried out on thienpyrazine model monomer and then applied on the two different viologen derivatives featuring thienpyrazine and quinoxaline rings, respectively. The model and two target molecules are shown in **Figure 3.6**.

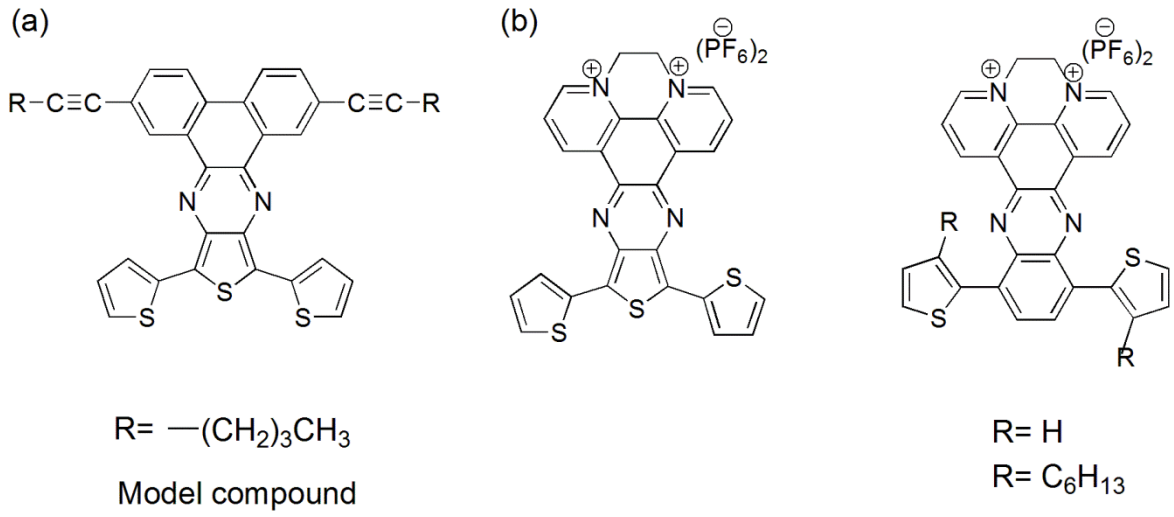

Figure 3.6. (a) Thienpyrazine model compound, (b) thienpyrazine and quinoxaline bipyridinium salts.

3.3. Results and discussion

a) Synthesis and spectroscopy of thienpyrazine model monomer12

3.3.1. Synthesis of model compound

The synthesis of the model monomer **12** is depicted in scheme **3.3** which started from iodination of phenanthrene 9,10-dione **6** using NIS in the presence of triflurometh ane-sulfonic acid gave compound **7** in 82 % yield. The resulting compound **7** was coupled with 1-hexyne *via* a Songoshira coupling to give compound **8** in 37% yield. To get the target model monomer **12**, simple condensation reaction between diamine compound **11** with compound **8** in presence of *p*-toluenesulfonic acid as a catalyst gave compound **12** in 45 % yield.

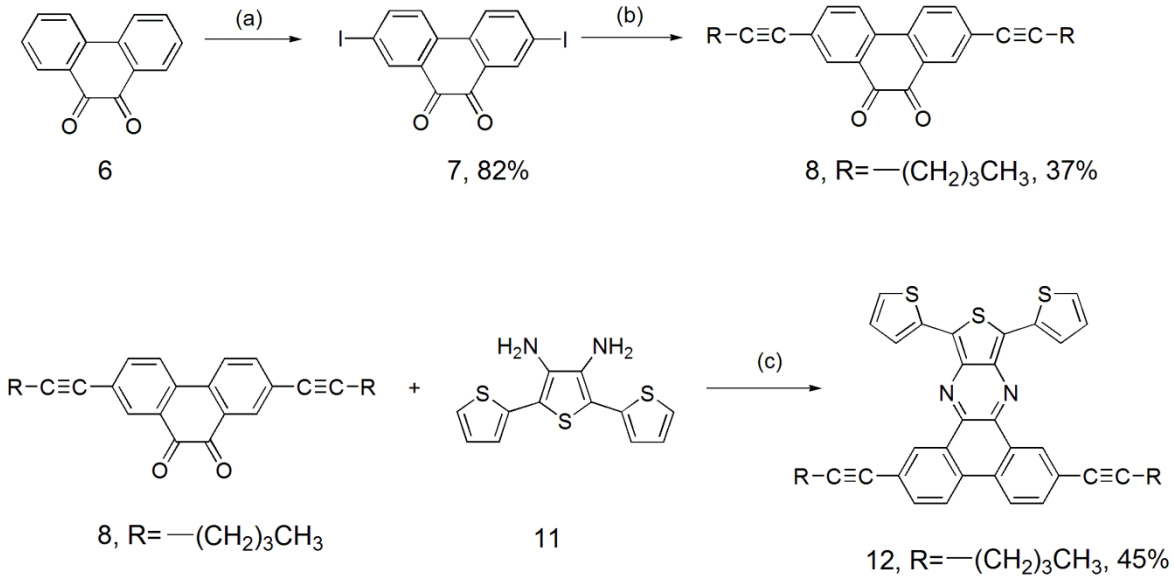

Scheme 3.3. Reagents and conditions: (a) NIS, trifluoromethanesulfonic acid, (b) 10% Pd /C, CuI, Ph_3P, K_2CO_3, H_2O: DME, 1- hexyne, N_2, (c) *p*-toluene sulfonic acid, chloroform, N_2.

3.3.2. UV-vis Spectroscopy of thienpyrazine model monomer

UV-vis absorption spectrum of compound **12** was recorded in CH_2Cl_2 (1×10^{-5}M). Compound **12** exhibited four main peaks, three of them in the higher energy region and one broad band in the lower energy region as shown in **Figure 3.7.** The UV absorption bands at λ = 232, 303 and 368 nm can be attributed to n- π^* and π–π^* transition, whereas the broad absorption band maximum a round 520-720 nm and can be attributed to intramolecular charge transfer CT between donor and acceptor moieties and resulted in an optically determined band gap of around 1.59 eV.

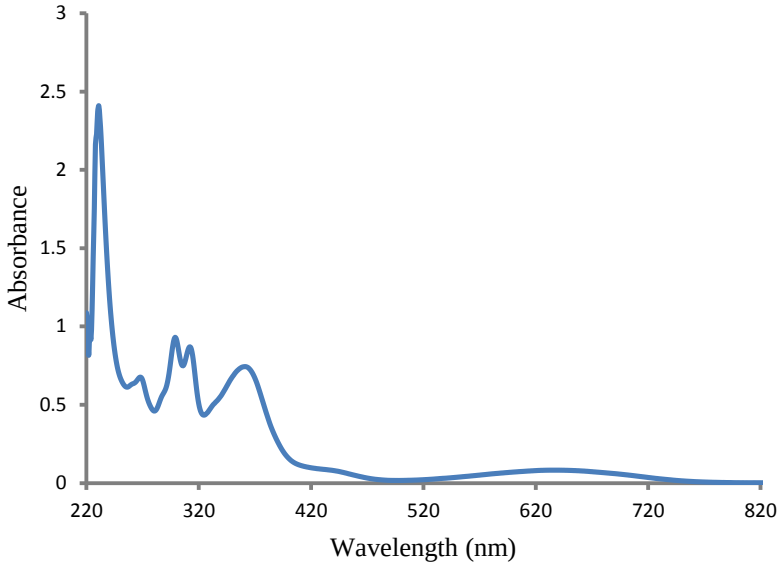

Figure 3.7. UV-vis absorption spectrum of compound **12** (1×10^{-5}M) recorded in CH_2Cl_2.

3.3.3. Electrochemical studies of thienpyrazine model monomer 12

3.3.3.1. Electrochemical study of monomer 12

Electrochemical properties of monomer **12** were investigated using cyclic voltammetry. The redox properties of the monomer was carried out in a conventional three electrode cell containing a platinum button as working electrode, silver wire as a reference electrode and Pt counter electrode. The study was performed in a solution of **12** (1×10^{-4}M) containing ($TBAPF_6$) as supporting electrolyte in CH_2Cl_2 solution and the collected data was referenced to the Fc/Fc^+ couple = 0.0 V.

A quasi-reversible oxidation wave and an irreversible reduction wave were observed for compound **12**. The oxidation wave occurs at $E_{1/2}$= + 0.37V and can be assigned to the formation of thiophene radical cation units, whereas the reduction potential was observed at $E_{1/2}$= -1.41V and can be explained in terms of the electron accepting ability of phenanthrene unit as shown in **Figure 3.8**. The approximate electrochemically determined band gap for compound **12** is 1.37 eV.

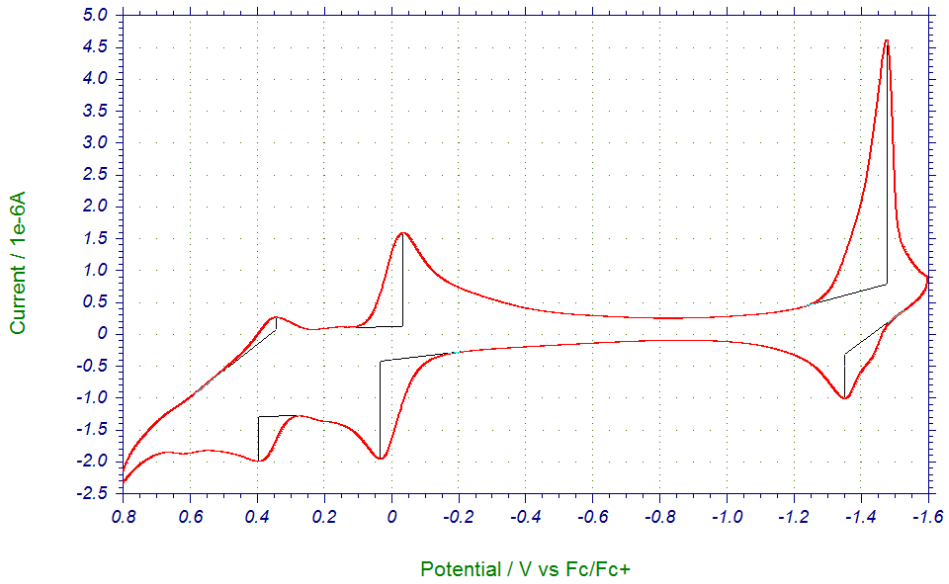

Figure 3.8. Cyclic voltammetry of compound **12** (1×10^{-4}M) recorded in CH_2Cl_2, with $TBAPF_6$ (0.1 M) as supporting electrolyte and at a scan rate of 100 mV/s.

3.3.3.2. Electrochemical studies of oligomer 12

Attempts were made to polymerize monomer **12** from solution. The attempts were carried out using a platinum working electrode with a silver wire reference electrode and a platinum counter electrode using a potentiol dynamic scan. The potentials were referenced to the Fc/Fc^+ redox couple. The growth of the oligomers was achieved through repetitive oxidation cycles monitored by cyclic voltammetry. The growth of the oligomers **12** over 200 cycles is presented in **Figures 3.9**, and shows an increase in the current with each cycle and development of a new peak at a lower oxidation potential corresponding to the formation of a polymer on the electrode surface.

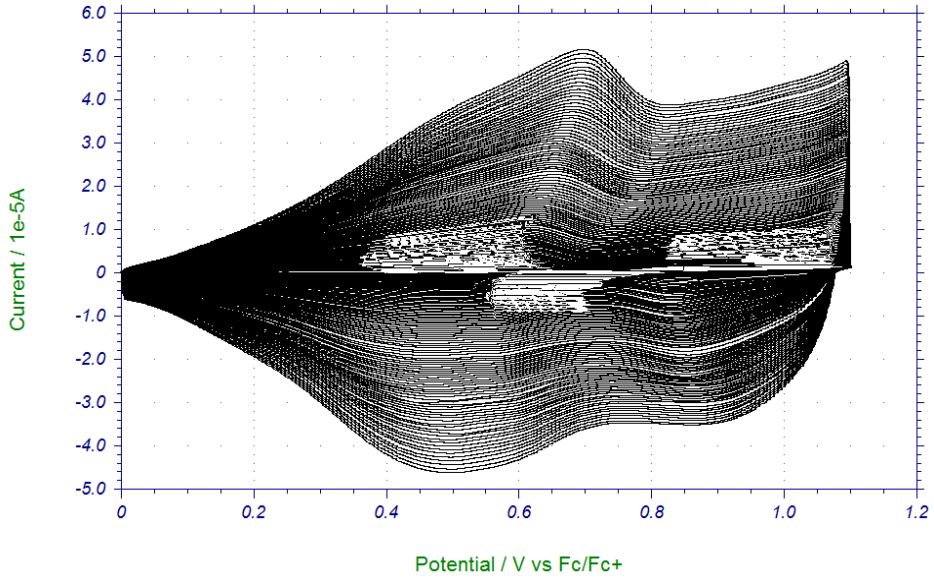

Figure 3.9. Polymer growth of monomer **12** over 200 segments on platinum working electrode.

The coated electrode was transferred into a solution of pure electrolyte in MeCN solution and the electrochemical properties of the polymer were investigated. The result is shown in **Figure 3.10**. One reversible oxidation wave at $E_{1/2}$= + 0.45 V and one irreversible reduction wave at $E_{1/2}$= -1.26 V corresponding to the phenanthrene unit were observed. The electrochemically determined band gap (calculated from the oxidation and reduction onset potentials of the polymer) is 0.95 eV. This small band gap indicates formation of a longer π-conjugation path compared with the monomer **12**.

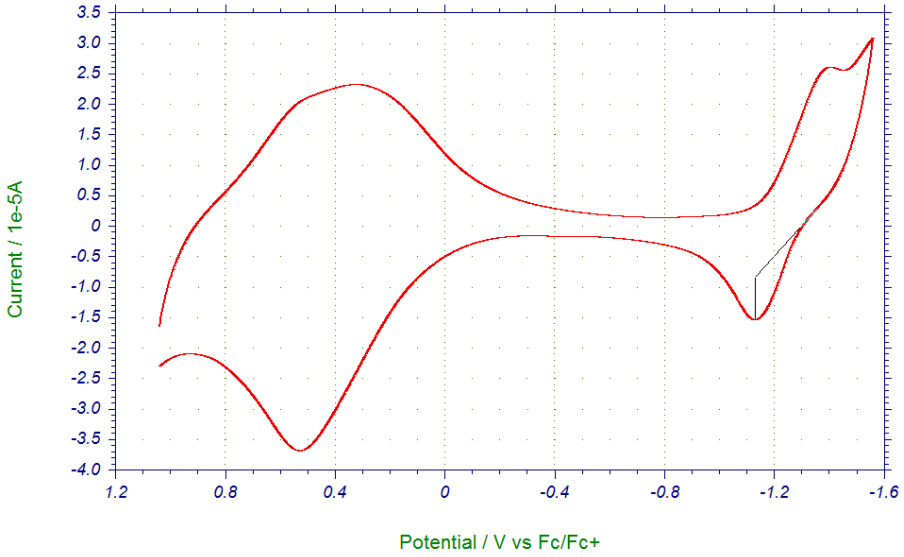

Figure 3.10. Cyclic voltammetry of oligomer **12** (1×10^{-4} M) recorded in CH_2Cl_2, with $TBAPF_6$ (0.1 M) as supporting electrolyte and at a scan rate of 100 mV/s.

Table 3.1. Electrochemical data of monomers and oligomers **12** (1×10^{-4} M) observed by cyclic voltammetry in CH_2Cl_2 solution, with $TBAPF_6$ (0.1 M), all potentials are given *vs.* Fc/Fc^+ redox couple used as internal standard.

Compounds	*Oxidation onset / V*	E_{HOMO} / *eV*	*Reduction onset / V*	E_{LUMO} / *eV*	*Electrochemically determined band gap / eV*
Monomer 12	+ 0.25	- 5.05	- 1.12	- 3.68	1.37
Oligomer 12	+ 0.18	- 4.61	- 1.13	- 3.67	0.95

To investigate the stability of the resulting oligomer **12** towards *p*-doping process, repetitive cycling of the deposited film on the working electrode in free monomer solution was carried out and the results show reasonably stable polymers as shown in Figure **3.11.** In addition, the polymer film displayed reasonably good electrochemical stability upon changing the scan rates. This was determined by plotting scan rates against maximum current of the resulting peak. The obtained linear relationship is shown in **Figures 3.12**.

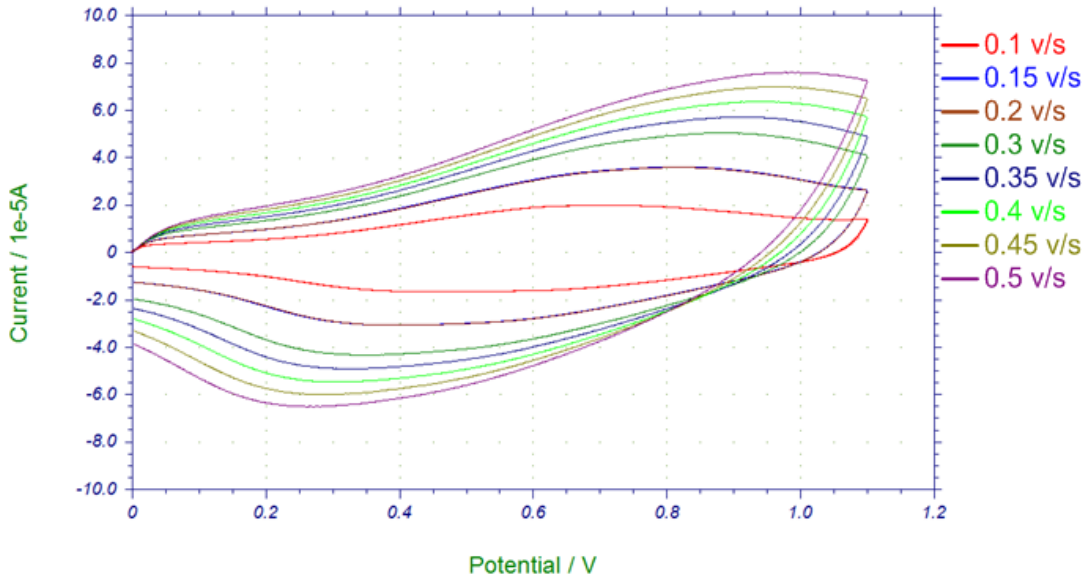

Figure 3.11. Oxidation scans of deposited oligomer **12** on the electrode surface recorded at different scan rates.

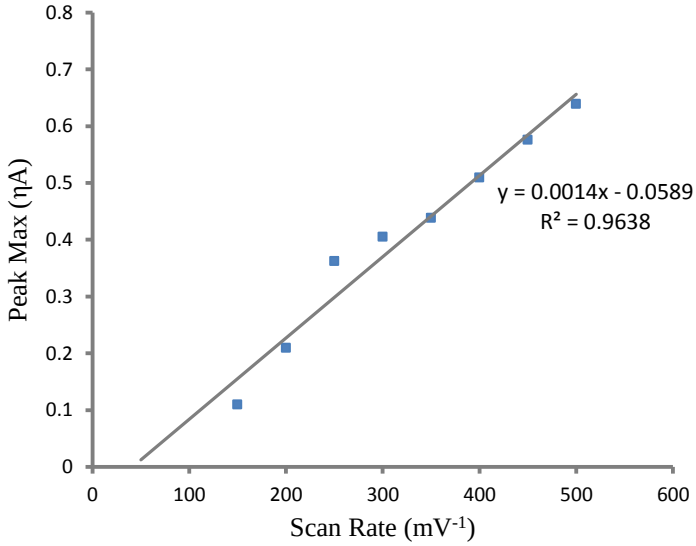

Figure 3.12. Variable scan rate versus maximum current measured for the oligomer formed from monomer **12**.

b) Synthesis and spectroscopy of viologen derivatives featuring thienpyrazine and quinoxaline rings 17, 25 and 26

3.3.4. Synthesis of the compounds

The synthesis of the target molecule **17** is described in **Scheme 3.4**. 2,5-Dibromo-3,4-dinitrothiophene **9** was prepared by the nitration of dibromothiophene **13** using a mixture of fuming nitric and concentrated sulfuric acids. The resulting compound **9** was reacted with 2-(tributylstannyl)-thiophene using a Stille coupling reaction with $Pd(PPh_3)Cl_2$ as a catalyst and tetrahydrofuran THF as solvent and gave dinitro compound **10** in 74% yield. Reduction of the resulting dinitro compound **10** using tin (II) chloride as reducing agent gave diamine compound **11** in 84% yield. Following this reaction, a simple condensation reaction between the diamine compound with 1,10-phenanthroline5,6-dione **15** gave compound **16** in 100% yield. To obtain the target bipyridinium derivative, compound **16** was heated under reflux overnight with 1,2-dibromoethane followed by exchanging the bromine ions with hexaflourophosphate ions (PF_6) and precipitation with petroleum ether gave compound **17** in 23%.

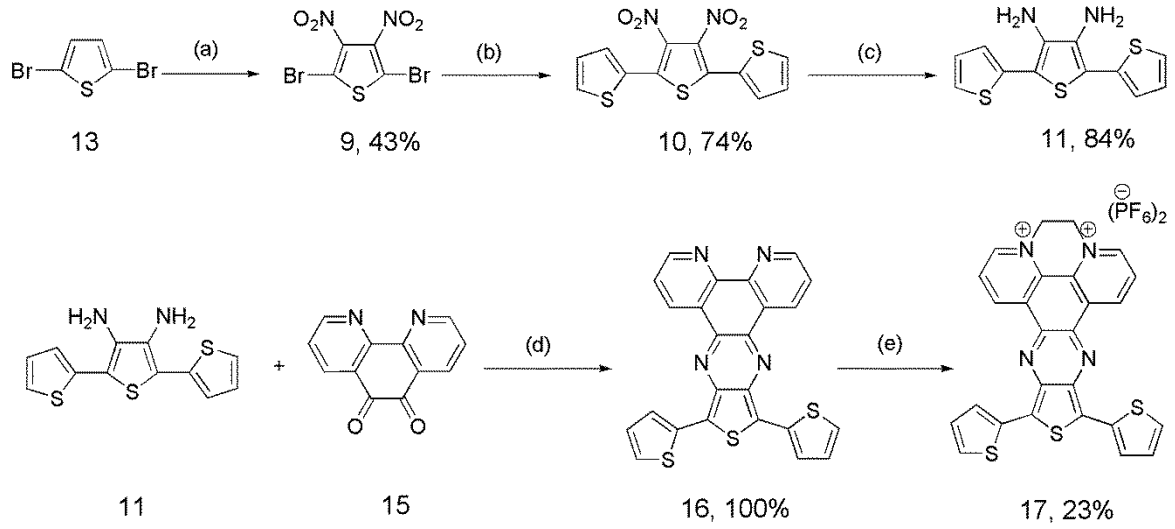

Scheme 3.4. Reagents and conditions: (a) fum. HNO_3: con. H_2SO_4, (b) 2-(tributylstannyl)-thiophene, $Pd(PPh_3)Cl_2$, THF, (c) $SnCl_2$, EtOH: con. HCl: toluene, (d) *p*-toluenesulfonic acid, chloroform, (e) 1,2-dibromoethane, KPF_6.

The synthesis of compounds **25** and **26** is described in **Scheme 3.5** and started from a Suzuki cross coupling of 4,7-dibromo-benzo[1,2,5]-thiadiazole **18** and 3-hexythiophene-2-boronic acid pinacol ester in the presence of $Pd(PPh_3)_4$ as a catalyst. This produced compound **20** in 47% yield. Reduction of compounds **19** (commercially available) and **20**, respectively, using heterogeneous catalytic system $NaBH_4/CoCl_2$ and ethanol as solvent, gave the desired aromatic diamine compounds **21** and **22** in 51 and 75% yield, respectively. To get the target bipyridinium derivatives **25** and **26**, simple reaction between the diamine compounds **21** and **22**, respectively, with phenanthrene-9,10-dione **15** gave compound **23** and **24**, respectively, in good yield. Heating compounds **23** and **24** under reflux in 1,2-dibromoethane overnight and over 48 h, respectively, gave the dibromo salt of the viologen, which after exchanging with hexaflourophosphate ions (PF_6) gave compound **25** and **26** in 45 and 61% yield, respectively.

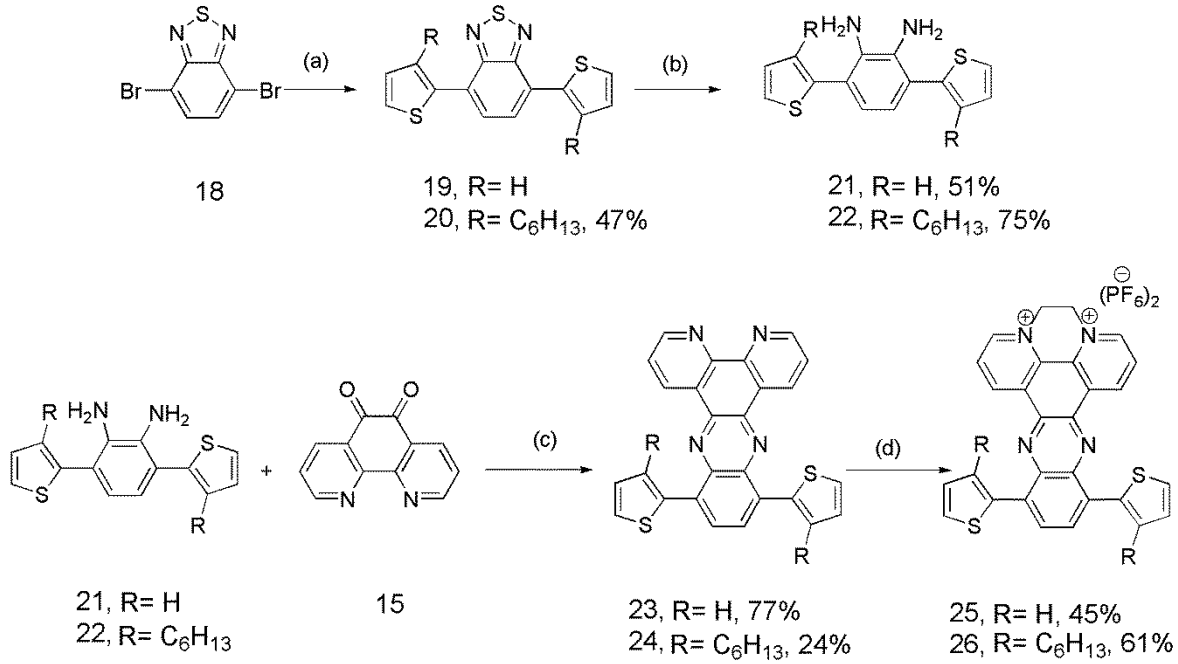

Scheme 3.5. Reagents and conditions: (a) 3-hexythiophene-2-boronic acid pinacol ester, $Pd(PPh_3)_4$, aliquat, Na_2CO_3, N_2 (b) $NaBH_4/CoCl_2$, ethanol, (c) *p*-toluene sulfonic acid, chloroform, (d) 1,2-dibromoethane, KPF_6.

3.3.5. UV-vis spectroscopy of monomers

UV-vis absorption spectra of bipyridinium derivatives **17**, **25** and **26** were recorded in CH_2Cl_2 (1×10^{-5}M). Significant differences in the absorption spectra of resulting compounds were observed (**Figure 3.13**). Compound **25** and **26** featuring a quinoxaline ring displayed two different absorption bands, one of these bands can be attributed to π–π* transition and showed a strong absorption band at 280 nm for compound **25** and a strong and red shifted band at 327 nm for compound **26**. The other absorption band attributed to intramolecular charge transfer (ICT) showed a broad absorption bands maximum around 387-648 nm and resulted in an optically determined band gap of 1.92 eV for compound **25** and 1.75 eV for compound **26**. Whereas compound **17** featuring thienopyrazine ring showed three main peaks in the absorption spectra; two of them in the higher energy region with intensive absorption bands at 280 nm and 366 nm and can be attributed to π–π*

transition and one in the lower energy region maximum a round 600-850 nm and can be attributed to ICT. Compared with compounds **25** and **26**, compound **17** also showed strong bathchromic shift in the intramolecular charge transfer band resulting from increasing the conjugation through the system due to the formation of quinoid structure of thienopyrazine unit and the introduction of phenanthrene unit into the conjugated system which resulted in an optically determined band gap of around 1.29 eV for compound **17**.

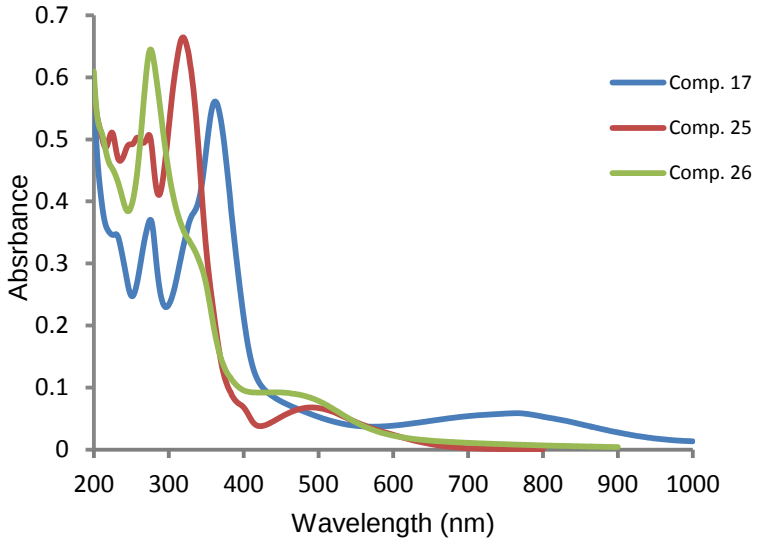

Figure 3.13. UV-vis absorption spectra of compounds **17, 25** and **26** (1×10^{-5}M) recorded in CH_2Cl_2.

3.3.6. Electrochemical and spectroelectrochemical studies

3.3.6.1. Electrochemical studies of monomers

Electrochemical properties of monomer **17** and **25** were studied using cyclic voltammetry. The redox properties of these monomers were carried out in a conventional three electrode cell containing a glassy carbon working electrode, Ag wire as a reference electrode and Pt counter electrode. The samples were prepared in (1×10^{-4} M) in MeCN with $TBAPF_6$ (0.1 M) as supporting electrolyte and the collected data was referenced to the Fc/Fc^{+} redox couple.

Two reduction waves on the reduction scans were observed, a reversible one at $E_{1/2}$= -1.08 V and a quasi-reversible peak at $E_{1/2}$= -1.51V for compound **17** as shown in **Figure 3.14**. Compound **25** exhibited two reversible reduction peaks at $E_{1/2}$= -1.45V and $E_{1/2}$= -1.99V which can be assigned to the two-step reduction of viologen to a neutral species via a cation radical intermediate as illustrated in **Figure 3.15**. During the anodic scan, two quasi-reversible peaks at $E_{1/2}$= + 0.18 and $E_{1/2}$= + 0.83V were observed for compound **17** and two quasi-reversible peaks at $E_{1/2}$= + 0.42 and $E_{1/2}$= + 0.66 V for compound **25**.

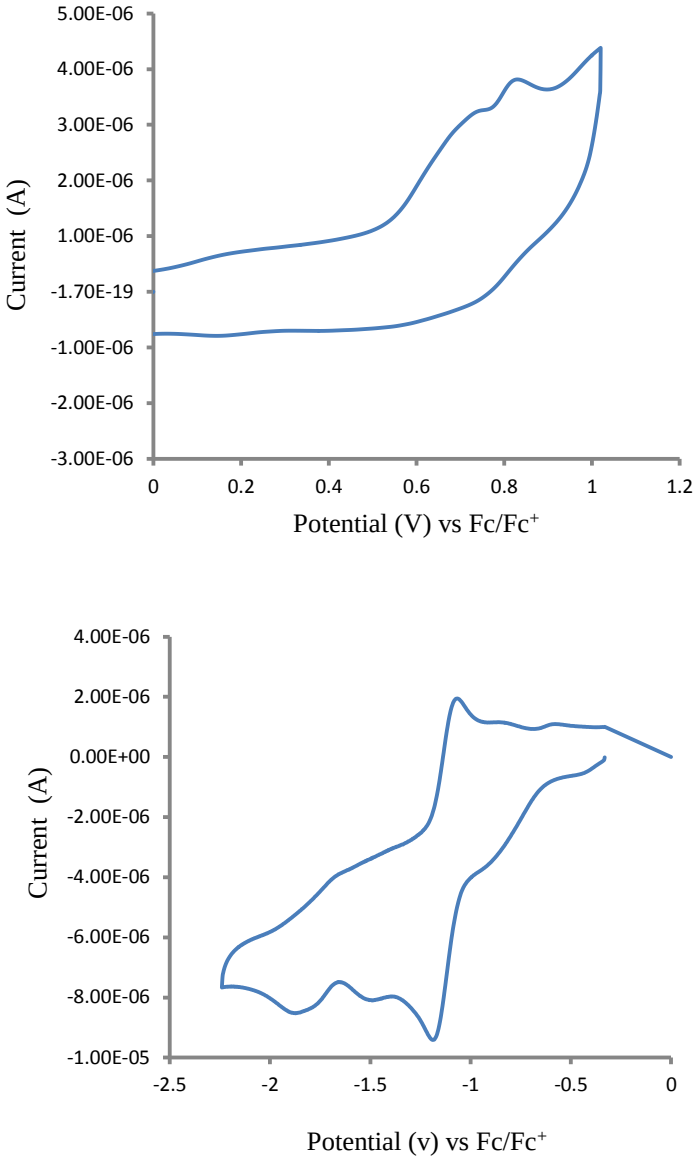

Figure 3.14. Monomer oxidation (up) and reduction (down) of compound **17** (1×10^{-4} M) recorded in MeCN, with $TBAPF_6$ (0.1 M) as supporting electrolyte and at a scan rate of 100 mV/s.

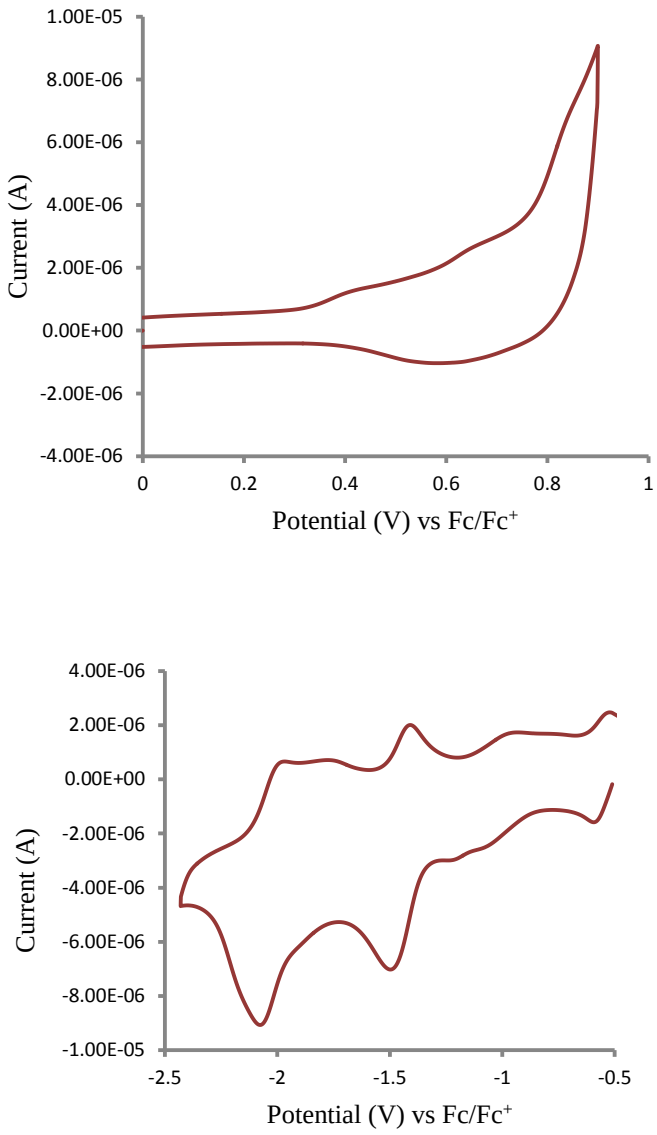

Figure 3.15. Monomer oxidation (up) and reduction (down) of compound **25** (1×10^{-4} M) recorded in MeCN, with $TBAPF_6$ (0.1 M) as supporting electrolyte and at a scan rate of 100 mV/s.

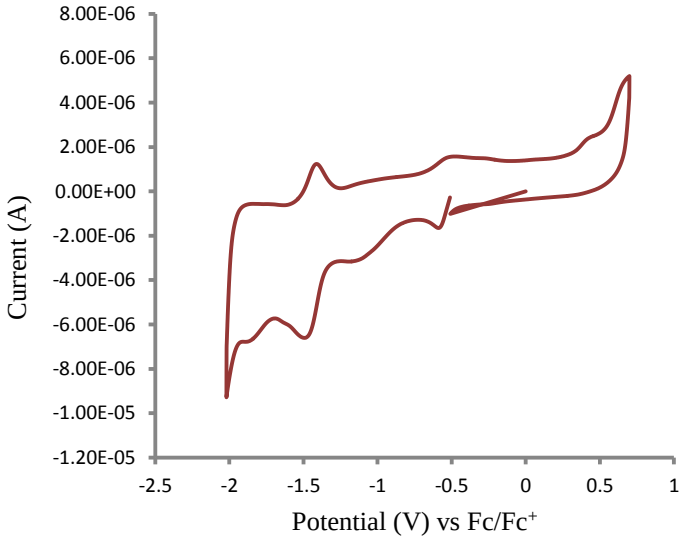

Figure 3.16. Cyclic voltammetry of monomer **25** (1×10^{-4} M) recorded in MeCN, with $TBAPF_6$ (0.1 M) as supporting electrolyte and at a scan rate of 100 mV/s.

3.3.6.2. Electrochemical studies of oligomers

Attempts were made to polymerize both monomers **17** and **25** from solution. The attempts were carried out using a glassy carbon working electrode with a silver wire reference electrode and a platinum counter electrode using a potentioldynamic mode. The potentials were referenced to the Fc/Fc^+ redox couple. The growth of the oligomers was achieved through repetitive oxidation cycles monitored by CV. The growth of the oligomers **17** and **25** over 300 cycles is presented in **Figures 3.17** and **3.17**, respectively, which shows an increase in the current with each cycle and the development of a new peak at a lower oxidation potential corresponding to the formation of a polymer on the electrode surface.

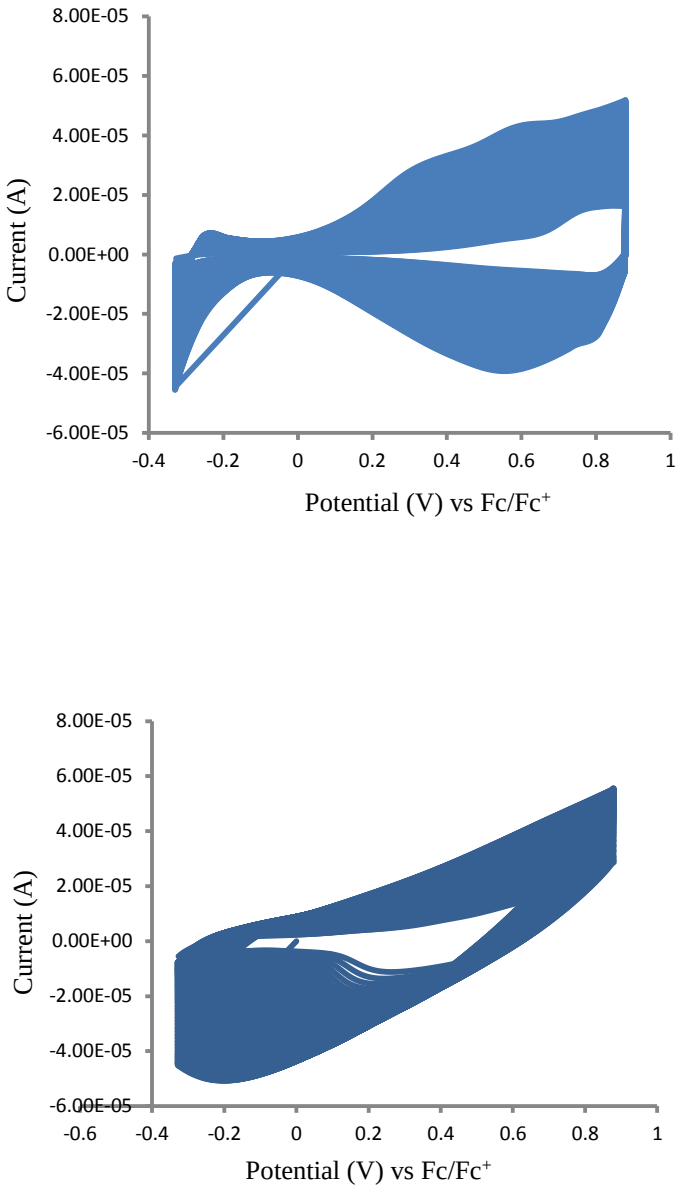

Figure 3.17. Polymer growth of monomer **17** over 300 segments on glassy carbon (up) and ITO slide working (down) as working electrodes.

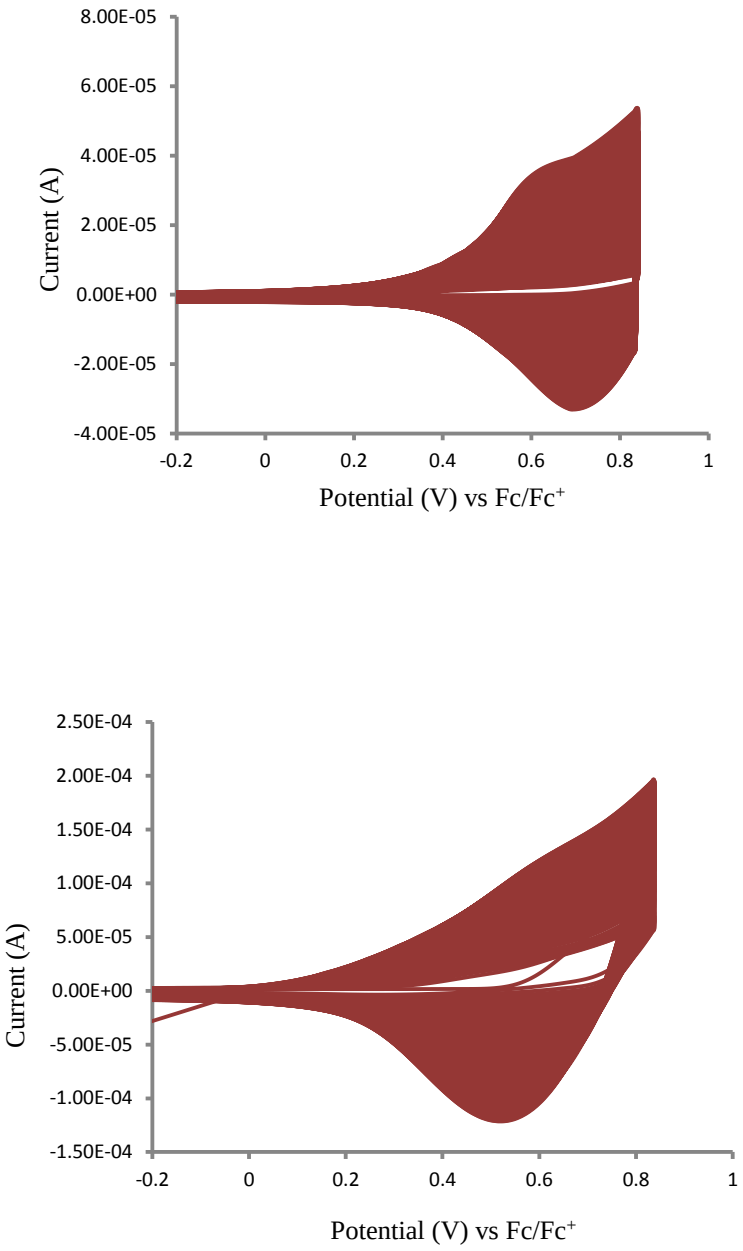

Figure 3.18. Polymer growth of compound **25** over 300 segments on glassy carbon (up) and ITO slide working (down) as working electrodes.

Electropolymerization for both monomers was also carried out into a ITO slide instead of glassy carbon working electrode. The coated electrode was transferred into a solution of monomer free electrolyte in MeCN solution for electrochemical study using same potential scan. The results are shown in **Figure 3.19**. Two quasi-reversible oxidation peaks at $E_{1/2}$= + 0.24 and + 0.59 V and two reversible reduction waves at $E_{1/2}$= -1.24 V and $E_{1/2}$= -1.79 V corresponding to the two-step reduction of the diquat moiety of oligomer **17**. The approximate electrochemically determined band gap calculated from the oxidation and reduction onset potentials of the polymer is 0.87 eV.

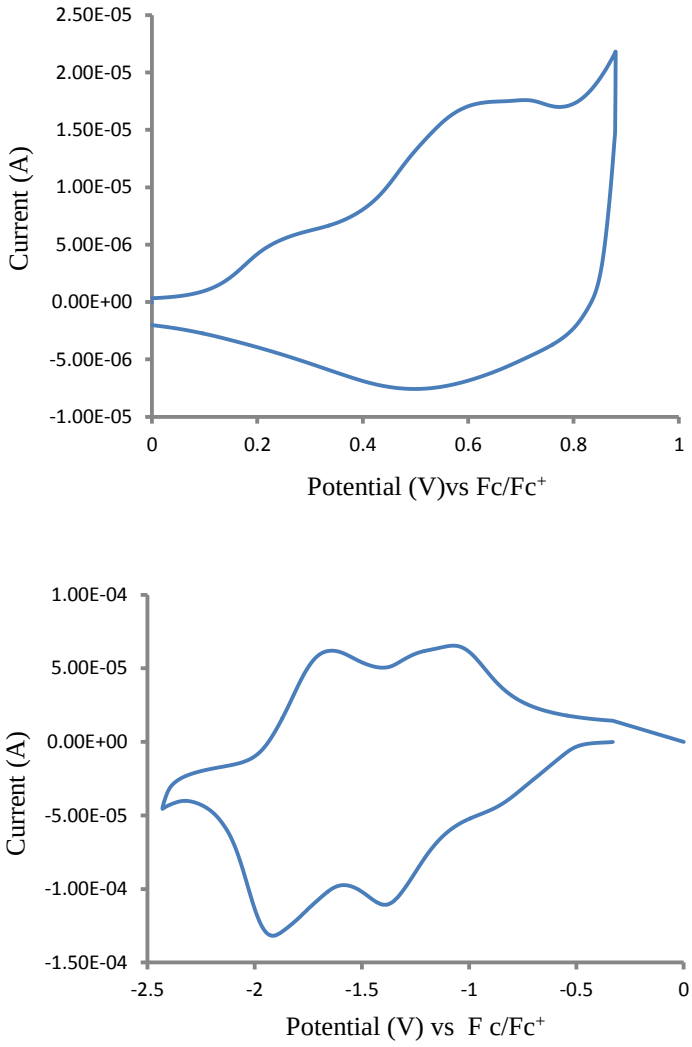

Figure 3.19. Polymer oxidation (up) and reduction (down) for compound **17** in monomer free MeCN solution.

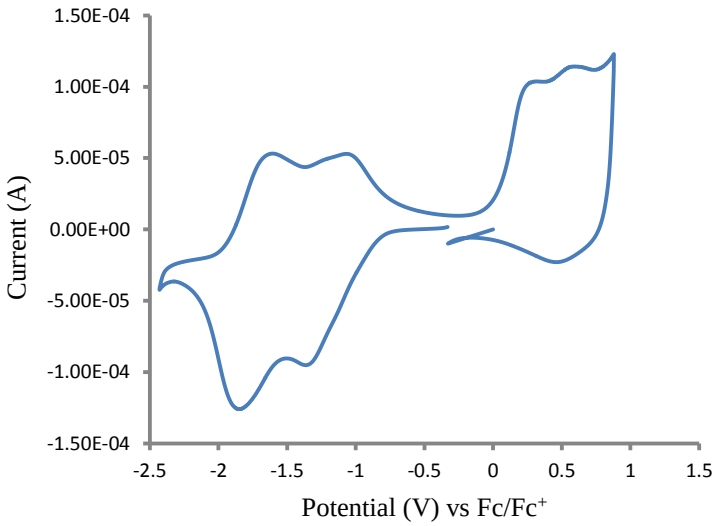

Figure 3.20. Cyclic voltammetry of oligomer **17** (1×10^{-4} M) recorded in MeCN, with $TBAPF_6$ (0.1 M) as supporting electrolyte and at a scan rate of 100 mV/s.

The CV of the resulting oligomer **25** displayed a quasi-reversible oxidation peak at $E_{1/2}$= + 0.53 V, and a shoulder at $E_{1/2}$= - 1.43 V and two reversible reduction waves at $E_{1/2}$= -1.68 V and $E_{1/2}$= - 2.16 V corresponding to the reduction of the diquat moiety of oligomer **25** as shown in **Figure 3.21**. The observed cathodic shift for compound **25** indicates the donating ability of quinoxaline unit compared with thienopyrazine unit. The electrochemically determined band gap calculated from the onset of the oxidation and reduction waves is 1.79 eV.

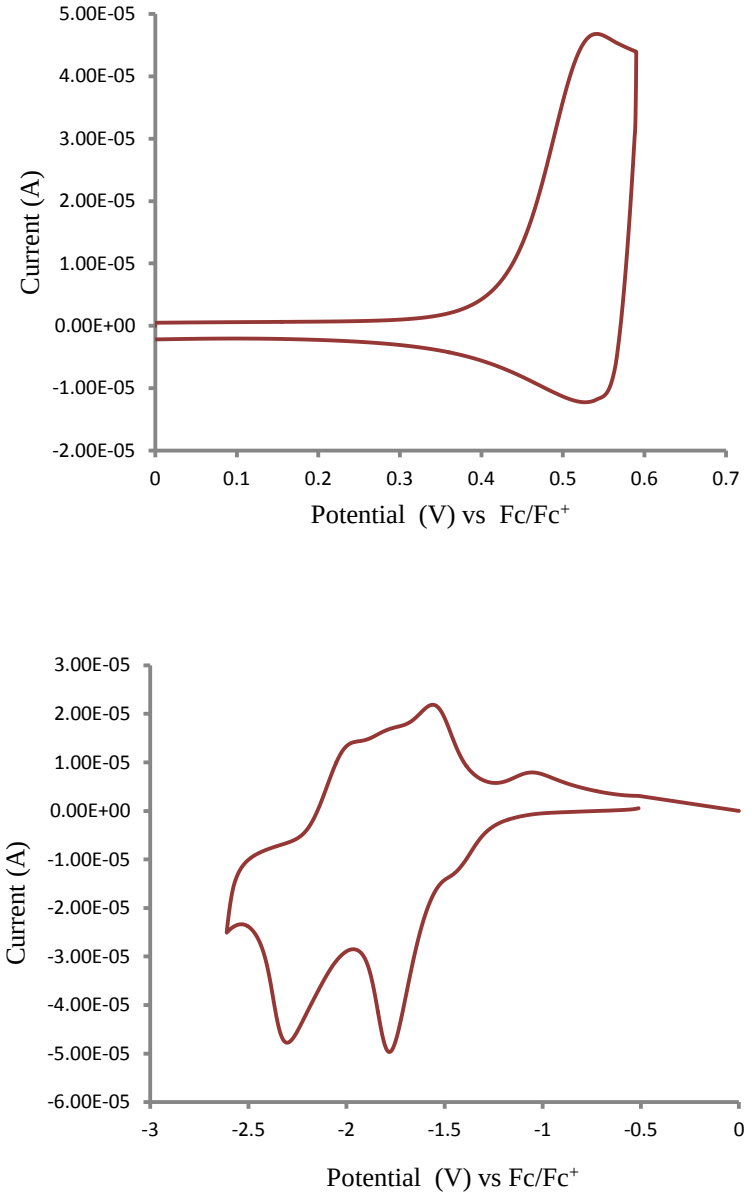

Figure 3.21. Polymer oxidation (up) and reduction (down) for compound **25** in monomer-free MeCN solution.

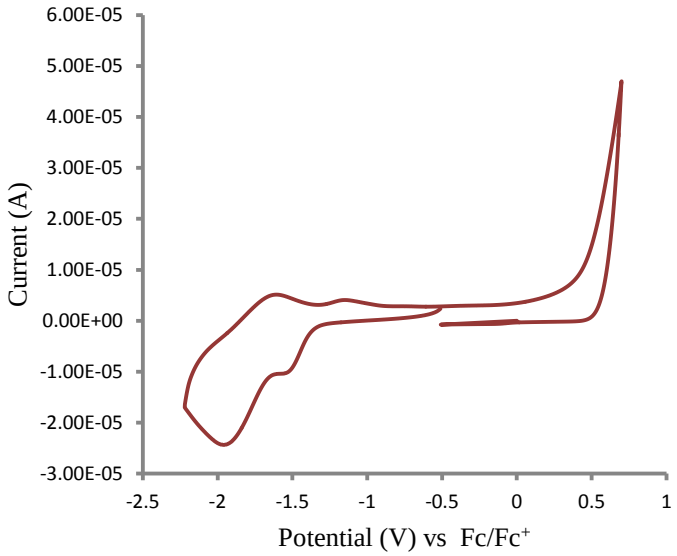

Figure 3.22. Cyclic voltammetry of polymer **25 (**1×10^{-4} M) recorded in MeCN, with $TBAPF_6$ (0.1 M) as supporting electrolyte and at a scan rate of 100 mV/s.

Table 3.2. Electrochemical data of monomers and oligomers **17** and **25** (1×10^{-4} M) observed by cyclic voltammetry in MeCN, with $TBAPF_6$ (0.1 M), all potentials are given vs. Fc/Fc^+ redox couple used as internal standard.

Compounds	*Oxidation onset / V*	E_{HOMO} / *eV*	*Reduction onset / V*	E_{LUMO} / *eV*	*Electrochemically determined band gap / eV*
Monomer 17	+ 0.12	- 4.92	- 0.60	- 4.20	0.72
Monomer 25	+ 0.30	- 5.10	- 1.34	- 3.46	1.64
Oligomer 17	+ 0.02	- 4.82	- 0.85	- 3.95	0.87
Oligomer 25	+ 0.43	- 5.23	- 1.36	- 3.44	1.79

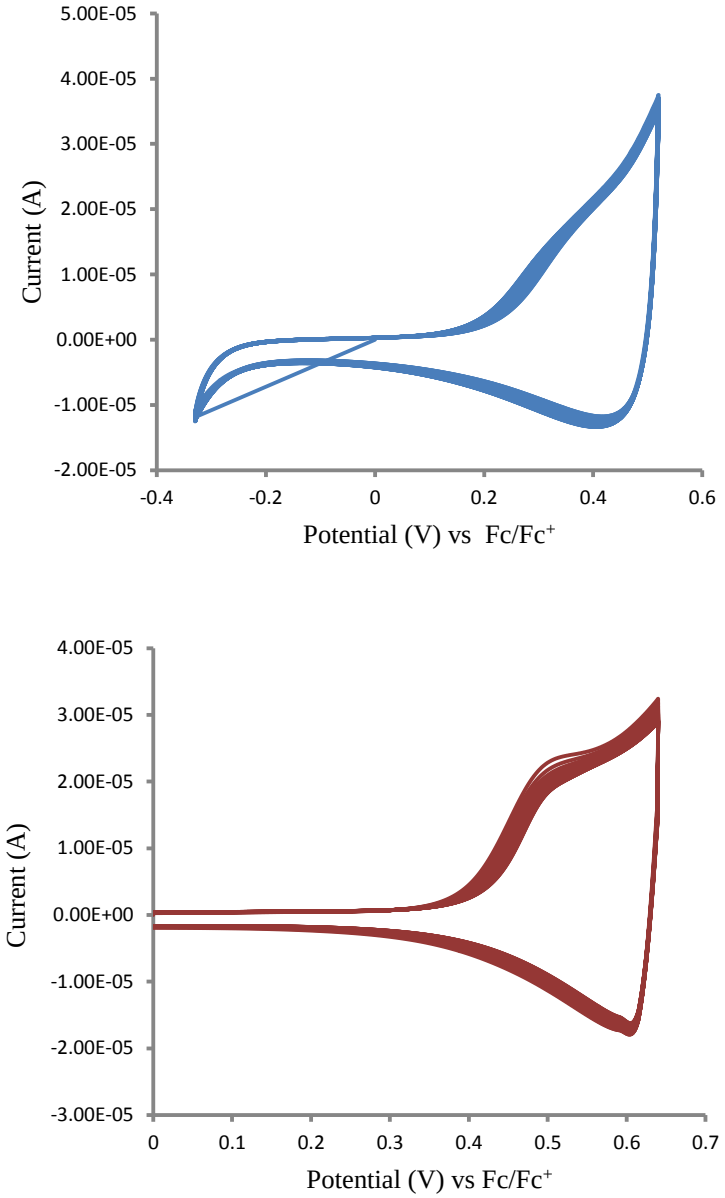

Figure 3.23. Oxidation stability of polymer **17** (up) and **25** (down) over 100 segments.

To investigate the stability of the resulting polymers **17** and **25** towards *p*-doping process, repetitive cycling over 100 cycles on the oxidation potential scans of the deposited film on the ITO slide in free monomer solution was carried out and the results show reasonably stable polymers Figure **3.23**. In addition both films of **17** and **25** displayed reasonably good electrochemical stability upon changing the scan rates as shown in **Figures 3.24** and **3.26**. This was determined by plotting the relationship between scan rates against resulting

maximum peak current. The obtained linear relationship is shown in **Figures 3.25** and **3.27.**

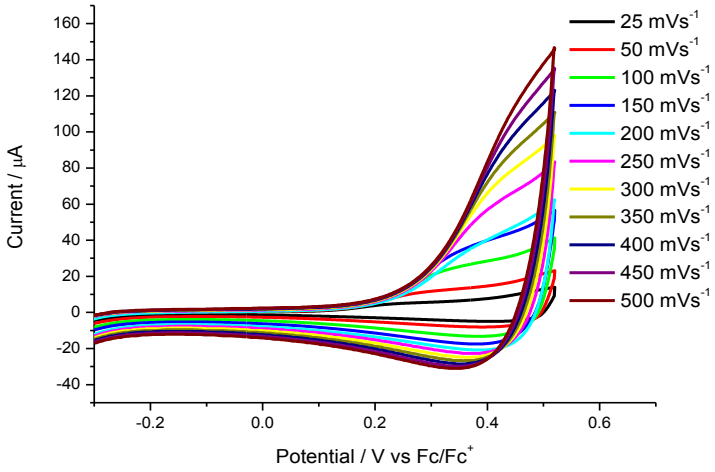

Figure 3.24. Oxidation scans of deposited oligomer **17** on electrode surface recorded at different scan rates.

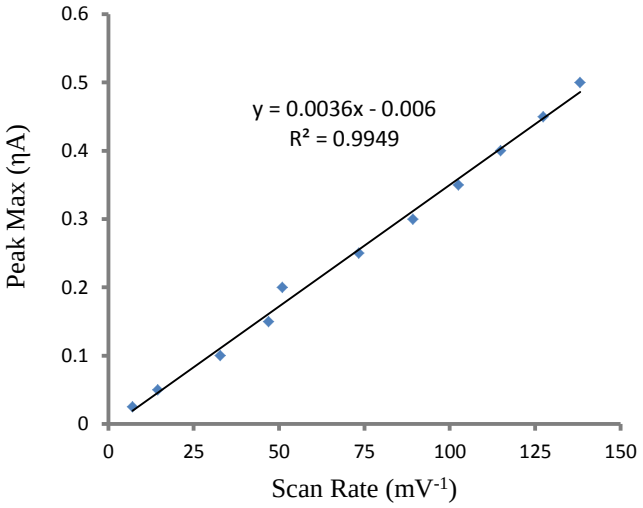

Figure 3.25. Plot of scan rate versus maximum current measured for polymer formed from compound **17**.

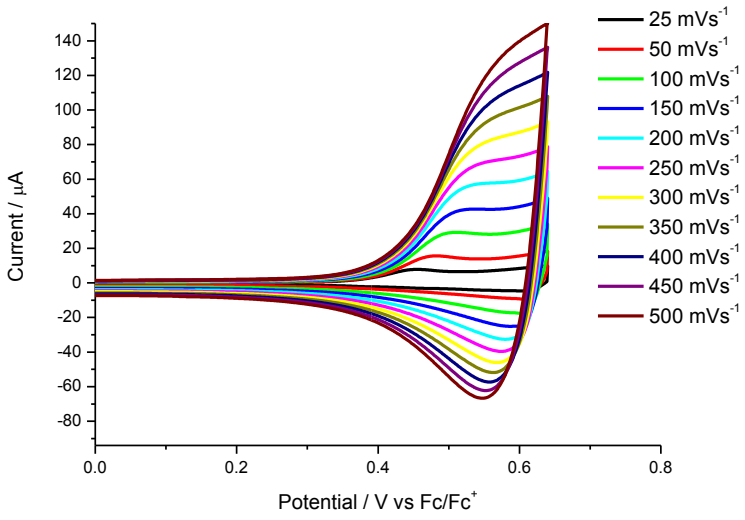

Figure 3.26. Oxidation scans of deposited oligomer **25** on electrode surface recorded at different scan rates.

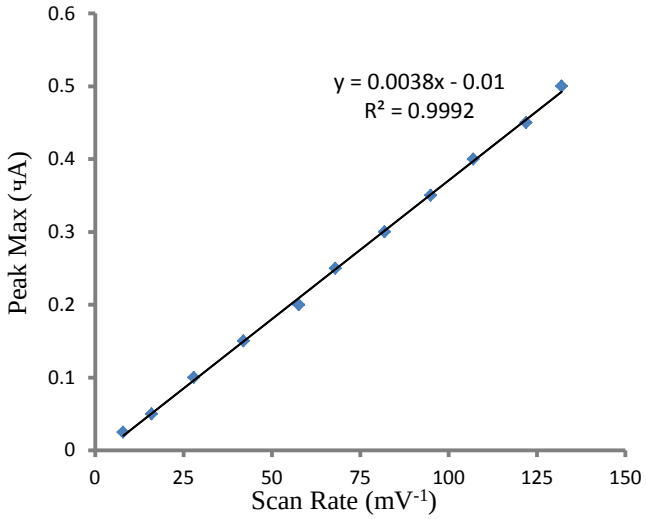

Figure 3.27. Plot of scan rate versus maximum current measured for polymer formed from compound **25**.

The absorption spectra of polymer **17** and **25** were obtained from thin films on an ITO coated glass slide. By cycling the potential between 0 and 1200 mV vs. Fc/Fc^{+} the polymers were de-doped. The UV-vis spectra of polymer **17** showed a maximum peak λ_{max} at 755 nm attributed to π-π* transition from the conjugated chain of the polymer as shown in **Figure 3.28**. The optically determined band gap of 1.24 eV is slightly lower than the determined optical band gap for the monomer 1.29 eV. In addition, the bathochromic shift of the π-π* transition band for oligomer **17** of around 122 nm compared to polymer **25** is assigned to an increase in the delocalization of π-electrons along the thienpyrazine unit due to the formation of a quinoid structure.

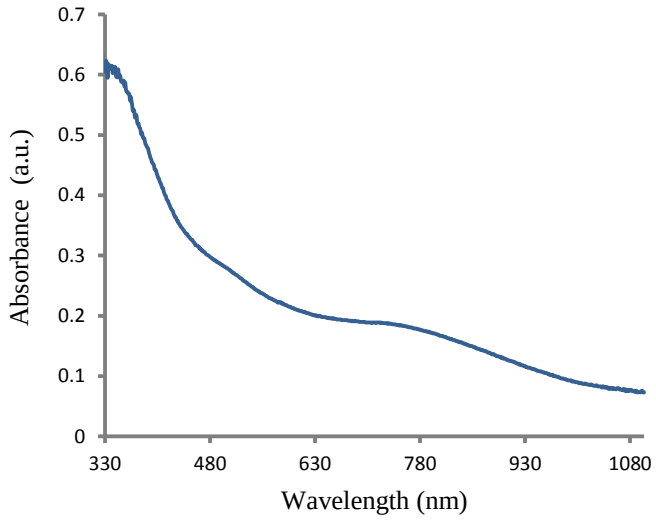

Figure 3.28. Solid state absorption spectrum of polymer **17** on ITO-coated glass.

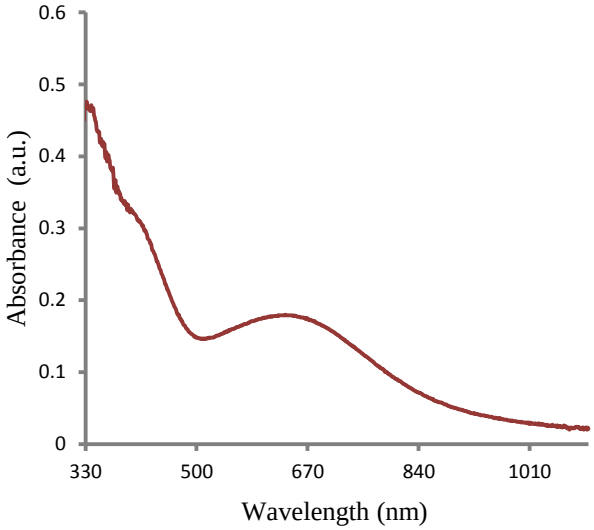

Figure 3.29. Solid state absorption spectrum of polymer **25** on ITO-coated glass.

For polymer **25**, by cycling between 0 and 1330 mV vs. Fc/Fc^{+} the film was de-doped and UV-vis spectra displayed a broad peak at 632 nm which can be attributed to π-π* transition as it shown in **Figure 3.29** and resulted in an optically determined band gap of 1.43 eV. This is lower than the optically determined band gap of the monomer 1.92 eV.

The UV-vis spectroelectrochemical measurements of the deposited polymer **25** on ITO glass slide were also investigated in monomer-free solution during the oxidation process and the electronic absorption spectra of the film at different potentials are summarised in 3D plots in **Figure 3.30**.

During potential cycling, the spectroelectrochemical plot shows further bathchromic shift and generation of a new broad absorption band in the region of 800-1100 nm at the same time of losing the intensity of π-π* band at 820 nm which indicates the formation of delocalised polaron species within the oligomer chain.

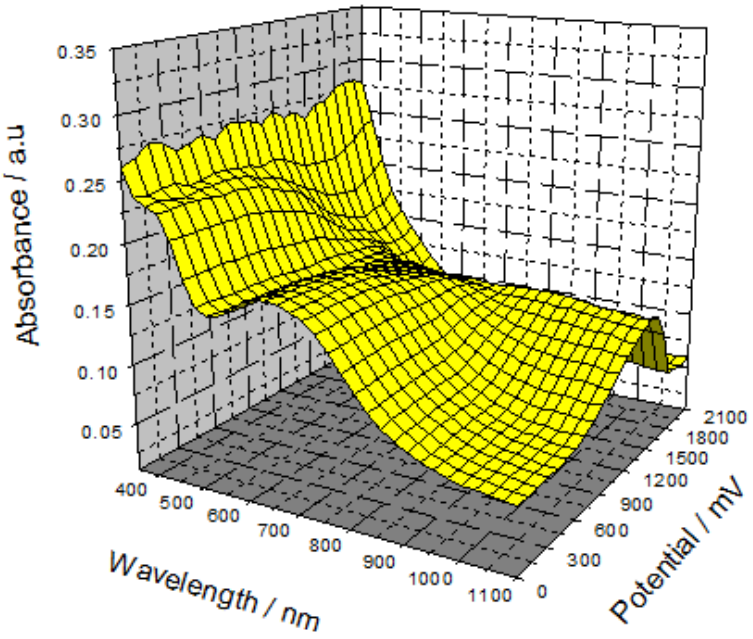

Figure 3.30. 3D absorption spectroelectrochemical plots for oligomer **25** as a thin film on ITO coated glass.

3.4. Conclusions and future work

3.4.1. Conclusion

Oligomers featuring bipyridinium unit with different thienopyrazine and quinoxaline moieties have been successfully synthesised and electropolymerized to investigate the effect of these moieties have on the energy levels and the band gap of resulting oligomers. The UV-vis results suggested that enhanced intramolecular charge transfer was achieved by incorporating thienopyrazine moiety into the oligomer backbone due to the formation of

quinoid structure of the thienopyrazine unit. Electropolymerization of both compounds **17** and **25** was successfully achieved through repetitive oxidative cycling.

The spectroelectrochemical plot of compound **25** indicated the generation of a new broad absorption wave between 800-1100 nm, whilst at the same time losing the intensity of π-π* transition band at 820 nm which indicates the formation of delocalised polaron species within the oligomer chain.

3.4.2. Future work

With more time available, an extension to the work could focus upon forming new conjugated polymers by chemical polymerisation using Stille and Suzuki coupling with appropriately functionalised viologen systems. Additional investigations could be carried out to examine the conductivity of the resulting polymer systems and the possibility of applying them to photovoltaic applications.

3.5. Acknowledgements

The author gratefully acknowledges Saadeldin Elmasly and Prof. Peter Skabara from the University of Strathclyde, Scotland, for assisting in the CV and polymerisation studies.

Chapter 4;

Optical and electrochemical properties of new push-pull chromophores.

4.1. Introduction

4.1.1. Nonlinear optical materials

The discovery of two-photon fluorescence in 1961 by pumping a quartz inorganic crystal with intense laser source has raised the interest of developing new second order nonlinear materials for use in optoelectronic applications.[128] In addition to this phenomenon in inorganic material such as lithium niobate ($LiNbO_3$) and potassium dihydrogenephosphate (KDP), nonlinear organic materials have undergone significant development in recent years. The key advantages of these materials include the improvement in the conductivity, processability and response time as well as the resistance to optical damage.[129]

Applying a strong electric field on molecules featuring polarizable electron density causes two types of NLO phenomena. Depending on the wavelength of the incident laser's light, occurrence of these phenomena can take place simultaneously through either perturbation of the ground state of the molecules, which can lead to second and third harmonic generation. Alternatively the promotion of electrons from ground state to the first or other excited states by absorption of two or multi different frequency photons has led to the formation of resonant nonlinear optical phenomena as shown in **Figure 4.1**.

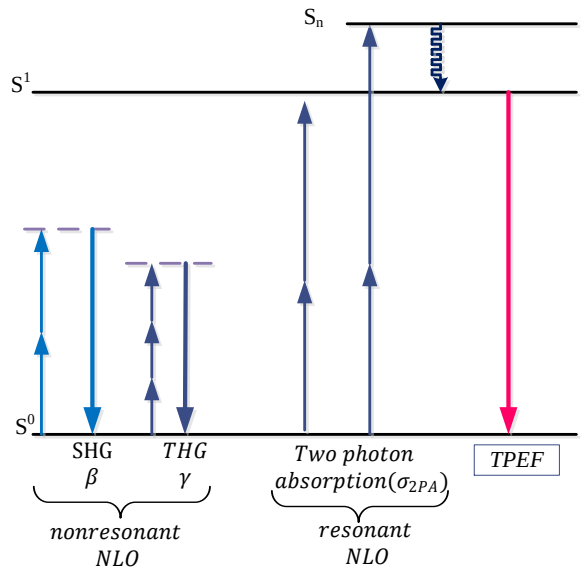

Figure 4.1. Jablonski diagram of NLO phenomena.[130]

The principle concept of nonlinear optics in a molecule involves forming new electric fields. The new resulted fields have different physical properties compared with the applied electromagnetic field (E) due to the interaction with the polarisable electron density of the molecules. Depending on the strength of the applied electromagnetic field, fluctuation in the electrons occurs and a dipole moment will be formed. Increasing the field leads to an increase in the dipole moment giving rise to a nonlinear response. The formed polarization (dipole moment) response can be expressed in equation **(4-1)**;

$$\Delta\mu = \alpha E + \beta E^2 + \gamma E^3 + \cdots \qquad (4\text{-}1)$$

Whereas α represents linear polarisability, and β, γ represents first and second hyper-polarisability, respectively.[130]

However, there are strict requirements for optoelectronic devices in terms of supplying materials with high processibility, thermal, mechanical and environmental stability as well as strong sensitivity to the applied electromagnetic fields. Therefore, focusing on building and modification of the structure of organic materials could contribute to achieving highly polarisability materials with strong sensitivity to the applied electromagnetic field.[131]

Noncentrosymmetry molecules having the ability to show intense intramolecular charge transfer is one of the criteria to achieve second order NLO organic molecules. The other criterion is the molecules should posse high molecular hyperpolarzability β. Therefore, a typical organic structure (D–π–A) consisting of strong electron donors (D) and strong electron acceptors (A), separated by a π-conjugated system is considered as a typical blueprint for NLO molecular components to be used in optoelectronic applications. Compounds of this type provide successful strategies to build polarisable molecules with intense and low energy intramolecular charge transfer and large values of second order electronic hyperpolarizability (β).[132]

Urea and their derivatives play important role in preparing second order materials with high photo-induced electron transfer due to the existence of lone electrons pairs giving them the property to be the simplest and readily available electron rich functional group. These materials provides hyperpolarizability (β) values of around 0.5×10^{-30} esu for urea determined by the electric field induced second harmonic (EFISH) technique. However, *p*-nitro aniline (PNA) and 4'-dimethylamino-4-nitrostilbene (DANS) showed prototypical organic nonlinear materials possessing a high hyperpolarzability β values of 34.5×10^{-30} esu for (PNA) and 248×10^{-30} esu for (DANS) by increasing the conjugation between the donor unit (Me_2N) and acceptor unit (NO_2) (**Figure 4.2**).[133]

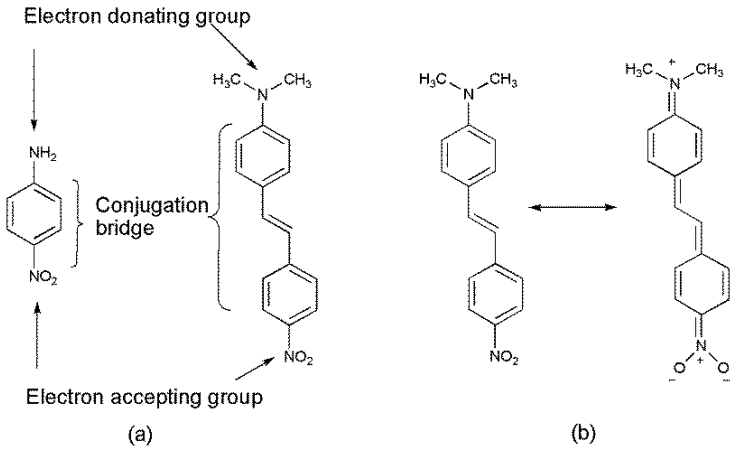

Figure 4.2. (a) Typical π-conjugated organic donor-acceptor chromophores; (b) charge transfer between donor and acceptor units.

An investigation of the hyperpolarizabilities of organic molecules was carried out on D-A substituted diphenyl polyenes **4.1** using EFISH and third harmonic generation (THG) techniques **Table 4.1**. The results showed that both β, γ are sensitive to the π-electron delocalization from one repeat unit to another in the molecular structure, whereas the nature of donor and acceptor affect the β value. Thus, for designing third order material two factors should be taken into account; controlling the absorption edges toward near IR region by choosing a strong donor and acceptor at the same time maximizing the γ value either by increasing the conjugation length. Alternatively designing molecules with multiple donor or acceptor substitutions which assist in increasing the electron density of the π-system in the donor system or creating a polarizing state toward the end of the π-system.[134]

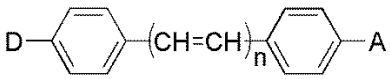

4.1

Table 4.1. β and ɤ values for D-A substituted diphenyl Polyenes.[134]

n	*D*	*A*	λ_{max}*(nm)*	*β(*10^{-30}*esu)*	*ɤ (*10^{-36}*esu)*
1	MeO	CN	340	19	54
2	MeO	CN	360	27	122
3	MeO	CN	380	40	234
1	MeO	NO_2	376	34	93
2	MeO	NO_2	397	47	130
3	MeO	NO_2	414	76	230
4	MeO	NO_2	430	101	-----
1	Me_2N	NO_2	430	73	225
2	Me_2N	NO_2	442	107	-----
3	Me_2N	NO_2	458	131	-----
4	Me_2N	NO_2	464	190∓ 50	-----

4.1.2. Bulk heterojunction devices based push-pull system

BHJ device is one of the most significant device architectures for organic solar cells. The device architecture and the working principles are described in more details in chapter one. The donor-acceptor blend in BHJ devices results in increasing the interpenetrating network between the two components at the same time assisting in providing large exciton diffusion interfaces in the area not far from the absorption area which helps to increase the power conversion efficiencies of the polymeric donor to be around 6-8 %. However, the improvement in the efficiencies of polymeric devices encountered a number of difficulties such as low stability and low reproducibility as well as problematic purification due to the growth in the molecular weight and poor solubility of the resulting polymer. Although only around 4 % PCE has been achieved for BHJ devices constructed using small molecules,

the resulting device has raised a number of attractive advantages compared with polymeric systems including higher charge carrier mobility, well-defined molecular structures as well as the ability to purify and produce these materials in large scale.[135, 136]

4.1.3. Non-planar push-pull system

Controlling the morphology of the resulting thin film in optoelectronic applications is a crucial issue associated with increasing the PCE. Therefore, instead of using planar D-π-A compounds which tend to form crystalline thin films and causes trapping of impurities between the blend of D-A components, non-planar compounds raises the possibility of forming amorphous thin films with a number of advantages such as good processability, optical transparency and homogeneous properties as well as increasing solubility and resisting aggregation.[137]

Increasing the intramolecular charge transfer from the donor moiety to acceptor moiety can effectively expand the absorption band into the near-IR region, leading to better adsorption of the low energy photons in the solar spectrum. Since increasing in ICT between the donor and acceptor molecules depends on the strength of associated units, the length and nature of π-conjugated spacer, tuning these parameters will optimize the energy levels and the optical band gap of the designed molecules. In addition, modification the nature of the donor and acceptor units of these molecules assists in improving the physical and chemical properties such as solubility, thermal and photoelectric properties.[138]

In this regard, *N*,*N*-dialkyl aniline compounds have significant features (i.e. strong donating ability, separated hole stability and hole transporting capability), and therefore may be considered as a promising units in preparing solution processed small molecules for BHJ devices. This is particularly true if coupled to powerful acceptors such a tetracyanoethene (TCNE), 7,7,8,8-tetracyano-*p*-quinodimethane (TCNQ) and DCV. These acceptor units can react with electron-rich alkynes to form promising nonlinear optic materials via [2 + 2] cycloaddition reaction in nearly quantitative yield without the need of catalyst. This reaction is followed by electrocyclic ring opening of the formed cyclobutenes to form donor-substituted 1,1,4,4-tetracyanobuta-1,3-dienes[139] as illustrated in **Scheme 4.1**.

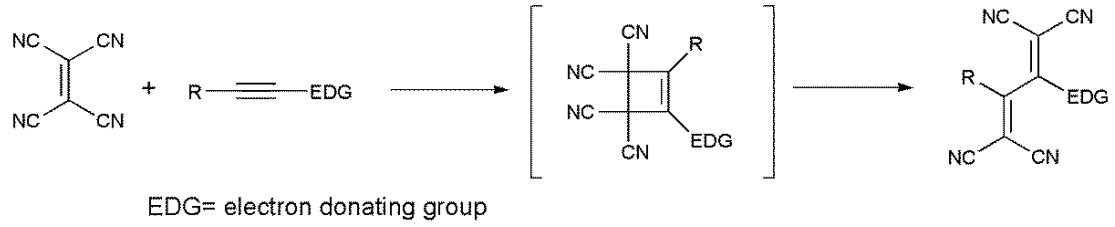

Scheme 4.1. Reaction between TCNE and an alkyne, substituted with an electron-donating group (EDG).

The mechanism of the [2 + 2] cycloaddition reaction between donor-substituted alkyne and 1,1-dicyanoethene (DCE) has been studied computationally using density functional methods in the gas phase. The mechanism shown in **Scheme 4.2** revealed the formations of four basic steps starting with the formation of two transition intermediate states with a small barrier energy difference. The first transition state was formed with a high energy γ-β bond formation resulting from the nucleophilic addition of the γ-carbon in donor-substituted alkyne to the β-position of the alkene. Then a closed ring product is formed in the second transition state with a lower energy value compared with the first transition state. The second transition state was formed through cyclisation process leading to α-δ

bond formation. The process is followed by highest energy consumption to break α-β bond and forming a *cis*-push-pull chromophore. Transition state between *cis* and *trans* configuration occurs through a low energy barrier, therefore, due to the stability of *trans* conformer, the mechanism concludes with the formation of a stable *trans* conformer push-pull chromophore.[138]

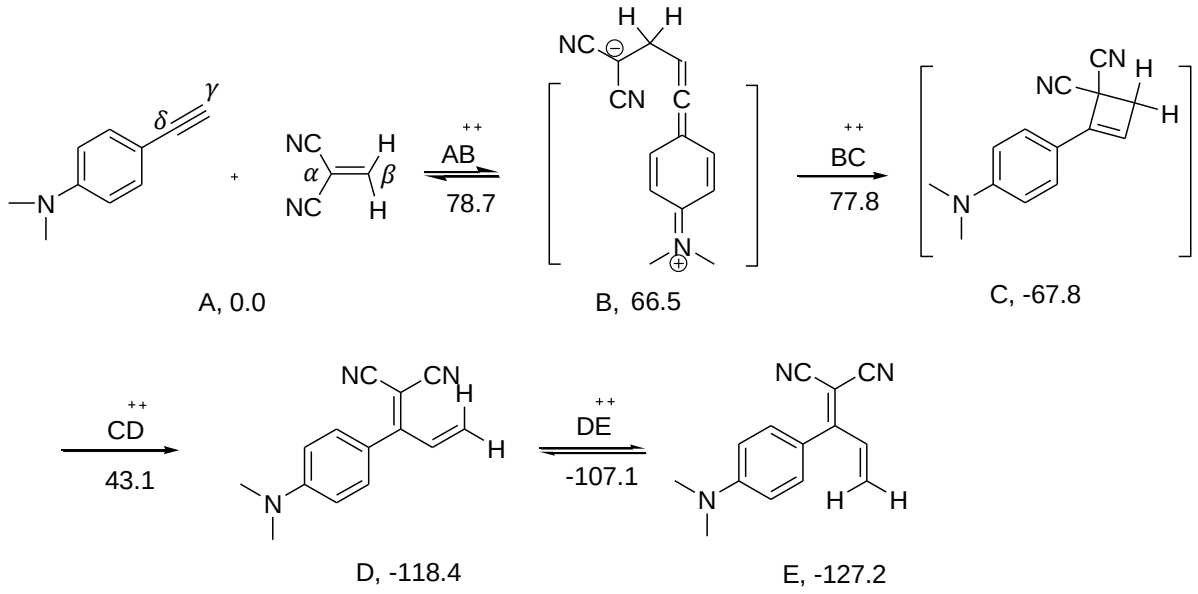

Scheme 4.2. Proposed mechanism of the reaction between 1,1 dicyanoethane and dimethylaniline with calculated free energy from B3LYP/6-31G.[138]

Michinobu and co-workers studied the reactivity between different electron rich substituted alkynes and TCNE (**Figure 4.3**). These investigations revealed that the reaction conditions depend strongly on the strength of the donor moieties as well as the steric hindrance of the compounds. Comparing the reactivity of *para, ortho or meta–N,N*-dimethyl aniline (DMA) derivatives with TCNE, effective reactions at room temperature in quantitative yield was mainly observed for *para*-dimethyl aniline substituted alkynes **4.2**. *Meta* and *ortho* derivatives did not react at room temperature instead harsh conditions were required to complete the reactions due to poorer electron donating ability of *meta*-derivatives and

steric hindrance in case of *ortho* compounds. In addition, the reactivity of TCNE was studied on *para*-dimethyl aniline systems featuring two triple bonds which showed that the closest triple bond to the *para*-dimethyl aniline unit was the most reactive.

This work also examined the reactivity of weaker electron donating groups such as 2-thienyl compound **4.3** and *para*-methoxy functionalized compound **4.4** toward cyclo-addition reaction with TCNE. The reactions of these weaker donating derivatives with TCNE required high temperature in order to complete the transformation.[139]

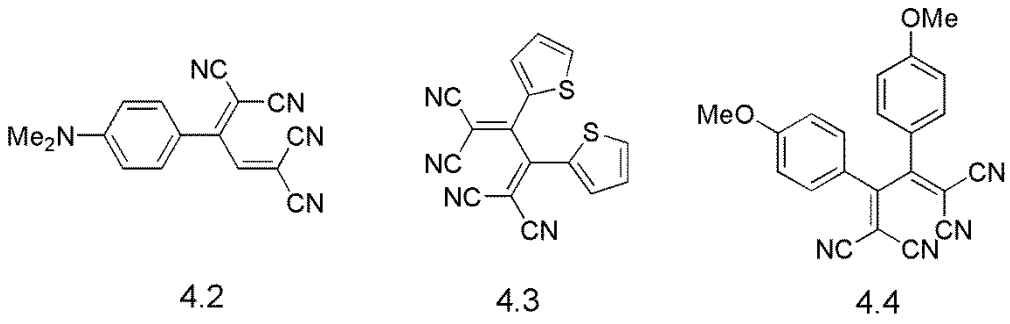

Figure 4.3. Molecular structures resulting from cycloaddition reaction of different alkynes.

4.1.4. Multiple donor and acceptor push-pull system

Variation in the number and position of cyano units on a series of 1,1-dicyano-4-[4-(diethylamino)phenyl]buta-1,3-dienes was investigated in order to identify the affects of the cyano substituent on the optical and electrochemical properties of resulting chromophores. Bathchromic shift and increase in the intensity of the intramolecular charge transfer band were observed with increasing number of cyano groups. However, compound **4.10** showed low intensity and energy transfer bands indicating strong non-planarity in the buta-1,3-diene backbone. In addition, attaching DMA compounds causes a strong bathochromic shift in the UV-vis spectra due to the formation of quinoid character and reflecting the high planarity of the π-conjugation chromophores. Anodic shift was also observed for the oxidation and reduction peaks upon increasing the number of cyano group on the π-conjugated butadiene backbone.[140]

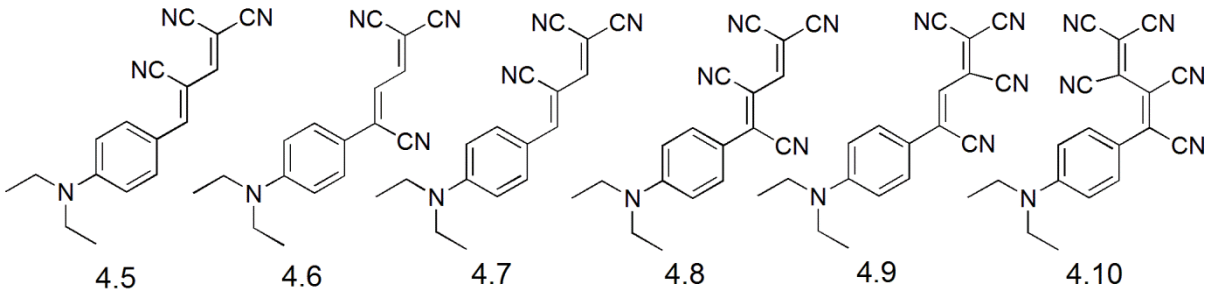

Investigation of structure-activity relationships for increasing the hyperpolarazability of molecules revealed that high third order optical nonlinearity of molecules resulted from two different factors: (i) the efficiency and extinction of donor and acceptor conjugation path way could be improved by utilizing low molecular symmetry and a two dimensional conjugation system; (ii) the energy of the longest charge transition wavelength. For example, high nonlinear efficiency was observed in a series of push-pull organic donor-

substituted cyanoethynylethene molecules (**Figure 4.4**). In these systems, DMA represents the donor unit and cyano group acts as acceptor units which are separated by a two-dimensional conjugated system forming three possible conjugation paths as illustrated in compound **4.13.** The third-order molecular polarizability of these molecules reaches around 3.8×10^{-33} esu, which corresponds to 1.7×10^{-48} m^5 V^{-2} per delocalized electron. This study revealed that the high hyperpolarazability value does not depend on the strength of the donor and acceptor unit as the conjugation between them appears to play a more important role.[141]

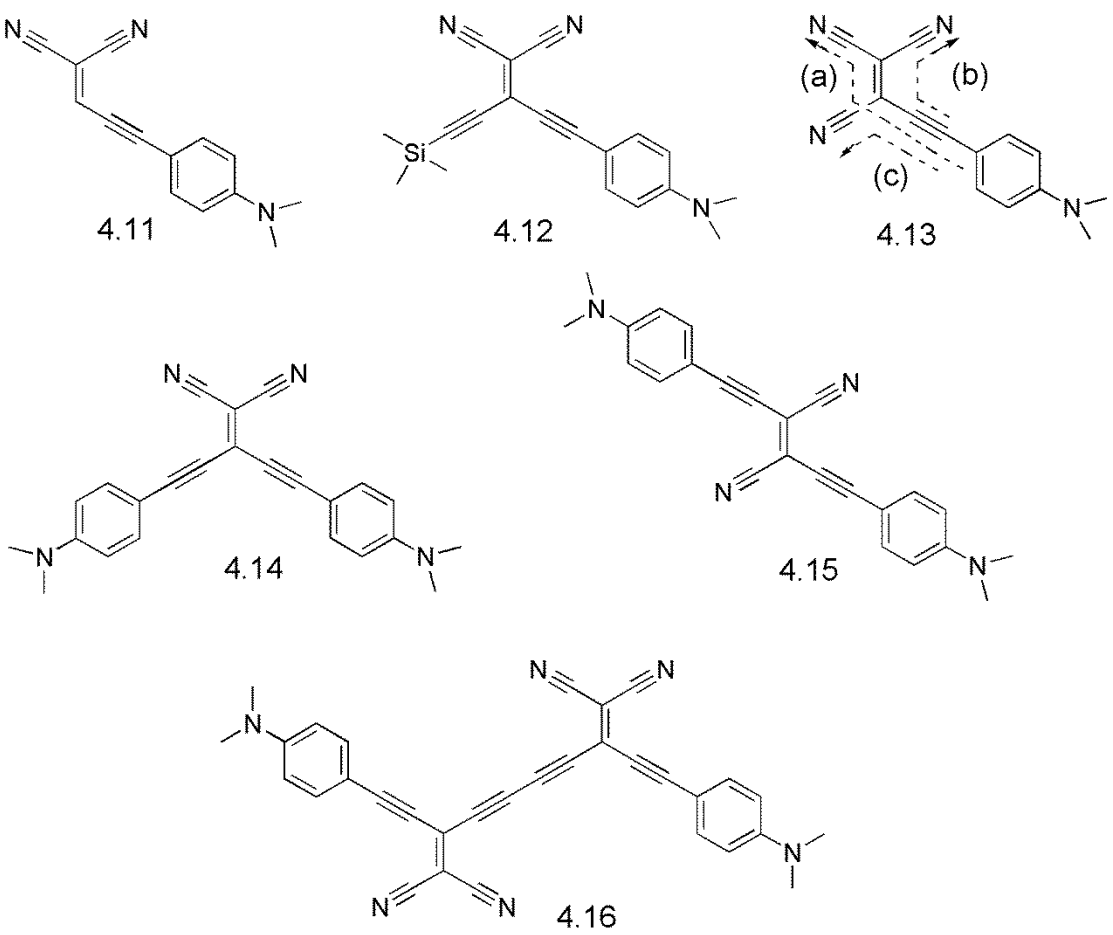

Figure 4.4. Series of push-pull organic donor-substituted cyanoethynylethene molecules featuring two-dimensional conjugated systems.

The need of third order optical molecules has led to the study of the electrochemical properties of series of molecules containing DMA ring attached directly to the $C(CN)_2$ or through a variety of different unsaturated spacers (**Figure 4.5**). The results revealed that small band gaps and lowest energy transitions were observed for the two dimensional compounds **4.22a** and **4.22b**, whereas a decrease in the band gap for the other molecules featuring unsaturated spacers was observed which resulted from decreasing the conjugation between donor and acceptor moieties.[142]

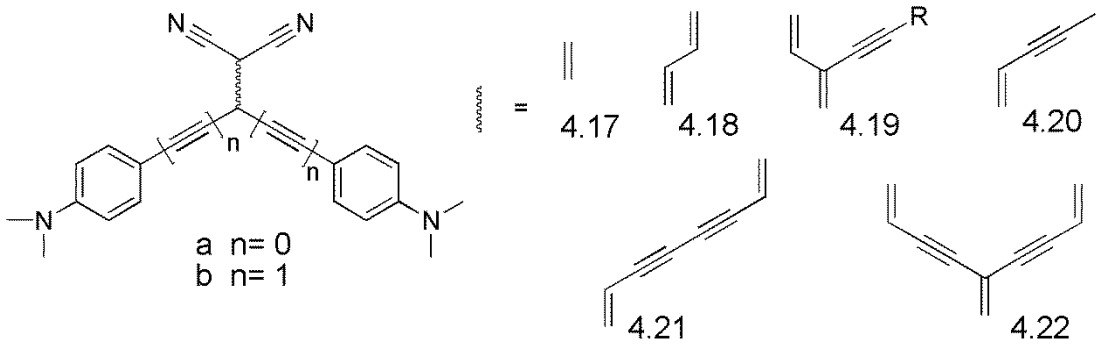

Figure 4.5. Showing a serie of DMA substituted cyanoethynylenes with different π-conjugated spacers.

Increasing the bond-length alternation (BLA) of the conjugated backbones is another way of reducing the band gap of organic chromophores and maintaining the β value. However, the influence on the BLA values depends primarily on increasing the conjugation path between the donor and acceptor units. In the case of the arene organic chromophores **4.23** and **4.24**, in which the aromatic structure represents the basic structure and is responsible for the stability of the overall molecules. Polarization of the aromatic ring will result in the loss of aromaticity. Therefore, increasing the double bond character by using quinoid spacers would facilitate the polarization in the organic push-pull chromphore and modulate the band gap. Wu and co-workers synthesized series of donor-acceptor chromophors

featuring quinoid spacers. Theoretical and electrochemical studies revealed that these molecules show low energy absorption band leading to a low band gap. Also comparing the bond-length alternation for these compounds with a reference aromatic compound revealed a degree of aromaticity in these D-Q-A systems.[143]

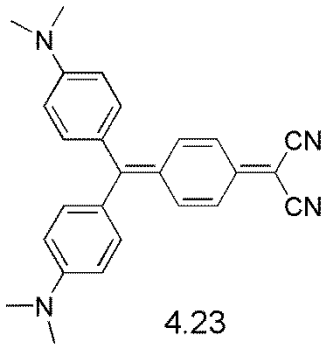

4.23

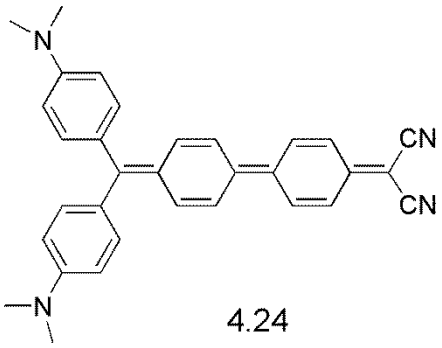

4.24

From the point of assembling strong donating and accepting units with a quinoid spacer, Bures and co-workers synthesized new push-pull chromophores featuring quinoid π-spacer by using tetracyano-9,10-anthraquinoidimethane (TCAQ) as an acceptor and different donor moieties compound **4.25-4.27**. Utilizing TCAQ in the system introduces other features to the system including thermal and chemical stability. In addition, the TCAQ unit increases the conjugation of the system and shows electro-active properties when incorporated with another acceptor unit either by attaching the TCAQ unit in a neutral form or in a reduced form such as the anion or dianion radical forms. Furthermore, TCAQ unit has the ability to participate in intramolecular charge transfer interaction through dipole moment formation.[144]

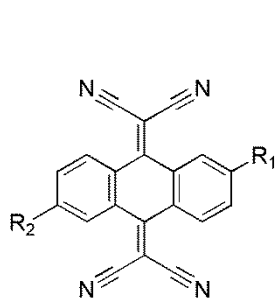

4.25

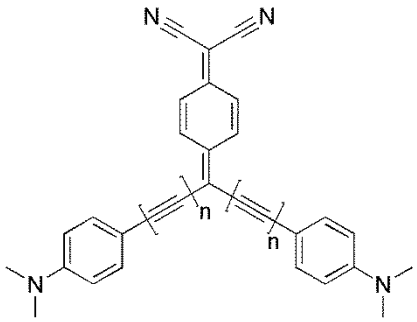

4.26

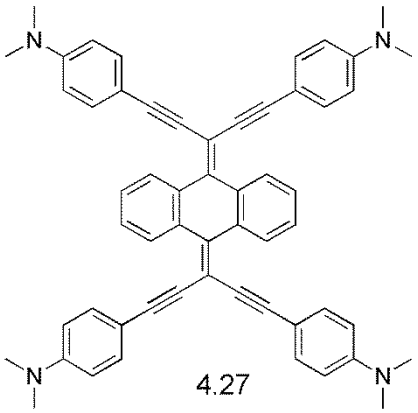

4.27

4.1.5. Oligothiophene based push-pull system

Oligothiophenes are characterized by good chemical stability, ideal π-delocalization, and simplicity in modification. Combining the properties of oligothiophene with cyano derivatives could assist in covering the limitation of the oligothiophene derivatives as promising materials for use as semiconductors in optoelectronic devices. Thus, applying cyano based oligothiophene to bulk heterojunction devices may assist in increasing the PCE via raising the charge carrier mobility, promoting separation and collection of charges at the respective electrode. Therefore, investigation of the optical and electrochemical properties was carried out on a series of cyano oligothiophene derivatives aiming to improve the design of new organic molecules for organic electronics devices. The existence of cyanovinyl moieties brings significant features including; tuning the absorptions and fluorescence wavelength, improving in the solid state organization and contribution in enhancing the nonlinear optical response.[145]

Therefore, the electronic and optical properties of push-pull oligothiophene derivatives was investigated by incorporating a TPA group as strong donating group and DCV or cyanopyridone as an acceptor group into oligothiophene moieties. The comparison between the two donor-acceptor oligothiophene derivatives **4.28** and **4.29** revealed that the addition of cyanopyridone unit reflected more positively on the absorption of the charge transfer band toward near IR region and led to a lowering LUMO energy level as well as improving the PCE of the device.[146]

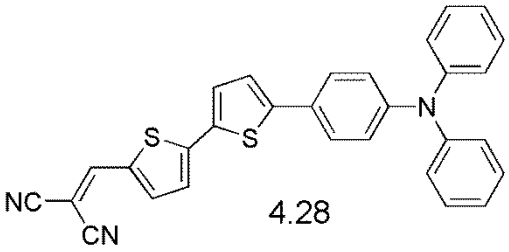

4.28

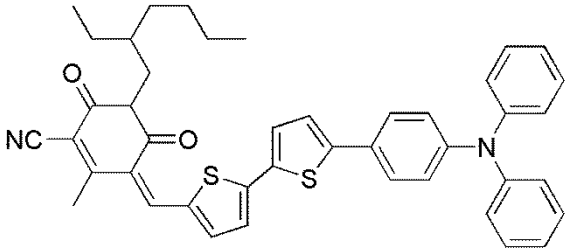

4.29

Further investigation was carried out by studying different number of symmetrical and unsymmetrical oligothiophene moieties terminated with TPA units and linked by a 1,1,4,4-tetracyanobuta-1,3-diene unit (**4.30-4.32**) in order to facilitate intermolecular charge transfer. The resulting NLO compounds showed improvement in the solubility and stability as well as the oxidation potentials which reflect positively on the future investigation of associated compounds as donor moieties in bilayer heterojunction solar cells.[41]

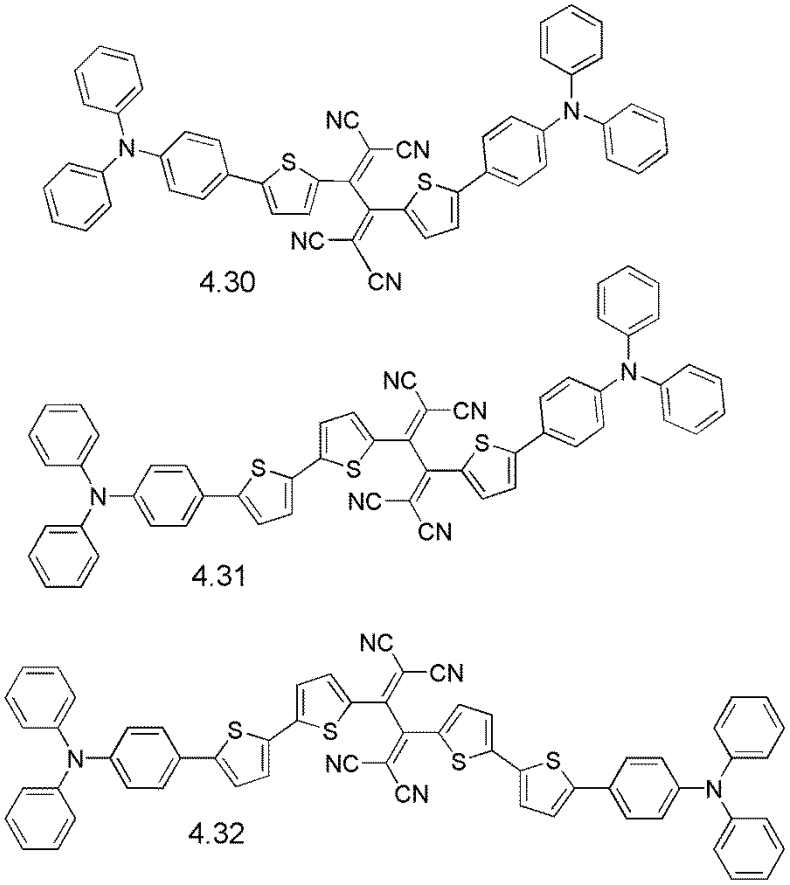

Two series of push-pull chromophores **4.33** and **4.34** combining the properties of oligothiophene as an effective spacer and capped with different amino donor groups and DCV or tricyanovinyl TCV moieties as acceptor groups were synthesized. Attractive electrochemical properties were observed for the resulting compounds due to formation of stable oxidation and reduction species. These results were supported by molecular geometry optimization studies which indicate the formation of quinoid character in both series of molecules. In addition, a theoretical study of atomic charge distribution indicated an increase in the electron charge density on the acceptor moieties (more than the donor unit) which leads to the formation of a strongly polarized conjugated system.[147]

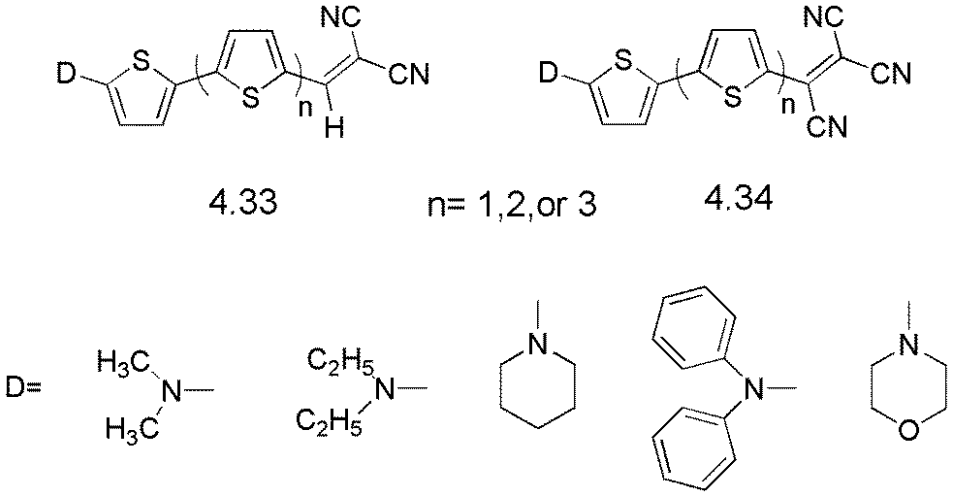

4.2. Aim and objectives

This part of the thesis describes the synthesis and electrochemical properties of two different series of powerful push-pull systems containing DMA moieties as a strong donating group and TCNE or TCNQ as electron accepting groups. One of the series features 9,10-phenanthraquinone or/ and TCAQ units as an electron accepting spacer (**Figure 4.6(a)**). As quinone derivatives have shown interesting electrochemical properties the 9,10-phenanthraquinone unit has attractive properties such as: (i) convenient modification of the unit by introducing different alkyl or aryl groups without affecting the planarity of the system; (ii) the presence of fused aromatic groups assist in increasing the conjugation along the system; (iii) this unit shows good stacking ability which leads to effective thin film order and facilitate electron transfer between the chains.

The second series features thiophene units as electron donating spacers (**Figure 4.6(b)**). These target compounds could have NLO properties and absorption in the near-IR region. Furthermore, the molecules attractive redox and photochemical properties indicate that these compounds may be attractive targets for fabricating of photovoltaic devices.

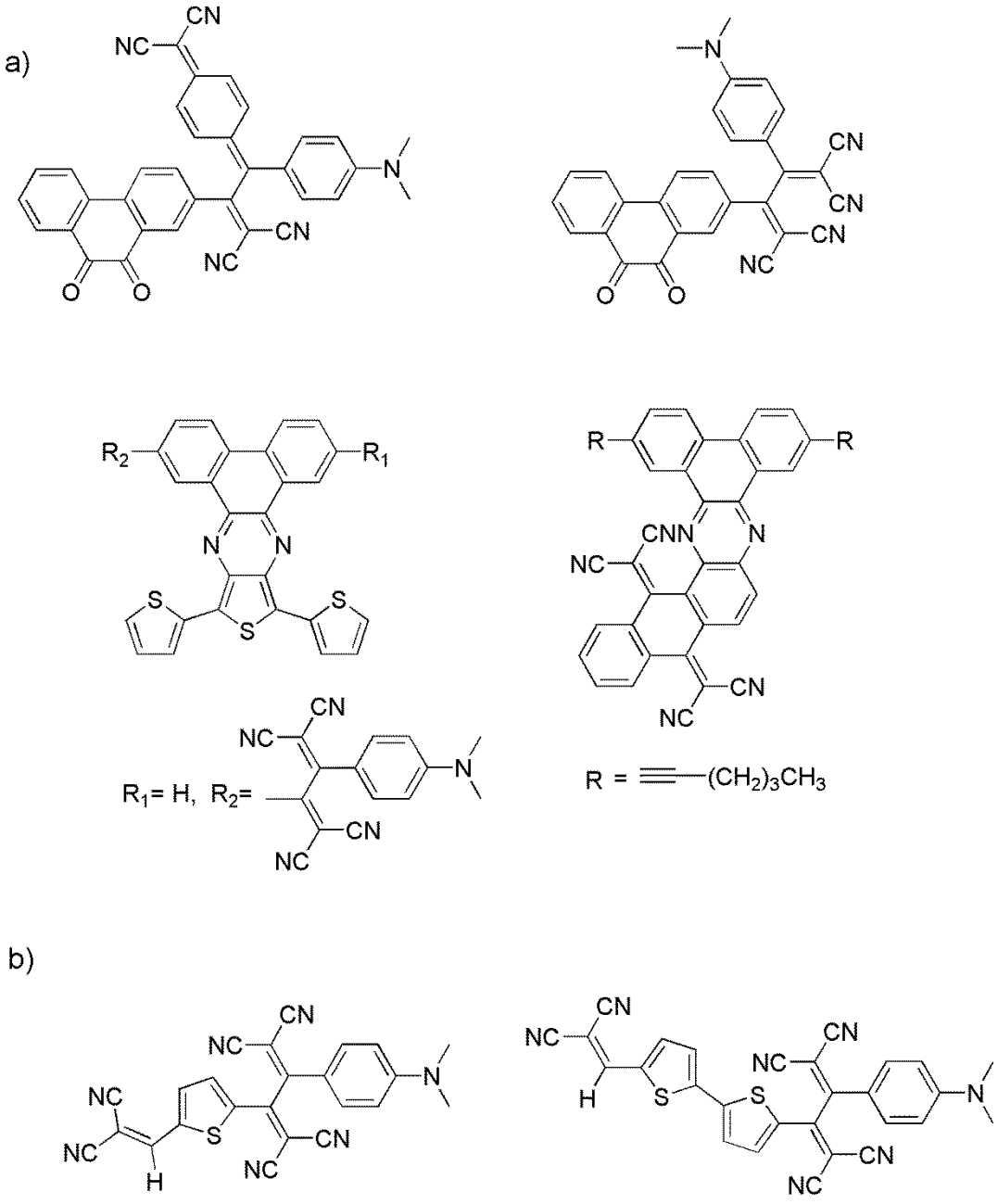

Figure 4.6. (a) Push-pull systems featuring 9,10-phenanthraquinone; (b) Push-pull system featuring thiophene spacers.

4.3. Results and discussion

4.3.1. Synthesis and optical properties of phenanthrenequinone push-pull systems

This section focuses on forming powerful new push-pull compounds featuring phenanthrenequinone with different donating groups such as DMA, ethnylthiophene, 2-ethnyl ferrocene, and TCNE or TCNQ as secondary acceptor moieties.

4.3.1.1. Synthesis of the compounds 29, 30, 31 and 32

The synthesis of compounds **29**, **30**, **31** is outlined in **Scheme 4.3**. The preparation started from the iodination of phenanthrene-9,10 dione **6** in acetic acid solution and gave compound **27** in 84% yield. The resulting monoiodo compound **27** was coupled with 4-ethynyl *N*-*N*-dimethyl aniline **28** *via a* Songoshira coupling reaction to give compound **29**. The preparation of compound **29** was studied under different conditions in order to increase the yield. The best yield of 46% was achieved by heating the reagents to 80ºC in degassed solution under nitrogen.

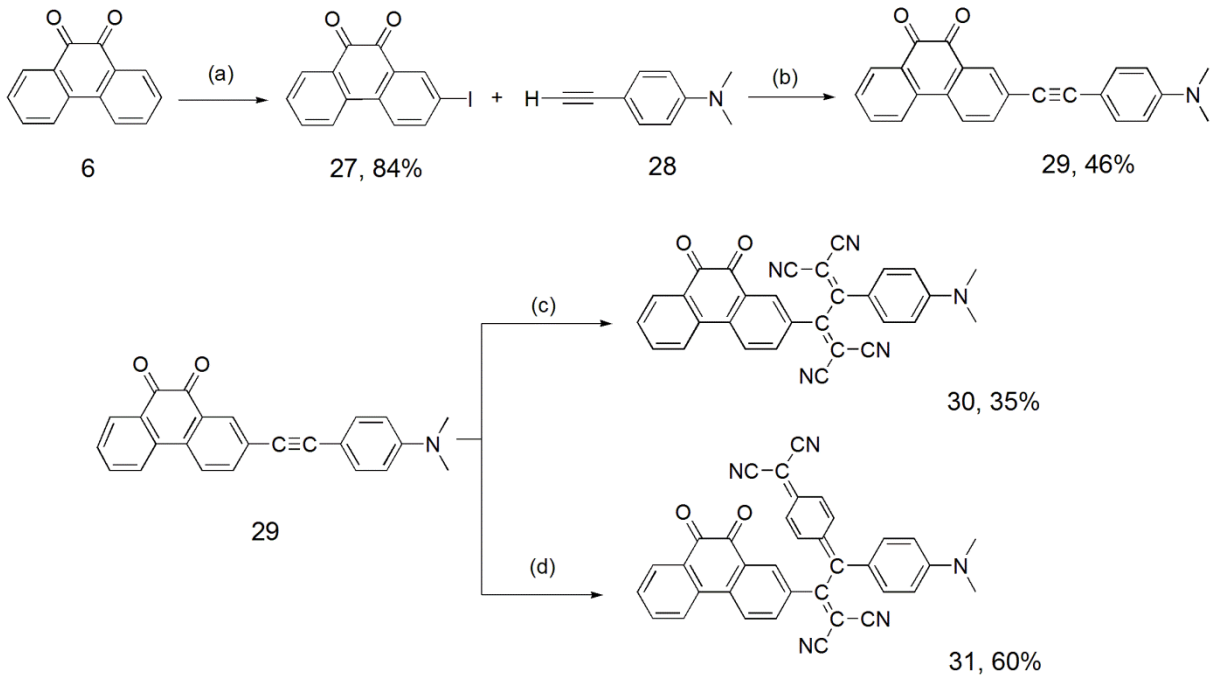

Scheme 4.3. Reagents and conditions: (a) I_2, H_2SO_4, CH_3COOH (b) 10% Pd/C, CuI, Ph_3P, K_2CO_3, Δ 80 °C (c) TCNE, THF, Δ 20 °C (d) TCNQ, THF, Δ 20 °C.

With the aim to prepare dipolar push-pull chromophores of the type D-A-A, compound **29** underwent [2+2] cycloaddition reactions at room temperature with TCNE and TCNQ, respectively, followed by retro-electrocyclisation to give **30** and **31** in 35% and 60%, respectively.

Further reactions were carried out by reacting compound **30** with diamino compound **11** *via* a simple condensation reaction (**Scheme 4.4**). The reaction was done by heating the resulting mixture in chloroform under nitrogen and in presence of *p*-toluene sulfonic acid as a catalyst to give compound **32** in 35% yield.

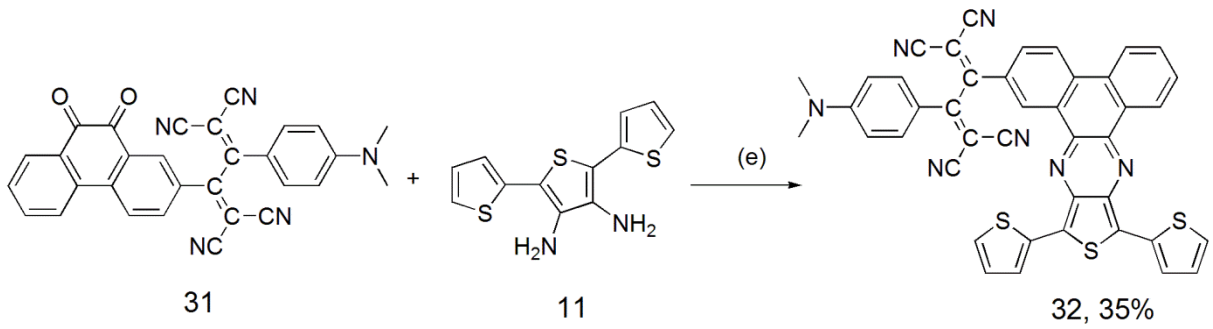

Scheme 4.4. Reagents and conditions: (e) $CHCl_3$, *p*-toluene sulfonic acid, N_2.

Similar Songoshira coupling reactions were attempted between compound **27** and 3-ethnyl thiophene **1** or 2-ethnyl ferrocene **35,** respectively. The synthesis of compound **33** was achieved from a coupling reaction with 3-ethnyl thiophene in 27% yield, whereas, the coupling of **27** with 2-ethnyl ferrocene **35** did not provide the expected compound and a new compound **36** was formed in 27% yield.

In order to synthesize nonplanar D-A-A compounds, compound **33** was reacted with TCNE. However**,** the reaction did not occur even with excess TCNE and applying high temperatures. This suggests that the electron donating ability of thiophene unit toward [2+2] cycloaddition reactions is not sufficient to provide compound **34** (S**cheme 4.5**).

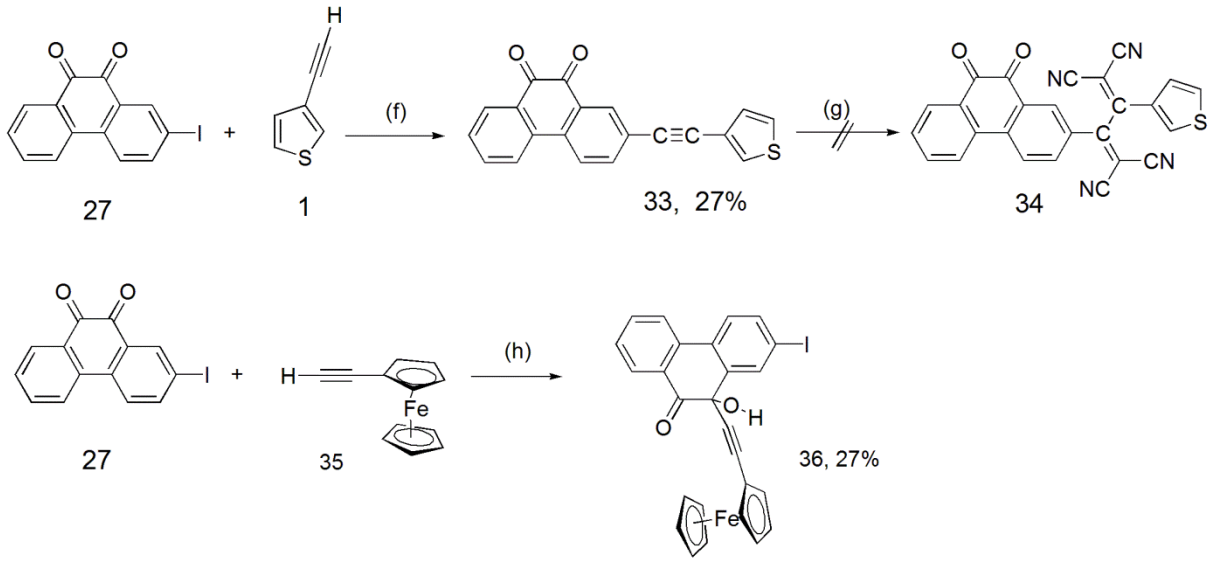

Scheme 4.5. Reagents and conditions (f) 10% Pd/C, CuI, Ph_3P, K_2CO_3, Δ 80 °C (g) TCNE, THF (h) 10% Pd/C, CuI, Ph_3P, K_2CO_3, Δ 80 °C.

4.3.1.2. X-ray structure

Crystals of compound **36** which were suitable for X-ray structure determination were obtained by slow evaporation of a 1:1 mixture of DCM and petroleum ether. It can clearly be seen that the 2-ethnyl ferrocene is attached to carbon number 9 on phenanthrenequinone derivative and the rest of the molecule is slightly twisted. **Figure 4.7** shows the crystal structure of compound **36**.

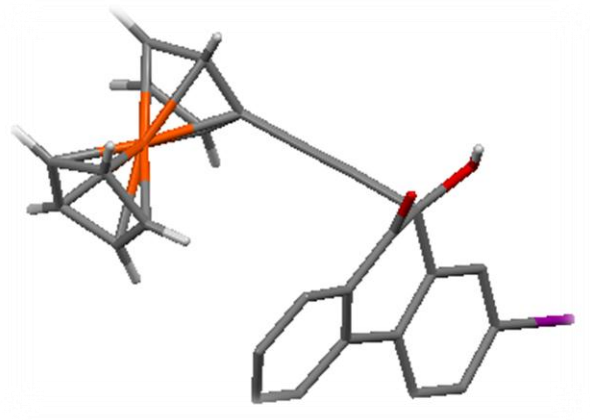

Figure 4.7. Crystal structure of **36** obtained by slow evaporation of a 1:1 mixture of DCM and petroleum ether.

4.3.1.3. UV-vis spectroscopy

UV-vis absorption spectra of compounds **29**, **30** and **31**, respectively, were recorded in CH_2Cl_2 (1×10^{-5} M). The results of UV-vis spectra are shown in **Figure 4.8**. These compounds displayed an intense absorption band towards the near IR region. Compound **29** showed two strong absorption peaks at λ= 277 and 351 nm. On the other hand, a weak peak was observed at about λ= 590 nm which provides an optically determined band gap around 2.2 eV. A strong absorption peak observed for compound **30** at λ= 450 nm with abroad tail last up to λ= 622 nm. Compound **31** displayed two bands; a weak absorption in the UV region at about λ= 450 nm and an intense and broad absorption band at around λ= 688 nm, which provides an optically determined band gap of 1.4 eV.

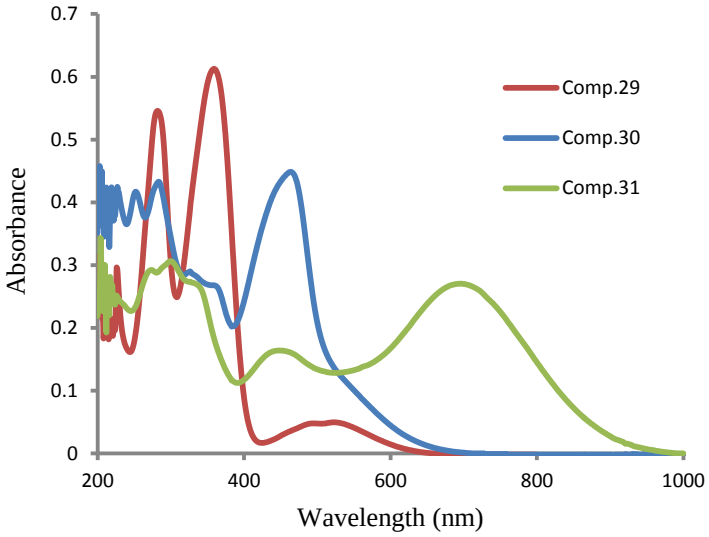

Figure 4.8. UV-vis absorption spectra of compound **29**, **30** and **31** (1×10^{-5}M) recorded in CH_2Cl_2.

An important simple test to probe possible NLO properties of these compounds is to record their UV-vis spectra in solvents of different polarity to check whether solvatochromism is observed. Compound **29** shows a slight difference in UV-vis absorption peaks upon varying the polarity of the solvents (DCM and DMSO). Negative solvatochromism in the maximum wavelength absorption was observed in the visible absorption bands of compound **29** (λ= 516 nm in DCM to λ= 478 nm in DMSO). This indicates that the ground state is stabilized in comparison with the first excited state suggesting a twisting between the donor and acceptor units (**Figure 4.9**).

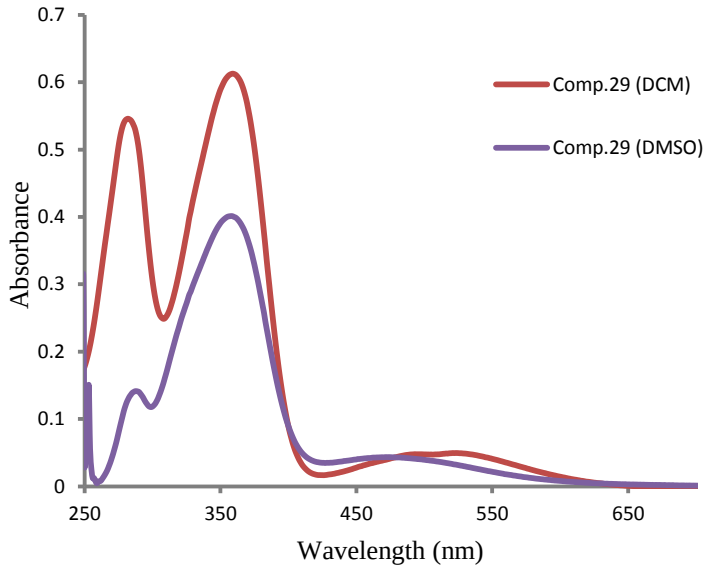

Figure 4.9. UV-vis absorption spectra of compound **29** (1× 10^{-5}M) recorded in DCM and DMSO.

Compound **31** exhibits very similar UV-vis absorption peaks in DCM and CH_3CN. Increasing the polarity of the solvents to DMSO resulted in a bathochromic shift from λ= 675 nm in CH_3CN to λ= 740 nm in DMSO (**Figure 4.10**).

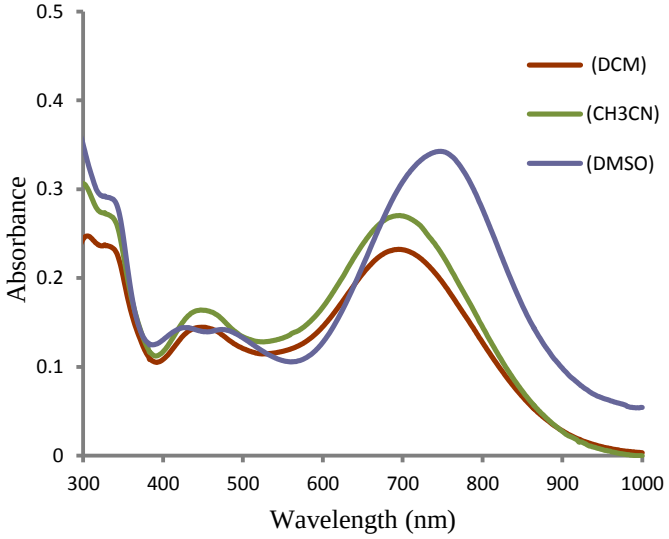

Figure 4.10. UV-vis absorption spectra of compound **31**(1× 10^{-5}M) in different solvents.

4.3.1.4. Cyclic voltammetry

Electrochemical properties of compounds **29**, **30** and **31** were studied using cyclic voltammetry. The redox properties of the molecules were investigated using a conventional three electrode cell containing a platinum button working electrode, silver wire as a reference electrode and Pt counter electrode. The samples recorded in CH_2Cl_2 (1×10^{-4} M) solution, containing 0.1 M of $TBAPF_6$ as supporting electrolyte. The data are summarized in **Table 4.2** and are referenced to the Fc/Fc^+ redox couple = 0.0 V.

Three reversible one-electron reduction waves were observed for compound **30** in comparison with compound **29** which showed only one reversible reduction peak at $E_{1/2}$= -1.05 V as illustrated in **Figure 4.11**. Compound **30** displayed two reversible peaks at $E_{1/2}$= -0.80 V and -1.31V assigned to the reduction of DCV moieties and the third reduction at -1.09 V has been assigned to phenanthrenequinone unit. Quasi-reversible oxidation peaks assigned for DMA electron donating unit was observed for compound **29** at $E_{1/2}$= + 0.40 and + 0.46 V**.** Compound **31** exhibited three reversible one-electron reduction peaks at $E_{1/2}$= - 0.63 V and $E_{1/2}$= - 0.76 V assigned to TCNQ moiety, and a third reduction peak at a more cathodic value at $E_{1/2}$= -1.23V which is presumably due to the phenanthrene-quinone unit**.** Oxidative cycling of compound **31** provided an oxidation wave at $E_{1/2}$= + 0.37 and + 0.45 V, whereas compound **29** displayed an oxidation wave at $E_{1/2}$= + 0.40 and + 0.46 V as shown in **Figure 4.12**.

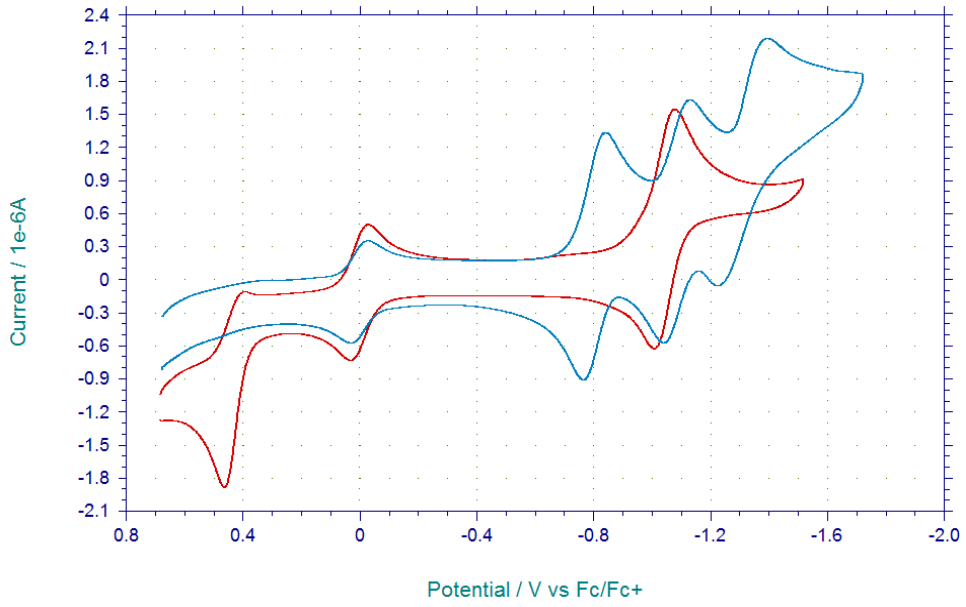

Figure 4.11. Cyclic Voltammetry of compound **29** (red line) and **30** (blue line) (1×10^{-4} M) recorded in CH_2Cl_2, with $TBAPF_6$ (0.1 M) as supporting electrolyte and scan rate of 100 mV/s.

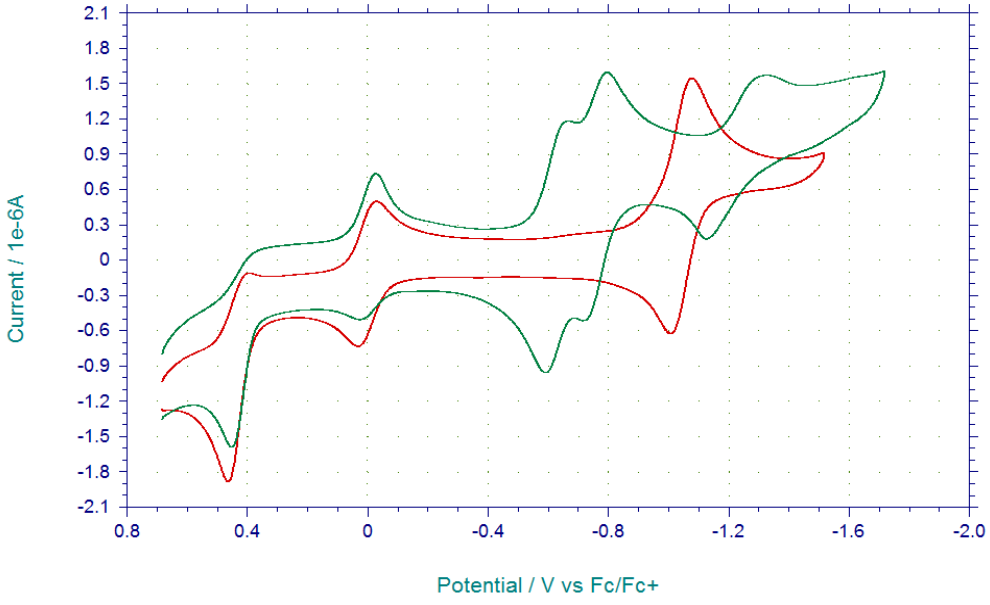

Figure 4.12. Cyclic Voltammetry of compound **29** (red line) and **31** (green line) (1×10^{-4} M) recorded in CH_2Cl_2, with $TBAPF_6$ (0.1 M) as supporting electrolyte and scan rate of 100 mV/s.

Table 4.2: Optical and electrochemical data of compounds **29, 30** and **31** (1×10^{-4} M) observed by cyclic voltammetry in CH_2C1_2, with $TBAPF_6$ (0.1 M), all potentials are given *vs.* Fc/Fc^+ redox couple used as internal standard.

Compound	λ_{max}*(nm)* / λ_{onset}*(nm)*	*Optically determined band gap (eV)*	$E^2_{1/2}$ *(V)*	$E^2_{1/2}$ *(V)*	$E^3_{1/2}$ *(V)*	$E^4_{1/2}$ *(V)*	E_{LUMO} *(eV)*	E_{HOMO} *(eV)*	E_g *(eV)*
29	516/ 620	2.2	-1.04	----	----	+0.43	-3.76	-5.23	1.47
30	462/ 601	2.0	- 0.80	-1.09	-1.31	----	-3.19	----	----
31	710/ 899	1.4	-0.63	-0.76	-1.23	+0.41	-4.17	-5.22	1.05

4.3.2. Optical properties of push-pull system featuring oligothiophenes

This section describes the synthesis of novel push-pull systems featuring thiophene units, DMA as donor units, and cyanovinyl as acceptor units. Improvement in the absorption of the resulting compounds into the near infrared region was achieved by further reaction with TCNE.

4.3.2.1. Synthesis of compounds 41, 42, 43 and 44

The synthetic approach for preparing the chromophores **43** and **44** is outlined in **Scheme 4.6**. The preparation started from coupling 4-ethynyl N-N dimethyl aniline **28** with 5-bromo-2-thiophenecarboxaldehyde **35** and 5-bromo-2,2'-bithiophene-5'-carboxal-dehyde **36** *via* a Songoshira coupling to give compounds **37** and **38**, respectively. Compounds **37** and **38** further underwent [2+2] cycloaddition reactions at 66 °C with TCNE followed by retro-electrocyclisation to provide compound **39** and **40** in high yield.

Target compounds **43** and **44** were obtained *via* Knoevenagel condensation reactions of compounds **39** and **40,** respectively, with malononitrile.

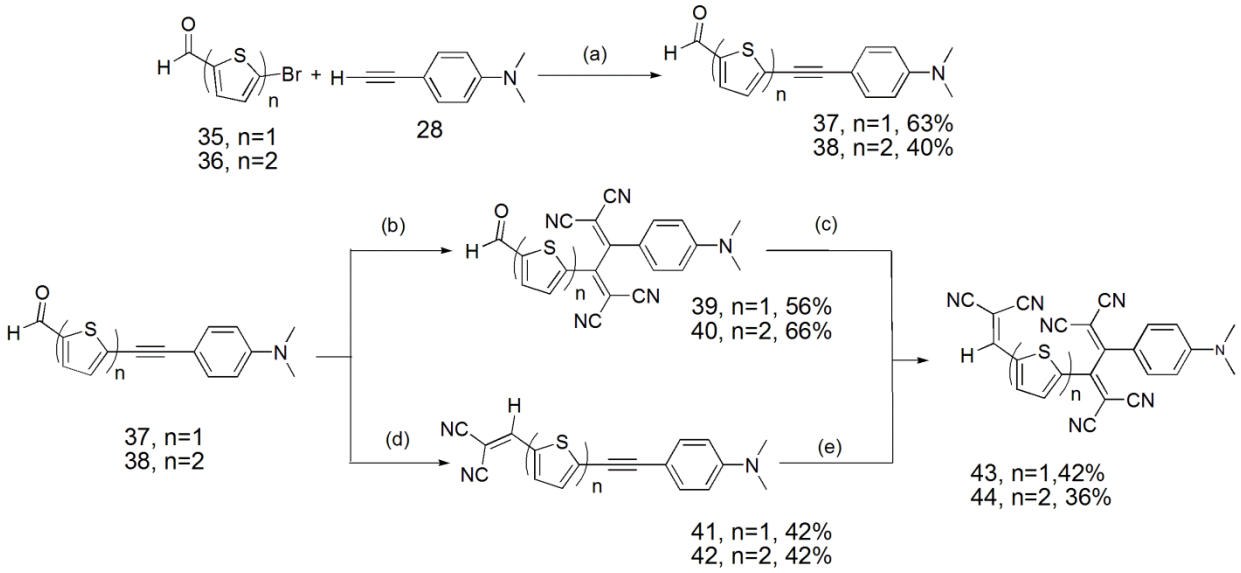

Scheme 4.6. Reagents and conditions: (a) Pd/ C, 10%, CuI, Ph_3P, K_2CO_3, DME: H_2O; (b) (e) TCNE, THF; (c) (d) malononitrile, piperidine, EtOH.

4.3.2.2. UV-vis spectroscopy

UV-vis absorption spectra of compounds **43** and **44** were recorded in CH_2C1_2 (1×10^{-5} M). These compounds displayed a broad and strong absorption maximum around λ= 400-680 nm as shown in **Figure 4.13**. Charge transfer bands resulting from intramolecular charge transfer from electron donating DMA unit into electron accepting dicyanvinyl moieties were observed in the spectra.

Interestingly, increased molar extinction coefficients and bathchromic shifts in the absorption was observed in the spectra of compound **44** compared to compound **43**, which likely results from increasing the conjugation length. A bathchromic shift was also observed for compound **43** relative to compound **37**, presumably likewise due to an increase in conjugation length.

Two absorption bands were observed in the spectra of compound **43**; the first one provides a higher intensity band at **λ**= 450–520 nm range with end absorption around **λ**= 750 nm which provides an optically determined band gap of 2.4 eV**.** The second one displayed a lower and broader intensity band within the **λ**= 400-440 nm range. The higher intensity absorption band can be assigned to an ICT band**,** whereas, the lower intensity band could be assigned to a π–π*transition. A noticeable shift in the broad intense visible band at λ= 535 nm was observed for compound **44**, which resulted in lower optically determined band gap of 2.3 eV relative to compound **38**, which exhibited two weaker and broad absorption bands in the UV and vis regions.

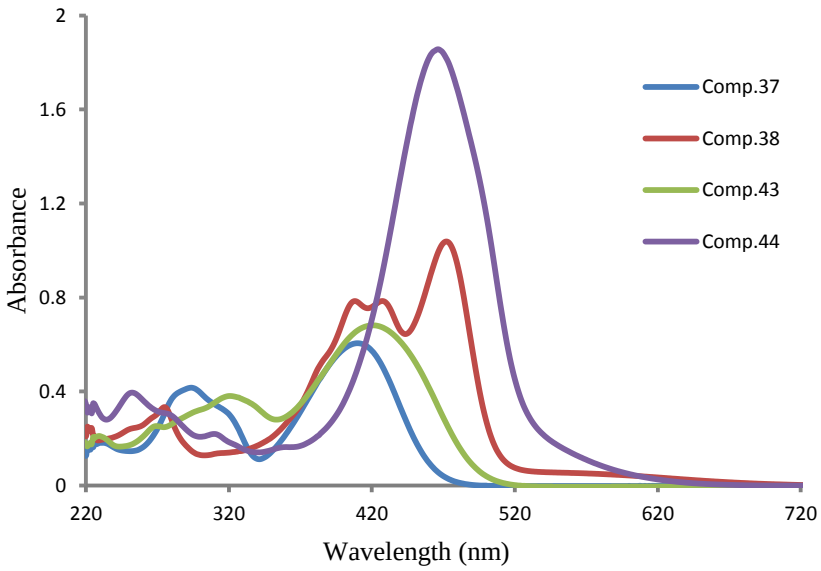

Figure 4.13. UV-vis absorption spectra of compounds **37, 38**, **43** and **44** (1×10^{-5}M) recorded in CH_2Cl_2.

4.3.2.3. Cyclic voltammetry

The electrochemical properties of push-pull systems **43** and **44** were evaluated by cyclic voltammetry. The electrochemical data of compound **43** and **44** were recorded at room temperature in CH_2Cl_2 ($1x10^{-4}$ M) containing $TBAPF_6$ (0.1 M) as supporting electrolyte and a platinum button working electrode, platinum wire as counter electrode and silver wire as a reference electrode. All potentials are given *vs.* Fc/Fc^+ redox couple = 0.0 V, which was utilized as internal standard.

Three reversible peaks were observed for compounds **43** and **44** upon reduction, which presumably are due to the reduction of 1,1,4,4- tetracyanobuta-1,3-diene (TCBD) moieties and dicyanvinyl moieties. A single reversible oxidation peak at $E_{1/2}$= +0.96 for compound **43** and $E_{1/2}$= +0.93 V for compound **44** was assigned to the oxidation of the electron donating DMA moiety as shown in **Figure 4.14**. The LUMO and HOMO energy levels were estimated from the onset of the reduction and oxidation waves of compounds **43** and **44** are provided in **Table 4.3**. Whilst there is no significant difference in the HOMO energy, the LUMO energy of compound **44** is higher than the LUMO energy of compound **43**, resulting in a larger bandgap for the bithiophene derivative **44**. This could indicate that the molecules are more twisted which leads to an increase in the energy bandgap levels. On the other hand, it is worth mentioning that the reduction of the DCV moieties in **43** appears at $E_{1/2}$ = -0.67 V indicating the better acceptor ability than the DCV moieties in **44** which appears at $E_{1/2}$= -0.86 V.

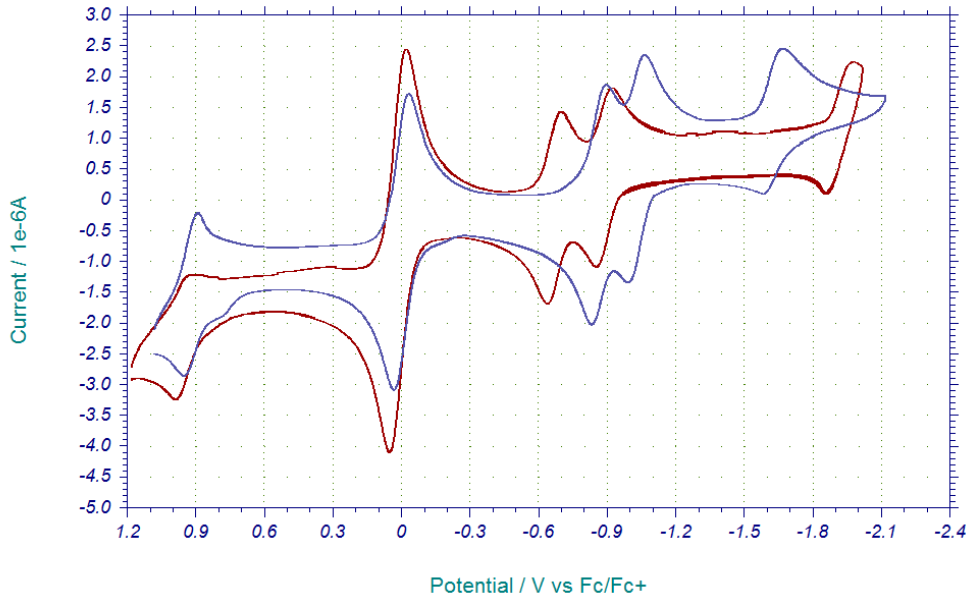

Figure 4.14. Cyclic voltammetry of compound **43** (red line) and **44** (blue line) (1 x 10^{-4}M) recorded in CH_2Cl_2, with $TBAPF_6$ (0.1M) as supporting electrolyte and at scan rate of 100 mV/s.

Table 4.3: Optical and electrochemical data of compounds **43** and **44** recorded using cyclic voltammetry in CH_2C1_2, with $TBAPF_6$ (0.1 M), all potentials are given *vs.* Fc/Fc^+ redox couple used as internal standard.

Compounds	λ_{max} *(nm)*/ λ_{onset} *(nm)*	$E^1_{1/2}$ *(V)*	$E^2_{1/2}$ *(V)*	$E^3_{1/2}$ *(V)*	$E^4_{1/2}$ *(V)*	E_{LUMO} *(eV)*	E_{HOMO} *(eV)*	E_g *(eV)*
43	467/ 489	-0.67	-0.89	-1.92	+0.96	-4.13	-5.76	1.63
44	459 / 557	-0.86	-1.03	-1.63	+0.93	-3.94	-5.73	1.79

4.3.2.4. Molecular modelling

Calculation of the HOMO and LUMO levels of the push-pull compounds **43** and **44** were performed using Spartan 08 software using DFT B3LYP 6-311G level of theory. Compatible results between modelled and electrochemical data were found for both compounds. The calculated HOMOs and LUMOs energies are showed in **Figure 4.15**.

For both compounds, it is clear that the HOMO is located on the DMA and TCBD moieties, whereas the LUMO is located on thiophene and DCV moieties. Comparison of the DFT calculated results with the cyclic voltammetry data showed small differences in the HOMO and LUMO energy levels for both compounds (**Table 4.4**). The reason for these differences could be referred to the variation in the conditions and the media of obtaining the results (solution versus gas phase).

Table 4.4. Predicated HOMO and LUMO energy levels for compounds **43** and **44** using DFT calculation and cyclic voltammetry.

Compounds	*Predicated energy levels using DFT calculation*			*Predicated energy levels using cyclic voltammetry*		
	HOMO (eV)	LUMO (eV)	Eg (eV)	HOMO (eV)	LUMO (eV)	Eg (eV)
43	-6.40	-4.30	2.1	-5.76	-4.13	1.6
44	-6.30	-4.00	2.3	-5.73	-3.94	1.8

The calculated LUMO energy of compound **44** occurs at a more negative value (-4.0 eV) compared with the calculated LUMO energy of compound **43** (-4.3eV) which results in a larger band gap for the more conjugated compound **44**. These results are roughly

compatible with the electrochemical data which show that the first and second reduction peaks of compound **44** are shifted to a higher potential than compound **43**.

a)

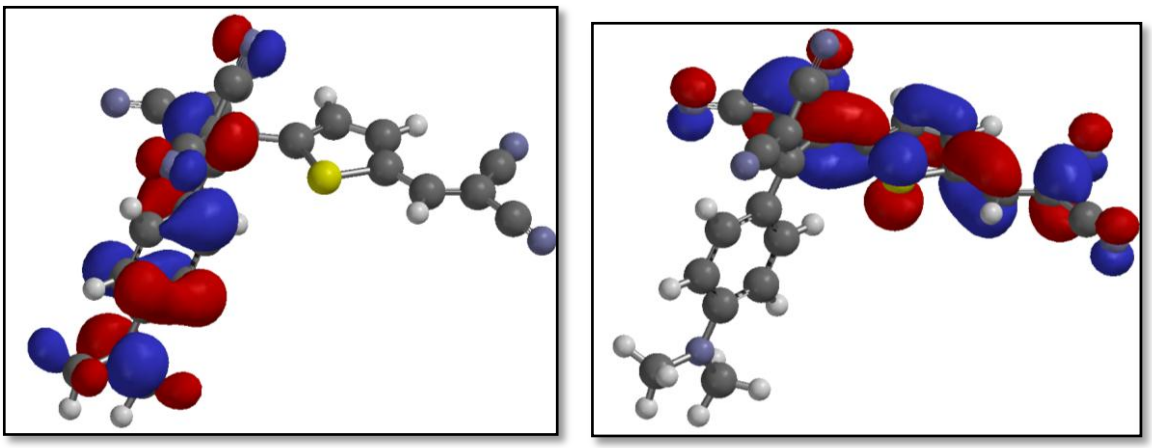

HOMO= -6.40 eV LUMO = -4.30 eV

b)

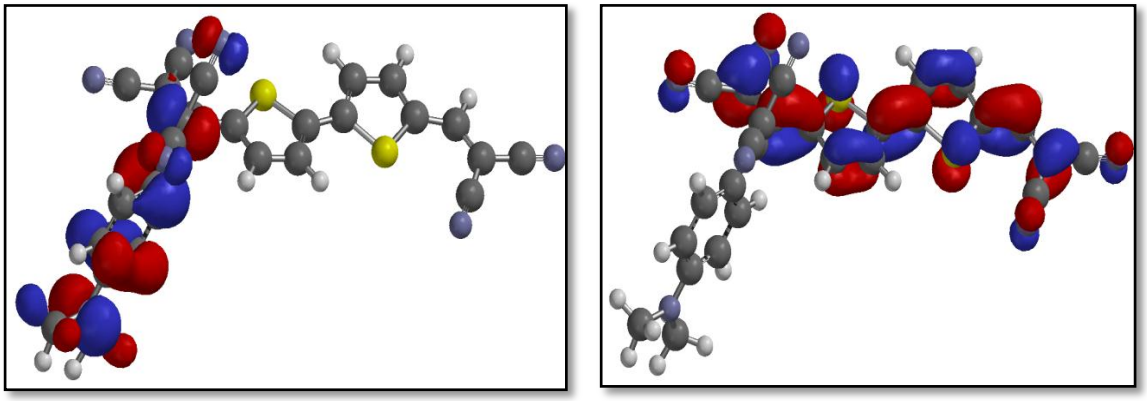

HOMO= -6.30 eV LUMO = -4.00 eV

Figure 4.15. Orbital plots of a) compound **43** and b) compound **44** performed on spartan 08 program using DFT B3LYP/6-311G calculations.

4.3.3. Optical properties of new acceptor featuring a quinoid π-spacer

This section focus on forming a new A-π-A system featuring a quinoid π-spacer by combining two acceptor moieties, i.e. phenanthrenequinone and TCAQ derivatives, in order to investigate the properties of the resulting juxtaposed acceptor units.

4.3.3.1. Synthesis of compounds 46 and 47

The synthesis of TCAQ derivative **47** was carried out by Knoevenagel condensation reaction **Scheme 4.7** from synthesized anthraquinone derivative **46** by reaction with Lehnert's reagent ($TiCl_4$, malononitrile, pyridine) in dry CH_2Cl_2 solution. The TCAQ derivative was obtained as a stable red solid in 69 % yield. The synthesis started by preparing 2,7-diiodo-9,10-phenanthrenequinone **7** in a good yield by iodination of phenanthrene 9,10-dione with NIS in presence of trifluromethane sulfonic acid. Compound **7** further underwent Songoshira coupling reaction with 1-hexyne to give compound **8** in 37 % yield. Then simple condensation reaction between commercially available 1,2-diamino-anthraquinone **45** with the synthesized derivative **8** was achieved by heating the reaction mixture under reflux in chloroform solution and in presence of *p*-toluene sulfonic acid as a catalyst to give anthraquinone derivative **46** in 65 % yield.

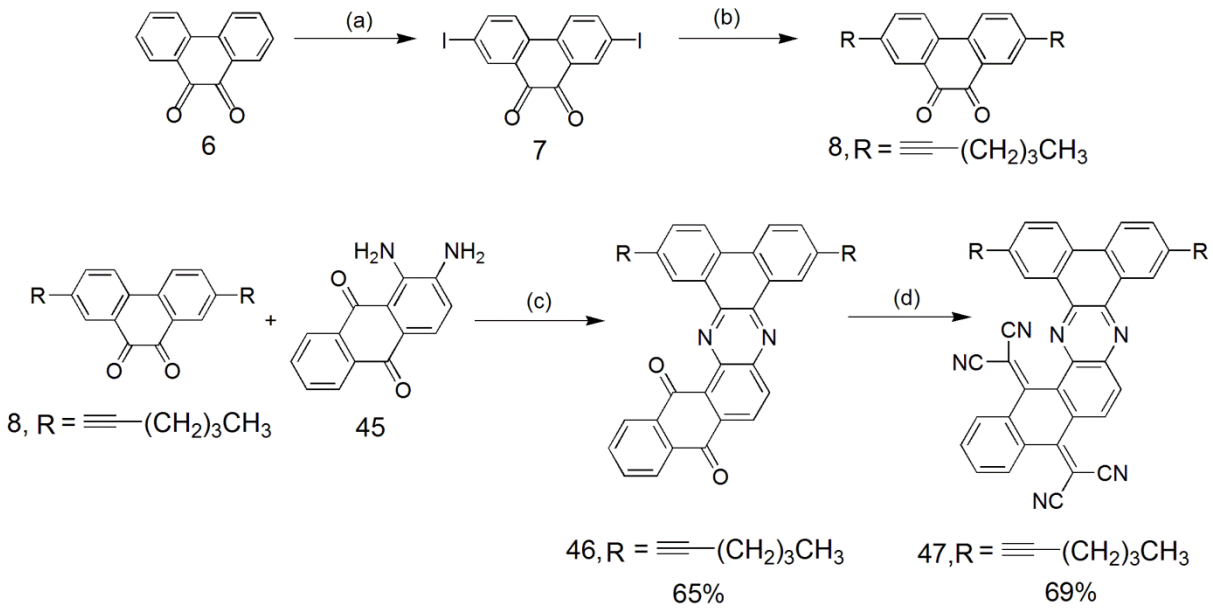

Scheme 4.7. Reagents and conditions: (a) trifluromethanesulfonic acid, N-Iodosuccinamide, (b) Pd/ C, 10%, CuI, Ph_3P, K_2CO_3, 1-hexyne, DME: H_2O; (c) *p*-toluene sulfonic acid, chloroform; (d) titanium chloride, malononitrile, pyridine, dry CH_2Cl_2.

4.3.3.2. UV-vis spectroscopy

UV-vis absorption spectra of compounds **46** and **47** were recorded in CH_2Cl_2 (1×10^{-5} M). These compounds displayed broad and strong UV absorption bands around λ= 250-350 nm and a broad, weak intensity band in the visible region as shown in **Figure 4.16**.

Absorption were observed for compound **46** at λ= 274 nm with three shoulders appearing at λ= 303, 325 and 349 nm. The second band appears at λ= 420 nm and showed a long tail up to around λ= 520 nm resulting in optically determined band gap of 2.7 eV.

A bathchromic shift ca. 16 nm was observed in the visible region for compound **47** compared with compound **46**. The optically determined band gap for compound **47** was 2.5 eV, which is narrower than the calculated band gap of compound **46** (2.7 eV).

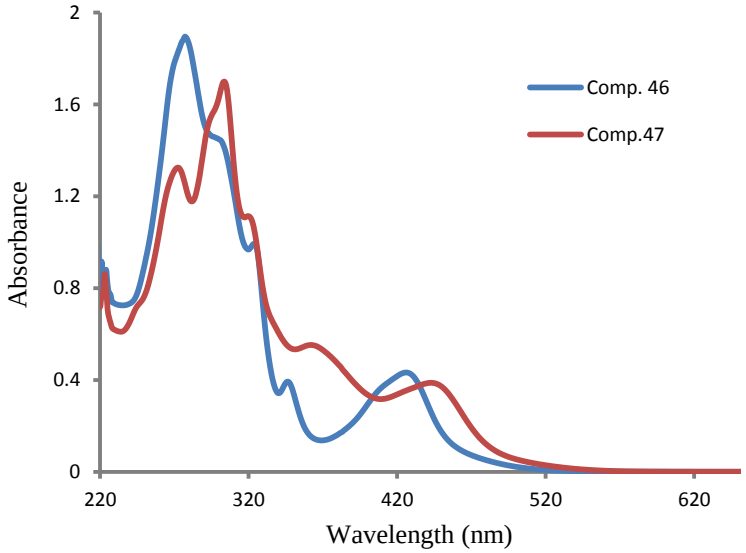

Figure 4.16. UV-vis absorption spectra of compound **46** and **47** (1×10^{-5} M) recorded in CH_2Cl_2.

4.3.3.3. Cyclic voltammetry

Electrochemical properties of the TCAQ derivative **47** were carried out and compared with anthraquinone derivative **46** by CV. The resulting reduction peaks are shown in **Figure 4.17**. The redox and oxidation behaviors of the resulting compounds were investigated on a conventional three electrode cell containing glassy carbon working electrode, Ag wire a reference electrode and Pt counter electrode. The samples were prepared in CH_2Cl_2 (1×10^{-4} M) solution with 0.1 M of $TBAPF_6$ as supporting electrolyte and E_{LUMO} values for the compounds are referenced to the potential of the Fc/Fc^+ redox couple =0.0 V. The resulting electrochemical data of compounds **46** and **47** are summarized in **Table 4.5**.

Three reversible one-electron reduction peaks were observed for anthraquinone derivative **46** and are assigned to the anthraquinone and phenanthrenequinone moieties, whereas TCAQ derivative **47** is reduced in two reversible reduction peaks; a single reversible two-electron reduction peak at a more negative potential with respect to anthraquinone

derivative **46** was assigned to the TCAQ moiety and a second one electron reduction peak assigned for phenanthrenequinone moiety shifted to more cathodic value.

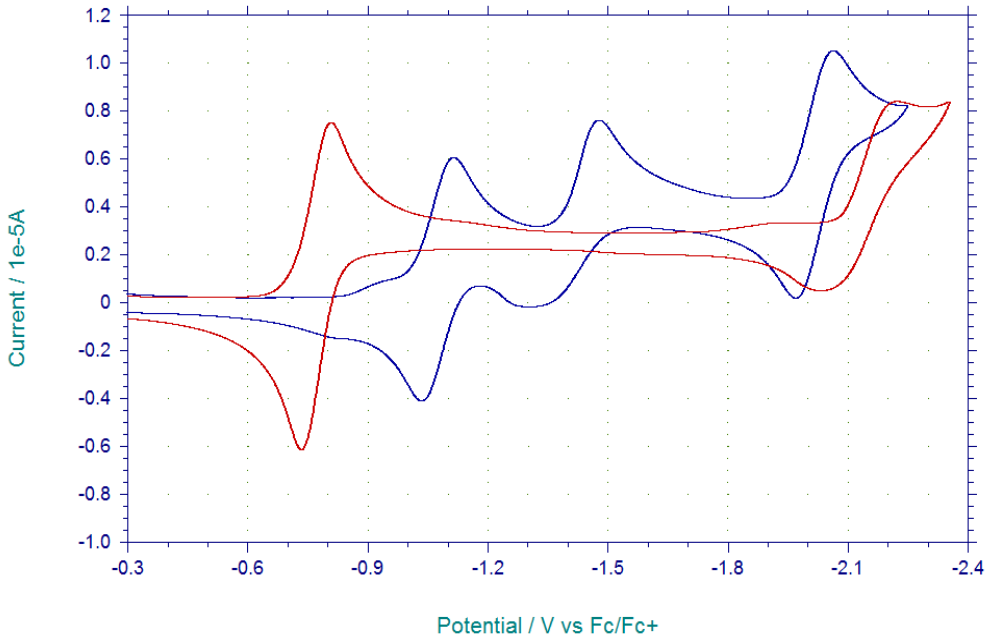

Figure 4.17. Cyclic voltammetry of compound **46** (blue line) and **47** (red line) (1×10^{-4} M) recorded in CH_2Cl_2, with $TBAPF_6$ (0.1 M) as supporting electrolyte and at scan rate of 100 mV/s.

Table 4.5. Optical and electrochemical data of compounds **46** and **47** observed by cyclic voltammetry in CH_2C1_2, with $TBAPF_6$ (0.1 M), all potentials are given *vs.* Fc/Fc^+ redox couple used as internal standard.

Compounds	λ_{max} *(nm)*/ λ_{onset} *(nm)*	*Optically determined band gap (eV)*	$E^1_{1/2}$ *(V)*	$E^2_{1/2}$ *(V)*	$E^3_{1/2}$ *(V)*	E_{LUMO} *(eV)*
46	420/ 468	2.7	-1.08	-1.40	-2.02	-3.72
47	440/ 487	2.5	-0.78	-2.14	-----	-4.02

4.4. Conclusion and future work

4.4.1. Conclusion

To summarize, we have successfully synthesized two different series of push-pull chromophores containing DMA moieties as a strong donating group and TCNE or TCNQ as electron accepting units with different conjugated spacers. One of the series features 9,10-phenanthraquinone or/ and TCAQ units and the second series features oligothiophene unit as donor unit**.**

More soluble and highly coloured NLO molecules were synthesized *via* [2+2] cycloaddition reaction in moderated yield. The compounds solvatochromic properties were studied using different polarity solvents. An increase in the intensity and shift the intermolecular charge transfer band into near IR region was observed by using high polarity solvents.

Electrochemical studies of the resulting dipolar compounds showed significant reversible peaks assigned for TCBD or TCNQ units in the reductive scan and dimethylaniline DMA in the oxidative scan. Observation the first reduction peak of the TCNQ derivative at more negative value in comparison with TCBD derivative indicates significant difference in the LUMO energies leading to a small band gap value.

A larger band gap value was observed for compound **44** in comparison with the one thiophene derivative **43** resulting from a greater anodic shift in the first reduction peak for the bithiophene derivative. In contrast the oxidation peaks assigned to DMA units remain approximately the same value for both compounds. For the TCAQ derivatives the reduction peaks occurs at more positive value indicating a lower energy value for LUMO level compared with the anthraquinone derivative.

4.4.2. Future work

With more time available, a new series of push-pull chromophore with different numbers of thiophene units could be prepared and studied in order to investigate the change in the band gap. In due course, some of the compounds described in this chapter will be screened for NLO and photovoltaic properties.

Chapter 5;

Synthesis of new planar and non-planar push-pull systems featuring thiophene moieties for DSSCs.

5.1. Introduction

5.1.1. The history of organic sensitizer

Significant progress in the organic DSSCs occurred when Grätzel and O'Regan revealed considerable PCE of around 7 % for a Ru (II) pyridyl dye. The efficiency was later increased to 10 and 11.1 % for **N3** dye (or its salt **N719**) and black dye **N749**, respectively. **Figure 5.1** shows the molecular structures of common Ru (II) pyridyl dyes.[148, 149]

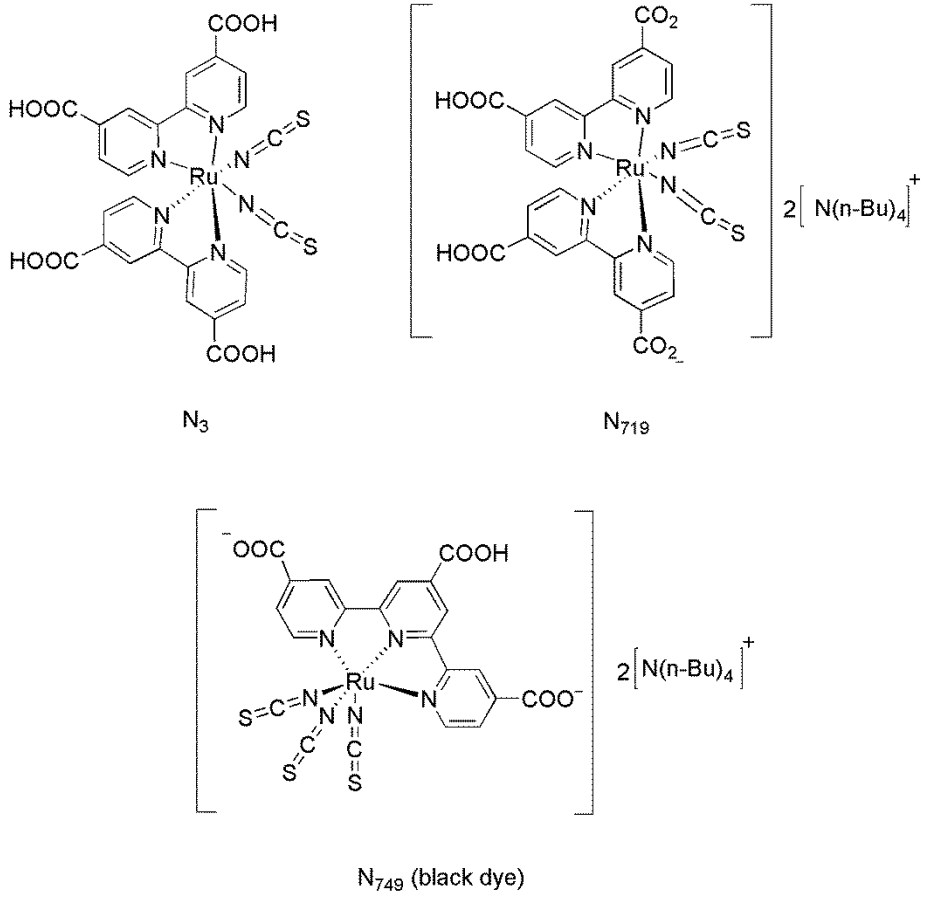

Figure 5.1. Molecular structures of common Ru (II) pyridyl dyes.

Before the aforementioned significant advances, many attempts were focused on applying a monolayer or multilayer of the inorganic sensitized dyes on a smooth semiconductor surface in order to increase the efficiency. Although early attempts of using monolayer of dye on flat surface gave efficiency around 1 %, this was much too low for practical applications. The poor ability of the monolayer in harvesting a significant fraction of incident light and the possibility of losing this incident light through the process are key reasons for the poor efficiency. Further unsuccessful progress resulted from applying multilayer of the dye on a flat semiconductor surface. In both cases, the formed excited state of the dye occurred at a distance far away from the semiconductor interface and led to poor electron injection ability. In addition, the oxidized dye could be formed in low dielectric constant area of the film which could lead to unwanted recombination.[150] Therefore, Grätzel and O'Regan replaced the planar and smooth semiconductor electrode with mesopourous metal oxide electrode in order to increase the adsorbed number of dyes on the surface at the same time allowing direct contact with the redox electrolyte**.** By applying this technique significant increase in light harvesting by the dye and the number of electrons injected into the semiconductor was recorded.[151] The improvement in the efficienency of this process is shown in **Figure 5.2**.

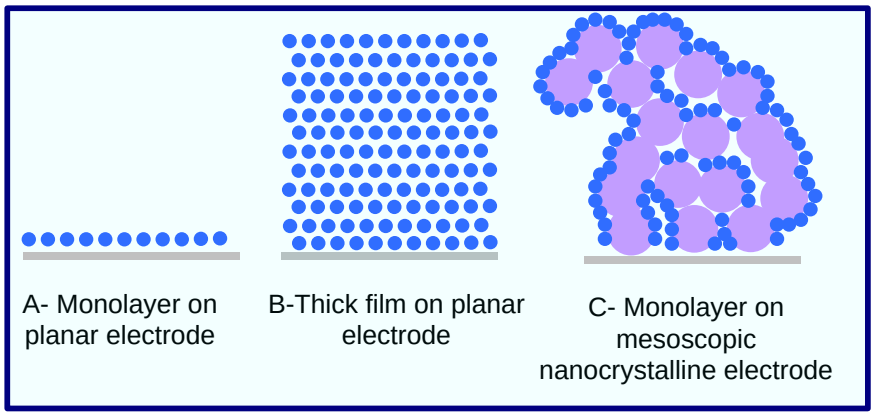

Figure 5.2. Improvement in efficiency of electrodes for DSSCs.[150]

The challenge of moving from conventional solar cell devices based on silicon with efficiency reaching around 25 % into alternative approaches with efficiency reaches 10-11% resulting from organic solar cell is governed by number of factors; including reducing the production and fabrication cost to a fraction of the value compared with the cost of silicon solar cell production, increasing the processability to fit a large scale area.[16] In this context, DSSC have been extensively investigated in order to improve the physical properties and enhance the performance of the cells. The evaluation of DSSCs conversion efficiencies is shown in **Figure 5.3**. Since 1992 until now, significant progress has been noticed for ruthenium polypyridyl complexes with highest efficiency reached 11 % under standard solar illumination.[149] However, limitation in long term stability and poor extinction coefficient values of Ruthenium complex based dyes cause a reduction in the harvesting ability even with increased thickness of the TiO_2 surface. Therefore, applying organic sensitizer as an alternative approach assists in solving these problems through tuning and modifying the chemical structure easily, improving the extinction coefficient, as well as reducing the cost and solving some of the toxicity problems.[16] Although poor performance was observed in the beginning of 1998 for applying organic sensitizers with efficiency limited to 1.3 %, a significant enhancement was observed in the efficiency reached about 9.5 % for applying organic indoline dyes in 2008. In between these periods, coumarines and polyene dyes show modest improvement in the efficiency resulting from molecular aggregation on TiO_2 surface which leads to quenching of the excited dye and poor electron injection.[152] These results were followed in 2009 by higher value of efficiency reaching around 9.8 % with dye containing triphenylamine as donor unit.[153] **Figure 5.4** shows molecular structure of common metal free organic sensitizers.

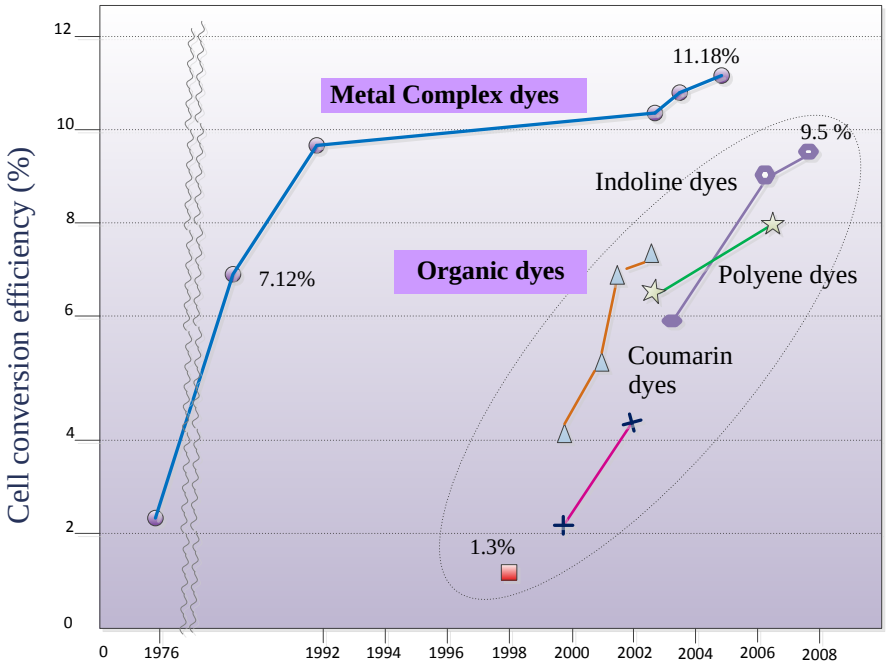

Figure 5.3. Evaluation of DSSCs conversion efficiencies under standard illumination.[154]

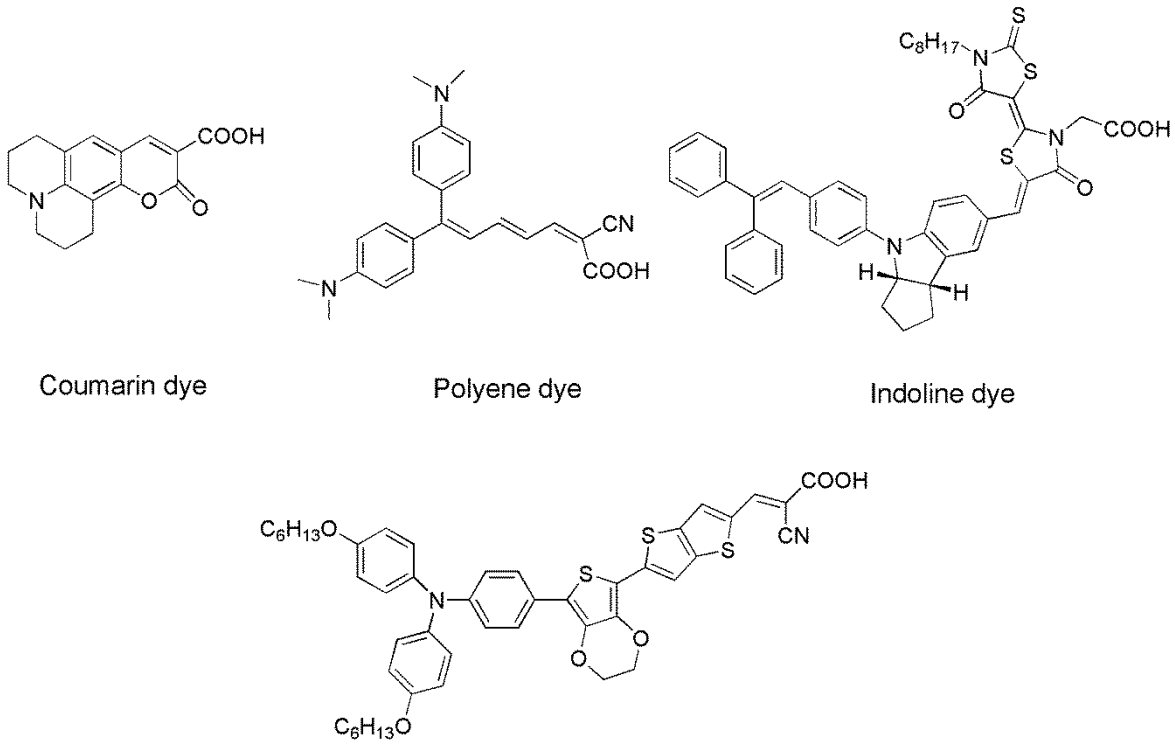

Figure 5.4. Molecular structure of some metal free organic sensitizers.

Therefore, adjusting the molecular structure of the dyes plays an important role toward improving the performance of DSSCs. These dyes have a common basic chemical structure containing of electron donor unit attached to electron acceptor unit through π-conjugated spacer. Arylamines is the most used electron rich unit in DSSCs due to effective stability and powerful aggregation resistance ability; whereas cyanoacrylic acid, phosphonic acid or sulfonic acid represents examples of electron accepting units. Importantly these units at the same time are used as anchoring groups onto the TiO_2 film. The design structures of these dyes are completed by a π-conjugation system between the associated units in order to tune the properties of resulting dye toward enhancing light harvesting. The result dipolar structures assist in producing intermolecular charge transfer between the donor and acceptor unit during the photoexcitation process.[154]

5.1.2. Dye-sensitized Solar Cells

The device architecture of DSSCs shown in **Figure 5.5**; consists of noncrystalline mesoporous titanium dioxide film which is the working electrode. This film is deposited on glass substrate covered with a TCO substrate (usually fluorine doped with SnO_2). The thickness of the applied TiO_2 film is typically around 10 μm with nanoparticle dimensions around 10-30 nm and the band gap is around 3.2 eV. These features of TiO_2 form an internal contact surface with the adsorbed dye greater than a smooth electrode surface. A monolayer of adsorbed dye attached to TiO_2 surface through anchoring groups is responsible of absorbing a large amount of spectral light. The device architecture is completed with a conducting glass substrate and activated with a platinum catalyst. This used as a counter electrode to regenerate the hole transport material by the electrons coming from TiO_2 through the external circuit. The fast rate of electron transfer between iodine and triiodine species, the high diffusion coefficient of these species to reach the

counter electrode and the satisfactory rate of oxidized dye regeneration make iodine and triiodine species the most accepted redox couple used in the DSSC devices.[16,155]

5.1.3. DSSCs light converting process

The general principle of converting light into electricity in DSSCs differs from conventional semiconductor solar cells in which the sensitizer is responsible for transferring adsorbed photons from incident light into electrical charges (equation **(5-1)**). In addition, the light harvesting and transport of charge carriers occurs in two separate states. Whereas the light harvesting is completed by the synthesized dye, the transportation of electrons and holes is completed by TiO_2 electrode and electrolyte, respectively (equations **(5-2)** and **(5-3)**). The injected electrons into the semiconductor surface travel through the external circuit to the counter electrode and contribute in oxidizing the redox electrolyte **Figure 5.5**. The process of injecting electrons into TiO_2 is a fast process (occurs in subpicoseconds) and contributes in forming an efficient oxidized dye. The produced oxidized dye is regenerated through reduction process with iodide species forming an initial dye-iodine complex as illustrated in the equations below. This process is followed by the formation of diiodide radicals ($I_2^{-\bullet}$) after dissociation of the dye-iodine complex in the solution. Two of diiodide radicals react to form triiodide and iodide species (equation **(5-4)**). The counter electrode is responsible for passing the injected electrons and reducing triiodine species to ensure sufficient iodine species (equation **(5-6)**). This process continues all over again unless quenching of the oxidized dye occurs.[156]

$$D + h\upsilon \rightarrow D^* \quad (5\text{-}1)$$

$$D^* \rightarrow D^+ + e^-_{TiO_2} \quad (5\text{-}2)$$

$$D^+ + I^- \rightarrow (D \ldots I) \quad (5\text{-}3)$$

$$(D \ldots I) + I^- \rightarrow D + I_2^{-\cdot} \quad (5\text{-}4)$$

$$2I_2^{-\cdot} \rightarrow I_3^- + I^- \quad (5\text{-}5)$$

$$I_3^- + 2e^- \rightarrow 3I^- \quad (5\text{-}6)$$

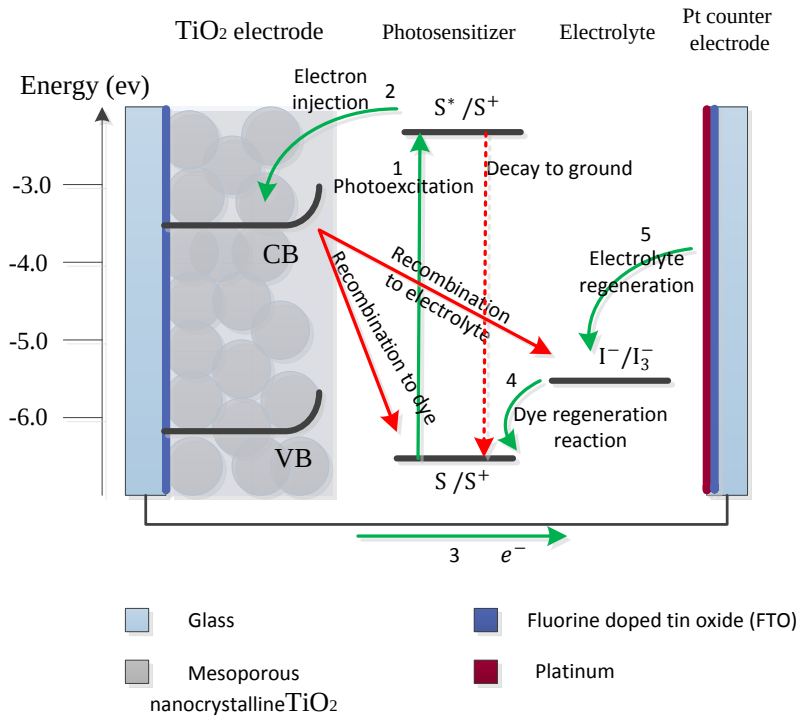

Figure 5.5. Schematic diagram representing the device architecture and the working principle of DSSCs.[16]

During the illumination process, variation in the electron density occurs on the photoelectrode and the counter electrode surface. This variation forms an electrochemical potential difference and leads to motion of the charges through the circuit and generation of a photocurrent.[157]

However, device performance is hampered by losses during the conversion process. Quenching of the dye's charge is an example of energy loss. It could result from either slow injection of electrons into the TiO_2 conduction band or an increase in the concentration of iodine species in the medium. In case of increasing the concentration of iodine, the iodine species are responsible for reducing the excited dye and forming reduced dye species (equation **(5-7)**). The resulting reduced dye species either inject their electrons into the conducting band of TiO_2 or complete the process normally (equation **(5-9)**), or they may counter recombination by reacting with triiodide species in the medium (equation **(5-10)**). At the same time, the formed radical idodide and the existence of iodide ions in the electrolyte react to form two diiodide radicals (equation **(5-8)**).[156]

$$D^* + I^- \rightarrow D^- + I^{\cdot} \quad (5\text{-}7)$$

$$I^{\cdot} + I^- \rightarrow I_2^{-\cdot} \quad (5\text{-}8)$$

$$D^- \rightarrow D + e^-_{TiO_2} \quad (5\text{-}9)$$

$$D^- + I_3^- \rightarrow D + I_2^{-\cdot} + I^- \quad (5\text{-}10)$$

In the case of slow electron injection, the efficiency of this process depends not only on the rate of moving electrons into the conduction band; but is also affected by the rate of excited state decay of the dye to the ground state. Although triplet state has longer life time compared with singlet excited state dye, it is a less energetic state which could negatively affect the efficiency of injected electrons. However, increasing the rate of this process depends on a number of factors; i.e. the overlap between the LUMO level of the dye and conduction band of TiO_2, the electron density on the anchoring group of the dye and the nature of the excited state.[155]

However, the injected electrons could also be prone to charge recombination before reaching the external circuit. This could occur because of the slow electron transportation

through metal oxide film, which is affected by the trapping of the electrons in the film. This results in a low open circuit voltage and an increase in the dark current value. Therefore, the electron could recombine with the dye cation due to poor regeneration of oxidized dye, or into the hole transport material due to the insufficient injected electrons passing through the circuit into the electrolyte.

Therefore, strict demands upon improving the optical and electrochemical properties of the selected organic dyes should be considered in order to minimize the energy loss and improve the DSSCs device efficiency. These demands can be concluded in three main approaches; (i) develop a low band gap covering the visible and near-infrared region to allow photons from this area in solar spectrum to be absorbed; (ii) consider the LUMO and HOMO level of the dye compared with the position of the TiO_2 conducting level and redox electrolyte, respectively. The LUMO level of dye should be higher in energy compared to the conduction band while the HOMO level should be lower in energy compared with HOMO level of the electrolyte to insure sufficient electron injection into TiO_2 and regeneration of oxidized dye from the redox electrolyte as illustrated in **Figure 5.5**;[157] (iii) the positive charge on the oxidized dye should be localized on the donor unit and attached to π- conjugated spacer to insure less recombination of the injected electron by increasing the distance between the cation and TiO_2 surface. Conversely the electron density should be located on the acceptor unit for sufficient electron injection into TiO_2 surface. Achieving these conditions can be done by choosing different electron-donating groups and different π- conjugated spacer groups attached to a cyanoacrylic acid residue in the dye molecules.[158]

5.1.4. Non-planar push-pull organic dye

Significant progress in modulating the organic DSSCs was observed by Hara et al. using DMA units as donor and cyanoacrylic acid as an acceptor. These units were connected with diene or triene π-conjugated spacers. Satisfactory results were recorded for the performance of these dyes in DSSCs with efficiencies of around 5 % for the associated dyes and a maximum value reach around 6.8 % for dye **5.3** which showed maximum IPCE after adding deoxycholic acid (DCA) as assisting agent during the adsorption of the dye onto the TiO_2 surface.[159]

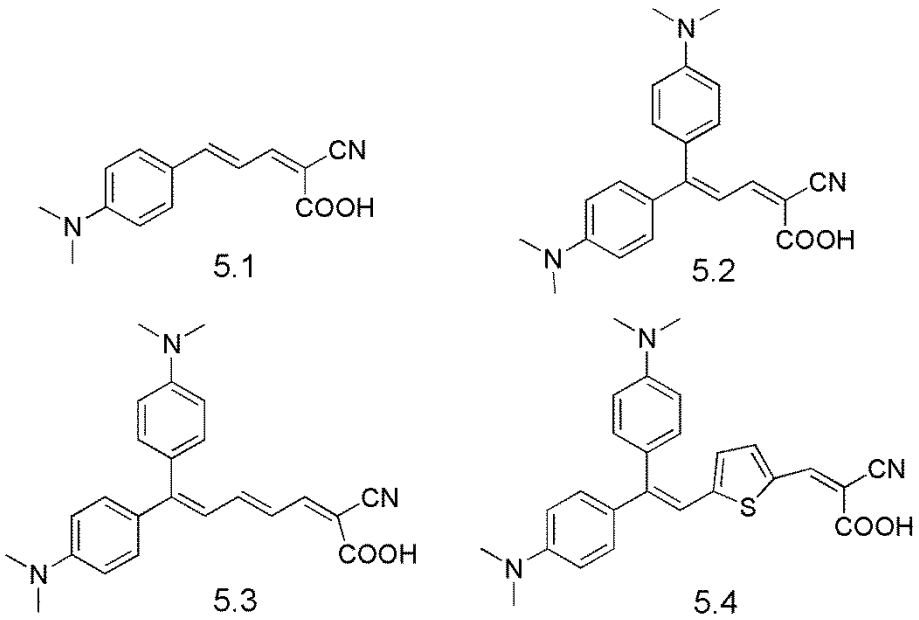

The modification in the optical properties of organic dyes can be done through varying the π-conjugated spacers between the donor and acceptor moieties. This modification could have a significant effect on adjusting the energy levels and improving the physical properties of organic sensitizers. Therefore, a variety of heterocyclic linkers have been used in organic sensitizers to study the influence on the device performance. The results showed power conversion efficiency of 6.6 % obtained for the dyes containing a thiophene

linker with CPDT bridge dye **5.6**. This value results from increasing the J_{sc}. In addition, the photocurrent decay measurements of the synthesized dyes indicated that the dyes with phenyl linkers in **5.5** and **5.7** have the longest electron injection life time in TiO_2 films compared with thiophene and thiazole linkers, and resulted in increasing both V_{oc} and power conversion efficiency.[160]

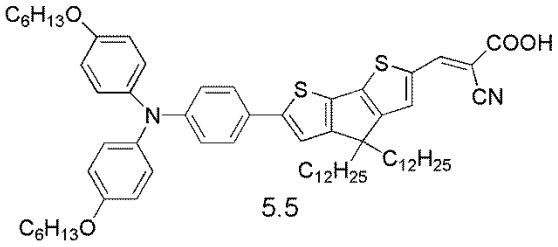

5.5

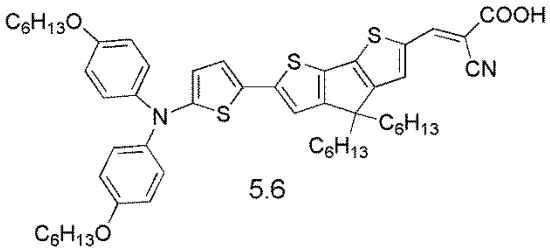

5.6

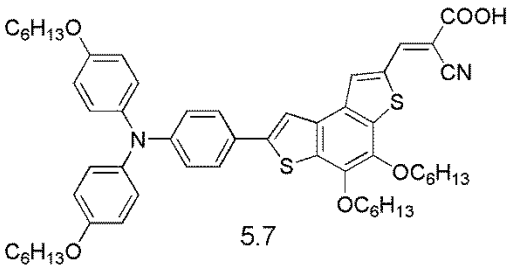

5.7

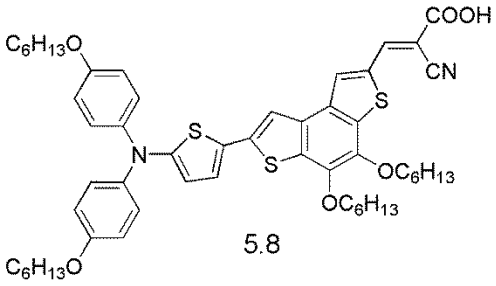

5.8

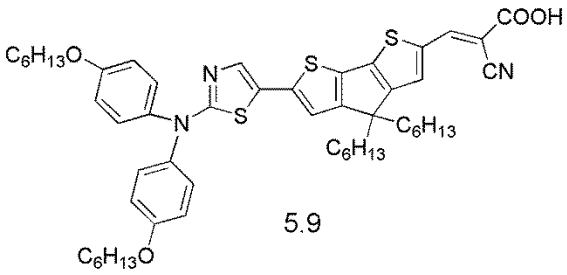

5.9

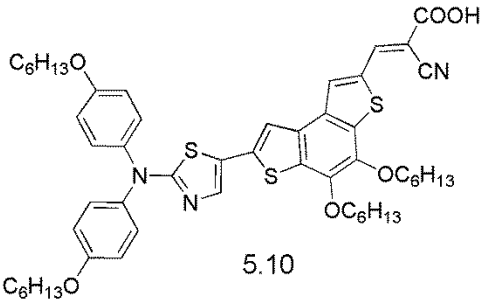

5.10

In addition, introducing a sterically hindered moiety into the π-conjugated spacer of an organic dye could assist in preventing dye aggregation by reducing the recombination on a TiO_2 surface and could lead to better performance. Therefore, Kozma *et al.* incorporated 3-dialkylthiophene as a linker into different π-conjugated spacers containing tetrathiophene or dithieno[3,2-b:2’,3’-d]thiophene attached to triphenylamine to increase the conjugation length and prevent π-stacking. Both dyes exhibited high V_{oc} values indicating efficient

injection of electrons into the TiO_2 surface which led to efficiency value of 7.17 % and 6.27 % for dye **5.11** and **5.12,** respectively.[161]

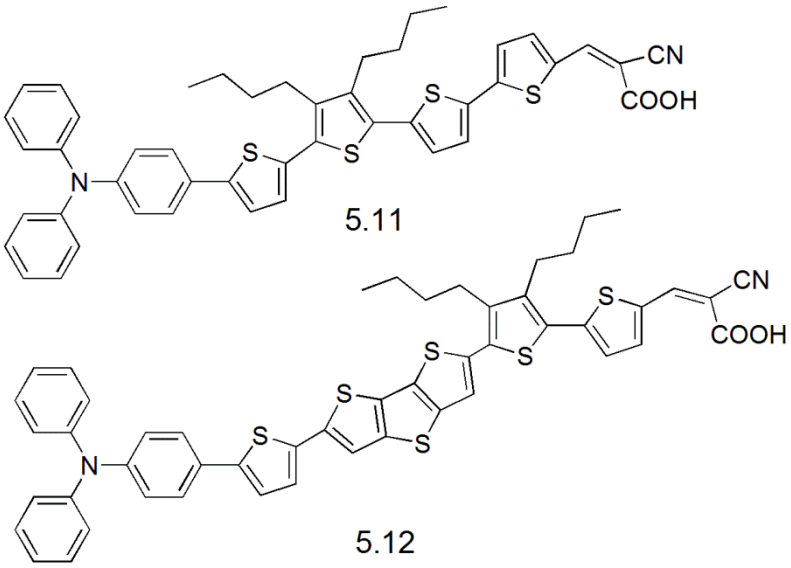

Using rigid π-conjugated polycyclic structures such as benzo[1,2-b:4,3-b']dithiophene and benzo[1,2-b:4,5-b']dithiophene and TPA as donor units could increase conductivity and π-π stacking in the solid state, as well as reducing the recombination of excited electrons. Good efficiency was observed for dye **5.13** compared with dye **5.14** due to localized electron density on the benzo[1,2-b:4,3-b']dithiophene unit closer to the anchoring group which resulted in stabilizing the LUMO level and increasing the conjugation between donor and acceptor units.[162]

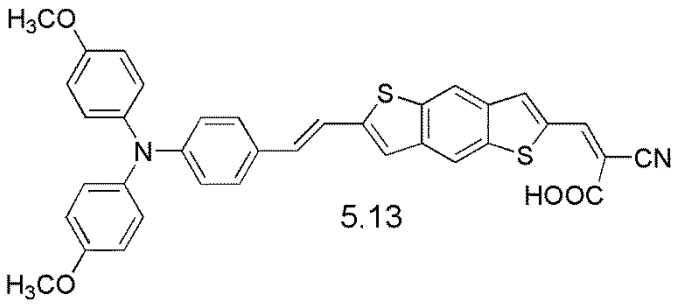

5.13

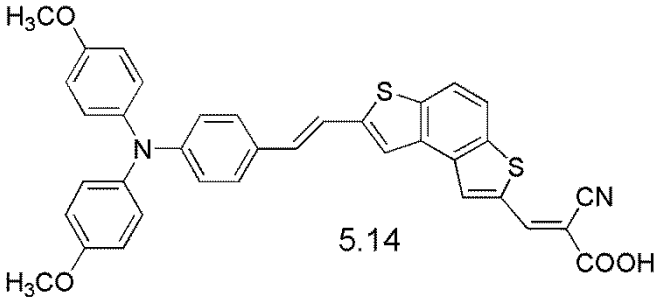

5.14

A variety of electron rich and electron deficient units has been incorporated with the EDOT unit to form binary π-conjugated spacer in a typical D-π-A dye. One study revealed that among the synthesized dyes, dye **5.18** had a better performance as a photosensitizer in DSSCs with efficiency reaching 6.11 %. The improvement in efficiency results from red shift in the wavelength of IPCE spectrum and an increase in the maximum IPCE peak. In addition, the small molecular size of this dye **5.18** contributes to its anchoring on the TiO_2 surface and leads to high electron density surface and effective performance.[163]

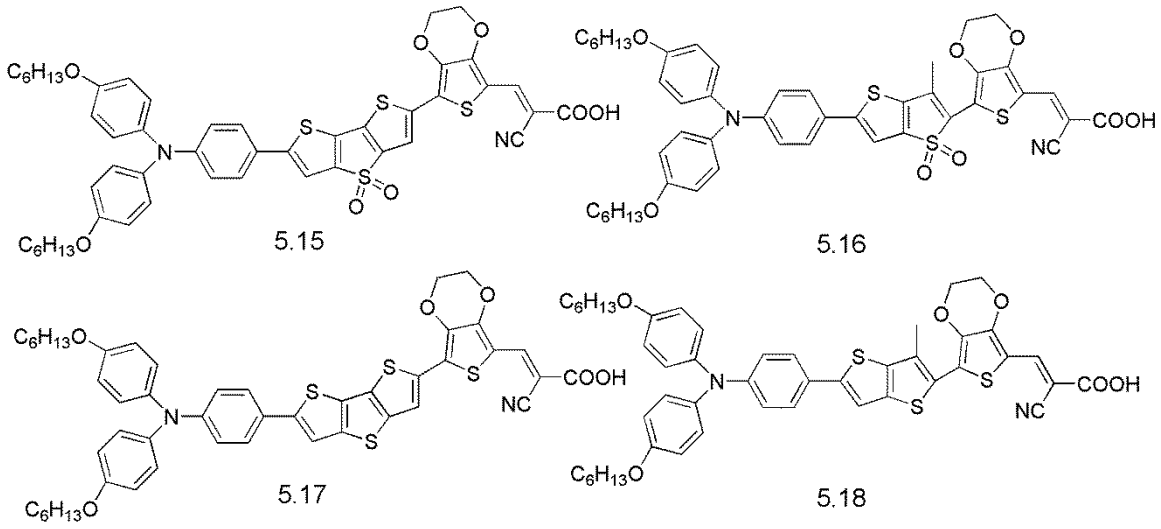

Exploiting the properties of oligothiophene materials has played an important role in improving their performance. This is due to the unique combination between chemical stability, ideal π-delocalization, simplicity in modification and ability to tune the optical and electrochemical proprieties.[145] Therefore, Wang *et al.* synthesized new organic dyes containing a carbazole donor unit and cyanoacrelic acid acceptor unit with differently positioned n-hexyl substituted oligthiophene units acting as the π-conjugated spacer. The alkyl groups were used in order to control the amount and thickness of the adsorbed dye on the TiO_2 surface and reduce the recombination of injected electrons with the electrolyte. All synthesized dyes showed long electron injection life times and an increased V_{oc} resulting from increasing the number of adsorbed dyes on the TiO_2 film. These features lead to a maximum efficiency of 8.3 % for dye **5.20**.[164]

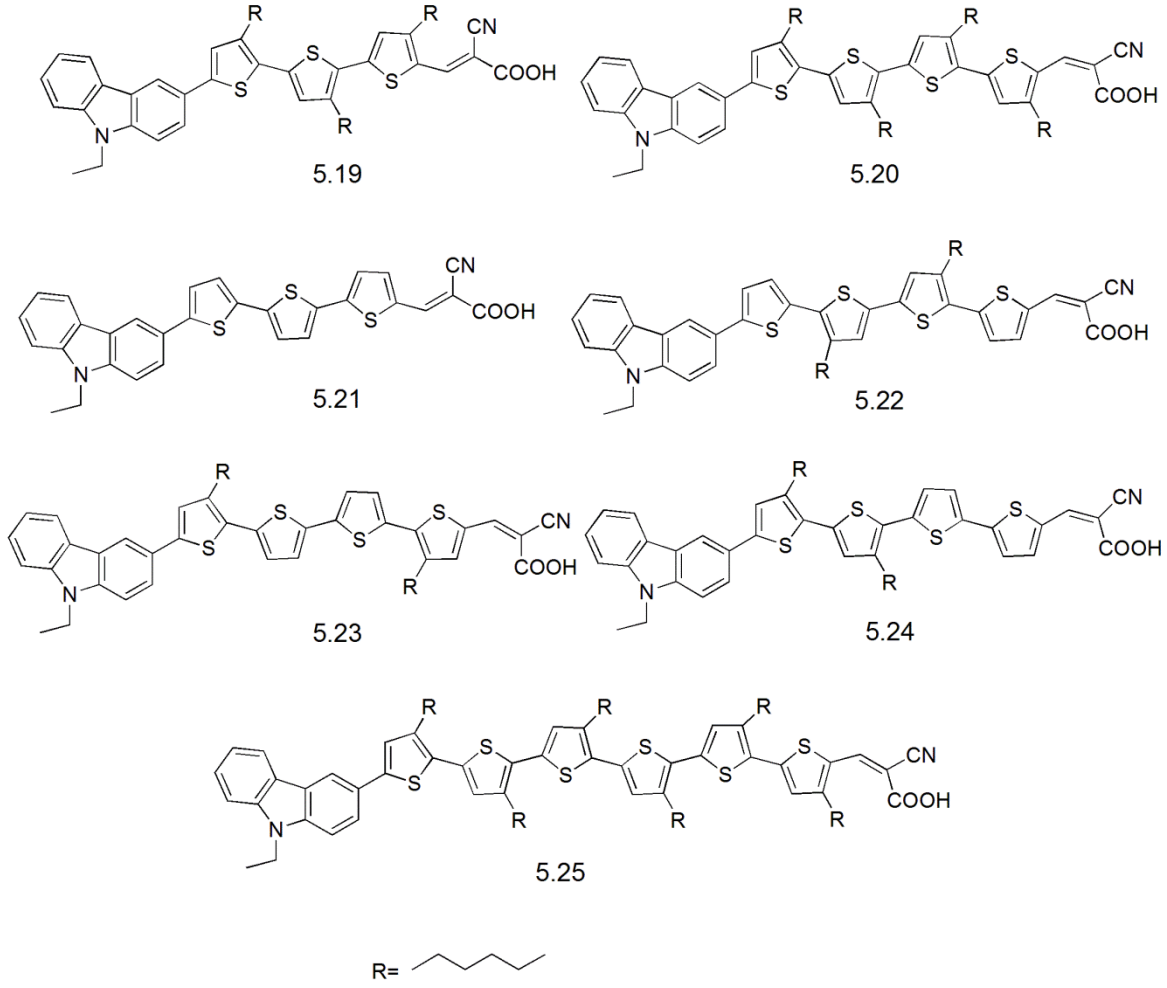

In addition to electron donating ability and effective stability of TPA in DSSCs, aggregation resistance of this unit also has significant effects on the performance of organic sensitizers. Other features include ultrafast electron injection and reduction in the recombination of injected electrons with the electrolyte. Therefore, the effect of reducing electron recombination and enhancing light harvesting on the performance of dyes featuring TPA was investigated by synthesizing a series of planar dyes consisting of different flexible rotational bridges. Improving in the power conversion efficiency was observed for dye **5.28** due to an increase in the conjugation path between the donor and acceptor units and improvement in the overlap between the LUMO energy level of the dye and conduction band of TiO_2.[165, 166]

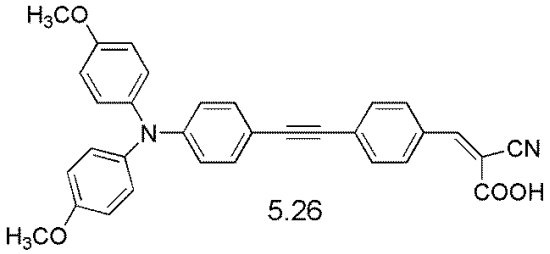

5.26

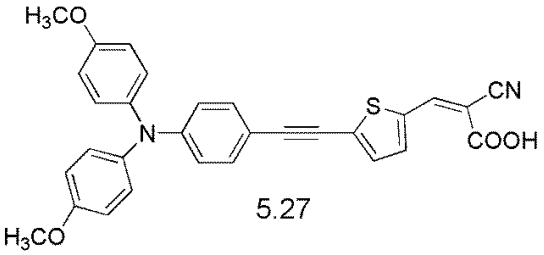

5.27

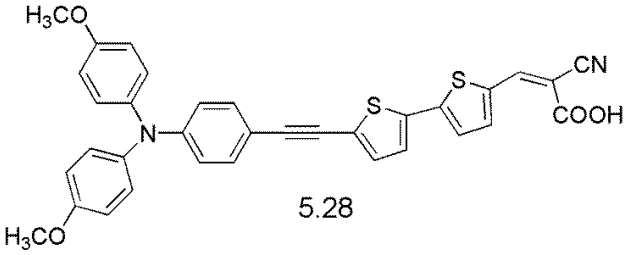

5.28

Moreover, the bis-dimethylfluoreneaniline moiety can improve the PCE of the dye *via* reducing the aggregation of the dye on the semiconductor surface at the same time increasing light absorption ability. Applying thiophene units as π-conjugated spacers in these dyes reflected positively on the performance through increasing the conjugation between the donor and acceptor units and enhancing the molar extinction coefficient of the dyes. Efficiency of dye **5.30** was observed to be around 8.01 % and was attributed to increasing the conjugation between donor and acceptor units and enhancing the J_{sc} value compared with dye **5.29**.[167]

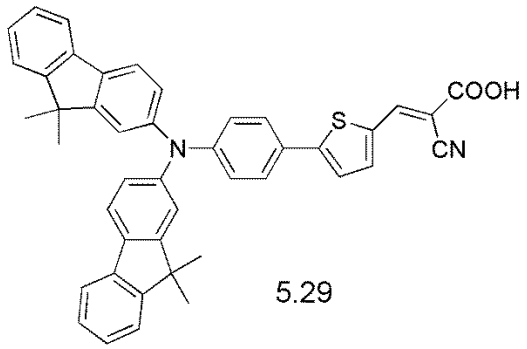

5.29

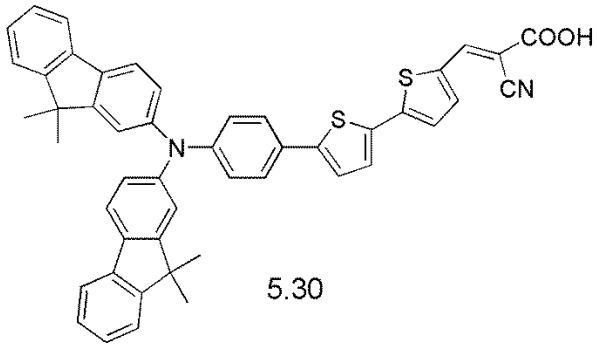

5.30

Further investigations were carried out relating to the efficiency of new photosensitizers which are structurally similar to the organic dyes **5.29** and **5.30**. The study focused on expanding the absorption region by introducing dienes into the conjugation spacer in dyes **5.29** and **5.30**. However, compared with previously prepared dyes poor efficiency was recorded for associated dyes **5.31** and **5.32**. This could be due to quenching of the excited electrons by the solvent and poor electron injection into the semiconductor surface.[168]

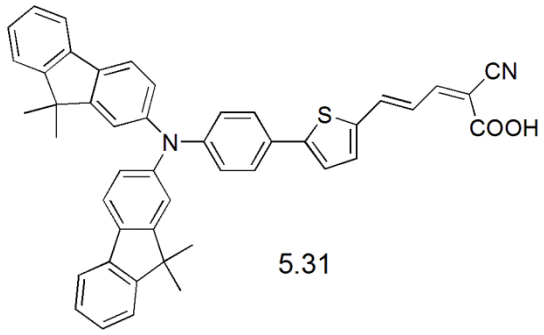

5.31

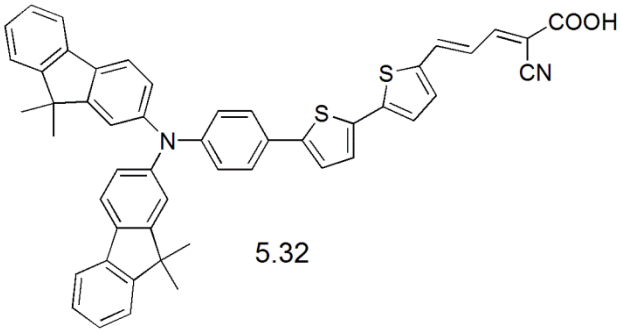

5.32

Enhancing the efficiency of DSSCs has been investigated by locking the phenyl units attached to amine unit from rotation. Therefore, incorporation of 5-phenyl-iminodibenzyl or 5-phenyliminostilbene as donor units into organic sensitizers has been shown to improve the efficiency especially for dye **5.36**.[169]

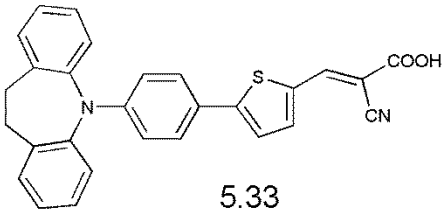

5.33

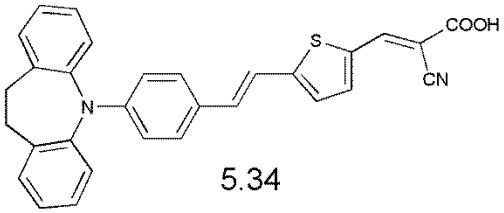

5.34

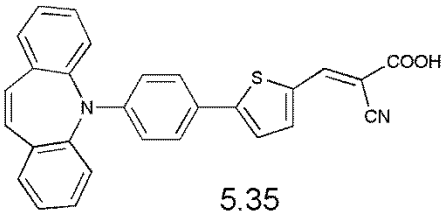

5.35

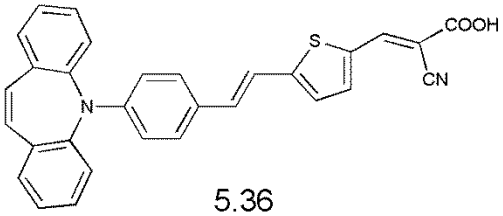

5.36

Using bulky substituted amines instead of triphenylamine in a D-π-A system has improved the power conversion efficiency to about 8.71 % for dye **5.39**. This significant improvement in the efficiency resulted from an increase in both the short circuit current and open circuit voltage compared with other associated dyes. The increase in V_{oc} was attributed to the long life time of separated charges and the aggregation resistance of the dye.[170]

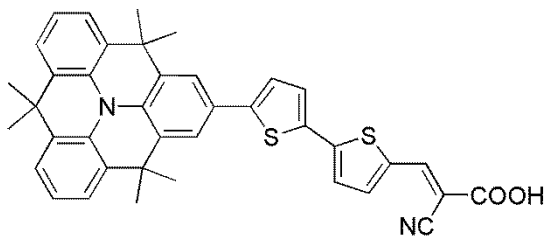

5.37

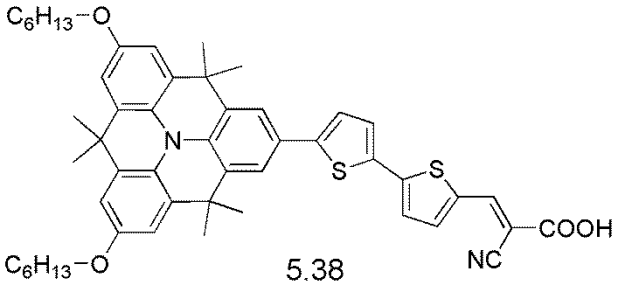

5.38

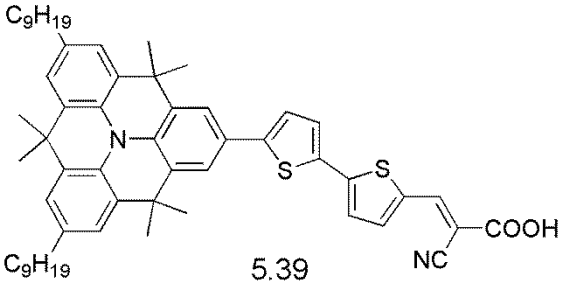

5.39

5.2. Aims and objectives

The aim of this project was to synthesize new series of metal free organic dyes that could improve the efficiency of DSSCs by modulating the absorption of light towards the near-IR region. Therefore, this chapter describes the synthesis of two different series of powerful organic dyes containing DMA moieties as a strong donating group and cyanoacrylic acid as acceptor and anchoring group. These units are connected together with different π-conjugated systems containing thiophene and bithiophene units attached to alkynes or TCNE units as linkers in order to increase the conjugation and prevent the interaction between the two thiophene units due to the non-planarity of the latter systems. The molecular structures of these dyes are shown in **Figure 5.6**.

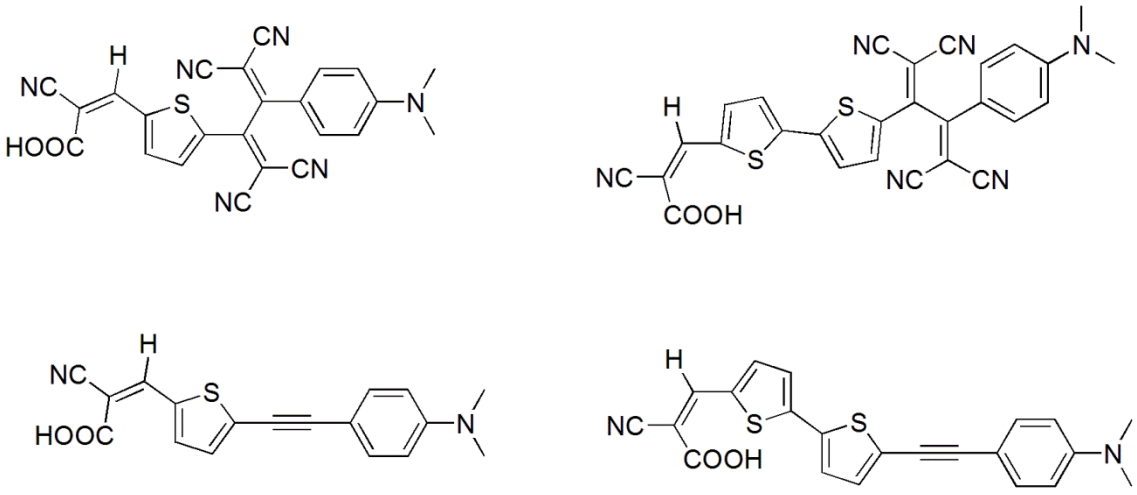

Figure 5.6. Metal free organic dyes featuring an alkyne or TCNE as the π-conjugated spacer.

5.3. Results and discussion

5.3.1. Synthesis of the compounds

The synthesis of metal free organic dyes **48** and **49-51** is outlined in **Scheme 5.1**. The synthesis started from coupling 4-ethynyl-*N*-*N*-dimethyl aniline **28** with 5-bromo-2-thiophenecarboxaldehyde **35** or 5-bromo-2,2'-bithiophene-5'-carboxaldehyde **36** *via* Songoshira coupling in the presence of 10% Pd/C and CuI as catalysts to give compound **37** and **38,** respectively, in good yields**.** To synthesize the non-planar organic dyes, compounds **37** and **38** underwent [2+2] cycloaddition reactions at 66 °C with TCNE. Retro-electrocyclisation afforded and gave compounds **39** and **40** in 56 % and 66 % yields, respectively. Organic dyes **48** and **49** were obtained *via* Knoevenagel condensation reaction of compounds **39** and **40**, respectively, with cyanoacrylic acid. The reaction conditions involved the use of piperidine as a catalyst and CH_2Cl_2 as solvent. Organic dyes **50** and **51** were obtained *via* Knoevenagel condensation reaction of compounds **37** and **38**, respectively, with cyanoacetic acid and in the presence of piperidine as a catalyst and CH_3CN as solvent.

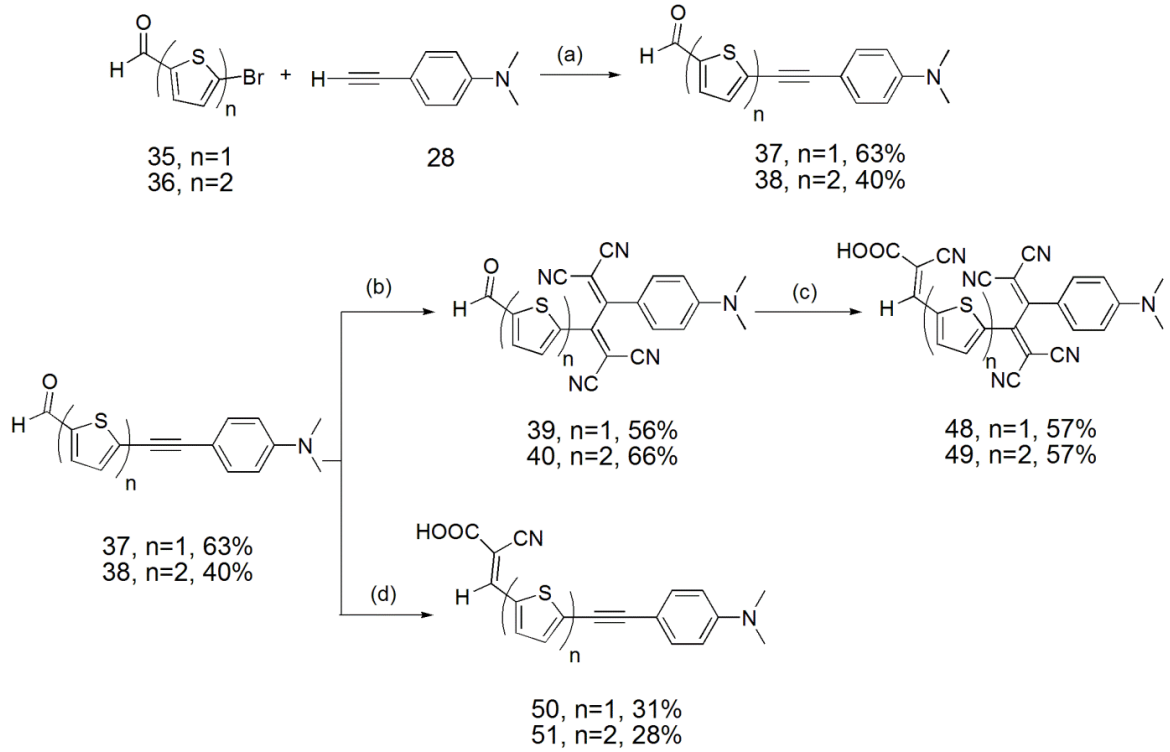

Scheme 5.1. Reagents and conditions: (a) Pd/C 10%, CuI, Ph_3P, K_2CO_3, DME: H_2O; (b) TCNE, THF; (c) cyanoacetic acid, piperidine, CH_2Cl_2; (d) cyanoacetic acid, piperidine, CH_3CN.

5.3.2. UV-Vis spectroscopy

The UV-vis absorption spectra of dyes **48** and **49** were recorded in CH_2Cl_2 (1×10^{-5} M) and dyes **50** and **51** were recorded in DMF (1×10^{-5}M) **Figure 5.7** and **Figure 5.8**, respectively. An intense absorption band in the UV region with an abroad tail toward the near IR region was observed for all the synthesized dyes. All prepared organic dyes displayed π–π* transition bands with variation in the molar extinction values. These bands could be assigned to intermolecular charge-transfer between the electron-donating DMA unit and the electron accepting cyanoacrylic acid units.

An increase in the molar extinction coefficients and a shift in CT band towards near IR region was observed in the spectra of compound **49** relative to compound **48** which exhibited two weak intensity broad absorption bands in the UV and visible regions. The resulting wavelength shift could be assigned to increase conjugation length and intramolecular charge-transfer between donor and acceptor units.

However, the ICT absorption bands of compound **50** and **51** were of higher intensity and broader ranging between λ= 360 nm and 540 nm with end absorption around 650 nm. Bathchromic shift ca. 19 nm was observed in the maximum absorption band for compound **51** compared with **50** indicating effective π communications between the donor and acceptor units.

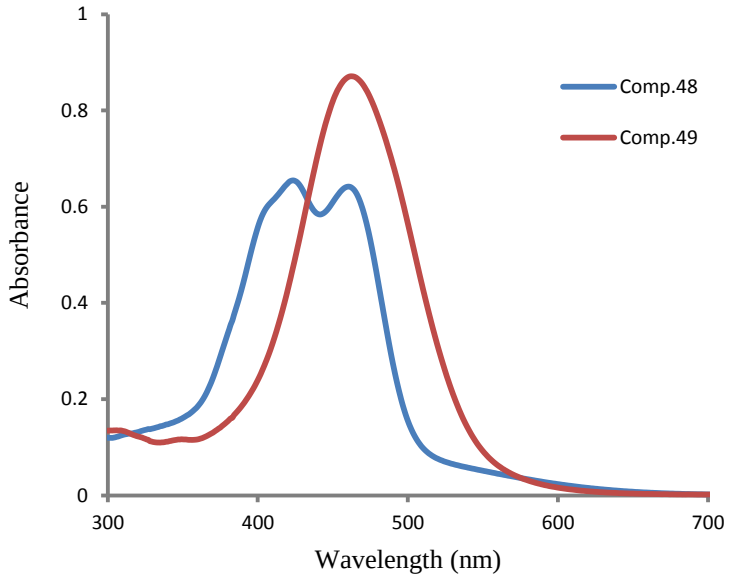

Figure 5.7. UV-vis absorption spectra of compounds **48** and **49** (1×10^{-5}M) recorded in CH_2Cl_2.

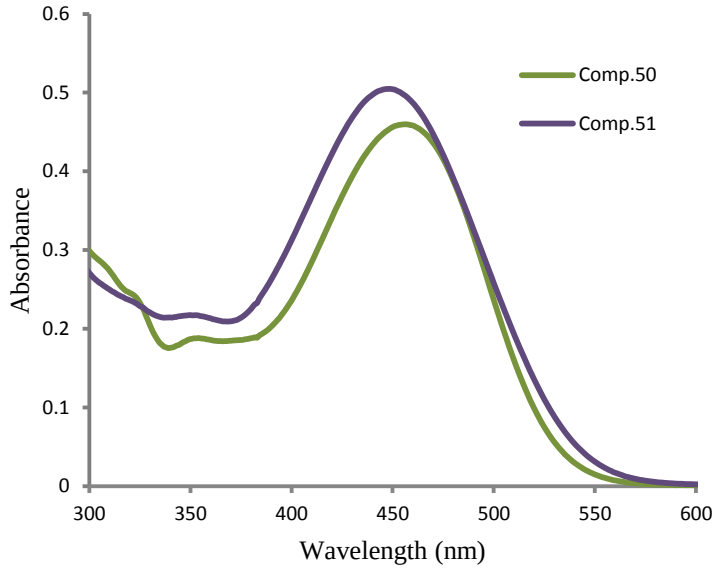

Figure 5.8. UV-vis absorption spectra of compounds **50** and **51** (1×10^{-5} M) recorded in DMF.

5.3.3. Fluorescence spectroscopy

The fluorescence emission spectra of the four dyes were recorded in DMF (1×10^{-5}M) as shown in **Figure 5.9** and **5.10**. Bathchromic emission shift and reduced intensity of the emission bands were observed for the synthesized dyes **50** and **51** compared with the starting materials compound **37** and **38**, respectively. These results are in accordance with increasing in the intramolecular charge transfer between the electron donating DMA units and the acceptor cyanoacrylic acid units. A maximum emission peak at λ= 560 nm was observed for compound **38** under excitation wavelength λ= 432 nm, however, under the same excitation wavelength compound **51** exhibited red shift with the maximum absorption wavelength occurs at λ= 575 nm.

Similarly, compound **50** displayed bathchromic emission shift and drop in intensity relative to the corresponding band of compound **37**, after excitation with λ= 432 nm. However, organic dyes **48** and **49** displayed a strong quenching of the emission after excitation with different excitation wavelengths (λ= 432 and at λ= 410 nm).

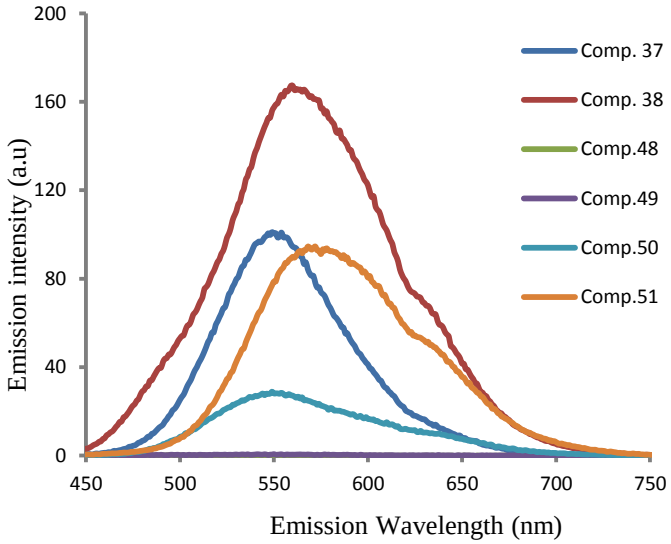

Figure 5.9. Fluorescence emission spectra of dyes and starting materials ($1x10^{-5}$ M) recorded at an excitation wavelength of λ = 432 nm in DMF.

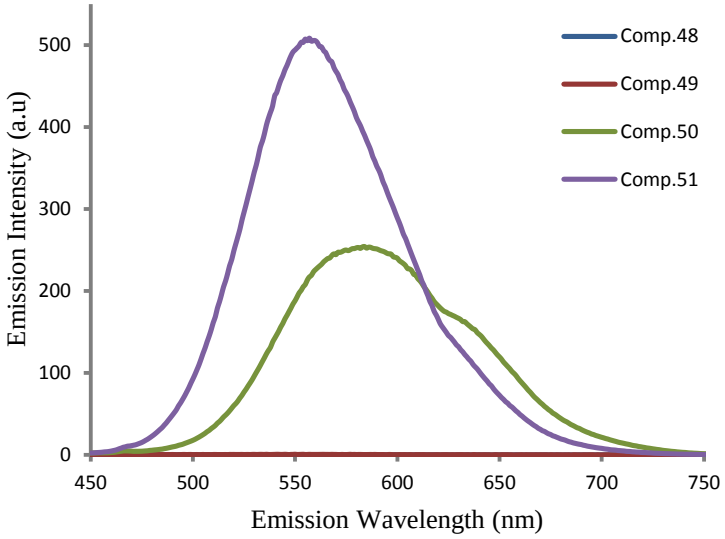

Figure 5.10. Fluorescence emission spectra of dyes ($1x10^{-5}$M) recorded at an excitation wavelength of λ = 410 nm in DMF.

5.3.4. Cyclic voltammetry

The electrochemical properties of dyes **48** and **49** were evaluated using cyclic voltammetry in order to investigate the influence of increasing the conjugation on LUMO energy levels and hence the band gaps. The electrochemical data in **Table 5.1** were obtained at room temperature in THF (1×10^{-4} M) containing $TBAPF_6$ (0.1 M) as supporting electrolyte, a platinum button as working electrode, silver wire as a reference electrode and pt counter electrode. The data are referenced to the redox couple Fc/Fc^{+}=0.0.

Two reversible peaks were observed for compounds **48** and **49** on the reduction scans which are presumably be assigned to the reduction of TCBD moieties **Figure 5.11**. The LUMO energy levels were estimated from reduction onsets of compounds **48** and **49**, whereas the HOMO energy levels were estimated from the onset wavelength of the

absorption spectra together with the LUMO energy calculated by CV. It is clear from reduction potential that the LUMO of compound **49** is higher than that of compound **48**.

Table 5.1. Optical and electrochemical data of metal free organic dyes **48** and **49** recorded using cyclic voltammetry (CV) in THF, with $TBAPF_6$ (0.1 M), all potentials are given *vs.* Fc/Fc^+ redox couple used as internal standard.

Compound	*UV results (nm)* λ_{max} / λ_{onset}	*Optically determined band gap (eV)*	*Extinction Coefficient* ($M^{-1}cm^{-1}$)	*CV results (Volts)* $E_{½}(ox)$	$E_{½}(red)$	*Calculated Energy (eV)* $E_{HOMO(optic)}$	E_{LUMO}
48	430/ 510	2.43	65,000	–	-0.89	- 6.34	-3.91
49	455 / 560	2.21	87,000	–	-0.97	- 6.04	-3.83

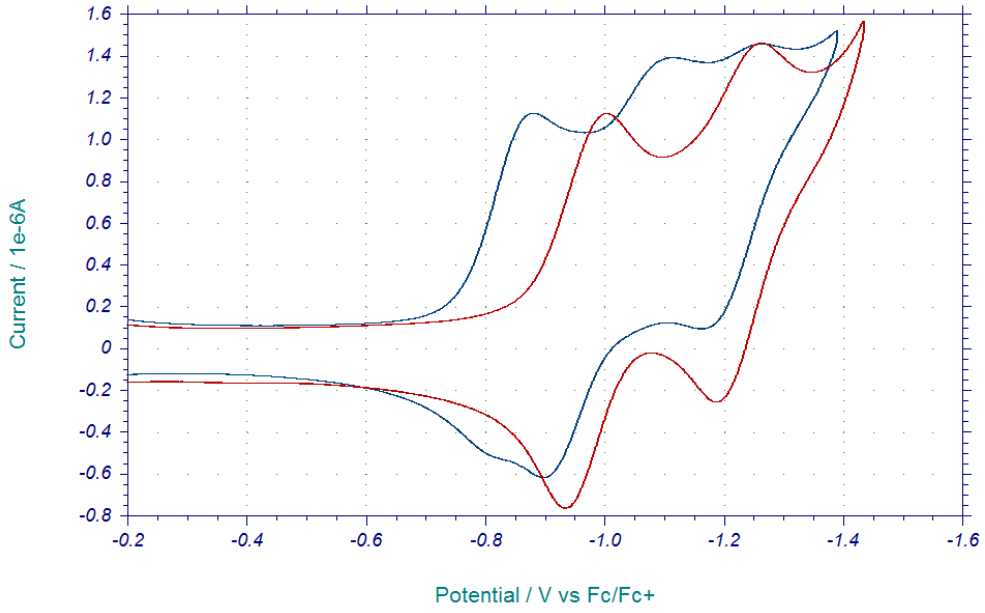

Figure 5.11. Cyclic Voltammetry of compounds 4**8** (blue line) and **49** (red line) (1 x 10^{-4} M) recorded in THF, with $TBAPF_6$ (0.1 M) as supporting electrolyte and at scan rate of 100 mV/s.

The electrochemical properties of dyes **50** and **51** were evaluated using square wave and cyclic voltammetry. The collected electrochemical data in **Table 5.2** were measured at room temperature in DMF ($5x10^{-4}$ M) containing $TBAPF_6$ (0.1 M) as the supporting electrolyte. The cyclic voltammetry data of dyes **50** and **51** showed reversible one-electron wave assigned to the reduction of cyanoacrylic moiety and quasi-reversible oxidation peak on the oxidation scan assigned for DMA unit (**Figure 5.12**). These results were compatible with the square wave voltammetry data (**Figure 5.13**). The oxidation potentials of compound **50** and **51** were determined to be 0.42 V and 0.37 V *vs.* Fc/Fc^+, respectively, and the reduction potentials were determined to be -2.09 V and -1.99 V. It is worth mentioning that increasing the conjugation length of compound **51** decreased the LUMO level to -2.81 eV compared with compound **50** which appears at -2.71 eV**.** Also the conjugation length effects positively on the HOMO level by increasing the energy level to -5.17 eV compared with compound **50** which appears at -5.22 eV. A small electro-chemically determined band gap was observed for compound **51** (2.36 eV).

Table 5.2. Optical and electrochemical data of organic dyes **50** and **51** recorded using cyclic voltammetry (CV) in DMF, with $TBAPF_6$ (0.1 M), all potentials are given *vs.* Fc/Fc^+ redox couple used as internal standard.

Compound	*UV results (nm)* λ_{max} / λ_{onset}	*Optically determined band gap (eV)*	*CV results (Volts)* $E_{½}(ox)$	$E_{½}(red)$	*SW results (Volts)* $E_{diff}(ox)$	$E_{diff}(red)$	*Calculated Energy (eV)* E_{HOMO}	E_{LUMO}	E_{GAP}
50	408 / 426	2.56	0.41	-2.09	0.42	-2.09	-5.22	-2.71	2.51
51	426 / 508	2.44	0.36	-1.99	0.37	-1.99	-5.17	-2.81	2.36

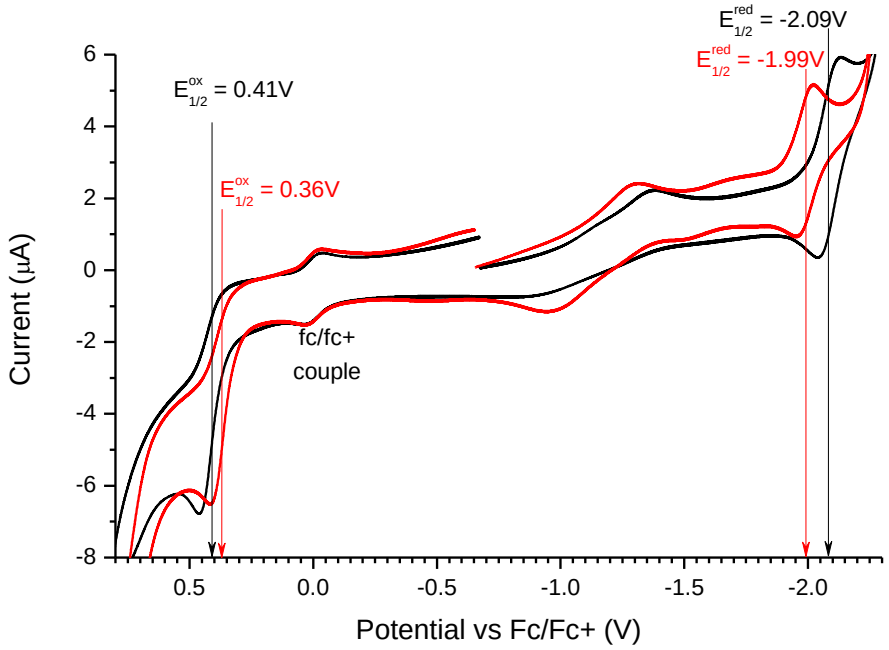

Figure 5.12. Cyclic voltammetry of compound **50** (black line) and **51** (red line) ($5x10^{-4}$ M) recorded in DMF, with (0.1 M) $TBAPF_6$ as supporting electrolyte and at scan rate of 100 mV/s.

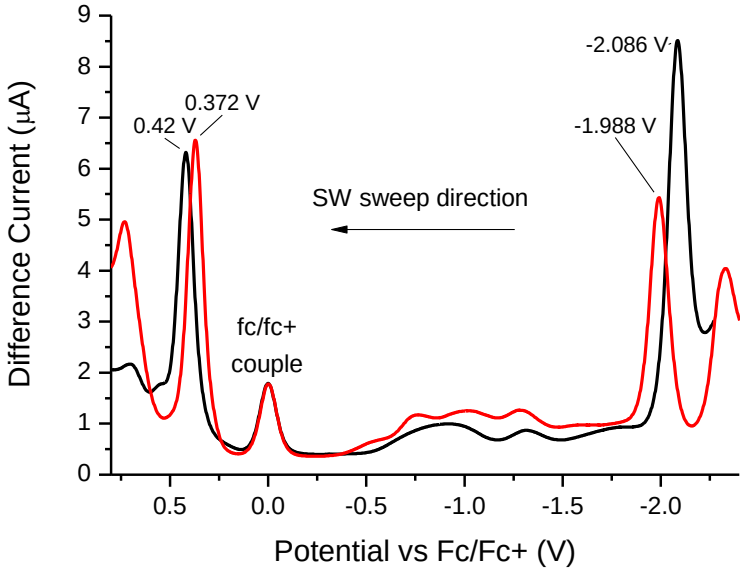

Figure 5.13. Square wave voltammogram of compound **50** (black line) and **51** (red line) ($5x10^{-4}$ M) recorded in DMF**,** with (0.1 M) $TBAPF_6$ as supporting electrolyte and at $\boldsymbol{E_{Incr} = 2\ mV}$, $\boldsymbol{E_{Amp} = 25\ mV}$ and $\boldsymbol{SW_{freq} = 25\ Hz}$.

5.3.5. Preliminary photovoltaic measurements

The preparation for the photovoltaic measurements is described in the experimental section. A solar cell I-V measurement system was used to mesure the photovoltaic characteristics of the devices under AM 1.5 global one sun illuminations (100 mW/cm^2).

Figure 5. 14 shows I-V characteristics of DSSCs based on the synthesized dyes **50** and **51.** The results were compared and preformed under the same condition of the common **N719** dye. The electrical conversion efficiencies of the DSSCs are largely in agreement with the optical properties of the synthesized dyes. The photovoltaic parameters are summarized in **Table 5.3**. The performance of dye **50** in DSSCs exhibited a J_{sc} of 8.68 mA/cm^2, an V_{oc} of 0.52 V, and an overall electrical conversion efficiency (η) of 2.9 %. Under similar conditions, the addition of extra thiophene bridging unit in dye **51** resulted in higher J_{sc} and V_{oc}, and better photovoltaic performance with efficiency (η) reach around 3.9 %. The increase in the efficiency of about 35 % can be ascribed to the improvement of the electron-donating ability. Although the efficiencies are lower than that obtained for the ruthenium-based DSSCs (4.9 %), the improvement in the efficiency can be achieved by increasing the number of thiophene unit between electron donor and acceptor units.

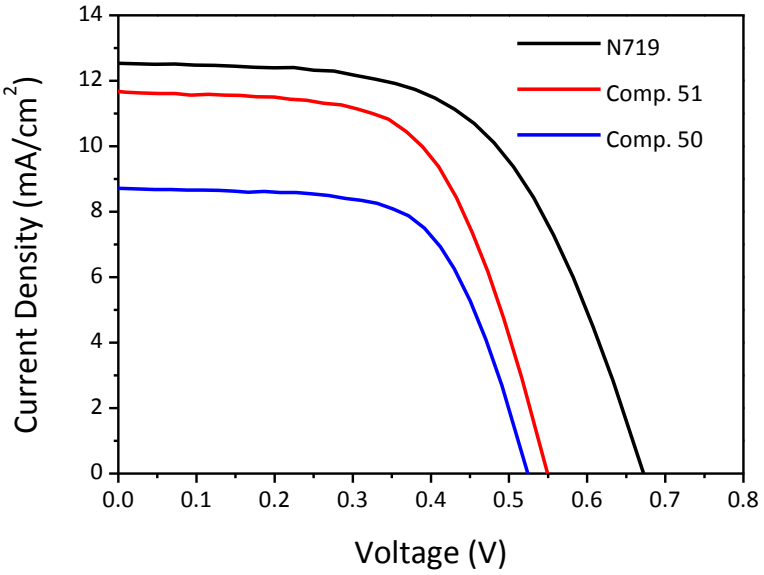

Figure 5. 14. Current-potential (I-V) curves for DSSCs based on the synthesized dyes **50**, **51** and **N719** under an irradiation of 100 mW cm^{-2}.

Table 5.3. Photovoltaic performance parameters of DSSCs based on dye **50** and **51** and referenced to **N719** dyes. The parameters were measured under an irradiation of 100 mW cm^{-2} (AM 1.5 G simulated sunlight) at room temperature.

Dyes	J_{sc} *(mA/cm^2)*	V_{oc} *(V)*	*FF*	*η(%)*
50	8.68	0.52	64.4	2.9
51	11.67	0.54	60.6	3.9
N719	12.58	0.67	57.4	4.9

5.4. Conclusions and Future work

5.4.1. Conclusion

Several numbers of metal free organic dyes with different conjugated spacers have been successfully synthesized. The dyes featured DMA as a strong donating group and cyanoacrylic acid as an acceptor and anchoring group. The associated units were connected together with different π-conjugated system containing thiophene or bithiophene units attached to an alkyne or TCNE as linkers in order to increase the conjugation length of the system.

The influence of the π-conjugated spacer on the optical and physical properties of the dyes has been investigated using UV-vis, fluorescence and cyclic voltametry. The UV-vis results suggested that considerable increase in the absorption coefficients and slight change in the maximum absorption wavelength were observed upon increasing the conjugation length between the donor and acceptor units. Strong quenching of fluorescence was observed for the dyes featuring TCNE as linker. Preliminary DSSCs fabricated from dye **50** and **51** provided moderately efficient devices.

5.4.2. Future work

With additional time, a new series of metal free organic dyes with different donating groups and different conjugation spacers could be synthesized. Investigation of the influence of the π-conjugated spacers on the physical and optical properties of the new organic dyes would be a key extension to this work. DSSCs are currently being fabricated from dyes **48** and **49**.

5.5. Acknowledgements

I gratefully acknowledge Brian Fitzpatrick, the postdoctoral in our group, for assisting in the CV and SW studies. Also my special thanks to the Jong In Hong group, Chung Ang university in Korea, for preliminary DSSC measurements.

Chapter 6;

Experimental.

6.1. General experimental and materials

All chemicals were supplied from commercial sources and were used without purification unless stated. All reactions were performed under a nitrogen atmosphere unless stated. Flash column chromatography was carried out using Fisher Matrix silica 60. Macherey-Nagel aluminium backed plates pre-coated with silica gel 60 (UV254) were used for thin layer chromatography. All melting points recorded are uncorrected.

^{1}H NMR and ^{13}C NMR spectra were run on Bruker Avance 400 MHz, and Bruker Avance 500 MHz spectrometers. All NMR spectra used tetramethylsilane (TMS) as reference (δ = 0.0 ppm). Mass spectra were obtained from the Mass Spectrometry laboratory in the School of Chemistry, University of Glasgow. High resolution mass spectra were run on a JEOL JMS-700 spectrometer with the measurements recorded under the conditions of electron impact (EI) ionisationon, chemical ionization (CI) or fast atom bombar-dment (FAB) conditions.

Transmission infrared spectra IR were obtained by using Perkin-Elmer RX FT-IR system. Cyclic Voltammetry experiments were carried out on a CH Instruments 440 Electrochemical Workstation. UV-Vis Spectrometers used were Perkin-Elmer LAMBDA 25 UV-Vis Spectrometer and the fluorescence measurements were run on a Shimadzu Spectrophotometer RF-5301PC using 1 cm quartz fluorescence cells.

6.2. Experimental section

1,4-Bis(3-thienyl)buta-1,3-diyne (2)[171]

3-Ethynylthiophene (0.44 g, 4.0 mmol) and copper (II) chloride (0.04 g, 0.29 mmol) were added to a mixture of triethylamine (0.05 mL, 0.36 mmol) and dry toluene (6 mL). Then the reaction mixture was heated at 60 °C for 6 hours. After cooling to room temperature, the solvent was evaporated under reduced pressure and the crude product was purified by column chromatography (SiO_2; petroleum ether: 10% toluene) to afford a white solid (0.35 g, 41 %); mp. 108-110 ºC (lit. 110-112 ºC); ^{1}H NMR (400 MHz, $CDCl_3$) δ 7.59 (dd, *J* = 2.5, 5.0 Hz, 2H), 7.28 (dd, *J* = 2.5, 5.0 Hz, 2H), 7.17 (dd, *J* = 2.5, 5.0 Hz, 2H) ppm; ^{13}C NMR (100 MHz, $CDCl_3$) δ 131.3 (C-H), 130.2 (C-H), 125.6 (C-H), 120.9 (C-C), 76.6 (C≡C), 73.5 (C≡C) ppm; HRMS (EI^+) calculated for $C_{12}H_6S_2$ 213.9911 found 213.9913.

1,3,5-(3-Thienyl)-2,4,6 tris-[2(3-thienylethynyl)]benzene (3)

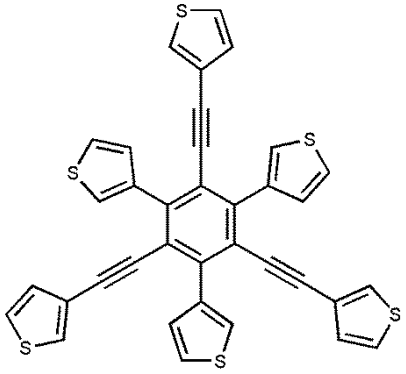

A mixture 1,4-bis(3-thienyl)buta-1,3-diyne (2) (0.20 g, 0.94 mmol) and cobalt octacarbonyl (0.04 mg, 0.12 mmol) were dissolved in 1,4-dioxane (5mL). The reaction mixture was stirred at 110 °C overnight. Then the reaction mixture was filtered and the filtrate was collected and dried under reduced pressure. The crude product was then purified by using column chromatography (SiO_2; DCM: petroleum ether; 3:6) to afford a pale yellow solid (0.06 g, 10%); mp. Dec. >258 ºC; ^{1}H NMR (400 MHz, $CDCl_3$) δ 7.65 (dd, *J* = 1.2, 3.0 Hz, 3H), 7.47 (dd, *J* = 1.2, 5.0 Hz, 3H), 7.41 (dd, *J* = 3.0, 5.0 Hz, 3H), 7.18 (dd, *J* = 3.0, 5.0 Hz, 3H), 7.10 (dd, *J* = 1.2, 3.0 Hz, 3H), 6.76 (dd, *J* = 1.2, 5.0 Hz, 3H) ppm; ^{13}C NMR (100 MHz, $CDCl_3$) δ 140.9 (C-C), 139.0 (C-C), 130.1 (C-H), 129.4 (C-H), 128.6 (C-H), 125.7 (C-H), 125.2 (C-H), 123.3 (C-H), 122.7 (C-C), 122.2 (C-C), 92.4 (C≡C), 87.6 (C≡C) ppm; IR (film) υ 3099 (C-H), 2217 (C≡C), 1737 (C=C) cm^{-1}; HRMS (FAB $(M+H)^+$) calculated for $C_{36}H_{19}S_6$ 642.9811 found 642.9813.

1,4-Bis(2-thienyl)buta-1,3-diyne (5)[172]

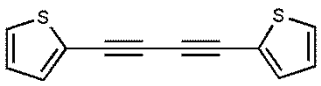

2-Ethynylthiophene (1.0 g, 9.25 mmol) and copper (II) chloride (0.07 g, 0.52 mmol) were added to a mixture of triethylamine (0.12 mL, 0.86 mmol) and dry toluene (15 mL). Then the reaction mixture was heated at 60 °C for 6 hours. After cooling to room temperature, the solvent was evaporated and the crude product was purified by column chromatography (SiO_2; petroleum ether) to afford pale an yellow solid (0.50 g, 25 %); mp. 99-110 ºC (lit. 92-93 ºC); ^{1}H NMR (400 MHz, $CDCl_3$) δ 7.24 (dd, *J* = 4.0, 1.1 Hz, 2H), 7.22 (dd, *J* = 5.0, 1.1 Hz, 2H), 6.89 (dd, *J* = 5.0, 4.0 Hz, 2H) ppm; ^{13}C NMR (100 MHz, $CDCl_3$) δ 134.3 (C-H), 128.7 (C-H), 127.1 (C-H), 122.1 (C-C), 77.8 (C≡C), 76.6 (C≡C) ppm; HRMS (EI^+) calculated for $C_{12}H_6S_2$ 213.9911 found 213.9911.

1,3,5-(2-Thienyl)-2,4,6 tris-[2(2-thienylethynyl)]benzene (6)

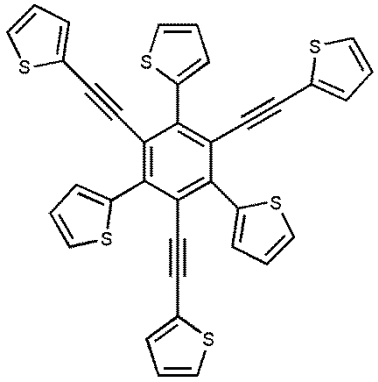

A mixture of 1,4-bis(2-thienyl)buta-1,3-diyne (5) (1.0 g, 4.67 mmol) and cobalt octacarbonyl (0.15 mg, 0.45 mmol) were dissolved in 1,4-dioxane (10 mL). The reaction mixture was stirred at 110 °C overnight. The reaction mixture was filtered and the filtrate was collected and dried under reduced pressure. Then the crude product was purified by using column chromatography (SiO_2: toluene: petroleum ether; 3:6) to afford a pale yellow solid (0.30 g, 10 %); mp. Dec.> 258 ºC; ^{1}H NMR (400 MHz, $CDCl_3$) δ 7.56 (dd, *J* = 5.0, 1.2 Hz, 3H), 7.43 (dd, *J* = 3.6, 1.2 Hz, 3H), 7.26 (dd, *J* = 5.0, 1.2 Hz, 3H), 7.22 (dd, *J* = 5.0, 3.6 Hz, 3H), 6.92 (m, 6H) ppm; ^{13}C NMR (100 MHz, $CDCl_3$) δ 139.1 (C-C), 138.1 (C-C), 132.1 (C-H), 129.4 (C-H), 128.0 (C-H), 127.0 (C-H), 126.6 (C-H), 126.3 (C-H), 125.1 (C-C), 122.9 (C-C), 92.6 (C≡**C**), 91.4 (C≡**C**) ppm; IR (film) υ 3099 (C-H), 2207 (C≡**C**), 1520 (C=**C**), 1387 (C=**C**) cm^{-1}; HRMS (FAB $(M+H)^+$) calculated for $C_{36}H_{19}S_6$ 642.9811 found 642.9815.

2,7-Diiodo-9,10-phenanthrenequinone (7)[173]

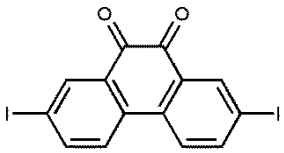

9,10-Phenathrenquinone (2.50 g, 12.0 mmol) in trifluromethanesulfonic acid (25.0 g, 166 mmol) was cooled to 0 °C before under N_2 before N-iodosuccinamide (5.0 g, 22 mmol) was added slowly to the mixture. After stirring the reaction mixture for 6 h at room temperature, the mixture was poured into ice and the precipitates were filtered off and dried to afford a dark orange solid (4.50 g, 82 %); mp. 250- 252°C (lit. >250 °C); ^{1}H NMR (400 MH_Z, $CDCl_3$) δ 8.49 (d, *J* =1.9 H_Z, 2H), 8.04 (dd, *J* = 8.0, 1.9 H_Z, 2H), 7.70 (d, *J* = 8.0 H_Z, 2H) ppm; HRMS (FAB M^+) calculated for $C_{14}\,H_6\,I_2\,O_2$ 459.8457 found 459.8434.

2,7-Dihex-1-ynyl-phenanthrene-9,10-dione (8)

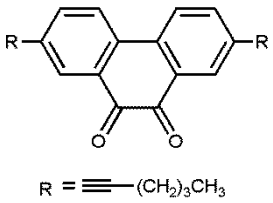

2,7-Diiodo-9,10 phenathrenequinone (7) (1.0 g, 2.17 mmol), 10 % Pd /C (0.05 g, 0.04 mmol), CuI (0.20 g, 1.0 mmol), Ph_3P (0.60 g, 2.4 mmol) and K_2CO_3 (1 g, 7.24 mmol) were dissolved at room temperature in a 1:1 mixture of water (10 mL) and DME (10 mL) at room temperature. The reaction mixture was degassed with N_2 for 5 min and stirred for 30 min under N_2. Then 1-hexyne (0.30 g, 3.65 mmol) was added to the mixture and the reaction mixture was heated to 80 °C for 2 h. After cooling to room temperature, the mixture was extracted with DCM (40 mL) until the organic layer was clear. Then the extracted layers were combined, dried over $MgSO_4$ and filtered. After evaporation the solvent, the residue was purified on a column chromatography (SiO_2; DCM: hexane; 1:1) to give an orange solid (0.29 g, 37 %); mp. 144-146 °C; ^{1}H NMR (400 MH_Z, $CDCl_3$) δ 8.16 (d, *J* = 1.8 H_Z, 2H), 7.87 (d, *J* = 8.3 H_Z, 2H), 7.66 (dd, *J* = 8.3, 1.8 H_Z, 2H), 2.44 (t, *J* = 7.2 H_Z ,4H), 1.60 (m, 4H), 1.49 (m, 4H), 0.97 (t, *J* = 7.2 H_Z ,6H) ppm; ^{13}C NMR (100 MH_Z, $CDCl_3$) δ 179.6 (C=O), 138.4 (C-H), 134.1 (C-C), 133.4 (C-H), 130.6 (C-C), 125.9 (C-C), 124.0 (C-H), 94.4 (C≡C), 78.9 (C≡C), 30.5 ($C-CH_2$), 22.0 ($C-CH_2$), 19.1 ($C-CH_2$), 13.6 ($C-CH_3$) ppm; IR (film) υ 2931 (C-H), 2870 (C-H), 2225 (C≡C), 1610 (C=O) cm^{-1}; HRMS (EI^+) calculated for $C_{26}H_{24}O_2$ 368.1776 found 368.1779.

2,5-Dibromo-3,4-dinitrothiophene (9)[174]

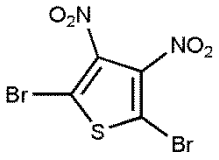

2,5-Dibromothiophene (3.50 mL, 31.0 mmol) was added to a mixture of H_2SO_4 (33 mL, 619 mmol), and fuming nitric acid (11 mL, 264 mmol) at 0 °C. The reaction mixture was then poured into ice and the precipitate was collected by filtration followed by recrystalization from methanol gave the pure product as a pale yellow solid (4.44 g, 43 %); mp. 138-140 °C (lit.135-137 °C); ^{13}C NMR (100 MHz, $CDCl_3$) δ 139.6 (2×C-C), 116.9 (2×C-C); HRMS (EI^+) calculated for $C_4O_4N_2Br_2S$ 329.7946 found 329.7948.

3',4'-Dinitro-(2,2',5',2'')-terthiophene (10)[175]

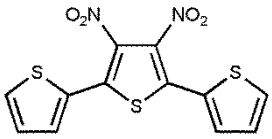

2,5-Dibromo-3,4-dinitrothiophene (9) (3.60 g, 10.8 mmol), 2-(tributylstanyl)-thiophene (12 g, 32.0 mmol) and dichlorobis(triphenylphosphino)palladium (1.0 g, 1.5 mmol) were dissolved in dry THF (96 mL). The reaction mixture was heated under reflux under nitrogen for 18 h. After cooling, the reaction mixture was concentrated under reduced pressure then washed carefully with hexane. The resulting product was purified by column chromatography (SiO_2; petroleum ether: dichloromethane; 3:2) to give the desired product

as an orange solid (2.73 g, 74 %); mp. 142-144 °C (lit. 149-151 °C); ^{1}H NMR (400 MH_Z, $CDCl_3$) δ 7.60 (dd, *J* = 5.0, 1.2 H_Z, 2H), 7.54 (dd, *J* = 4.0, 1.2 H_Z, 2H), 7.17 (dd, *J* = 5.0, 4.0 H_Z, 2H) ppm; HRMS (EI^+) calculated for $C_{12}H_6O_4N_2S_3$ 337.9490 found 337.9496.

3',4'-Diamino-[2,2':5',2'']-terthiophene (11)[176]

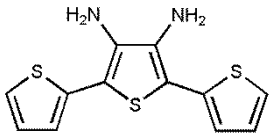

A mixture of 3',4'-dinitro-(2,2':5',2")-terthiophene (10) (1.0 g, 2.96 mmol) and anhydrous tin (II) chloride (5.68 g, 29.9 mmol) was dissolved in a mixture of concentrated HCl (20 mL, 817 mmol), ethanol (40 mL) and toluene (40 mL). The reaction mixture was then heated under reflux overnight. Then the resulting mixture was poured into 25% cold NaOH (70 mL) and the suspension was kept alkaline. The resulting suspension was extracted with toluene (100 mL) and the combined organic layers were washed with brine (30 mL), dried over $MgSO_4$ and filtered. Then the solvent was evaporated to afford the oily product which was then carefully washed with ethanol to afford the product as a brown solid (0.70 g, 84 %); ^{1}H NMR (400 MH_Z, $CDCl_3$) δ 7.24 (dd, *J* = 5.0, 1.2 H_z, 2H), 7.06 (m, 4H), 3.71 (S, 4H) ppm. HRMS (EI^+) calculated for $C_{12}H_{10}N_2S_3$ 278.0006 found 279.20. The crude product was used for the next step without further purification.

Dibenzo[*f*,*h*]thieno[3,4-b]quinoxaline,10,12-di-2-thienyl-2,7-dihex-1-ynyl (12)

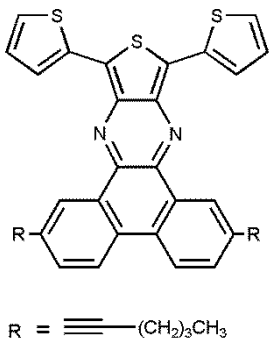

A mixture of 2,7-dihex-1-ynyl-phenanthrene-9,10-dione (8) (0.20 g, 0.50 mmol) and 3',4'-diamino-[2,2':5',2"]-terthiophene (11) (0.20 g, 0.60 mmol) was dissolved in $CHCl_3$ (8 mL). *p*-toluene sulfonic acid (0.03 g, 0.20 mmol) was added to the reaction. The mixture then was heated under reflux and nitrogen overnight. After cooling, the precipitates were collected by filtration to afford a green solid (0.14 g, 45 %); mp. > 250 ºC; ^{1}H NMR (400 MHz, $CDCl_3$) δ 9.09 (d, *J* = 1.0 Hz, 2H), 8.17 (d, *J* = 8.0 Hz, 2H), 7.67 (d, *J* = 4.0 Hz, 2H), 7.63 (dd, *J* = 1.0, 8.0 Hz, 2H), 7.45 (d, *J* = 4.0 Hz, 2H), 7.16 (t, *J* = 4.0 Hz, 2H), 2.55 (t, *J* = 7.0 Hz, 4H), 1.69 (m, 4H), 1.59 (m, 4H), 1.05 (t, *J* = 7.0 Hz, 6H) ppm; ^{13}C NMR (100 MHz, $CDCl_3$) δ 142.3 (C-H), 138.4 (C-H), 134.9 (C-H), 133.4 (C-H), 131.0 (C-C), 130.5 (C-C), 129.9 (C-H), 127.2 (C-H), 126.8 (C-H), 124.2 (C-H), 124.1 (C-H), 124.0 (C-H), 123.0 (2×C-H), 92.2 (C≡**C**), 80.8 (C≡**C**), 30.8 (C-CH_2), 22.0 (C-CH_2), 19.3 (C-CH_2), 13.8 (C-CH_3) ppm; IR (film) υ 2955 (C-H), 2924 (C-H), 2225 (C≡C), 1722 (C-N) cm^{-1}; HRMS (EI^+) calculated for $C_{38}H_{30}S_3N_2$ 610.1571 found 610.1576.

3,3''-Dihexyl-3',4'-dinitro-2,2':5',2''-terthiophene (13)[177]

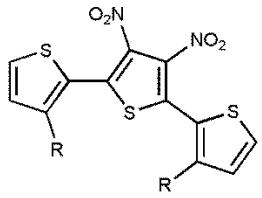

R=C_6H_{13}

A mixture of 2,5-dibromo-3,4-dinitro thiophene (9) (1.0 g, 3.0 mmol) and 3-hexy-thiophene-2-boronic acid pinacol ester (2.0 g, 8.0 mmol) in dry toluene (30 mL) was purged with N_2 before a solution of 2.0 M Na_2CO_3 in water and degassed solution of tetrakis (triphenylphosphine) palladium (0) (0.05 g, 0.04 mmol) with Aliquat (2 mL) in dry toluene (10 mL) were added to the reaction mixture. Then the reaction mixture was heated under reflux 105 ºC under N_2 for 2 days. After cooling, the organic layer was extracted with toluene (50 mL), dried over $MgSO_4$ and filtered. The solvent was evaporated and the residue was purified by column chromatography, eluting with petroleum ether to afford the desired product as a pale yellow oily compound (0.85 g, 56 %); ^{1}H NMR (400 MHz, $CDCl_3$) δ 7.47 (d, *J* = 4.7 Hz, 2H), 7.00 (d, *J* = 4.7 Hz, 2H), 2.86 (t, *J* = 7.4, 15.1 Hz, 4H), 1.58 (m, 4H), 1.29 (m, 12H), 0.88 (t, *J* = 7.4 Hz, 6H) ppm; HRMS (EI^+) calculated for $C_{24}H_{30}O_4N_2S_3$ 506.1368 found 507.4.

5,5''-Dibromo-3',4'-dinitro-2,2':5',2'-terthiophene (14)

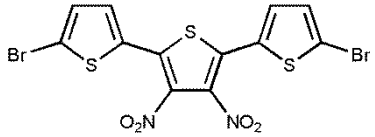

NBS (0.30 g, 2.0 mmol) was added to a solution of 3',4'-dinitro-(2,2',5',2")-terthiophene (10) (1.50 g, 4.30 mmol) in DMF (15 mL). The reaction mixture was heated at 50 ºC overnight. The precipitates were collected by filtration and washed with methanol to afford an orange solid (0.20 g, 50 %); ^{1}H NMR (400 MHz, $CDCl_3$) δ 7.15 (d, *J* = 3.0 Hz, 2H), 7.30 (d, *J* = 3.0 Hz, 2H) ppm.

Thieno[3',4':5,6] pyrazino[2,3-*f*][1,10] phenanthroline (16)[178]

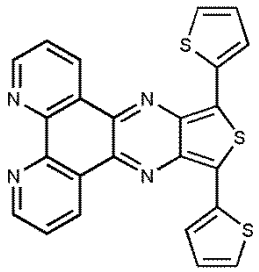

A mixture of 1,10-phenanthroline5,6-dione (0.50 g, 2.4 mmol) and 3',4'-diamino-[2,2':5',2"]-terthiophene (11) (0.50 g, 1.79 mmol) was dissolved in $CHCl_3$ (22 mL) and *p*-toluene sulfonic acid (0.08 g, 0.53 mmol) was added to the reaction. The reaction mixture was heated under reflux overnight under N_2. After cooling, a green solid compound was collected by filtration (1.15 g, 100%); mp.>300 ºC (lit. > 300 ºC); ^{1}H NMR (400 MHz, $CDCl_3$) δ 9.39 (dd, *J* = 8.0, 1.7 H_Z, 2H), 9.21 (dd, *J* = 4.4, 1.7 H_Z, 2H), 7.72 (t, *J* = 8.0 ,4.4 H_Z, 2H), 7.65 (dd, *J* = 4.0, 1.7 H_Z, 2H), 7.51 (dd, *J* = 5.0, 1.2 H_Z, 2H), 7.19 (t, *J* = 5.0, 4.0 H_Z, 2H) ppm; HRMS(FAB $(M+H)^+$) calculated for $C_{24}H_{13}N_4S_3$ 453.0302, found 453.0298.

Thieno[3',4':5,6] pyrazino[2,3-*f*][1,10] phenanthroline, hexafluorophosphate (1:1) (17)

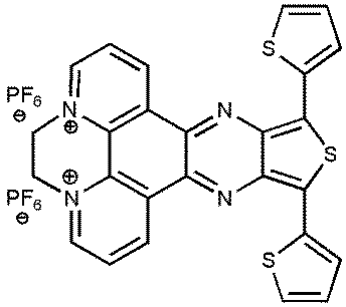

A mixture of thieno[3',4':5,6] pyrazino[2,3-*f*][1,10] phenanthroline (16) (0.10 g, 0.28 mmol) and 1,2-dibromoethane (5.0 mL, 58.0 mmol) was heated overnight at 114 ºC. After cooling, the product was precipitated by addition to petroleum ether. Then the collected precipitates were washed carefully with chloroform until the filtrate becomes clear. Halogen exchange was achieved by dissolving the green product and an excess amount of potassium hexaflourophosphate in small amount of DMF. The prepared solution was added dropwise to water (50 mL). The resulting precipitates were collected by filtration and washed carefully with water to yield dark green compound (0.05 g, 23 %); mp. > 300 ºC; ^{1}H NMR (400 MHz, CD_3CN) δ 10.19 (dd, *J* = 8.3, 1.0 Hz, 2H), 9.32 (dd, *J* = 5.0, 1.0 Hz, 2H), 8.65 (t, *J* = 7.1, 14.4 Hz, 2H), 7.86 (d, *J* = 4.0 Hz, 2H), 7.73 (d, *J* = 5.0 Hz, 2H), 7.27 (t, *J* = 8.3, 4.0 Hz, 2H), 5.48 (s, 4H) ppm; ^{13}C NMR (100 MHz, CD_3CN) δ 149.2 (C-H), 144.0 (C-H), 129.9 (C-H), 129.1(C-H), 128.2 (C-H), 126.7 (C-H), 52.5 (N-CH_2) ppm; IR (film) υ 3668 (C-H), 3120 (C-H), 827 cm^{-1}; MS *m/z* 769.98; anal. calculated for $C_{26}H_{16}N_4S_3P_2F_{12}$; C, 40.53; H, 2.08; N, 7.27, Found; C, 40.19; H, 2.30; N, 7.39.

4,7-Bis-(3-hexylthiophen-2-yl)benzo[1,2,5]thiadiazole (20)[179]

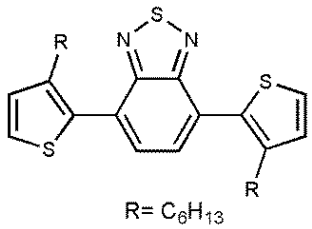

A mixture of 4,7-dibromo-benzo[1,2,5]thiadiazole (1.0 g, 3.4 mmol) and 3-hexythiophene-2-boronic acid pinacol ester (2.2 g, 8.8 mmol) in dry toluene (30 mL) was purged with N_2 before a solution of Na_2CO_3 2 M (10 mL) in water and a degassed solution of tetrakis (triphenylphosphine) palladium (0) (0.06 g, 0.05 mmol), aliquat (1 mL) in dry toluene (10 mL) were added to the reaction mixture. Then the reaction mixture was heated under reflux under N_2 overnight. After cooling, the organic layer was extracted with toluene (50 mL), dried over $MgSO_4$ and filtered. The solvent was evaporated and the residue was purified by column chromatography (SiO_2; petroleum ether: 30% DCM) to afford the desired product as yellow oily compound (0.75 g, 47 %); ^{1}H NMR (400 MHz, $CDCl_3$) δ 7.65 (s, 2H), 7.43 (d, *J* = 5.4 Hz, 2H), 7.10 (d, *J* = 5.4 Hz, 2H), 2.66 (t, *J* = 7.7, 15.6 Hz, 4H), 1.62 (m, 4H), 1.21 (m, 12H), 0.81 (t, *J* = 7.7, 13.7 Hz, 6H) ppm; ^{13}C NMR (100 MHz, $CDCl_3$) δ 154.3 (C-C), 141.7 (C-C), 132.3 (C-H), 129.9 (C-H), 129.2 (C-H), 127.7 (C-C), 125.8 (C-C), 31.6 (C-H_2), 30.6 (C-H_2), 29.4 (C-H_2), 29.0 (C-H_2), 22.4 (C-H_2), 13.9 (C-H_3) ppm; HRMS(EI$^+$) calculated for $C_{26}H_{32}N_2S_3$ 468.1728 found 468.1721.

1,2-Diamino-3,6-dithien-2-ylbenzene (21)[175]

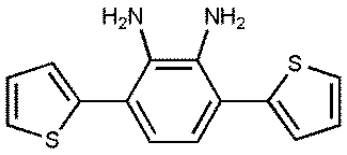

To a mixture of 4,7-di-thiophen-2-yl-benzo[1,2,5]thiadiazole (0.50 g, 2.17 mmol) and cobalt (II) chloride (0.06 g, 0.43 mmol) in ethanol (15 mL) was added sodium borohydride (0.16 g, 4.35 mmol). The reaction mixture was heated under reflux overnight. After cooling, the mixture was extracted with DCM (50 mL) and the organic layers were combined, dried over $MgSO_4$ and filtered. Then the solvent was evaporated under reduced pressure to afford brown solid (0.30 g, 51 %); mp 115-120 ºC (lit. 109-109.5 ºC); ^{1}H NMR (400 MHz, $CDCl_3$) δ 7.40 (dd, *J* = 5.2, 1.2 Hz, 2H), 7.22 (dd, *J* = 3.5, 1.2 Hz, 2H), 7.17 (dd, *J* = 5.2, 3.5 Hz, 2H), 6.91(s, 2H), 3.89 (s, 4H) ppm; ^{13}C NMR (100 MHz, $CDCl_3$) δ 140.9 (C-N), 132.6 (C-C), 127.5 (2×C-H), 126.2 (C-H), 125.6 (C-H), 121.8 (C-C) ppm. Due to the easy exposure to decomposition, the crude product was used for the next step without further purification.

4,7-Bis-(3-hexylthiophen-2-yl)- 1,2 diaminobenzene (22)

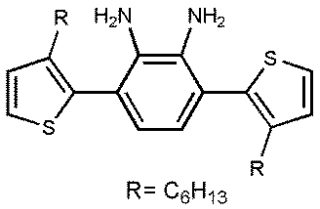

To a mixture of 4,7-bis-(3-hexyl-thiophen-2-yl)-benzo[1,2,5] thiadiazole (20) (1.0 g, 2.13 mmol) and cobalt (II) chloride (0.06 g, 0.43 mmol) in ethanol (30 mL) was added sodium borohydride (0.12 g, 3.12 mmol). The reaction mixture was heated under reflux for 2 days. After cooling, the mixture was extracted with DCM (50 mL) and the organic layers were combined, dried over $MgSO_4$ and filtered. Then the solvent was evaporated under reduced pressure to afford dark brown oily compound (0.70 g, 75 %); ^{1}H NMR (400 MHz, $CDCl_3$) δ 7.33 (d, *J* = 5.1 Hz, 2H), 7.05 (s, 2H), 7.01 (d, *J* = 5.1 Hz, 2H), 4.14 (s, 4H), 2.68 (t, *J* = 7.7, 15.2 Hz, 4H), 1.60 (m, 4H), 1.26 (m, 12H), 0.85 (t, *J* = 6.7, 13.7 Hz, 6H) ppm. The crude product was used for the next step without further purification.

Dipyrido[3,2-*a*:2',3'-*c*]phenazine (23)[178]

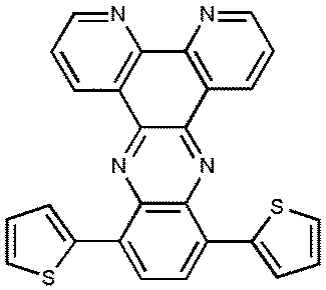

A mixture of phenanthroline–5,6-dione (0.30 g, 1.44 mmol) and 3,6-dithienl-o-phenylene-diamine (21) (0.30 g, 1.44 mmol) was dissolved in $CHCl_3$ (30 mL) and *p*-toluene sulfonic acid (0.07 g, 0.30 mmol) was added to the reaction mixture. Then the mixture was heated under reflux 2 days under N_2. After cooling, the precipitate was collected by filtration to afford an orange compound (0.50 g, 77 %); mp. > 300 °C (lit. 323-325 °C). Due to poor solubility in common NMR solvents no NMR spectra was obtained. The crude product was used for the next step without further purification. MS *m/z* 446.06; anal. calculated for $C_{26}H_{14}N_4S_2$; C, 70.00; H, 3.16; N, 12.56, Found; C, 64.81; H, 3.26; N, 10.23.

Dipyrido[3,2-*a*:2',3'-*c*]phenazine,10,13-bis(4-hexyl-2-thienyl) (24)

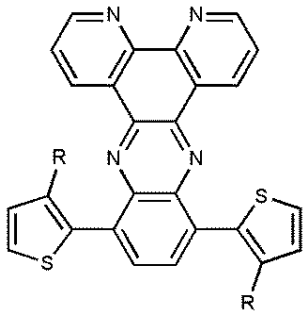

A mixture of 1,10-phenanthroline-5,6-dione (0.34 g, 1.62 mmol) and 3,6-bis-(3-hexyl-thiophen-2-yl)-benzene-1,2-diamine (22) (0.70 g, 1.62 mmol) was dissolved in $CHCl_3$ (30 mL), then *p*-toluene sulfonic acid (0.03 g, 0.20 mmol) was added to the reaction. The reaction mixture was then heated under reflux and nitrogen overnight. After cooling, the solvent was evaporated and the crude product was purified by column chromatography (SiO_2; DCM: 30 % ethyl acetate) to afford orange oily compound (0.24 g, 24 %); ^{1}H NMR (400 MHz, $CDCl_3$) δ 9.46 (dd, *J* = 8.0, 1.6 Hz, 2H), 9.25 (d, *J* = 4.4 Hz , 2H), 8.01 (s, 2H), 7.75 (dd, *J* = 14.4, 8.0 Hz, 2H), 7.58 (d, *J* = 5.2 Hz, 2H), 7.21 (d, *J* = 5.2 Hz, 2H), 2.72 (t, *J* = 8.0, 15.9 Hz, 4H), 1.64 (m, 4H), 1.21 (m, 4H), 1.12 (m, 8H), 0.72 (t, *J* = 6.8, 13.4 Hz, 6H) ppm; ^{13}C NMR (100 MHz, $CDCl_3$) δ 152.5 (C-C), 148.7 (C-H), 141.7 (C-H) , 141.1 (C-H), 140.4 (C-H), 134.4 (C-C), 134.0 (C-H), 132.9 (C-H), 131.8 (C-C), 128.7 (C-C), 127.8 (C-H), 125.9 (C-C), 124.1 (C-C), 31.4 ($C-H_2$), 30.6 ($C-H_2$), 29.4 ($C-H_2$) , 28.9 ($C-H_2$) , 22.4 ($C-H_2$), 13.8 ($C-H_3$) ppm; IR (film) υ 3056 (C-H), 2924(C-H), 2854 (C=N) cm^{-1}; HRMS(EI^+) calculated for $C_{38}H_{38}N_4S_2$ 614.2538 found 614.2540.

Dipyrido[3,2-*a*:2',3'-*c*]phenazine, hexafluorophosphate (1:1) (25)

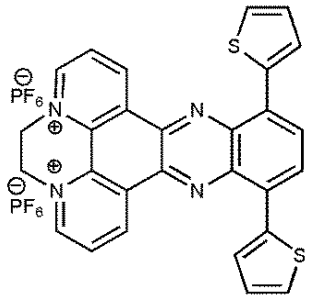

A mixture of dipyrido[3,2-*a*:2',3'-*c*]phenazine (24) (0.30 g, 0.67 mmol) and 1,2 dibromo-ethane (5 mL, 58 mmol) was heated overnight at 114 ºC. After cooling, the product was precipitated by addition of petroleum ether. Then the collected precipitates were washed carefully with chloroform until the filtrate becomes clear. Halogen exchange was achieved by dissolving the red product and an excess amount of potassium hexaflourophosphate in small amount of DMF. The prepared solution was added dropwise to water (50 mL). The resulting precipitates were collected by filtration and washed carefully with water to yield dark purple solid (0.23 g, 45 %); mp. > 300 ºC; ^{1}H NMR (400 MHz, CD_3CN) δ 10.57 (d, *J* = 8.3 Hz, 2H), 9.47 (dd, *J* = 7.0, 1.0 Hz, 2H), 8.82 (t, *J* = 14.2, 7.0 Hz, 2H), 8.59 (s, 2H), 8.02 (dd, *J* = 4.0, 1.0 Hz, 2H), 7.82 (dd, *J* = 4.0, 1.0 Hz, 2H), 7.34 (t, *J* = 8.3, 4.0 Hz, 2H), 5.60 (s, 4H) ppm; ^{13}C NMR (100 MHz, DMSO) δ 149.2 (C-H), 143.9 (C-H), 135.9 (C-C), 135.7 (C-C), 134.4 (C-C), 131.3 (C-H), 130.7 (C-C), 130.4 (C-C), 129.7 (C-C), 129.6 (C-C), 127.6 (C-H), 127.2 (C-H), 52.5 (N-CH_2) ppm; IR (film) υ 3655 (C-H), 3120 (C-H), 827 cm^{-1}; MS *m/z* 764.03; anal. calculated for $C_{28}H_{18}F_{12}N_4P_2S_2$; C, 44.01; H, 2.36; N, 7.33, Found; C, 50.56; H, 2.48; N: 8.68.

Dipyrido[3,2-*a*:2',3'-*c*]phenazine, 10,13-bis(4-hexyl-2-thienyl) hexafluorophosphate (1:1) (26)

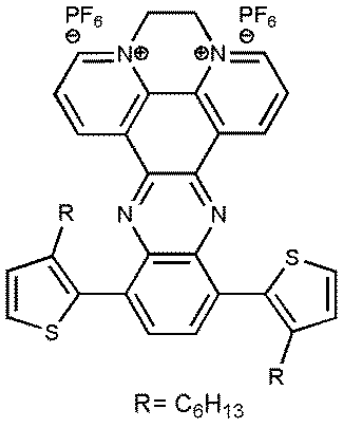

A mixture of dipyrido[3,2-*a*:2',3'-*c*]phenazine,10,13-bis(4-hexyl-2-thienyl) (25) (0.14 g, 0.23 mmol) and 1,2-dibromoethane (5 mL, 58 mmol), was heated for 3 days at 114 ºC. After cooling to room temperature, the product was precipitated by addition of petroleum ether. Then the collected purple precipitates were washed carefully with chloroform until the filtrate becomes clear. Halogen exchange was achieved by dissolving the purple product and excess amount of potassium hexaflourophosphate in small amount of DMF. The solution was added drop wise to water (50 mL). The resulting precipitates were collected by filtration and washed carefully with water to yield a brown solid (0.10 g, 61%); mp. > 300 ºC; ^{1}H NMR (400 MHz, DMSO) δ 10.02 (dd, *J* = 8.3, 1.0 Hz, 2H), 9.82 (dd, *J* = 4.8, 1.0 Hz, 2H), 8.91 (dd, *J* = 14.4, 8.3 Hz, 2H), 8.36 (s, 2H), 7.89 (d, *J* = 5.2 Hz, 2H), 7.33 (d, *J* = 5.2 Hz, 2H), 5.65 (s, 4H), 2.73 (t, *J* = 14.0, 7.0 Hz, 4H), 1.58 (m, 4H), 1.14 (m, 4H), 1.06 (m, 8H), 0.67 (t, *J* = 14.0, 7.0 Hz, 6H) ppm; ^{13}C NMR (100 MHz, DMSO) δ 149.7 (C-H), 142.5 (C-H), 142.0 (C-C), 141.5 (C-C), 136.5 (C-C), 134.6 (C-H), 133.5 (C-C), 132.4 (C-C), 131.3 (C-C), 130.9 (C-C), 129.8 (C-H), 129.2 (C-H), 127.7 (C-H), 52.5 (N-CH_2), 30.7 (C-H_2), 29.9 (C-H_2), 28.7 (C-H_2), 28.1 (C-H_2), 21.8 (C-H_2), 13.7 (C-H_3) ppm; IR (film) υ 3668 (C-H), 2924 (C-H), 2854 (C=N), 829 cm^{-1}. MS *m/z* 932.21;

anal. calculated for $C_{40}H_{42}N_4S_2P_2F_{12}$; C,51.54; H, 4.54; N, 6.01, Found; C, 52.83; H, 4.43; N, 6.03.

2-Iodo-9,10-phenanthrenquinone (27)[180]

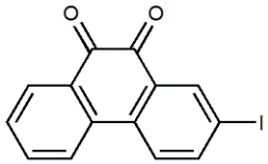

A mixture of nitric acid (2 mL, 48 mmol) and sulfuric acid (5 mL, 94 mmol) was added to a solution of phenanthrene- 9,10 dione (2.0 g, 10 mmol) and iodine (2.56 g, 10 mmol) in acetic acid (100 mL). The solution was then heated under reflux for 4 h. The reaction mixture was left to cool for 10 h, then crude product was purified by column chromatography (SiO_2: toluene) to afford an orange solid (2.80 g, 84 %); mp. 210-220 ºC (lit. 225 ºC); ^{1}H NMR (400 MHz, $CDCl_3$) δ 8.49 (d, *J* = 2.0 Hz, 1H), 8.20 (dd, *J* = 1.4, 8.0 Hz, 1H), 8.04 (dd, *J* = 2.0, 8.0 Hz, 1H), 7.98 (d, *J* = 8.0 Hz, 1H), 7.74 (d, *J* = 8.0 Hz, 1H), 7.71 (dt, *J* = 1.4, 8.0 Hz, 1H), 7.50 (dt, *J* = 1.4, 8.0 Hz, 1H) ppm; ^{13}C NMR (100 MHz, $CDCl_3$) δ 179.3 (C=O), 179.2 (C=O), 144.6 (C-H), 139.1 (C-H), 136.1 (C-H), 135.2 (C-C), 135.1 (C-C), 131.9 (C-C), 131.0 (C-C), 130.8 (C-H), 130.0 (C-H), 125.5 (C-H), 123.9 (C-H), 95.1 (C-I) ppm; HRMS m/z (EI+) calculated for $C_{14}H_7O_2I$ 333.9491 found 333.9495.

2-(4-(Dimethyl amino phenyl)ethynyl) phenanthrene-9,10-dione (29)

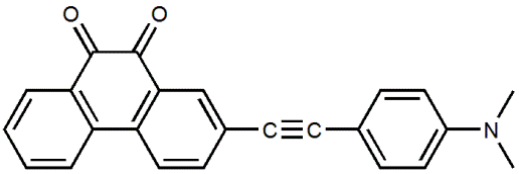

2-Iodo-9,10-phenanthrenquinone (27) (0.30 g, 0.89 mmol), 10% Pd/C (0.03 g, 0.03 mmol), CuI (0.06 g, 0.31 mmol), Ph_3P (0.19 g, 0.72 mmol) and K_2CO_3 (0.30 g, 2.17 mmol) were dissolved at room temperature in a 1:1 mixture of water (10 mL) and DME (10 mL). The mixture was degassed with N_2 for 5 min and stirred for 30 min under N_2. Then 4-ethynyl-*N*,*N*-dimethylaniline (0.20 g, 1.38 mmol) was added to the mixture. The reaction mixture was heated under reflux to 80 °C overnight. The mixture was then cooled, extracted with (50 mL) DCM and the organic layers were combined, dried over $MgSO_4$ and filtered. Then the solvent was evaporated under reduced pressure. The residue was then purified by column chromatography (DCM: 20% petroleum ether) to give a purple compound (0.10 g, 46 %); mp. 215-220 ºC; ^{1}H NMR (400 MHz, $CDCl_3$) δ 8.27 (d, *J* =1.8 Hz, 1H), 8.18 (dd, *J* =1.3, 7.5 Hz, 1H), 7.97 (m, 2H), 7.77 (dd, *J* = 1.8, 7.5 Hz, 1H), 7.71 (dt, *J*= 1.3, 7.5 Hz, 1H), 7.46 (dt, *J* = 1.3, 7.5 Hz, 1H), 7.42 (d, J = 8.5 Hz, 2H), 6.67 (d, J = 8.5 Hz, 2H), 3.03 (s, 6H) ppm; ^{13}C NMR (100 MHz, $CDCl_3$) δ 180.1 (C=O), 179.9 (C=O), 150.4 (C-N), 137.8 (C-H), 136.0 (C-H), 135.7 (C-C), 134.1 (C-C), 133.0 (C-H), 132.9 (2×C-H), 130.8 (C-C), 130.9 (C-C) 130.6 (C-H), 129.5 (C-H), 126.0 (C-C), 124.1 (C-H), 124.0 (C-H), 111.7 (2×C-H), 108.9 (C-C), 94.5 (C≡**C**), 85.9 (C≡**C**), 40.1 (2×C-**N**) ppm; IR (film) υ 2615 (C-H), 2015 (C≡**C**), 1880 (C=O), 1329 (C-**N**) cm^{-1}; HRMS m/z (EI$^+$) calculated for $C_{24}H_{17}O_2N$ 351.1259 found 351.1261.

(2-(4-(Dimethyl amino phenyl)ethynyl)-3-(9,10-phenanthrenedione))buta-1,3-diene-1,1,4,4-tetracarbonitile (30)

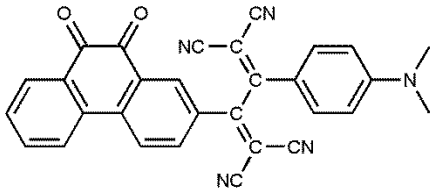

Tetracyanoethylene (0.10 g, 0.70 mmol) was added to a solution of 2-(4-(dimethyl amino phenyl)ethynyl) phenanthrene-9,10-dione (29) (0.10 g, 0.30 mmol) in THF (15 mL). The reaction mixture was stirred overnight at 20 ºC. After evaporation of the solvent, the solid was purified by column chromatography (SiO_2; hexane: ethyl acetate, 3:2) to give a brown solid (0.05 g, 35 %); mp. > 270 ºC; ^{1}H NMR (400 MHz, d_6) δ 8.62 (d, *J* = 2.2 Hz,1H), 8.57 (d, *J* = 7.8 Hz, 1H), 8.42 (d, *J* =7.8 Hz, 1H), 8.32 (dd, *J* = 2.2, 4.0 Hz, 1H), 8.20 (dd, *J* = 1.4, 4.0 Hz, 1H), 8.05 (d, *J* = 9.3 Hz, 2H), 7.90 (dt, *J* = 1.4, 7.8 Hz, 1H), 7.7 (dt, *J* = 1.0, 7.5 Hz, 1H), 6.91 (d, *J* = 9.3 Hz, 2H), 3.23 (s, 6H) ppm; ^{13}C NMR (100 MHz, d_6) δ 179.5 (C=O), 179.3 (C=O), 167.2 (C-C), 162.9 (C-C), 155.7 (C-C), 141.1 (C-C), 136.6 (C-H), 136.2 (C-H), 135.1 (C-C), 133.6 (2×C-H), 133.4 (C-C), 133.2 (C-C), 133.0 (C-C), 131.8 (C-H), 130.9 (C-H), 130.6 (C-H), 126.7 (C-H), 126.3 (C-H), 117.6 (C-C), 115.4 (C≡N), 115.0 (C≡N), 113.2 (2×C-H), 113.0 (C≡N), 112.7 (C≡N), 90.6 (C-C), 75.3 (C-C), 40.2 (2×C-**N**) ppm; IR (film) υ 2599 (C-H), 2530 (C≡N), 2029 (C≡N), 1865 (C=O), 1325 (C-**N**) cm^{-1}; HRMS (FAB (M+H)$^+$) calculated for $C_{30}H_{18}N_5O_2$ 480.1460 found 480.1455.

[2- (4-(Dicyanomethylidene)-2,5-cyclohexadien-1-ylidene)(4-(dimethylamino)phenyl) ethynl)-3-(9,10-phenanthrenedione)]-1,3-butadiene-1,1,4,4-tetracarbonitrile (31)

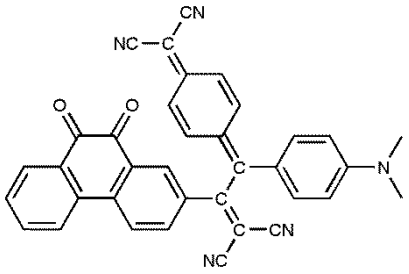

7,7,8,8-Tetracyanoquinodimethane (0.10 g, 0.44 mmol) was added to a solution of 2-(4-(dimethyl amino phenyl)ethynyl) phenanthrene-9,10-dione (29) (0.10 g, 0.30 mmol) in THF (15 mL). The reaction mixture was stirred overnight at 20 ºC. After evaporation all the solvent, the precipitate was purified by column chromatography (SiO_2; hexane: ethyl acetate, 3:2) to give a dark green solid (0.10 g, 60 %); mp. > 280 ºC; ^{1}H NMR(400 MHz, CD_3CN) δ 8.49 (d, *J* = 2.0 Hz, 1H), 8.25 (d, *J* = 8.0 Hz, 1H), 8.19 (d, *J* = 8.0, 1H), 8.15 (dd, *J* = 1.0, 7.5, 1H), 7.94 (dd, *J* = 2.0, 8.0 Hz, 1H), 7.83 (dt, *J* = 1.0, 7.5 Hz, 1H), 7.62 (dt, *J* = 1.0, 7.5 Hz, 1H), 7.46 (d, *J* = 9.3 Hz, 4H), 7.23 (d, *J* = 9.3 Hz, 2H), 6.80 (d, *J* = 9.3 Hz, 2H), 3.10 (s, 6H) ppm; ^{13}C NMR (100 MHz, d_6) δ 179.5 (C=O), 179.4 (C=O), 170.4 (C-H), 155.0 (C-C), 154.4 (C-C), 153.3 (C-C), 140.1 (C-N), 136.8 (C-H), 136.7 (C-H), 136.6 (C-H), 136.0 (C-C), 135.2 (C-C), 133.1 (C-C), 133.0 (2×C-H), 132.7 (C-C), 131.6 (2×C-H), 131.4 (2×C-H), 130.6 (C-H), 126.4 (C-H), 126.1 (C-H), 125.3 (C-H), 123.7 (C-C), 115.6 (C-C), 113.9 (2×C≡N), 113.5 (2×C-H), 113.4 (2×C≡N), 91.2 (C-C), 70.2 (C-C), 40.3 (2×C-N) ppm; IR (film) υ 2597 (C-H), 25430 (C≡N), 2015 (C≡N), 1864(C=O), 1326 (C-N) cm^{-1}; HRMS m/z (FAB $(M+H)^+$) calculated for $C_{36}H_{22}N_5O_2$ 556.1774 found 556.1777.

3-(Dibenzo[*f*,*h*]thieno[3,4-*b*]quinoxaline, 10,12-(di-2-thienyl)-(2-(4-(dimethyl amino phenyl)ethynyl)-buta-1,3-diene-1,1,4,4-tetracarbonitile) (32)

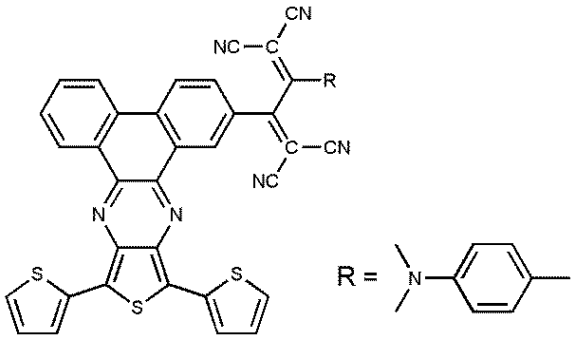

(2-(4-(Dimethyl amino phenyl) ethynyl)-3-**(**9,10-phenanthrenedione))-buta-1,3-diene-1,1,4,4-tetracarbonitile (30) (0.10 g, 0.20 mmol) and 3',4'-diamino-[2,2':5',2'']-terthiophene (11) (0.10 g, 0.36 mmol) were dissolved in chloroform (12 mL). *p*-toluene sulfonic acid (0.03 g, 0.17 mmol) was added to the solution. The reaction mixture was heated under reflux overnight under nitrogen. After cooling, the solvent was evaporated under reduced pressure and the precipitates were purified by column (SiO_2: DCM: 20 % petroleum ether) to afford a dark brown solid (0.05 g, 35 %); mp. > 300 ºC; ^{1}H NMR (400 MHz, $CDCl_3$) δ 9.43 (s, 1H), 9.24 (m, 1H), 8.61 (d, *J* = 9.2 H_Z, 1H), 8.52 (dd, *J* = 9.2, 1.8 H_Z, 1H), 8.45 (m,1H), 7.94 (dd, *J* = 9.2, 7.9 H_Z, 2H), 7.79 (m, 2H), 7.68 (d, *J* = 3.5 H_Z, 1H), 7.57 (d, *J* = 3.5 H_Z, 1H), 7.47 (d, *J* = 5.0 H_Z, 1H), 7.37 (d, *J* = 5.0 H_Z, 1H), 7.15 (t, *J* = 8.8, 5.0 H_Z, 1H), 7.09 (t, *J* = 8.8, 4.5 H_Z, 1H), 6.76 (d, *J* = 9.7 H_Z, 2H), 3.20 (s, 6H) ppm; HRMS(FAB M^+) calculated for $C_{42}H_{23}N_7S_3$ 721.8877 found 721.8837.

2-(3-Thienyl)ethynyl)phenanthrene-9,10-dione (33)

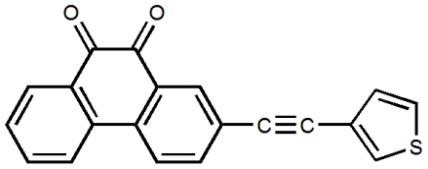

2-Iodo-9,10-phenanthrenquinone (27) (0.40 g, 1.20 mmol), 10% Pd/C (0.03 g, 0.04 mmol), CuI (0.10 g, 0.50 mmol), Ph_3P (0.20 g, 0.70 mmol) and K_2CO_3 (0.40 g, 3.0 mmol) were mixed in a 1:1 solution of water (10 mL) and ethylene glycol dimethyl ether (10 mL) at room temperature. The mixture was stirred under N_2 for 30 min, then 3-ethynylthiophene (0.30 g, 3.0 mmol) was added to the mixture. The reaction mixture was heated under reflux overnight. After cooling, the mixture was extracted with (50 mL) DCM. The organic layers were combined, dried over $MgSO_4$ and filtered. Then the solvent was evaporated and the residue was purified by column chromatography (DCM: 10 % ethyl acetate) to afford an orange solid (0.10 g, 27 %); mp. 147-149 ºC; ^{1}H NMR (400 MHz, $CDCl_3$) δ 8.26 (d, *J* = 1.8 H_Z, 1H), 8.16 (dd, *J* = 1.3, 7.6 H_Z, 1H), 7.98 (m, 2H), 7.77 (dd, *J* = 1.8, 8.3 H_Z, 1H), 7.72 (dt, *J* =1.3, 7.6 H_Z, 1H), 7.58 (dd, *J* =1.1, 3.0 H_Z, 1H), 7.46 (dt, *J* = 1.1, 7.5 H_Z, 1H), 7.33 (dd, *J* = 3.0, 4.9 H_Z, 1H), 7.21 (dd, *J* =1.1, 4.9 H_Z, 1H) ppm; ^{13}C NMR (100 MHz, $CDCl_3$) δ 179.8 (C=O), 179.7 (C=O), 138.0 (C-H), 136.1 (C-H), 135.3 (C-C), 134.9 (C-C), 133.2 (C-H), 130.9 (C-C), 130.9 (C-H), 130.6 (C-H), 129.8 (C-H), 129.8 (C-H), 129.6 (C-H), 125.7 (C-H), 125.0 (C-C), 124.2 (C-H), 124.1 (C-H), 121.5 (C-H), 87.8 (C≡**C**), 87.1 (C≡**C**) ppm; IR (film) υ 3107(C-H), 2218 (C≡**C**), 1674 (C=O) cm^{-1}; HRMS m/z (EI$^+$) calculated for $C_{20}H_{10}SO_2$ 314.0402 found 314.0403.

10-Hydroxy-2-iodo-10-(ferrocenyl) phenanthren-9(10H)-one (36)

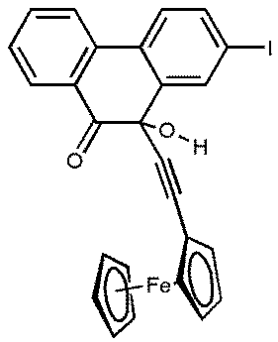

2-Iodo-9,10-phenanthrenquinone (27) (0.30 g, 0.90 mmol), 10% Pd /C (0.01 g, 0.01 mmol), CuI (0.03 g, 0.18 mmol), Ph_3P (0.2 g, 0.72 mmol) and K_2CO_3 (0.30 g, 2.16 mmol) were dissolved at room temperature in a 1:1 mixture of water (10 mL) and DME (10 mL). The mixture was degassed with N_2 for 5 min and stirred for 30 min under N_2. Then ethylferrocene (0.30 g, 1.35 mmol) was added to the mixture. The reaction mixture was heated under reflux to 80 °C overnight. The mixture was then cooled, extracted with (50 mL) DCM and the organic layers were combined, dried over $MgSO_4$ and filtered. Then the solvent was evaporated under reduced pressure and the residue was then purified by column chromatography (DCM: 20% petroleum ether) to give an orange compound (0.10 g, 27%); mp. dec. > 177 ºC; ^{1}H NMR (400 MHz, $CDCl_3$) δ 8.24 (d, *J* = 1.8 Hz, 1H), 8.06 (dd, *J* = 1.5, 7.7 Hz, 1H), 7.93 (d, *J* = 8.0 Hz, 1H), 7.80 (dd, *J* = 1.5, 7.7 Hz, 1H), 7.74 (dt, *J* = 1.5, 7.7 Hz, 1H), 7.58 (dd, *J* = 1.8, 8.0 Hz, 1H), 7.49 (dt, *J* = 1.5, 7.7 Hz, 1H), 4.39 (s, 1H), 4.24 (m, 1H), 4.19 (m, 1H), 4.08 (m, 2H), 3.86 (s, 5H) ppm; ^{13}C NMR (100 MHz, $CDCl_3$) δ 195.7 (C=O), 139.2 (C-C), 138.0 (C-H), 136.7 (C-C) ,135.4 (C-H), 135.2 (C-H), 128.9 (C-H), 128.6 (C-C), 128.4 (C-H), 127.8 (C-C), 126.0 (C-H), 123.3 (C-H), 95.3 (C-I), 85.0 (C≡C), 83.8 (C≡C), 71.9 (C-H), 71.8 (C-H), 71.7 (C-C), 69.8 (C-H), 69.1 (5×C-H), 69.0 (C-H), 62.6 (C-OH) ppm; IR (film) υ 3458 (O-H), 2922 (C-H), 2210 (C≡C), 1699

(C=O) cm^{-1}; HRMS m/z (FAB $(M+Na)^+$) calculated for $C_{26}H_{17}O_2NaFeI$ 566.9520 found 566.9519.

5-(4-(Dimethyl amino phenyl)ethynyl) thiophene-2-carbaldehyde (37)

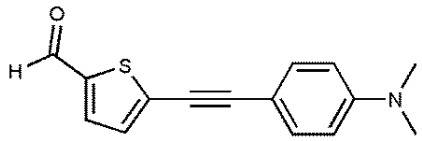

5-Bromo-2-thiophenecarboxaldehyde (0.50 g, 2.30 mmol), 10% Pd /C (0.07 g, 0.07 mmol), CuI (0.13 g, 0.68 mmol), Ph_3P (0.47 g, 1.80 mmol) and K_2CO_3 (0.50 g, 3.6 mmol) were dissolved at room temperature in a 1:1 mixture of water (15 mL) and DME (15 mL). The mixture was degassed with N_2 for 5 min and stirred for 30 min under N_2. Then 4-ethynyl-N,N-dimethylaniline (0.50 g, 3.40 mmol) was added to the mixture. The reaction mixture was heated under reflux to 80 °C overnight. The mixture was then cooled, extracted with DCM (80 mL) and the organic layers were combined, dried over $MgSO_4$ and filtered. The solvent was evaporated under reduced pressure and the residue was purified by column chromatography (toluene: 10 % DCM) to give an orange solid (0.37 g, 63 %); mp. 147-149 ºC; ^{1}H NMR (400 MHz, $CDCl_3$) δ 9.84 (s, 1H), 7.64 (d, *J* = 3.9 Hz, 1H), 7.41 (d, *J* = 8.9 Hz, 2H), 7.22 (d, *J* = 3.9 Hz, 1H), 6.65 (d, *J* = 8.9 Hz, 2H), 3.02 (s, 6H) ppm; ^{13}C NMR (100 MHz, $CDCl_3$) δ 182.2 (C=O), 150.7 (C-N), 142.7 (C-H), 136.3 (C-H), 134.4 (C-C), 132.9 (2×C-H), 131.2 (C-H), 111.6 (2×C-H), 108.1 (C-C), 100.3 (C≡C), 80.6 (C≡C), 40.0 (2×C-**N**) ppm; IR (film) υ 2807(C-H), 2182 (C=C), 1656 (C=O), 1229 (C-N) cm^{-1}; HRMS m/z (EI+) calculated for $C_{15}H_{13}NOS$ 255.0718 found 255.0708.

5(5(4-(Dimethyl amino phenyl)ethnyl)thiophene-2-yl)thiophene-2-carbaldehyde (38)

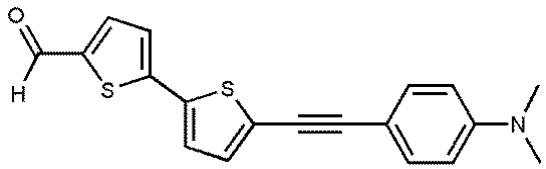

5-Bromo-2,2'-bithiophene-5'-carboxaldehyde (0.50 g, 1.83 mmol), 10% Pd /C (0.06 g, 0.06 mmol), CuI (0.10 g, 0.55 mmol), Ph_3P (0.40 g, 1.50 mmol) and K_2CO_3 (0.40 g, 2.90 mmol) were dissolved at room temperature in a 1:1 mixture of water (15 mL) and DME (15 mL). The mixture was degassed with N_2 for 5 min and stirred for 30 min under N_2. Then 4-ethynyl-N,N-dimethylaniline (0.40 g, 2.75 mmol) was added to the mixture. The reaction mixture was heated under reflux to 80 °C overnight. The mixture was then cooled, extracted with DCM (80 mL) and the organic layers were combined, dried over $MgSO_4$ and filtered. Then the solvent was evaporated under reduced pressure and the residue was then purified by column chromatography (SiO_2; DCM: 10 % petroleum ether) to give orange compound (0.37 g, 40 %); mp. 200-203 ºC; ^{1}H NMR (400 MHz, $CDCl_3$) δ 9.86 (s, 1H), 7.66 (d, *J* = 4.0 Hz, 1H), 7.39 (d, *J* = 8.9 Hz, 2H), 7.23 (d, *J* = 3.4 Hz, 1H), 7.22 (d, *J* = 3.4 Hz, 1H), 7.13 (d, *J* = 4.0 Hz, 1H), 6.66 (d, *J* = 8.9 Hz, 2H), 3.01 (s, 6H) ppm; ^{13}C NMR (100 MHz, $CDCl_3$) δ 182.4 (C-H), 150.4 (C-C), 146.6 (C-C), 141.6 (C-C), 137.3 (C-H), 135.8 (C-C), 132.7 (2×C-H), 131.8 (C-H), 126.3(C-C), 126.0 (C-H), 124.2 (C-H), 111.7 (2×C-H), 108.8 (C-C), 97.3 (C≡C), 80.2 (C≡C), 40.1 (2× CH_3-**N)** ppm; IR (film) υ 2787(C-H) , 2185(C=C), 1654 (C=O), 1228 (C-N) cm^{-1}; HRMS m/z (EI^+) calculated for $C_{19}H_{15}NOS_2$ 337.0595 found 337.0591.

2-(4-(Dimethylamino) phenyl)-3-(5-formylthiophene-2-yl)buta-1,3-diene-1,1,4,4-tetracarbonitrile (39)

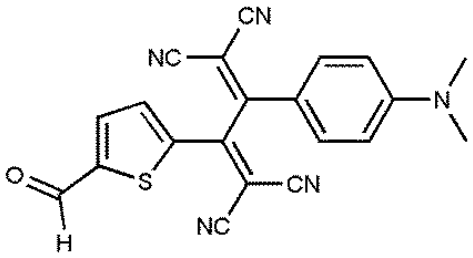

Tetracyanoethylene (0.11 g, 0.86 mmol) was added to a solution of compound [5-(4-(dimethyl amino phenyl)ethynyl) thiophene-2-carbaldehyde] (37) (0.20 g, 0.88 mmol) in THF (20 mL). The reaction mixture was stirred overnight at 66 ºC. After evaporation of all the solvent, the solid was purified by column chromatography (SiO_2; CH_2Cl_2: diethyl ether; 2:3) to give (0.19 g, 56 %) of a dark red solid; mp. 150-160 ºC; ^{1}H NMR (400 MHz, $CDCl_3$) δ 10.01 (s, 1H), 8.09 (d, *J* = 4.2 Hz, 1H), 7.83 (d, *J* = 4.2 Hz, 1H), 7.77 (d, *J* = 9.5 Hz, 2H), 6.74 (d, *J* = 9.5 Hz, 2H), 3.19 (s, 6H) ppm; ^{13}C NMR (100 MHz, $CDCl_3$) δ 182.3 (C-H), 161.0 (C=$C(CN)_2$), 159.4 (C=$C(CN)_2$), 154.7 (C-N phen), 150.3 (C-C), 141.4 (C-C), 135.7 (C-H), 135.2 (C-H), 132.5 (2×C-H) ,117.0 (C-C), 113.9 (C≡**N**), 113.1(C≡**N**), 112.4 (2×C-H), 111.9 (C≡**N**), 110.9 (C≡**N**), 85.1 (C=$C(CN)_2$), 74.4 (C=$C(CN)_2$), 40.3 (2×CH_3-**N)** ppm; IR (film) υ 2934 (C-H), 2213 (C≡**N**), 1666 (C=C), 1604 (C=C), 1173(C-**N**) cm^{-1}; HRMS m/z (EI+) calculated for $C_{21}H_{13}N_5OS$ 383.0841 found 383.0847.

2-(4-(Dimethyl amino)phenyl)-3-(5(5-formylthiophene-2-yl) thiophene-2-yl) buta-1,3-diene-1,1,4,4-tetracarbonitrile (40)

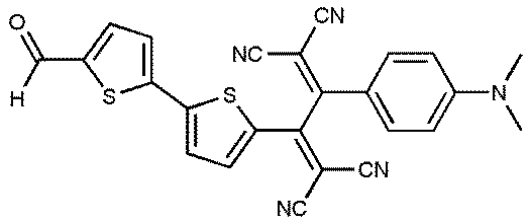

5(5(4-(Dimethyl amino phenyl) ethnyl) thiophene-2-yl) thiophene-2-carbaldehyde (0.20 g, 0.59 mmol) (38) and tetracyanoethane (0.08 g, 0.59 mmol) were dissolved in dry THF (20 mL). The reaction mixture was heated under reflux overnight. After cooling to room temperature, the solvent was evaporated and the crude product was purified by column chromatography (SiO_2: diethyl ether: DCM; 3:2) to afford a dark red compound (0.18 g, 66 %); mp. 180-190 ºC; ^{1}H NMR (400 MHz, $CDCl_3$) δ 9.93 (s, 1H), 7.82 (d, *J* = 4.2 Hz, 1H), 7.80 (d, *J* = 9.2 Hz, 2H), 7.74 (d, *J* = 4.0 Hz, 1H), 7.48 (d, *J* = 4.0 Hz, 1H), 7.43 (d, *J* = 4.2 Hz, 1H), 6.73 (d, *J* = 9.2 Hz, 2H), 3.18 (s, 6H) ppm; ^{13}C NMR (100 MHz, $CDCl_3$) δ 182.4 (C-H), 161.8 (C-C), 158.6 (C-C), 154.5 (C-C), 147.6 (C-C), 144.9 (C-C), 142.9 (C-C), 138.3 (C-H), 136.8 (C-H), 135.3 (C-C), 132.5 (2×C-H), 127.7 (C-H), 127.5 (C-H), 117.5 (C-C), 114.2 (C-C), 113.3 (C-C), 112.8 (C-C), 112.3 (2×C-H), 111.6 (C-C), 80.2 (C═C), 74.5 (C═C), 40.22 (2× CH_3-**N)** ppm; IR (film) υ 2934 (C-H), 2214 (C≡**N**), 1666 (C═C), 1602 (C═C), 1172 (C-N) cm^{-1}; HRMS (FAB $(M+H)^+$) calculated for $C_{25}H_{16}ON_5S_2$ 466.0796 found 466.0793.

5-(4-(Dimethyl amino) phenyl) ethynyl)-2 thienyl)methylene (41)

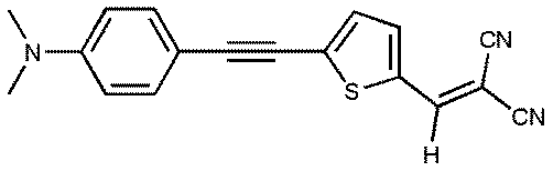

A mixture of 5-(4-(dimethyl amino phenyl)ethynyl) thiophene-2-carbaldehyde (37) (0.20 g, 0.78 mmol) and malonitrile (0.05 g, 0.78 mmol) in ethanol (40 mL) was purged with N_2 before 3-4 drops of piperidine was added. The reaction mixture was then heated under reflux at 78 ºC overnight. After cooling the mixture, the solvent was evaporated and the crude product was purified by column chromatography (SiO_2: DCM: 10 % petroleum ether) to afford a dark red compound (0.10 g, 42%); mp. 190-200 ºC; ^{1}H NMR (400 MHz, $CDCl_3$) δ 7.72 (s, 1H), 7.61 (d, *J* = 4.0 Hz, 1H), 7.41 (d, *J* = 9.0 Hz, 2H), 7.22 (d, *J* = 4.0 Hz, 1H), 6.66 (d, *J* = 9.0 Hz, 2H), 3.04 (s, 6H) ppm; ^{13}C NMR (100 MHz, $CDCl_3$) δ 150.9 (C-N phen), 149.8 (C-H), 138.9 (C-H), 136.8 (C-C), 134.5 (C-C), 133.2 (2×C-H), 131.2 (C-H), 114.2 (C≡**N**), 113.4 (C≡**N**), 111.7 (2×C-H), 107.6 (2×C-S), 104.1 (C≡**C**), 81.1 (C≡**C**), 76.5 (C=C$(CN)_2$), 40.0 (2×C-**N**) ppm; IR (film) υ 2889 (C-H), 2218 (C≡**N**), 2168 (C-H), 2144(C≡C) cm^{-1}; HRMS m/z (EI$^+$) calculated for $C_{18}H_{13}N_3S$ 303.0830 found 303.0829.

5(5(4-(Dimethyl amino phenyl)ethnyl)thiophene-2-yl)thienyl) methylene (42)

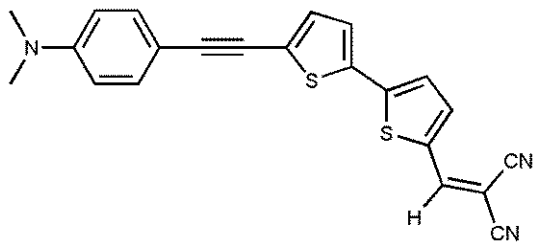

A mixture of 5(5(4-(dimethyl amino phenyl) ethnyl) thiophene-2-yl) thiophene-2-carbaldehyde (38) (0.30 g, 0.89 mmol) and malonitrile (0.06 g, 0.90 mmol) in ethanol (40 mL) was purged with nitrogen before 3-4 drops of piperidine was added. The reaction mixture was then heated under reflux at 78 ºC overnight under nitrogen. After cooling the mixture, the solvent was evaporated and the crude product was purified by column chromatography (SiO_2: DCM: 20 % petroleum ether) to afford a dark red compound (0.13 g, 42%); mp. 210-220 ºC; ^{1}H NMR (400 MHz, $CDCl_3$) δ 7.75 (s, 1H), 7.63 (dd, *J* = 4.2, 0.6 Hz, 1H), 7.39 (d, *J* = 9.0 Hz, 2H), 7.32 (d, *J* = 4.0 Hz, 1H), 7.25 (d, *J* = 4.2 Hz, 1H), 7.16 (d, *J* = 4.0 Hz, 1H), 6.66 (d, *J* = 9.0 Hz, 2H), 3.02 (s, 6H) ppm; ^{13}C NMR (100 MHz, $CDCl_3$) δ 150.5 (C-N phen), 150.0 (C-H), 148.8 (C-C), 140.1(C-H), 134.8 (C-C), 133.5 (C-C), 132.8 (2×C-H), 132.1 (C-H), 127.8 (C-C), 127.2 (C-H), 124.6 (C-H), 114.3 (C≡**N**), 113.4 (C≡**N**), 111.7 (2×C-H), 108.6 (2×C-S), 80.4 (C≡C), 76.7 (C=C(CN)$_2$), 40.2 (2×C-**N**) ppm; IR (film) υ 2923 (C-H), 2853, 2214 (C≡**N**), 1662 (C=C), 1383 (C-N); HRMS m/z (EI$^+$) calculated for $C_{22}H_{15}N_3S_2$ 385.0707 found 385.0717.

5-(4-(Dimethyl amino) phenyl) ethynyl)-2 thienyl) methylene)- buta-1,3-diene-1,1,4,4-tetracarbonitrile (43) (method 1)

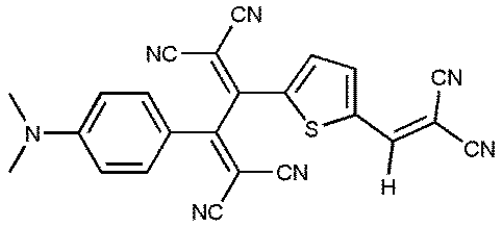

5-(4-(Dimethyl amino) phenyl) ethynyl)-2 thienyl) methylene (41) (0.10 g, 0.32 mmol) and tetracyanoethane (0.04 g, 0.32 mmol) were dissolved in dry THF (20 mL). The reaction mixture was heated under reflux at 66 ºC overnight. After cooling to room temperature, the solvent was evaporated and the crude product was purified by column chromatography (SiO_2: DCM: 2 % ethyl acetate) to afford a dark brown solid (0.10 g, 42 %); mp. Dec. > 125 ºC; ^{1}H NMR (400 MHz, $CDCl_3$) δ 7.99 (d, *J* = 4.4 Hz, 1H), 7.93 (d, *J* = 4.4 Hz, 1H), 7.82 (s, 1H), 7.76 (d, *J* = 9.2 Hz, 2H), 6.74 (d, *J* = 9.2 Hz, 2H), 3.20 (s, 6H) ppm; ^{13}C NMR (100 MHz, $CDCl_3$) δ 160.5 (C=C(CN)$_2$), 158.2 (C=C(CN)$_2$), 154.8 (C-N phen), 148.2 (C-H), 142.5 (C-C), 142.0 (C-C), 136.5 (C-H), 136.1 (C-H), 132.4 (2×C-H), 117.0 (C-C), 113.8 (C≡**N**), 113.2 (C≡**N**), 112.5 (2×C-H), 112.0 (2×C≡**N**), 111.9 (C≡**N**), 110.7 (C≡**N**), 85.6 (C=C(CN)$_2$), 84.6 (C=C(CN)$_2$), 74.3 (C=C(CN)$_2$), 40.0 (2×C-**N**) ppm; IR (film) υ 3087 (C-H), 2214 (C≡**N**), 1603 (C=**C**), 1173 (C-N) cm^{-1}; HRMS m/z (EI+) calculated for $C_{24}H_{13}N_7S$ 431.0953 found 431.0958.

5-(4-(Dimethyl amino) phenyl) ethynyl)-2 thienyl) methylene)- buta-1,3-diene-1,1,4,4-tetracarbonitrile (43) (method 2)

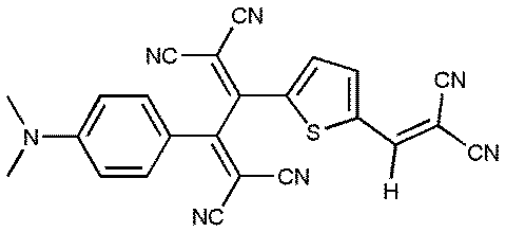

To a mixture of 2-(4-(dimethyl amino) phenyl)-3-(5-formylthiophene-2-yl)buta-1,3-diene-1,1,4,4-tetracarbonitrile (39) (0.10 g, 0.26 mmol) and malononitrile (0.02 g, 0.30 mmol) in CH_2Cl_2 (10 ml) was added 1 drop of piperidine. The reaction mixture was heated under reflux overnight. After cooling to room temperature, the solvent was evaporated and the crude product was purified by column chromatography (SiO_2: DCM: diethyl ether 2 %) to afford a dark green compound (0.04 g, 38 %); mp. 255-265 ºC; ^{1}H NMR (500 MHz, $CDCl_3$) δ 7.99 (d, *J* = 4.4 Hz, 1H), 7.93 (dd, *J* = 0.5, 4.4 Hz, 1H), 7.82 (s, 1H), 7.76 (d, *J* = 9.2 Hz, 2H), 6.74 (d, *J* = 9.2 Hz, 2H), 3.20 (s, 6H) ppm; ^{13}C NMR (125 MHz, $CDCl_3$) δ 160.5 (C=C(CN)$_2$), 158.2 (C=C(CN)$_2$), 154.8 (C-N phen), 148.2 (C-H), 142.5 (C-C), 142.0 (C-C), 136.5 (C-H), 136.1 (C-H), 132.4 (2×C-H), 117.0 (C-C), 113.8 (C≡**N**), 113.2 (C≡**N**), 112.5 (2×C-H), 112.0 (2×C≡**N**), 111.9 (C≡**N**), 110.7 (C≡**N**), 85.6 (C=C(CN)$_2$), 84.6 (C=C(CN)$_2$), 74.3 (C=C(CN)$_2$), 40.0 (2×C-**N**) ppm; IR (film) υ 3087 (C-H), 2214 (C≡**N**), 1603 (C=**C**), 1173 (C=**C**) cm^{-1}; HRMS m/z (EI$^+$) calculated for $C_{24}H_{13}N_7S$ 431.0953 found 431.0956.

5((5(4-(Dimethyl amino phenyl)ethnyl)thiophene-2-yl)thienyl) methylene)- buta-1,3-diene-1,1,4,4-tetracarbonitrile (44)

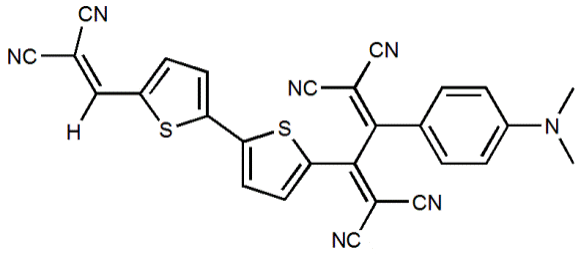

To a mixture of 2-(4-(dimethyl amino) phenyl)-3-(5(5-formylthiophene-2-yl) thiophene-2-yl) buta-1,3-diene-1,1,4,4-tetracarbonitrile (39) (0.20 g, 0.43 mmol) and malononitrile (0.03 g, 0.45 mmol) in CH_2Cl_2 (10 ml) was added 1 drop of piperidine. The reaction mixture was heated under reflux overnight. After cooling to room temperature, the solvent was evaporated and the crude product was purified by column chromatography (SiO_2: DCM: diethyl ether 5 %) to afford a dark red compound (0.08 g, 36 %); mp. 270-280 ºC; ^{1}H NMR (400 MHz, $CDCl_3$) δ 7.85 (d, *J* = 4.2, 1H), 7.82 (s, 1H), 7.80 (d, *J* = 9.5, 2H), 7.71 (d, *J* = 4.2, 1H), 7.49 (d, *J* = 4.2, 2H), 6.74 (d, *J* = 9.5, 2H), 3.18 (s, 6H) ppm; ^{13}C NMR (100 MHz, THF) δ 152.4 (C-N phen), 141.3 (C-C), 140.3 (C-C), 138.6 (C-H), 133.7 (2×C-H), 129.8 (C-C) , 129.7 (C-C), 113.5 (2×C-H), 40.8 (2× CH_3-**N)** ppm; IR (film) υ 3076 (C-H) , 2214 (C≡**N**), 1606 (C=**C**), 1174 (C=**C**) cm^{-1}; HRMS (FAB $(M+H)^+$) calculated for $C_{28}H_{16}N_7S_2$ 514.0909 found 514.0911.

2,7-Dihex-1-ynyl-dibenzo[*a*,*c*]phenazine-9,10-anthraquinone (46)

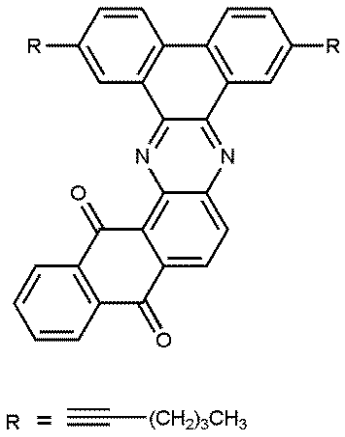

2,7-Dihex-1-ynyl-phenanthrene-9,10-dione (8) (0.20 g, 0.27 mmol) and 1,2-diamino-anthraquinone (0.14 g, 0.27 mmol) were dissolved in chloroform (10 mL). Then *p*-toluene sulfonic acid (0.04 g, 0.23 mmol) was added to the solution. The reaction mixture was heated under reflux under nitrogen for 2 days. After cooling, the solvent was evaporated under reduced pressure. The solid was purified by column chromatography (SiO_2; DCM: 10 % toluene) to afford an orange solid (0.10 g, 65 %); mp. 190-192 ºC; ^{1}H NMR (500 MHz, $CDCl_3$) δ 8.99 (d, *J* = 1.6 Hz, 1H), 8.84 (d, *J* = 1.6 Hz, 1H), 8.46 (d, *J* = 8.7 Hz, 1H), 8.32 (d, *J* = 8.7 Hz, 1H), 8.22 (dd, *J* = 7.6, 0.9 Hz, 1H), 8.15 (dd, *J* = 7.5, 0.9 Hz, 1H), 8.08 (d, *J* = 8.4 Hz, 1H), 8.05 (d, *J* = 8.4 Hz, 1H) 7.77 (dt, *J* = 7.4, 1.2 Hz, 1H), 7.71 (dt, *J* = 7.4, 1.2 Hz, 1H), 7.59 (dd, *J* = 8.3, 1.7 Hz, 1H), 7.51 (dd, *J* = 8.3, 1.7 Hz, 1H), 2.59 (t, *J* = 7.1 Hz, 2H), 2.49 (t, *J* = 7.1 Hz, 2H), 1.77 (m, 2H), 1.67 (m, 4H), 1.59 (m, 2H), 1.09 (t, *J* = 7.4 Hz, 3H), 1.04 (t, *J* = 7.4 Hz, 3H) ppm; ^{13}C NMR (125 MHz, $CDCl_3$) δ 183.3 (C=O), 182.2 (C=O), 143.9 (C-C), 143.7 (C-C), 141.7 (C-C), 139.2 (C-C), 135.3 (C-H), 135.2 (C-H), 134.8 (C-H), 134.2 (C-C), 133.8 (C-C), 133.7 (C-H), 133.1 (C-H) , 131.8 (C-C), 130.9 (C-C), 130.4 (C-C), 130.0 (C-H), 129.6 (C-C), 129.2 (C-H), 128.9 (C-C), 128.5 (C-C), 127.2 (C-H), 126.3 (C-H), 126.0 (C-H), 124.3 (C-C), 123.7 (C-C), 122.8 (C-H), 122.6 (C-H), 92.7 (C≡**C**), 92.4 (C≡**C**), 80.7 (C≡C), 80.3 (C≡C), 30.9 (C-H_2), 30.9 (C-H_2), 22.3 (C-H_2),

22.2 (C-H_2), 19.5 (C-H_2), 19.3 (C-H_2), 13.8 (C-H_3), 13.7 (C-H_3) ppm; IR (film) υ 2956 (C-H), 2928 (C-H), 2858 (C-H), 1660 (C=O), 1593 (C=N) cm^{-1}; HRMS (FAB $(M+H)^+$) calculated for $C_{40}H_{31}N_2O_2$ 571.2386 found 571.2380.

2,7-Dihex-1-ynyl-Dibenzo[*a,c*]phenazine -11,11,12,12-tetracyano-anthraquinodimethane (47)

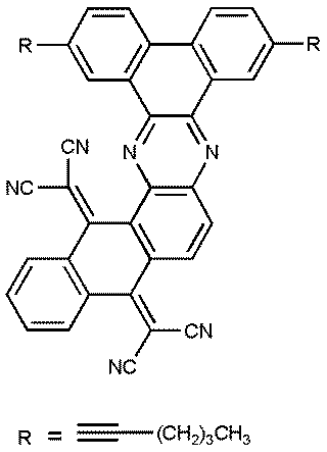

Titanium chloride (0.4 mL, 3.6 mmol) and pyridine (0.5 mL, 6.2 mmol) were added slowly to a mixture of **2,7**-dihex-1-ynyl-dibenzo[*a,c*]phenazine-9,10-anthraquinone (46) (0.15 g, 0.26 mmol) and malononitrile (0.26 g, 3.95 mmol) in dry DCM (30 mL) at 0 ºC under N_2. The reaction mixture was then heated under reflux at 40 ºC overnight under nitrogen. After cooling, the reaction mixture was poured into 5 % HCl (100 mL). Then the organic layer was extracted with $CHCl_3$ (50 mL), washed with sat. $NaHCO_3$ (50 mL), brine (50 mL) and dried over Na_2SO_4 and then filtered. Then the solvent was removed under reduced pressure and the crude product was purified using column chromatography (SiO_2; DCM: 10 % petroleum ether) to afford a red compound (0.12 g, 69 %); mp. Dec. > 246 ºC; ^{1}H NMR (400 MHz, $CDCl_3$) δ 9.32 (d, *J* = 1.8 Hz, 1H), 9.26 (d, *J* = 1.8 Hz, 1H), 8.62 (d, *J* = 15.0, 6.9 Hz, 2H), 8.53 (dd, *J* = 3.5, 1.1 Hz, 1H), 8.41 (t, *J* = 7.7 Hz, 2H), 8.35 (dd, *J* = 7.7,

1.1Hz, 1H), 7.81 (m, 4H), 2.61 (t, *J* = 6.9 Hz, 2H) 2.54 (t, *J* = 6.9 Hz, 2H), 1.67 (m, 8H), 1.07 (t, *J* = 7.3 Hz, 3H), 1.02 (t, *J* = 7.3 Hz, 3H) ppm; ^{13}C NMR (100 MHz, $CDCl_3$) δ 159.9 (C-C), 156.7 (C-C), 144.7(C-C), 142.9 (C-C), 142.5 (C-C), 136.8 (C-C), 134.8 (C-H), 133.8 (C-H), 132.4 (C-H), 132.1 (C-C), 131.9 (C-H), 131.6 (C-C), 131.5 (C-C), 130.5 (C-C), 130.0 (C-H), 129.9 (C-H), 129.7 (C-C), 129.1 (C-C), 128.8 (C-C), 127.7 (C-C), 127.5 (C-H), 126.0 (C-H), 124.7 (C-C), 124.5 (C-C), 123.4 (C-H), 123.3 (C-H), 113.2 (C≡N), 113.0 (C≡N), 112.8 (C≡N), 93.5 (C≡C), 93.2 (C≡C), 89.0 (C-$(CN)_2$), 84.4 (C-$(CN)_2$), 80.3 (C≡C), 80.1(C≡C), 30.9 (C-H_2), 30.8 (C-H_2), 22.1 (2×C-H_2), 19.4 (C-H_2), 19.3 (C-H_2), 13.8 (C-H_3), 13.7 (C-H_3) ppm; IR (film) υ 2956 (C-H) , 2928 (C-H), 2858 (C-H), 2225 (C≡N) cm^{-1}; HRMS (FAB $(M+H)^+$) calculated for $C_{46}H_{31}N_6$ 667.2610 found 667.2604.

2-Cyano-3-(5-(4-(dimethyl amino phenyl) ethynyl) thiophene-2-yl) buta-1,3-diene-1,1,4,4-tetracarbonitrile acrylic acid (48)

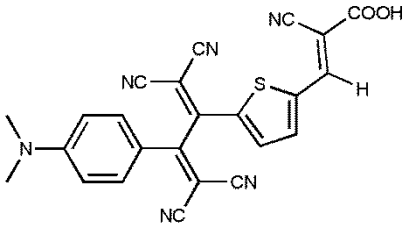

To a mixture of 2-(4-(dimethyl amino)phenyl)-3-(5-formylthiophene-2-yl)-buta-1,3-diene-1,1,4,4-tetracarbonitrile (39) (0.40 g, 1.04 mmol) and cyanoacetic acid (0.27 g, 3.13 mmol) in CH_2Cl_2 (20 mL) was added piperidine (0.2 mL, 2.0 mmol). The reaction mixture was heated under reflux for 2 days under nitrogen. After cooling to room temperature, the mixture was then poured into (1N) HCl (100 mL) and the organic layer was extracted with DCM (200 mL). The extracted organic layer was washed with brine ((100 mL), water (100 mL), dried over $MgSO_4$ and filtered. Then solvent was evaporated and the crude product was purified by column chromatography (SiO_2: chloroform: methanol 10%) to afford a

dark red solid (0.13 g, 57 %); mp. 260-270 ºC; ^{1}H NMR (500 MHz, DMSO) δ 8.58 (s, 1H), 8.08 (d, *J* = 4.4, 1H), 8.00 (d, *J* = 4.4, 1H), 7.92 (d, *J* = 9.2, 2H), 6.88 (d, *J* = 9.2, 2H), 3.17 (s, 6H) ppm; ^{13}C NMR (125 MHz, DMSO) δ 160.7 (C=C(CN) (COOH)), 157.9 (C=C(CN)$_2$), 154.7 (C-N phen), 144.5 (C-H), 139.2 (C-C), 138.8 (C-H), 138.4 (C-H), 132.7 (2×C-H), 116.4 (C-C), 114.9 (C≡N), 114.2 (C≡N), 112.5 (2×C-H), 112.1 (2×C≡N), 83.6 (C=C(CN)$_2$), 71.6 (C=C(CN)$_2$), 40.0 (2×C-N); IR (film) υ 3388 (O-H), 2835 (C-H), 2214 (C≡N), 1687 (C=O) cm^{-1}; $C_{24}H_{14}N_6O_2S$ 450.0899 found 450.0922.

2-Cyano-3-(5-(5-(4-(dimethyl amino phenyl)ethynyl)-thiophene-2-yl)thiophene-2-yl)-buta-1,3-diene-1,1,4,4-tetracarbonitrile acrylic acid (49)

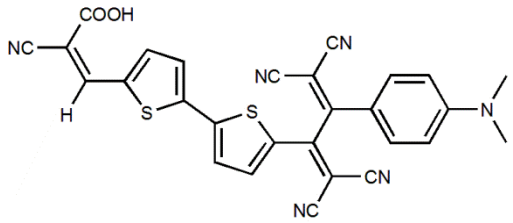

To a mixture of 2-(4-(dimethyl amino)phenyl)-3-(5(5-formylthiophene-2-yl) thiophene-2-yl) buta-1,3-diene-1,1,4,4-tetracarbonitrile (40) (0.20 g, 0.43 mmol) and cyanoacetic acid (0.11 g, 1.29 mmol) in CH_2Cl_2 (20 mL) was added piperidine (0.2 mL, 2.0 mmol). The reaction mixture was heated under reflux for 2 days under nitrogen. After cooling to room temperature, the mixture was then poured into (1N) HCl (100 mL) and the organic layer was extracted with DCM (200 mL). The extracted organic layer was washed with brine (100 mL), water (100 mL), dried over $MgSO_4$ and filtered. Then solvent was evaporated and the crude product was purified by column chromatography (SiO_2: chloroform: methanol 10 %) to afford a dark red compound (0.13 g, 57 %); mp. 285-295 ºC; ^{1}H NMR (500 MHz, DMSO) δ 8.09 (s, 1H), 7.95 (d, *J* = 4.4 Hz, 1H), 7.91 (d, *J* = 9.4 Hz, 2H), 7.81 (d, *J* = 4.4 Hz, 1H), 7.76 (d, *J* = 4.4 Hz, 2H), 6.89 (d, *J* = 9.4 Hz, 2H), 3.15 (s, 6H) ppm;

IR (film) υ 3398 (O-H), 2208 (C≡N), 1602 (C=O) cm^{-1}; HRMS (FAB $(M+H)^+$) calculated for $C_{28}H_{16}N_7S_2$ 514.0909 found 514.0911.

2-Cyano-3-(5-(4-(dimethyl amino phenyl) ethynyl) thiophene-2-yl) acrylic acid (50)

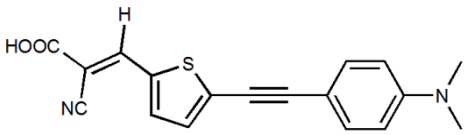

To a mixture of 5-(4-(dimethyl amino phenyl)ethynyl) thiophene-2-carbaldehyde (37) (0.40 g, 1.78 mmol) and cyanoacetic acid (0.30 g, 3.52 mmol) in CH_3CN (20 mL) was added piperidine (0.2 mL, 2.0 mmol). The reaction mixture was heated under reflux overnight under nitrogen. After cooling to room temperature, the mixture was then poured into (1N) HCl (100 mL) and the organic layer was extracted with chloroform (200 mL). The extracted organic layer was washed with brine (100 mL), water (100 mL), dried over $MgSO_4$ and filtered. Then solvent was evaporated and the crude product was purified by column chromatography (SiO_2: chloroform: acetic acid 10 %) to afford a red compound (0.18 g, 31 %); mp. 210-220 ºC; ^{1}H NMR (500 MHz, DMSO) δ 8.48 (s, 1H), 7.96 (d, *J* = 4.0, 1H), 7.45 (d, *J* = 4.0, 1H), 7.42 (d, *J* = 9.1, 2H), 6.73 (d, *J* = 9.1, 2H), 2.98 (s, 6H) ppm; ^{13}C NMR (125 MHz, DMSO) δ 163.2 (C-OOH), 150.9 (C-N phen), 145.6 (C-H), 139.7 (C-H), 135.5 (C-C), 132.8 (2×C-H), 132.0 (C-H), 131.8 (C-C), 116.5 (C≡**N**), 111.9 (2×C-H), 106.7 (C-C), 101.1 (C=CN,COOH), 81.3 (C≡**C**), 80.7 (C≡**C**), 39.9 (2×C-**N**) ppm; IR (film) υ 3200 (O-H), 2177 (C≡N), 1680 (C=O), 1600 (C=C) cm^{-1}; HRMS (FAB $(M+Na)^+$) calculated for $C_{18}H_{14}N_2O_2SNa$ 345.0674 found 345.0676.

2-Cyano-3-(5-(5-(4-(dimethyl amino phenyl)ethynyl)-thiophene-2-yl)thiophene-2-yl)acrylic acid (51)

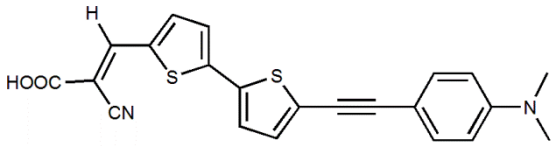

To a mixture of 5(5(4-(dimethyl amino phenyl) ethnyl)thiophene-2-yl) thiophene-2-carbaldehyde (38) (0.40 g, 1.20 mmol) and cyanoacetic acid (0.20 g, 2.35 mmol) in CH_3CN (20 mL) was added piperidine (0.2 mL, 2.0 mmol). The reaction mixture was heated under reflux overnight under nitrogen. After cooling to room temperature, the mixture was then poured into (1N) HCl (100 mL) and the organic layer was extracted with chloroform (200 mL). The extracted organic layer was washed with brine (100 mL), water (100 mL), dried over $MgSO_4$ and filtered. Then solvent was evaporated and the crude product was purified by column chromatography (SiO_2: chloroform: acetic acid 10 %) to afford a red compound (0.13 g, 28 %); mp. 235-245 ºC; ^{1}H NMR (400 MHz, DMSO) δ 8.40 (s, 1H), 7.92 (d, *J* = 4.0, 1H), 7.58 (d, *J* = 4.0, 1H), 7.54 (d, *J* = 4.0, 1H), 7.37 (d, *J* = 8.9, 2H), 7.33 (d, *J* = 4.0, 1H), 6.73 (d, *J* = 8.9, 2H), 2.97 (s, 6H) ppm; IR (film) υ 3308, 2177 (C≡N), 1633 (C=O), 1604 (C=C) cm^{-1}; HRMS (FAB (M-H)$^-$) calculated for $C_{22}H_{16}N_2O_2S_2$ 403.0574 found 403.0561.

2,7-Bis(carbazol-9-yl)-9,10-phenathrenequinone (52)

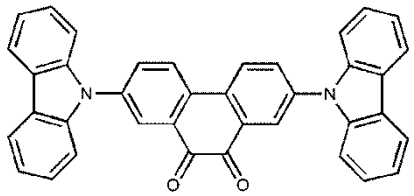

A mixture of 2,7-diiodo-9, 10 phenathrenequinone (0.50 g, 1.09 mmol), CuI (0.02 g, 0.10 mmol), carbazole (0.47 g, 2.17 mmol), K_2CO_3 (0.60 g, 4.34 mmol), 18-crown-6 (0.01g, 0.03 mmmol) and 1,3-dimethyl-3,4,5,6-tetrahydro-2(1H)- pyrimidinone (DMPU) (0.20 mL, 1.66 mmol) was heated at 170 °C under nitrogen for 2 days. After cooling, the reaction mixture was quenched with 1N HCl (100 mL). The solids were collected and washed with a mixture of 80 % ammonium hydroxide and water (100 mL). The crude sample was then purified by column chromatography (DCM: 20 % petroleum ether) to give a purple compound (0.06 g, 10 %); mp. 300-310 ºC; ^{1}H NMR (400 MHz, $CDCl_3$) δ 8.50 (d, *J* = 2.3 Hz, 2H), 8.33 (d, *J* = 8.6 Hz, 2H), 8.18 (dt, *J* = 7.3, 1.0 Hz, 4H), 8.04 (dd, *J* = 8.6, 2.3 Hz, 2H), 7.49 (m, 8H) 7.36 (dt, *J*= 1.0, 7.3 Hz, 1H) ppm; ^{13}C NMR (100 MHz, $CDCl_3$) δ 179.4 (C=O), 140.1 (C-N), 139.5 (C-N), 133.9 (C-H), 133.7 (C-C), 132.4 (C-C), 128.1(C-H), 126.4 (C-H), 126.1 (C-H), 123.9 (C-C), 120.9 (C-H), 120.6 (C-H), 109.7(C-H) ppm; IR (film) υ 2615 (C-H), 1880 (C=O), 1329 (C-N) cm^{-1}; HRMS m/z (EI^+) calculated for $C_{38}H_{22}O_2N_2$ 538.1681.

6.3. Preparation for photovoltaic measurements

Acetic acid, ethyl cellulose, terpineol, anhydride ethanol and other chemicals were purchased from Sigma Aldrich and used as received without further purification. Commercial TiO_2 powders (P_{25}) were obtained from Degussa AG, Germany. Transparent fluorine-doped SnO_2 (FTO) conducting glass (TEC 8, sheet resistance = 8 Ω/sq) were purchased from Pilkington.

TiO_2 paste was prepared as follows. TiO_2 powder (6 g), acetic acid (1 mL), H_2O (6 mL) and ethanol (30 mL) were mixed and then ground in an alumina mortar. The dispersion of TiO_2 nanoparticles was transferred to a beaker and then both anhydrous terpineol (20 g) and ethyl cellulose (10 % solution in ethanol) were added. The TiO_2 nanoparticle solution was stirred with a magnetic bar and then sonicated by using a sonicator (Wiseclean co.). Subsequently, it was concentrated by using a rotary evaporator. Nanocrystalline TiO_2 paste was deposited on the FTO glass substrates using a doctor-blade technique and TiO_2 thick films were annealed in a furnace at 500 ºC for 1 hour. The prepared TiO_2 electrodes were immersed in a 0.04 M $TiCl_4$ solution at 70 ºC for 1 hour. They were rinsed with water and ethanol and then sintered at 500 ºC for 30 min. The TiO_2 electrodes were exposed by O_2 plasma and then immersed into a 0.5 mM photosensitizer solution for 24 hours. Pt-counter electrode was prepared on the FTO glass by using a magnetron sputterer after two holes were drilled in the glass. The photosensitizer-adsorbed TiO_2 electrode and Pt-counter electrode were sealed with 25 μm-thick Surlyn (Solaronix). The electrolyte, 50 mM of tri-iodine in acetonitrile (Iodolyte AN-50, Solaronix) was filled through the holes in the backside of the counter electrode.

The photovoltaic characteristics of the devices under AM 1.5 global one sun illumination (100 mW/cm^2) were investigated by a solar cell I-V measurement system (McScience K3000 LAB, Korea). J_{sc}, V_{oc}, FF and overall conversion efficiency (η) were simultaneously measured.

Chapter 7;

Appendices.

Appendix 1; X-Ray crystal structure of compound **3**

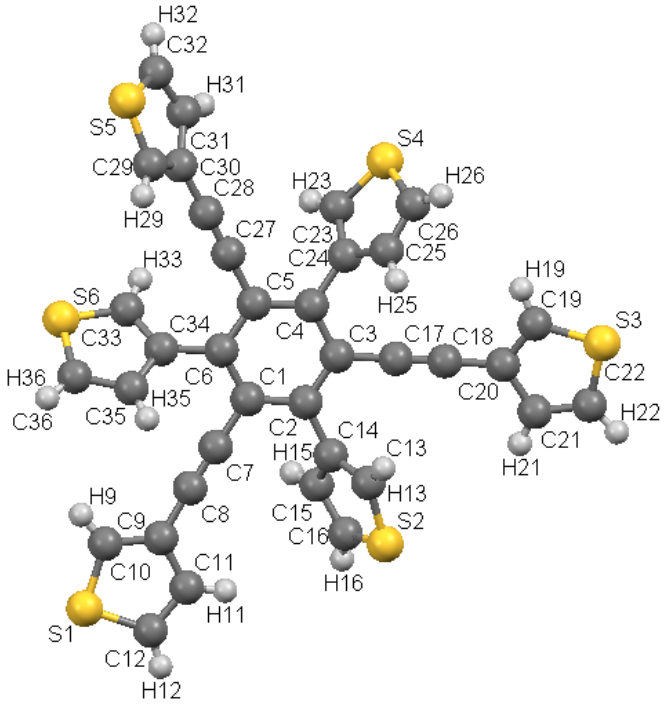

Table 7.1. Crystal data and structure refinement for compound **3**.

Identification code	compound **3**
Empirical formula	$C_{36}\ H_{18}\ S_6$
Formula weight	642.86
Temperature	150(2) K
Wavelength	0.71073 Å
Crystal system	Monoclinic
Space group	P2 (1)/c
Unit cell dimensions	a = 10.8017(4) Å alpha = 90 deg. b = 16.3130(6) Å beta = 93.459(2) deg. c = 17.0240(6) Å gamma = 90 deg.
Volume	2994.30 (19) A^3
Z, Calculated density	4, 1.426 Mg/m^3
Absorption coefficient	0.483 mm^{-1}

F(000)	1320
Crystal size	0.30 x 0.20 x 0.12 mm^3
Theta range for data collection	2.26 to 25.50 °.
Limiting indices	-10<=h<=13, -19<=k<=19, -18<=l<=20
Reflections collected / unique	22264 / 5564 [R(int) = 0.0327]
Completeness to theta = 25.50	99.8 %
Absorption correction	Empirical
Max. and min. transmission	0.9443 and 0.8686
Refinement method	Full-matrix least-squares on F^2
Data / restraints / parameters	5564 / 21 / 410
Goodness-of-fit on F^2	1.033
Final R indices [I>2sigma(I)]	R1 = 0.0447, wR2 = 0.1126
R indices (all data)	R1 = 0.0629, wR2 = 0.1265
Extinction coefficient	none
Largest diff. peak and hole	0.42 and -0.48 $e.A^{-3}$

Table 7.2. Atomic coordinates ($\times 10^4$) and equivalent isotropic displacement parameters ($A^2 \times 10^3$) for compound **3**, U(eq) is defined as one third of the trace of the orthogonalized Uij tensor.

	x	y	z	U(eq)
C(1)	2421(2)	5145(2)	4722(1)	24(1)
C(2)	3128(2)	5470(2)	5374(1)	24(1)
C(3)	3054(2)	5103(2)	6114(1)	24(1)
C(4)	2254(2)	4433(2)	6215(1)	25(1)
C(5)	1580(2)	4105(2)	5555(1)	24(1)
C(6)	1673(2)	4447(2)	4802(1)	23(1)
C(7)	2522(2)	5512(2)	3965(2)	27(1)
C(8)	2639(2)	5821(2)	3337(2)	30(1)
C(9)	2269(3)	5946(2)	1892(2)	39(1)
C(10)	2812(2)	6205(2)	2596(2)	30(1)
C(11)	3556(3)	6915(2)	2506(2)	35(1)
C(12)	3596(2)	7169(2)	1737(2)	31(1)
C(13)	5183(2)	6205(2)	5431(2)	33(1)
C(14)	3924(2)	6189(2)	5250(1)	24(1)
C(15)	3502(2)	6926(2)	4896(2)	29(1)
C(16)	4488(10)	7450(7)	4828(9)	39(3)
C(17)	3787(2)	5415(2)	6779(2)	27(1)
C(18)	4444(2)	5631(2)	7330(2)	28(1)
C(19)	5412(3)	5425(2)	8662(2)	48(1)
C(20)	5274(2)	5860(2)	7977(2)	32(1)
C(21)	6097(3)	6545(2)	7976(2)	42(1)
C(22)	6838(3)	6598(2)	8657(2)	58(1)

C(23)	969(3)	4015(2)	7348(2)	45(1)
C(24)	2113(3)	4082(2)	7006(2)	30(1)
C(25)	3073(3)	3779(2)	7501(2)	46(1)
C(26')	946(9)	3673(7)	8099(6)	33(2)
C(26)	2878(8)	3452(6)	8182(5)	48(3)
C(27)	862(2)	3375(2)	5646(1)	27(1)
C(28)	285(2)	2752(2)	5703(2)	29(1)
C(29)	-122(3)	1306(2)	5372(2)	38(1)
C(30)	-384(2)	2006(2)	5771(2)	29(1)
C(31)	-1380(3)	1886(2)	6274(2)	36(1)
C(32)	-1844(3)	1090(2)	6242(2)	42(1)
C(33)	-230(2)	3873(2)	4045(2)	31(1)
C(34)	1018(2)	4080(2)	4099(1)	26(1)
C(35)	1574(2)	3916(2)	3394(2)	33(1)
C(36)	700(10)	3584(8)	2829(6)	50(6)
C(36')	-609(13)	3590(14)	3280(9)	50(7)
S(1)	2681(1)	6542(1)	1132(1)	45(1)
S(2)	5841(1)	7084(1)	5151(1)	37(1)
S(3)	6544(1)	5838(1)	9284(1)	72(1)
S(4')	2439(3)	3450(1)	8374(1)	51(1)
S(4)	1261(4)	3581(2)	8265(2)	64(1)
S(5)	-1041(1)	513(1)	5613(1)	54(1)
S(6)	-730(2)	3502(3)	3182(2)	38(1)
S(6')	640(3)	3560(2)	2683(3)	33(1)
S(2')	4554(10)	7632(8)	4762(10)	32(2)
C(16')	5670(18)	6954(15)	5170(30)	74

Table 7.3. Bond lengths [A] and angles [deg] for compound **3**

C(1)-C(6)	1.408(3)
C(1)-C(2)	1.411(3)
C(1)-C(7)	1.431(4)
C(2)-C(3)	1.402(3)
C(2)-C(14)	1.478(3)
C(3)-C(4)	1.409(3)
C(3)-C(17)	1.435(3)
C(4)-C(5)	1.407(3)
C(4)-C(24)	1.480(4)
C(5)-C(6)	1.407(3)
C(5)-C(27)	1.436(3)
C(6)-C(34)	1.480(3)
C(7)-C(8)	1.196(4)
C(8)-C(10)	1.431(4)
C(9)-C(10)	1.369(4)
C(9)-S(1)	1.699(3)
C(10)-C(11)	1.423(4)
C(11)-C(12)	1.377(4)
C(12)-S(1)	1.721(3)
C(13)-C(14)	1.377(4)
C(13)-S(2)	1.681(3)

C(14)-C(15)	1.408(4)
C(15)-C(16)	1.376(10)
C(16)-S(2)	1.643(11)
C(17)-C(18)	1.196(4)
C(18)-C(20)	1.428(4)
C(19)-C(20)	1.365(4)
C(19)-S(3)	1.707(3)
C(20)-C(21)	1.427(4)
C(21)-C(22)	1.370(4)
C(22)-S(3)	1.679(4)
C(23)-C(24)	1.402(4)
C(23)-S(4)	1.724(4)
C(24)-C(25)	1.387(4)
C(25)-C(26)	1.304(9)
C(26')-S(4')	1.692(8)
C(26)-S(4)	1.774(8)
C(27)-C(28)	1.198(4)
C(28)-C(30)	1.424(4)
C(29)-C(30)	1.367(4)
C(29)-S(5)	1.696(3)
C(30)-C(31)	1.428(4)
C(31)-C(32)	1.392(4)
C(32)-S(5)	1.702(3)

C(33)-C(34)	1.387(4)
C(33)-S(6)	1.650(4)
C(34)-C(35)	1.399(4)
C(35)-C(36)	1.414(10)
C(36)-S(6)	1.696(11)
C(36')-S(6')	1.738(13)
S(2')-C(16')	1.750(16)
C(6)-C(1)-C(2)	120.9(2)
C(6)-C(1)-C(7)	120.0(2)
C(2)-C(1)-C(7)	119.0(2)
C(3)-C(2)-C(1)	119.3(2)
C(3)-C(2)-C(14)	122.1(2)
C(1)-C(2)-C(14)	118.6(2)
C(2)-C(3)-C(4)	120.6(2)
C(2)-C(3)-C(17)	120.0(2)
C(4)-C(3)-C(17)	119.4(2)
C(5)-C(4)-C(3)	119.2(2)
C(5)-C(4)-C(24)	120.2(2)
C(3)-C(4)-C(24)	120.6(2)
C(4)-C(5)-C(6)	121.0(2)
C(4)-C(5)-C(27)	119.2(2)
C(6)-C(5)-C(27)	119.7(2)
C(5)-C(6)-C(1)	118.8(2)

C(5)-C(6)-C(34)	121.4(2)
C(1)-C(6)-C(34)	119.8(2)
C(8)-C(7)-C(1)	178.3(3)
C(7)-C(8)-C(10)	178.2(3)
C(10)-C(9)-S(1)	111.8(2)
C(9)-C(10)-C(11)	111.8(2)
C(9)-C(10)-C(8)	124.4(3)
C(11)-C(10)-C(8)	123.7(2)
C(12)-C(11)-C(10)	113.4(2)
C(11)-C(12)-S(1)	109.9(2)
C(14)-C(13)-S(2)	112.4(2)
C(13)-C(14)-C(15)	111.7(2)
C(13)-C(14)-C(2)	124.0(2)
C(15)-C(14)-C(2)	124.2(2)
C(16)-C(15)-C(14)	109.5(5)
C(15)-C(16)-S(2)	115.1(7)
C(18)-C(17)-C(3)	175.8(3)
C(17)-C(18)-C(20)	177.1(3)
C(20)-C(19)-S(3)	111.2(3)
C(19)-C(20)-C(21)	111.8(3)
C(19)-C(20)-C(18)	123.7(3)
C(21)-C(20)-C(18)	124.5(3)
C(22)-C(21)-C(20)	112.4(3)

C(21)-C(22)-S(3)	111.6(3)
C(24)-C(23)-S(4)	106.8(3)
C(25)-C(24)-C(23)	111.4(3)
C(25)-C(24)-C(4)	125.2(3)
C(23)-C(24)-C(4)	123.3(2)
C(26)-C(25)-C(24)	122.1(5)
C(25)-C(26)-S(4)	103.6(6)
C(28)-C(27)-C(5)	177.8(3)
C(27)-C(28)-C(30)	179.2(3)
C(30)-C(29)-S(5)	112.0(2)
C(29)-C(30)-C(28)	123.5(3)
C(29)-C(30)-C(31)	111.7(2)
C(28)-C(30)-C(31)	124.7(2)
C(32)-C(31)-C(30)	112.8(3)
C(31)-C(32)-S(5)	110.1(2)
C(34)-C(33)-S(6)	114.4(2)
C(33)-C(34)-C(35)	111.3(2)
C(33)-C(34)-C(6)	124.5(2)
C(35)-C(34)-C(6)	124.2(2)
C(34)-C(35)-C(36)	110.7(5)
C(35)-C(36)-S(6)	112.0(7)
C(9)-S(1)-C(12)	93.00(13)
C(16)-S(2)-C(13)	91.3(4)

C(22)-S(3)-C(19)	92.98(16)
C(23)-S(4)-C(26)	96.0(4)
C(29)-S(5)-C(32)	93.36(15)
C(33)-S(6)-C(36)	91.7(4)

Symmetry transformations used to generate equivalent atoms:

Table 7.4. Anisotropic displacement parameters (A^2 x 10^3) for compound **3**.

The anisotropic displacement factor exponent takes the form:

$$-2\,pi^2\,[\,h^2\,a^{*2}\,U11 + ... + 2\,h\,k\,a^*\,b^*\,U12\,]$$

	U11	U22	U33	U23	U13	U12
C(1)	20(1)	27(1)	24(1)	-2(1)	0(1)	5(1)
C(2)	20(1)	24(1)	28(1)	-3(1)	-1(1)	4(1)
C(3)	21(1)	26(1)	24(1)	-3(1)	-4(1)	5(1)
C(4)	25(1)	23(1)	27(1)	-1(1)	-2(1)	6(1)
C(5)	21(1)	23(1)	27(1)	-2(1)	-2(1)	4(1)
C(6)	20(1)	25(1)	25(1)	-3(1)	-2(1)	5(1)
C(7)	25(1)	28(1)	27(1)	-6(1)	-1(1)	-1(1)
C(8)	29(1)	30(1)	31(2)	-4(1)	1(1)	-2(1)
C(9)	49(2)	38(2)	30(2)	-2(1)	2(1)	-8(1)
C(10)	31(1)	34(1)	26(1)	0(1)	3(1)	2(1)
C(11)	33(2)	40(2)	32(2)	-3(1)	2(1)	-5(1)
C(12)	32(1)	32(1)	29(1)	2(1)	2(1)	-2(1)

C(13)	25(1)	36(2)	37(2)	-5(1)	1(1)	1(1)
C(14)	23(1)	28(1)	22(1)	-6(1)	0(1)	0(1)
C(15)	27(1)	31(1)	26(1)	-1(1)	-1(1)	0(1)
C(16)	63(5)	26(6)	27(4)	10(4)	7(3)	3(3)
C(17)	26(1)	26(1)	28(1)	1(1)	-1(1)	3(1)
C(18)	25(1)	30(1)	30(1)	-1(1)	-2(1)	2(1)
C(19)	53(2)	48(2)	40(2)	-6(2)	-18(2)	12(2)
C(20)	24(1)	38(2)	33(2)	-9(1)	-5(1)	7(1)
C(21)	27(2)	50(2)	49(2)	-19(2)	3(1)	-2(1)
C(22)	25(2)	73(2)	75(2)	-47(2)	-5(2)	4(2)
C(23)	60(2)	41(2)	35(2)	1(1)	7(2)	4(2)
C(24)	40(2)	23(1)	26(1)	-4(1)	-5(1)	-1(1)
C(25)	60(2)	37(2)	40(2)	8(1)	-11(2)	-2(2)
C(27)	28(1)	27(1)	24(1)	-1(1)	-5(1)	4(1)
C(28)	31(1)	29(1)	25(1)	2(1)	-6(1)	2(1)
C(29)	44(2)	32(2)	37(2)	-2(1)	2(1)	-4(1)
C(30)	28(1)	29(1)	27(1)	5(1)	-10(1)	0(1)
C(31)	34(2)	42(2)	32(2)	6(1)	-5(1)	5(1)
C(32)	35(2)	54(2)	38(2)	17(1)	-1(1)	-4(1)
C(33)	26(1)	38(2)	29(1)	-3(1)	-2(1)	2(1)
C(34)	24(1)	27(1)	26(1)	-3(1)	-4(1)	2(1)
C(35)	28(1)	38(2)	31(2)	-11(1)	0(1)	0(1)
S(1)	58(1)	48(1)	30(1)	3(1)	-1(1)	-8(1)

S(2)	28(1)	41(1)	43(1)	-4(1)	4(1)	-8(1)
S(3)	72(1)	82(1)	56(1)	-29(1)	-40(1)	36(1)
S(4')	67(2)	47(1)	37(1)	13(1)	- 11(1)	-3(1)
S(4)	114(4)	44(1)	36(2)	6(1)	20(2)	-1(2)
S(5)	67(1)	35(1)	60(1)	0(1)	-1(1)	-14(1)
S(6)	28(1)	55(1)	31(1)	-9(1)	-4(1)	-4(1)
S(6')	28(1)	45(2)	26(1)	-14(1)	-1(1)	-4(1)
S(2')	39(3)	24(4)	34(3)	9(3)	7(2)	0(2)

Appendix 3; X-Ray crystal structure of compound **6**

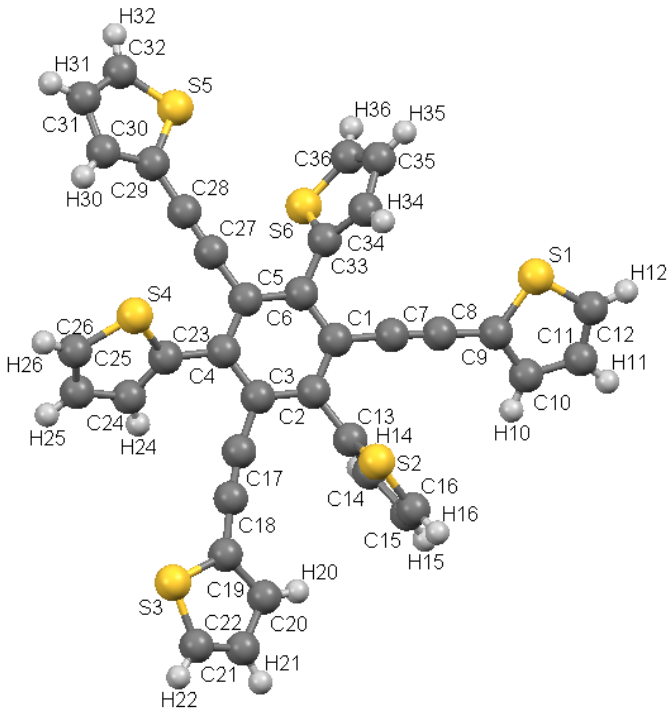

Table 7.5. Crystal data and structure refinement for compound **6**.

Identification code	compound **6**
Empirical formula	$C_{36}\ H_{18}\ S_6$
Formula weight	642.86
Temperature	150 (2) K
Wavelength	0.71073 Å
Crystal system	Monoclinic
Space group	C2/c
Unit cell dimensions	a = 49.9144 (16) Å alpha = 90 deg. b = 7.3196 (2) Å beta = 100.808(3) deg. c = 16.8057 (6) Å gamma = 90 deg.
Volume	6031.1(3) A^3
Z, Calculated density	8, 1.416 Mg/m^3
Absorption coefficient	0.480 mm^{-1}

F(000)	2640
Crystal size	0.14 x 0.06 x 0.03 mm^3
Theta range for data collection	2.45 to 26.00 °.
Limiting indices	-61<=h<=61, -9<=k<=6, -20<=l<=19
Reflections collected / unique	41837 / 5912 [R(int) = 0.0552]
Completeness to theta = 26.00	100.0 %
Absorption correction	Empirical
Max. and min. transmission	0.9857 and 0.9359
Refinement method	Full-matrix least-squares on F^2
Data / restraints / parameters	5912 / 24 / 426
Goodness-of-fit on F^2	1.040
Final R indices [I>2sigma(I)]	R1 = 0.0523, wR2 = 0.1391
R indices (all data)	R1 = 0.0722, wR2 = 0.1557
Extinction coefficient	none
Largest diff. peak and hole	0.88 and -0.69 $e.A^{-3}$

Table 7.6. Atomic coordinates ($\times 10^4$) and equivalent isotropic displacement parameters ($A^2 \times 10^3$) for compound **6**. U(eq) is defined as one third of the trace of the orthogonalized Uij tensor.

	x	y	z	U(eq)
C(1)	1227(1)	-2644(4)	4115(2)	20(1)
C(2)	1447(1)	-3633(4)	4561(2)	19(1)
C(3)	1397(1)	-5209(4)	4983(2)	20(1)
C(4)	1128(1)	-5820(4)	4969(2)	19(1)
C(5)	910(1)	-4831(4)	4504(2)	19(1)
C(6)	958(1)	-3240(4)	4081(2)	20(1)
C(7)	1282(1)	-1045(4)	3685(2)	23(1)
C(8)	1340(1)	294(4)	3348(2)	24(1)
C(9)	1413(1)	1850(4)	2936(2)	24(1)
C(10)	1658(1)	2088(4)	2626(2)	20(1)
C(11)	1653(1)	3781(5)	2223(2)	41(1)
C(12)	1425(1)	4752(5)	2219(2)	40(1)
C(13)	1728(1)	-2948(4)	4597(2)	22(1)
C(14)	1907(2)	-3140(20)	4060(7)	34(3)
C(15)	2160(1)	-2197(6)	4292(2)	40(1)
C(16)	2154(1)	-1366(5)	4995(2)	38(1)
C(17)	1633(1)	-6120(4)	5435(2)	21(1)
C(18)	1847(1)	-6688(4)	5779(2)	22(1)
C(19)	2112(1)	-7236(4)	6161(2)	24(1)
C(20)	2367(1)	-6661(4)	5909(2)	14(1)
C(21)	2586(1)	-7572(6)	6436(3)	50(1)
C(22)	2512(1)	-8622(6)	7005(3)	51(1)
C(23)	1079(1)	-7449(4)	5438(2)	21(1)
C(24)	1216(1)	-9097(4)	5488(2)	23(1)

C(25)	1122(1)	-10336(4)	6026(2)	30(1)
C(26)	927(1)	-9617(5)	6389(2)	33(1)
C(27)	635(1)	-5455(4)	4437(2)	23(1)
C(28)	402(1)	-5925(4)	4364(2)	25(1)
C(29)	127(1)	-6473(4)	4283(2)	24(1)
C(30)	2(2)	-7591(15)	4758(6)	27(2)
C(31)	-282(1)	-7803(5)	4495(3)	42(1)
C(32)	-362(1)	-6826(5)	3817(3)	41(1)
C(33)	731(1)	-2211(4)	3592(2)	22(1)
C(34)	646(2)	-410(14)	3675(7)	36(4)
C(14')	1881(4)	-1710(40)	5119(12)	54(8)
C(30')	-109(3)	-6090(40)	3664(14)	30(8)
C(34')	550(5)	-2710(30)	2867(14)	34(6)
C(35)	418(1)	139(5)	3046(2)	39(1)
C(36)	361(1)	-1284(5)	2548(2)	37(1)
S(1)	1201(1)	3680(1)	2700(1)	37(1)
S(2)	1878(1)	-1674(4)	5395(2)	34(1)
S(3)	2176(1)	-8669(2)	6970(1)	46(1)
S(4)	841(1)	-7451(1)	6064(1)	33(1)
S(5)	-112(1)	-5678(3)	3505(1)	39(1)
S(6)	534(1)	-3160(7)	2777(3)	30(1)
S(2')	1903(1)	-3414(11)	3848(4)	37(1)
S(5')	39(2)	-7881(15)	4952(6)	24(2)
S(6')	656(1)	-51(5)	3824(2)	28(1)

Table 7.7. Bond lengths [A] and angles [deg] for compound **6**.

C(1)-C(6)	1.402(4)
C(1)-C(2)	1.408(4)
C(1)-C(7)	1.430(4)
C(2)-C(3)	1.402(4)
C(2)-C(13)	1.479(4)
C(3)-C(4)	1.409(4)
C(3)-C(17)	1.441(4)
C(4)-C(5)	1.416(4)
C(4)-C(23)	1.474(4)
C(5)-C(6)	1.408(4)
C(5)-C(27)	1.431(4)
C(6)-C(33)	1.476(4)
C(7)-C(8)	1.194(4)
C(8)-C(9)	1.415(4)
C(9)-C(10)	1.426(4)
C(9)-S(1)	1.708(3)
C(10)-C(11)	1.410(5)
C(11)-C(12)	1.342(6)
C(12)-S(1)	1.692(4)
C(13)-C(14)	1.393(11)
C(13)-S(2)	1.690(4)
C(14)-C(15)	1.427(11)
C(15)-C(16)	1.334(5)
C(16)-S(2)	1.655(4)
C(17)-C(18)	1.191(4)
C(18)-C(19)	1.414(4)
C(19)-C(20)	1.478(4)
C(19)-S(3)	1.700(3)
C(20)-C(21)	1.436(5)
C(21)-C(22)	1.332(6)
C(22)-S(3)	1.667(4)
C(23)-C(24)	1.382(4)
C(23)-S(4)	1.727(3)
C(24)-C(25)	1.421(5)
C(25)-C(26)	1.352(5)
C(26)-S(4)	1.705(4)
C(27)-C(28)	1.196(4)
C(28)-C(29)	1.409(4)
C(29)-C(30)	1.373(9)
C(29)-S(5)	1.701(4)
C(30)-C(31)	1.410(9)

C(31)-C(32)	1.340(6)
C(32)-S(5)	1.666(4)
C(33)-C(34)	1.398(10)
C(33)-S(6)	1.679(5)
C(34)-C(35)	1.460(11)
C(35)-C(36)	1.333(5)
C(36)-S(6)	1.629(6)
C(6)-C(1)-C(2)	120.4(3)
C(6)-C(1)-C(7)	120.6(3)
C(2)-C(1)-C(7)	118.9(3)
C(3)-C(2)-C(1)	119.8(3)
C(3)-C(2)-C(13)	121.0(3)
C(1)-C(2)-C(13)	119.1(3)
C(2)-C(3)-C(4)	120.8(3)
C(2)-C(3)-C(17)	116.2(3)
C(4)-C(3)-C(17)	122.9(3)
C(3)-C(4)-C(5)	118.6(3)
C(3)-C(4)-C(23)	120.0(3)
C(5)-C(4)-C(23)	121.4(3)
C(6)-C(5)-C(4)	121.0(3)
C(6)-C(5)-C(27)	118.4(3)
C(4)-C(5)-C(27)	120.6(3)
C(1)-C(6)-C(5)	119.3(3)
C(1)-C(6)-C(33)	119.5(3)
C(5)-C(6)-C(33)	121.1(3)
C(8)-C(7)-C(1)	177.0(3)
C(7)-C(8)-C(9)	178.4(4)
C(8)-C(9)-C(10)	126.4(3)
C(8)-C(9)-S(1)	122.6(2)
C(10)-C(9)-S(1)	110.9(2)
C(11)-C(10)-C(9)	110.1(3)
C(12)-C(11)-C(10)	114.0(3)
C(11)-C(12)-S(1)	112.9(3)
C(14)-C(13)-C(2)	131.3(5)
C(14)-C(13)-S(2)	109.0(5)
C(2)-C(13)-S(2)	119.8(2)
C(13)-C(14)-C(15)	114.7(7)
C(16)-C(15)-C(14)	107.2(5)
C(15)-C(16)-S(2)	117.2(3)
C(18)-C(17)-C(3)	171.5(3)
C(17)-C(18)-C(19)	175.2(3)
C(18)-C(19)-C(20)	124.9(3)
C(18)-C(19)-S(3)	123.9(2)
C(20)-C(19)-S(3)	111.2(2)
C(21)-C(20)-C(19)	106.7(3)

C(22)-C(21)-C(20)	115.4(3)
C(21)-C(22)-S(3)	113.5(3)
C(24)-C(23)-C(4)	127.5(3)
C(24)-C(23)-S(4)	110.6(2)
C(4)-C(23)-S(4)	121.8(2)
C(23)-C(24)-C(25)	112.2(3)
C(26)-C(25)-C(24)	113.0(3)
C(25)-C(26)-S(4)	112.1(3)
C(28)-C(27)-C(5)	177.7(3)
C(27)-C(28)-C(29)	179.7(4)
C(30)-C(29)-C(28)	130.9(4)
C(30)-C(29)-S(5)	108.6(4)
C(28)-C(29)-S(5)	120.5(3)
C(29)-C(30)-C(31)	115.1(6)
C(32)-C(31)-C(30)	109.2(4)
C(31)-C(32)-S(5)	114.6(3)
C(34)-C(33)-C(6)	129.7(5)
C(34)-C(33)-S(6)	109.3(5)
C(6)-C(33)-S(6)	121.0(3)
C(33)-C(34)-C(35)	113.3(8)
C(36)-C(35)-C(34)	106.6(5)
C(35)-C(36)-S(6)	118.0(3)
C(12)-S(1)-C(9)	92.09(18)
C(16)-S(2)-C(13)	91.9(2)
C(22)-S(3)-C(19)	93.1(2)
C(26)-S(4)-C(23)	92.14(16)
C(32)-S(5)-C(29)	92.5(2)
C(36)-S(6)-C(33)	92.7(3)

Symmetry transformations used to generate equivalent atoms:

Table 7.8. Anisotropic displacement parameters ($A^2 \times 10^3$) for compound **6**.

The anisotropic displacement factor exponent takes the form:

$$-2\,pi^2\,[\,h^2\,a^{*2}\,U11 + ... + 2\,h\,k\,a^*\,b^*\,U12\,]$$

	U11	U22	U33	U23	U13	U12
C(1)	21(1)	17(1)	23(2)	-3(1)	3(1)	-1(1)
C(2)	15(1)	21(2)	21(2)	-4(1)	2(1)	-2(1)
C(3)	18(1)	19(2)	22(2)	-5(1)	2(1)	1(1)
C(4)	17(1)	19(2)	20(2)	-3(1)	2(1)	0(1)
C(5)	16(1)	19(2)	22(2)	-4(1)	2(1)	-1(1)
C(6)	19(1)	17(1)	22(2)	-4(1)	2(1)	2(1)
C(7)	19(1)	23(2)	25(2)	-2(1)	1(1)	-1(1)
C(8)	21(2)	26(2)	24(2)	-1(1)	1(1)	0(1)
C(9)	26(2)	22(2)	22(2)	1(1)	0(1)	-1(1)
C(10)	14(1)	26(2)	18(1)	7(1)	0(1)	-7(1)
C(11)	40(2)	46(2)	34(2)	10(2)	3(2)	-14(2)
C(12)	60(3)	24(2)	30(2)	4(1)	-6(2)	-10(2)
C(13)	17(1)	22(2)	25(2)	1(1)	2(1)	-1(1)
C(14)	34(4)	44(6)	20(6)	-21(4)	-7(4)	-15(3)
C(15)	28(2)	53(2)	42(2)	-1(2)	13(2)	-5(2)
C(16)	25(2)	34(2)	53(2)	-5(2)	4(2)	-9(2)

C(17)	21(2)	20(2)	21(2)	-3(1)	3(1)	-2(1)
C(18)	20(2)	19(2)	25(2))	-2(1)	2(1)	-1(1)
C(19)	20(2)	23(2)	27(2)	-4(1)	0(1)	0(1)
C(20)	2(1)	19(1)	21(1)	1(1)	-1(1)	-1(1)
C(21)	21(2)	57(3)	68(3)	-8(2)	-1(2)	0(2)
C(22)	42(2)	50(3)	51(3)	-1(2)	-20(2)	13(2)
C(23)	16(1)	21(2)	25(2)	-1(1)	2(1)	-3(1)
C(24)	25(2)	21(2)	22(2)	-1(1)	1(1)	-4(1)
C(25)	35(2)	22(2)	32(2)	6(1)	0(1)	0(1)
C(26)	30(2)	34(2)	36(2)	12(2)	6(2)	-6(2)
C(27)	20(2)	19(2)	28(2)	-1(1)	3(1)	1(1)
C(28)	23(2)	22(2)	30(2)	-2(1)	5(1)	2(1)
C(29)	18(1)	21(2)	34(2)	-5(1)	6(1)	-1(1)
C(30)	27(4)	28(4)	21(5)	13(3)	-6(3)	7(3)
C(31)	27(2)	39(2)	66(3)	-8(2)	23(2)	-11(2)
C(32)	19(2)	42(2)	59(3)	-13(2)	1(2)	-5(2)
C(33)	18(1)	21(2)	26(2)	0(1)	4(1)	-1(1)
C(14')	53(10)	77(13)	38(13)	-10(9)	25(8)	-2(7)
C(34')	49(10)	13(8)	44(9)	-11(5)	20(7)	6(6)
C(35)	41(2)	35(2)	43(2)	6(2)	10(2)	16(2)
C(36)	22(2)	57(2)	30(2)	4(2)	-2(1)	4(2)

S(1)	42(1)	30(1)	39(1)	-2(1)	8(1)	5(1)
S(2)	22(1)	37(1)	44(2)	-13(1)	7(1)	-11(1)
S(3)	40(1)	50(1)	44(1)	11(1)	-2(1)	0(1)
S(4)	27(1)	33(1)	42(1)	10(1)	14(1)	3(1)
S(5)	22(1)	47(1)	43(1)	7(1)	-4(1)	-1(1)
S(6)	27(1)	32(2)	27(1)	-1(2)	-5(1)	2(1)
S(2')	19(2)	64(3)	30(3)	-29(2)	7(2)	-19(1)
S(5')	15(3)	30(3)	24(4)	19(2)	-4(2)	-4(2)
S(6')	27(1)	21(1)	32(1)	-6(1)	-7(1)	8(1)

Appendix 2; X-Ray crystal structure of compound **36**

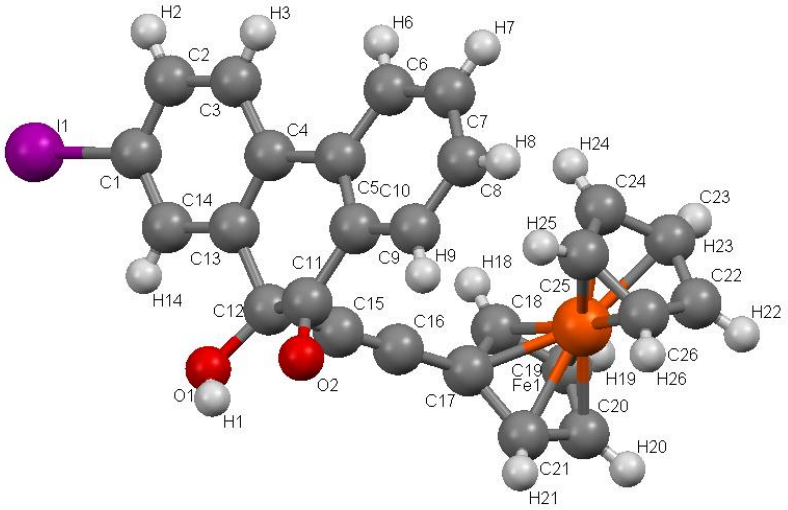

Table 7.9. Crystal data and structure refinement for compound **36**.

Identification code	compound **36**
Empirical formula	C_{26} H_{16} Fe I O_2
Formula weight	543.14
Temperature	293(2) K
Wavelength	0.71073 Å
Crystal system	Monoclinic,
Space group	P2 (1)/c
Unit cell dimensions	a = 7.8802(3) Å alpha = 90°. b = 22.9647(9) Å beta = 104.859(4)°. c = 11.7527(5) Å gamma = 90°.
Volume	2055.72(14) A^3
Z, Calculated density	4, 1.755 Mg/m^3
Absorption coefficient	2.256 mm^{-1}
F(000)	1068
Crystal size	0.22 x 0.05 x 0.03 mm^3
Theta range for data collection	2.82 to 25.71°.

Limiting indices	-9<=h<=9, -28<=k<=27, -14<=l<=14
Reflections collected / unique	16159 / 3901 [R(int) = 0.0570]
Completeness to theta = 25.71	99.6 %
Absorption correction	Analytical
Max. and min. transmission	0.9354 and 0.6367
Refinement method	Full-matrix least-squares on F^2
Data / restraints / parameters	3901 / 0 / 272
Goodness-of-fit on F^2	1.027
Final R indices [I>2sigma(I)]	R1 = 0.0374, wR2 = 0.0743
R indices (all data)	R1 = 0.0593, wR2 = 0.0841
Extinction coefficient	none
Largest diff. peak and hole	1.24 and -0.60 $e.A^{-3}$

Table 7.10. Atomic coordinates (x 10^4) and equivalent isotropic displacement parameters (A^2 x 10^3) for compound **36**. U(eq) is defined as one third of the trace of the orthogonalized Uij tensor.

	x	y	z	U(eq)
C(1)	4845(6)	2079(2)	1242(4)	22(1)
C(2)	6427(5)	1982(2)	955(4)	24(1)
C(3)	6548(5)	1547(2)	176(4)	23(1)
C(4)	5077(5)	1202(2)	-352(4)	18(1)
C(5)	5177(5)	728(2)	-1184(4)	17(1)
C(6)	6560(5)	687(2)	-1730(4)	23(1)
C(7)	6684(6)	210(2)	-2419(4)	28(1)
C(8)	5491(6)	-243(2)	-2574(4)	29(1)
C(9)	4114(6)	-208(2)	-2045(4)	26(1)
C(10)	3930(5)	274(2)	-1374(4)	17(1)
C(11)	2411(5)	318(2)	-857(4)	18(1)
C(12)	1884(5)	935(2)	-583(4)	16(1)
C(13)	3507(5)	1306(2)	-40(3)	15(1)
C(14)	3383(5)	1741(2)	756(4)	18(1)
C(15)	978(5)	1173(2)	-1761(4)	18(1)
C(16)	289(5)	1319(2)	-2745(4)	21(1)
C(17)	-565(5)	1516(2)	-3914(4)	22(1)
C(18)	-152(6)	2033(2)	-4456(4)	27(1)
C(19)	-1265(6)	2064(2)	-5599(4)	32(1)
C(20)	-2368(6)	1570(2)	-5785(4)	31(1)
C(21)	-1953(6)	1228(2)	-4754(4)	28(1)

C(22)	667(7)	935(2)	-6853(5)	42(1)
C(23)	1791(8)	1389(3)	-6516(6)	57(2)
C(24)	2771(8)	1281(5)	-5379(8)	99(4)
C(25)	2240(16)	752(6)	-5005(7)	130(6)
C(26)	900(12)	540(3)	-5937(8)	77(3)
O(1)	765(4)	928(1)	175(3)	21(1)
O(2)	1530(4)	-95(1)	-724(3)	24(1)
Fe(1)	208(1)	1325(1)	-5400(1)	27(1)
I(1)	4674(1)	2738(1)	2452(1)	31(1)

Table 7.11. Bond lengths [Å] and angles [°] for compound **36.**

C(1)-C(14)	1.386(6)
C(1)-C(2)	1.390(6)
C(1)-I(1)	2.104(4)
C(2)-C(3)	1.374(6)
C(3)-C(4)	1.410(6)
C(4)-C(13)	1.399(5)
C(4)-C(5)	1.479(6)
C(5)-C(6)	1.402(6)
C(5)-C(10)	1.410(6)
C(6)-C(7)	1.381(6)
C(7)-C(8)	1.383(6)
C(8)-C(9)	1.384(6)
C(9)-C(10)	1.389(6)
C(10)-C(11)	1.479(6)
C(11)-O(2)	1.209(5)
C(11)-C(12)	1.535(6)
C(12)-O(1)	1.405(5)
C(12)-C(15)	1.489(6)
C(12)-C(13)	1.532(5)
C(13)-C(14)	1.388(6)
C(15)-C(16)	1.193(6)
C(16)-C(17)	1.439(6)
C(17)-C(18)	1.425(6)
C(17)-C(21)	1.432(6)

C(18)-C(19)	1.405(6)
C(19)-C(20)	1.411(7)
C(20)-C(21)	1.409(7)
C(22)-C(23)	1.359(8)
C(22)-C(26)	1.384(9)
C(23)-C(24)	1.384(11)
C(24)-C(25)	1.391(14)
C(25)-C(26)	1.399(14)
C(14)-C(1)-C(2)	120.8(4)
C(14)-C(1)-I(1)	119.4(3)
C(2)-C(1)-I(1)	119.7(3)
C(3)-C(2)-C(1)	119.9(4)
C(2)-C(3)-C(4)	120.8(4)
C(13)-C(4)-C(3)	118.1(4)
C(13)-C(4)-C(5)	120.0(4)
C(3)-C(4)-C(5)	121.9(4)
C(6)-C(5)-C(10)	118.1(4)
C(6)-C(5)-C(4)	122.1(4)
C(10)-C(5)-C(4)	119.7(4)
C(7)-C(6)-C(5)	120.1(4)
C(6)-C(7)-C(8)	121.8(4)
C(7)-C(8)-C(9)	118.8(4)
C(8)-C(9)-C(10)	120.6(4)
C(9)-C(10)-C(5)	120.6(4)
C(9)-C(10)-C(11)	120.1(4)
C(5)-C(10)-C(11)	119.3(4)
O(2)-C(11)-C(10)	123.5(4)
O(2)-C(11)-C(12)	120.2(4)
C(10)-C(11)-C(12)	116.1(3)
O(1)-C(12)-C(15)	111.4(3)
O(1)-C(12)-C(13)	109.6(3)
C(15)-C(12)-C(13)	109.5(3)
O(1)-C(12)-C(11)	111.7(3)
C(15)-C(12)-C(11)	103.5(3)
C(13)-C(12)-C(11)	111.0(3)
C(14)-C(13)-C(4)	121.3(4)
C(14)-C(13)-C(12)	119.0(3)
C(4)-C(13)-C(12)	119.7(4)
C(1)-C(14)-C(13)	119.1(4)
C(16)-C(15)-C(12)	174.4(4)
C(15)-C(16)-C(17)	177.8(5)
C(18)-C(17)-C(21)	107.3(4)
C(18)-C(17)-C(16)	125.7(4)

C(21)-C(17)-C(16)	126.9(4)
C(19)-C(18)-C(17)	108.1(4)
C(18)-C(19)-C(20)	108.5(4)
C(21)-C(20)-C(19)	108.4(4)
C(20)-C(21)-C(17)	107.7(4)
C(23)-C(22)-C(26)	109.2(6)
C(22)-C(23)-C(24)	107.7(7)
C(23)-C(24)-C(25)	108.9(8)
C(24)-C(25)-C(26)	106.5(6)
C(22)-C(26)-C(25)	107.7(8)

Symmetry transformations used to generate equivalent atoms:

Table 7.12. Anisotropic displacement parameters ($A^2 \times 10^3$) for compound **36**.

The anisotropic displacement factor exponent takes the form:

$$-2\,pi^2\,[\,h^2\,a^{*2}\,U11 + ... + 2\,h\,k\,a^*\,b^*\,U12\,]$$

	U11	U22	U33	U23	U13	U12
C(1)	28(2)	19(2)	17(2)	-1(2)	1(2)	1(2)
C(2)	19(2)	28(2)	22(2)	0(2)	-1(2)	-5(2)
C(3)	15(2)	31(3)	23(2)	3(2)	7(2)	-3(2)
C(4)	21(2)	18(2)	14(2)	7(2)	5(2)	3(2)
C(5)	17(2)	19(2)	16(2)	6(2)	6(2)	5(2)
C(6)	17(2)	28(2)	26(3)	3(2)	8(2)	1(2)
C(7)	25(2)	39(3)	28(3)	2(2)	19(2)	5(2)
C(8)	33(3)	30(3)	27(3)	0(2)	16(2)	11(2)
C(9)	29(2)	24(2)	25(3)	-5(2)	9(2)	-1(2)
C(10)	16(2)	20(2)	15(2)	3(2)	4(2)	0 (2)

C(11)	20(2)	23(2)	10(2)	-1(2)	3(2)	-1(2)
C(12)	15(2)	20(2)	13(2)	2(2)	6(2)	-1(2)
C(13)	17(2)	17(2)	10(2)	4(2)	2(2)	-1(2)
C(14)	17(2)	24(2)	14(2)	1(2)	4(2)	1(2)
C(15)	14(2)	21(2)	20(2)	-2(2)	6(2)	-2(2)
C(16)	16(2)	24(2)	26(3)	3(2)	11(2)	-1(2)
C(17)	19(2)	29(2)	19(2)	1(2)	6(2)	7(2)
C(18)	27(2)	28(2)	24(3)	0(2)	4(2)	1(2)
C(19)	37(3)	36(3)	25(3)	8(2)	10(2)	12(2)
C(20)	26(2)	44(3)	19(3)	1(2)	-1(2)	4(2)
C(21)	23(2)	31(3)	28(3)	3(2)	3(2)	2(2)
C(22)	43(3)	56(4)	32(3)	-16(3)	18(2)	0(3)
C(23)	62(4)	63(4)	62(4)	-14(3)	44(4)	-11(3)
C(24)	24(3)	192(11)	77(6)	-87(7)	5(4)	19(5)
C(25)	143(9)	223(13)	35(5)	40(7)	40(5)	163(10)
C(26)	124(7)	42(4)	98(7)	14(4)	87(6)	35(4)
O(1)	24(2)	21(2)	23(2)	-3(1)	14(1)	-5(1)
O(2)	26(2)	23(2)	27(2)	-2(1)	12(1)	-6(1)
Fe(1)	28(1)	37(1)	16(1)	0(1)	7(1)	8(1)
I(1)	33(1)	28(1)	28(1)	-10(1)	-2(1)	2(1)

Chapter 8;

List of references.

[1] Günes S.; Neugebauer H.; Sariciftci N. S., *Chem. Soc. Rev.*, **2007**, *107*, 1324-1338.

[2] Nelson J., *The Physics of Solar Cells*, Imperial College Press, UK, 2003.

[3] Smestad G. P., *Optoelectronics of Solar Cells*, The International Society for Optical Engineering, USA, 2002.

[4] Chapin D. M.; Fuller C. S.; Pearson G. L., *J. of Appl. Phys.*, **1954**, *25*, 676-677.

[5] Langa F.; Nierengarten J., *Fullerenes: Principles and Applications*, 2nd edition, Royal Society of Chemistry,UK, 2007.

[6] Lynn P. A., *Electricity from Sunlight: An Introduction to Photovoltaics*, John Wiley and Sons Ltd, UK, 2010.

[7] Krebs F. C., *Polymer Photovoltaics: A Practical Approach*, the International Society for Optical Engineering, USA, 2008.

[8] Bundgaard E.; Krebs F. C., *Sol. Energy Mater. Sol. Cells*, **2007**, *91*, 954-985.

[9] Wallace C.H. Choy, *Organic Solar Cells: Materials and Device Physics*, Springer-Verlage London Ltd, UK, 2013.

[10] Nunzi J. M., *C. R. Physique*, **2002**, *3*, 523-542.

[11] Kroon R.; Lenes M.; Hummelen J. C.; Blom P. W.; Boer B., *Polymer Reviews*, **2008**, *48*, 531-582.

[12] Jiangeng X.; Soichi U.; Barry R.; Forrest S. R., *Appl. Phys. Lett.*, **2004**, *84*, 3013-3015.

[13] Winder C.; Sariciftci N. S., *J. Mater. Chem.*, **2004**, *14*, 1077-1086.

[14] Hoppea H.; Sariciftci N. S., *J. Mater. Res.*, **2004**, *19*, 1924-1945.

[15] Zang L.; Günes S., Eds. *Energy Efficiency and Renewable Energy Through Nanotechnology*, Springer-Verlag London Ltd, UK, 2011.

[16] Clifford J. N.; Martínez-Ferrero E.; Viterisi A.; Palomares E., *Chem. Soc. Rev.*, **2011**, *40*, 1635-1646.

[17] Li C.; Liu M.; Pschirer N. G.; Baumgarten M.; Müllen K., *Chem. Soc. Rev.*, **2010**, *110*, 6817-6855.

[18] Ma W.; Yang C.; Gong X.; Lee K.; Heeger A. J., *Adv. Funct. Mater.*, **2005**, *15*, 1617-1622.

[19] Sirringhaus H.; Tessler N.; Friend R. H., *Science*, **1998**, *280*, 1741-1744.

[20] Dang M. T.; Hirsch L.; Wantz G.; Wuest J. D., *Chem. Soc. Rev.*, **2013,** *113*, 3734-3765.

[21] Chen J.; Cao Y., *Acc. Chem. Res.*, **2009**, *42*, 1709-1718.

[22] Kitamura C.; Tanaka S.; Yamashita Y., *J. Chem. Mater.*, **1996**, *8*, 570-578.

[23] Brocks G.; Tol A., *J. Phys. Chem.*, **1996**, *100*, 1838-1846.

[24] Cheng Y.; Yang S.; Hsu C., *Chem. Soc. Rev.*, **2009**, *109*, 5868-5923.

[25] Kanibolotsky A. L.; Perepichka I. F.; Skabara P. J., *Chem. Soc. Rev.*, **2010**, *39*, 2695-2728.

[26] Grayson S. M.; Fréchet J. M. J., *Chem. Rev.*, **2001**, *101*, 3819-3868.

[27] Lo S.; Burn P., *Chem. Soc. Rev.*, **2007,** *107*, 1097-1116.

[28] Hasobe T.; Kashiwagi Y.; Absalom M. A.; Sly J.; Hosomizu K.; Crossley M. J.; Imahori H.; Kamat P. V.; Fukuzumi S., *Adv. Mater.*, **2004**, *16*, 975-979.

[29] Wong W.; Ma C.; Pisula W.; Mavrinskiy A.; Feng X.; Seyler H.; Jones D. J.; Müllen K.; Bäuerle P.; Holmes A., *Chem. Eur. J.*, **2011**, *17*, 5549- 5560.

[30] Wong W.; Ma C.; Pisula W.; Yan C.; Feng X.; Jones D. J.; Müllen K.; Janssen R.; Bäuerle P.; Holmes A., *Chem. Mater.*, **2010**, *22*, 457-466.

[31] John H.; Bauer R.; Espindola P.; Sonar P.; Heinze J.; Müllen K., *Angew. Chem. Int. Ed.*, **2005**, *44*, 2447-2451.

[32] Lin Y.; Lia Y.; Zhan X., *Chem. Soc. Rev.*, **2012**, *41*, 4245-4272.

[33] Tamayo A. B.; Walker B.; Nguyen T., *J. Phys. Chem. C*, **2008**, *112*, 11545-11551.

[34] Sun X.; Zhou Y.; Wu W.; Liu Y.; Tian W.; Yu G.; Qiu W.; Chen S.; Zhu D., *J. Phys. Chem. B*, **2006**, *110*, 7702-7707.

[35] Haid S.; Mishra A.; Uhrich C.; Pfeiffer M.; Bäuerle P., *Chem. Mater.*, **2011**, *23*, 4435-4444.

[36] Liu Y.; Wan X.; Wang F.; Zhou J.; Long G.; Tian J.; You J.; Yang Y.; Chen Y., *Adv. Energy Mater.*, **2011**, *1*, 771-775.

[37] Liu Y.; Wan X.; Yin B.; Zhou J.; Long G.; Yin S.; Chen Y., *J. Mater. Chem.*, **2010**, *20*, 2464-2468.

[38] Yin B.; Yang L.; Liu Y.; Chen Y.; Qi Q.; Zhang F.; Yin S., *Appl. Phys. Lett.*, **2010**, *97*, 023303-023305.

[39] Roncali J., *Macromol. Rapid Commun.*, **2007**, *28*, 1761-1775.

[40] Roncali J., *Acc. Chem. Res.*, **2009**, *42*, 1719-1730.

[41] Leliege A.; Blanchard P.; Rousseau T.; Roncali J., *Org. Lett.*, **2011**, *13*, 3098-3101.

[42] Chiu S. W.; Lin L. Y.; Lin H. W.; Liu Y. H.; Huang Z. Y.; Lin Y. T.; Lin F.; Chen Y. H.; Wong K. T., *Chem. Commun.*, **2012,** *48*, 1857-1859.

[43] Liu Q.; Jiang K.; Guan B.; Tang Z.; Pei J.; Song Y., *Chem. Commun.*, **2011**, *47*, 740-742.

[44] Zhang J.; Deng D.; He C.; He Y.; Zhang M.; Zhang Z. G.; Zhang Z.; Li Y., *Chem. Mater.*, **2011**, *23*, 817-822.

[45] Kroto H. W.; Heath J. R.; O'Brien S. C.; Curl R. F.; Smalley R. E.; *Nature*, **1985**, *318*, 162-163.

[46] Kratschmer W.; Lamb L. D.; Fostiropoulos K.; Huffman D. R., *Nature*, **1990**, *347*, 354-358.

[47] Giacalone F.; Martín N., *Chem. Rev.*, **2006**, *106*, 5136-5190.

[48] Janssen R. A. J.; Christiaans M. P. T.; Pakbaz K.; Moses D.; Hummelen J. C.; Sariciftci N. S., *J. Chem. Phys.*, **1995**, *102*, 2628-2635.

[49] Segura J. L.; Martín N.; Guldi D. M., *Chem. Soc. Rev.*, **2005**, *34*, 31-47.

[50] He Y.; Li Y., *J. Chem. Phys*., **2011**, *13*, 1970-1983.

[51] Sonar P.; Lim J. P. F.; Chan K. L., *Energy Environ. Sci.*, **2011**, *4*, 1558-1574.

[52] Wienk M.; Kroon J.; Verhees W.; Knol J.; Hummelen J. C.; Hal P.; Janssen R., *Angew. Chem., Int. Ed.*, **2003**, *42*, 3371-3375.

[53] Choi J. H.; Son K. I.; Kim T.; Kim K.; Ohkubo K.; Fukuzumi S., *J. Mater. Chem.*, **2010**, *20*, 475-482.

[54] Zhang Y.; Yip H. L.; Acton O.; Hau S. K.; Huang F.; Jen A. K. Y., *J. Chem. Mater*., **2009**, *21*, 2598-2600.

[55] Zheng L. P.; Zhou Q. M.; Deng X. Y.; Yuan M.; Yu G.; Cao Y., *J. Phys. Chem. B*, **2004**, *108*, 11921-11926.

[56] Knorr S.; Mehring M.; Grube G.; Effenberger F., *J. Chem. Phys.*, **1999**, *110*, 3502-3508.

[57] Armaroli N.; Accorsi G.; Gisselbrecht J.; Gross M.; Krasnikov V.; Tsamouras D.; Hadziioannou G.; Gómez-Escalonilla M.; Langa F.; Eckerte J.; Nierengarten J., *J. Mater. Chem.*, **2002**, *12*, 2077-2087.

[58] Murata Y.; Suzuki M.; Komatsu K., *Org. Biomol. Chem.*, **2003**, *1*, 2624-2625.

[59] Zhan X.; Facchetti A.; Barlow S.; Marks T. J.; Ratner M. A.; Wasielewski M. R.; Marder S. R., *Adv. Mater.*, **2011**, *23*, 268-284.

[60] Rim S. B.; Fink R. F.; Schoneboom J. C.; Erk P.; Peumans P., *Appl. Phys. Lett.*, **2007**, *91*, 173504-173506.

[61] Guo X. Y.; Bu L. J.; Zhao Y.; Xie Z. Y.; Geng Y. H.; Wang L. X., *Thin Solid Films*, **2009**, *517*, 4654-4657.

[62] Shin W. S.; Jeong H. H.; Kim M. K.; Jin S. H.; Kim M. R.; Lee J. K.; Lee J. W.; Gal Y. S., *J. Mater. Chem.*, **2006**, *16*, 384-390.

[63] Kamm V.; Battagliarin G.; Howard I. A.; Pisula W.; Mavrinskiy A.; Li C.; Müllen K.; Laquai F.; *Adv. Energy Mater.*, **2011**, *1*, 297-302.

[64] Mikroyannidis J. A.; Suresh P.; Sharma G.D., *Synth. Met.*, **2010**, *160*, 932-938.

[65] Sullivan P.; Duraud A.; Hancox I.; Beaumont N.; Mirri G.; Tucker J. H. R.; Hatton R. A.; Shipman M.; Jones T. S., *Adv. Energy Mater.*, **2011**, *1*, 352-355.

[66] Kietzke T.; Shin R. Y. C.; Egbe D. A. M.; Chen Z. K.; Sellinger A., *Macromolecules*, **2007**, *40*, 4424-4428.

[67] Woo C. H.; Holcombe T. W.; Unruh D. A.; Sellinger A.; Fréchet J. M. J., *J. Chem. Mater.*, **2010**, *22*, 1673-1679.

[68] Zhou T.; Jia T.; Kang B.; Li F.; Fahlman M.; Wang Y., *Adv. Energy Mater.*, **2011**, *1*, 431-439.

[69] Schwenn P. E.; Gui K.; Nardes A. M.; Krueger K. B.; Lee K. H.; Mutkins K.; Rubinstein-Dunlop H.; Shaw P. E.; Kopidakis N.; Burn P. L.; Meredith P., *Adv. Energy Mater.*, **2011**, *1*, 73-81.

[70] Schoeler U.; Tews; Kuhn H., *J. Chem. Phys.*, **1974**, *61*, 5009-5016.

[71] Noma N.; Tsuzuki T.; Shirota Y., *Adv. Mater.*, **1995**, *7*, 647-648.

[72] Perepichka I. F.; Perepichka D. F., *Handbook of Thiophene-Based Materials: Applications in Organic Electronics and photonic*, John Wiley & Son Ltd., UK, 2009.

[73] Purcell S. T.; Garcia N.; Binh V. T.; Jones L.; Tour J. M., *J. Am. Chem. Soc.*, **1994**, *116*, 11985-11989.

[74] Azumi R.; Gotz G.; Debaerdemaeker T.; Baüerle P., *Chem. Eur. J.*, **2000**, *6*, 735-744.

[75] Sakai J.; Taima T.; Yamanari T.; Saito K., *Sol. Energy Mater. Sol. Cells*, **2009**, *93*, 1149-1153.

[76] Fichou D., *J. Mater. Chem.*, **2000**, *10*, 571-588.

[77] Funahashi M.; Hanna J., *Adv. Mater.*, **2005**, *17*, 594-598.

[78] Mei J.; Graham K. R.; Stalder R.; Tiwari S. P.; Cheun H.; Shim J.; Yoshio M.; Nuckolls C.; Kippelen B.; Castellano R. K.; Reynolds J. R., *Chem. Mater.*, **2011**, *23*, 2285-2288.

[79] Yasuda T.; Kishimoto K.; Kato T., *Chem. Commun.*, **2006**, *32*, 3399-3401.

[80] Prehm M.; Gtz G.; Buerle P.; Liu F.; Zeng X.; Ungar G.; Tschierske C., *Angew. Chem. Int. Ed.*, **2007**, *46*, 7856-7859.

[81] Roncali J.; Leriche P.; Cravino A., *Adv. Mater.*, **2007**, *19*, 2045-2060.

[82] Taerum T.; Lukoyanova O.; Wylie R. G.; Perepichka D. F., *Org. Lett.*, **2009**, *11*, 3230-3233.

[83] Baroncini M., *Design, Synthesis and Characterization of new Supramolecular Architectures*, Springer, Italy, 2011.

[84] Steed J. W.; Atwood J. L., *Supramolecular Chemistry*, John Wiley & Son Ltd., UK, 2009.

[85] Cao X.; Zhang W.; Wang J.; Zhou X.; Lu H.; Pei J., *J. Am. Chem. Soc.*, **2003**, *125*, 12430-12431.

[86] Geng Y.; Fechtenkötter A.; Müllen K., *J. Mater. Chem.*, **2001**, *11*, 1634-1641.

[87] Kim D. C.; Lee T. W.; Lee J. E.; Kim K. H.; Cho M. J.; Choi D. H., *Macromolecular Res.*, **2009**, *17*, 491-498.

[88] Sun Y.; Xiao K.; Liu Y.; Wang J.; Pei J.; Yu G.; Zhu D., *Adv. Funct. Mater.*, **2005**, *15*, 818-822.

[89] Murphy A. R.; Fréchet J. M. J., *Chem. Rev.*, **2007**, *107*, 1066-1096.

[90] Liu T.; Prabhakar C.; Yu J.; Chen C.; Huang H.; Yang J., *Macromolecules*, **2012**, *45*, 4529-4539.

[91] Pappenfus T. M.; Mann K. R., *Org. Lett.*, **2002**, *4*, 3043-3046.

[92] Casado J.; Pappenfus T. M.; Mann K. R.; Hernández V.; Navarrete J. T., *J. Chem. Phys.*, **2004**, *120*, 11874-11881.

[93] Narita T.; Takase M.; Nishinaga T.; Iyoda M.; Kamada K.; Ohta K., *Chem. Eur. J.*, **2010**, *16*, 12108-12113.

[94] Kim K. H.; Chi Z.; Cho M. J.; Jin J.; Choi D. H.; Paek S. H., *Macromol. Symp.*, **2007**, *249-250*, 1-7.

[95] Nicolas Y.; Blanchard P.; Levillain E.; Allain M.; Mercier N.; Roncali J., *Org. Lett.*, **2004**, *6*, 273-276.

[96] Simpson C. D.; Wu J.; Watson M. D.; Müllen K., *J. Mater. Chem.*, **2004**, *14*, 494-504.

[97] Zheng W.; Hu Y.; Chiang C.; Ong C. W., *Int. J. Mol. Sci.*, **2010**, *11*, 943-955.

[98] Ponomarenko S. A.; Kirchmeyer S.; Elschner A.; Huisman B. H.; Karbach A.; Drechster D., *Adv. Funct. Mater.*, **2003**, *13*, 591-596.

[99] Aso Y.; Otsubo T.; Vill V.; Mori A.; Ujiie S., *J. Chem. Res.*, **1999**,*10*, 596-597.

[100] Takemoto K.; Karasawa M.; Kimura M., *ACS Appl. Mater. Interfaces*, **2012**, *4*, 6289-6294.

[101] Shang H.; Fan H.; Liu Y.; Hu W.; Li Y.; Zhan X., *Adv. Mater.*, **2011**, *23*, 1554-1557.

[102] Shirakawa H.; Louis E. J.; MacDiarmid A. G.; Chiang C. K.; Heeger A. J., *Chem. Comm.*, **1977**, *16*, 578-580.

[103] Skotheim T. A., *Handbook of conducting polymers*, Marcel Dekker Incorpereted, 1986.

[104] Heywang G.; Jonas F., *Adv. Mater.*, **1992**, *4*, 116-118.

[105] Heinze J.; Frontana-Uribe B. A.; Ludwigs S., *Chem. Rev.*, **2010,** *110*, 4724-4771.

[106] Roncali J., *Chem. Rev.*, **1992**, *92*, 711-738.

[107] Diaz A. F.; Castillo J. I.; Logan J. A.; Lee W. Y., *J. Electroanal. Chem.*, **1981**, *129*, 115-132.

[108] Genies E. M.; Bidan G.; Diaz A. F., *J. Electronal. Chem.*, **1983**, *149*, 101-113.

[109] Roncali J., *Chem. Soc. Rev.*, **1997,** *97*, 173-205.

[110] Silva K. M.; Hwang E.; Serem W. K.; Fronczek F. R.; Garno J. C.; Nesterov E. E., *ACS Appl. Mater. Interfaces*, **2012**, *4*, 5430-5441.

[111] Lorcy D.; Cava M. P., *Adv. Mater.*, **1992**, *4*, 562-564.

[112] Kastner J.; Kuzmany H.; Vegh D.; Land M.; Cuff L.; Kertesz M., *Macromolecules*, **1995**, *28*, 2922-2929.

[113] Kitamura C.; Tanaka S.; Yamashita Y., *Chem. Commun.*, **1994**, *13*, 1585-1586.

[114] Sonmez G.; Shen C. K. F.; Rubin Y.; Wudl F., *Angew. Chem., Int. Ed. Engl.*, **2004**, *43*, 1498-1502.

[115] Tarkuc S.; Unver E. K.; Udumb Y. A.; Tanyeli C.; Toppare L., *Electrochim. Acta*, **2010**, *55*, 7254-7258.

[116] Monk P. M. S., *The viologens: physicochemical properties, synthesis and applications of the salts of 4,4'-bipyridine*, John Wiley & Sons Ltd: UK, 1998.

[117] Mortimer R. J., *Annu. Rev. Mater. Res.*, **2011**, *41*, 241-268.

[118] Krompieca M.; Grudzkaa I.; Filapeka M.; Skorkaa L.; Krompieca S.; Lapkowskib M.; Kaniad M.; Danikiewicz W., *Electrochimica. Acta*., **2011**, *56*, 8108-8114.

[119] Kijima M.; Setoh K.; Shirakawa H., *Chem. Lett.*, **2000**, *8*, 936-937.

[120] Takahashi K.; Nihira T.; Akiyama K.; Ikegami Y.; Fukuyo E., *Chem. Commun.*, **1992**, *8*, 620-622.

[121] Alberto M. E.; Simone B. C.; Cospito S.; Imbardelli D.; Veltri L.; Chidichimo G.; Russo N., *Chem. Phys. Lett.*, **2012**, *552*, 141-145.

[122] Benniston A. C.; Hagon J.; He X.; Yang S.; Harrington R. W., *Org. Lett.*, **2012**, *14*, 506-509.

[123] Ko H. C.; Kang M.; Moon B.; Lee H., *Adv. Mater.*, **2004**, *16*, 1712-1716.

[124] Ko H. C.; Park S.; Paik W., Lee H., *Synth. Met.*, **2002**, *132*, 15-20.

[125] Ko H. C.; Yom J.; Moon B.; Lee H., *Electrochimica Acta.*, **2003**, *48*, 4127-4135.

[126] Ko H. C.; Kim S.; Lee H.; B. Moon, *Adv. Funct. Mater.*, **2005**, *15*, 905-909.

[127] Constantin V.; Bongard D.; Walder L., *Eur. J. Org. Chem.*, **2012**, *5*, 913-921.

[128] Franken P. A.; Hill A. E.; Peters C. W.; Weinreich G., *Phys. Rev. Lett.*, **1961**, *7*, 118-119.

[129] Hicks R., *Stable Radicals: Fundamentals and Applied Aspects of Odd-Electron Compounds*, John Wiley and Sons Ltd., UK, 2010.

[130] Bruce D. W.; O'Hare D.; Walton R. I., *Molecular Materials*, John Wiley and Sons Ltd., UK, 2010.

[131] Marder S. R.; Perry J. W., *Adv. Mater.*, **1993**, *5*, *11*, 804-815.

[132] Papadopoulos M.; Sadlej A.; Leszczynski J., *Non-Linear Optical Properties of Matter from Molecules to Condensed Phases*, Springer, Netherland, 2006.

[133] Marder S. R.; Sohn J. E.; Stucky G. D., *Materials for nonlinear optics chemical perspectives*, ACS Symposium series 455, USA, 1991.

[134] Ashwell G. J.; Bloor D., *Organic materials for non-linear optics III*, The Royal Society of Chemistry, 1993.

[135] Chen Y.; Lin L.; Lu C.; Lin F.; Huang Z.; Lin H.; Wang P.; Liu Y.; Wong K.; Wen J.; Miller D.; Darling S., *J. Am. Chem. Soc.*, **2012**, *134*, 13616-13623.

[136] Ko H. M.; Choi H.; Paek S.; Kim K.; Song K.; Lee J. K.; Ko J., *J. Mater. Chem.*, **2011**, *21*, 7248-7253.

[137] Heremans P.; Cheyns D.; Rand B. P., *Acc. Chem. Res.*, **2009**, *42*, 1740-1747.

[138] Jarowski P.; Wu Y.; Boudon C.; Gisselbrecht J.; Gross M.; Schweizer W.; Diederich F., *Org. Biomol. Chem.*, **2009**, *7*, 1312-1322.

[139] Michinobu T.; Boudon C.; Gisselbrecht J.; Seiler P.; Frank B.; Moonen N.; Gross M.; Diederich F., *Chem. Eur. J.*, **2006**, *12*, 1889-1905.

[140] Tancini F.; Wu Y.; Schweizer W.; Gisselbrecht J.; Boudon C.; Jarowski P. D.; Beels M. T.; Biaggio I.; Diederich F., *Eur. J. Org. Chem.*, **2012**, *14*, 2756-2765.

[141] May J. C.; Lim J. H.; Biaggio I.; Moonen N. N.; Michinobu T.; Diederich F., *Opt. Lett.*, **2005**, *30*, 3057-3059.

[142] Bures F.; Schweizer W.; May J.; Boudon C.; Gisselbrecht J.; Gross M.; Biaggio I.; Diederich F., *Chem. Eur. J.*, **2007**, *13*, 5378-5387.

[143] Wu Y.; Bures F.; Jarowski P., Schweizer W.; Boudon C.; Gisselbrecht J.; Diederich F., *Chem. Eur. J.*, **2010**, *16*, 9592-9605.

[144] Isoda K.; Yasuda T.; Kato T., *J. Mater. Chem.*, **2008**, *18*, 4522-4528.

[145] Gonzalez S.; Orduna J.; Alicante R.; Villacampa B.; McGee K.; Pina J.; Melo J.; Schwaderer K.; Johnson J.; Blackorbay B.; Hansmeier J.; Bolton V.; Helland T.; Edlund B.; Pappenfus T.; Navarrete J.; Casado J., *J. Phys. Chem. B*, **2011**, *115*, 10573-10585.

[146] Gupta A.; Ali A.; Bilic A.; Gao M.; Hegedus K.; Singh B.; Watkins S. E.; Wilson G. J.; Bach U.; Evans R. A., *Chem. Commun.*, **2012**, *48*, 1889-1891.

[147] Oliva M.; Casado J.; Raposo M.; Fonseca A.; Hartmann H.; Hernández V.; Navarrete J., *J. Org. Chem.*, **2006**, *71*, 7509-7520

[148] Nazeeruddin M. K.; Kay A.; Rodicio I.; Humpbry-Baker R.; Müller E.; Liska P.; Vlachopoulos N.; Grätzel M., *J. Am. Chem. Soc.*, **1993**, *115*, 6382-6390.

[149] Chiba Y.; Islam A.; Watanabe Y.; Komiya R.; Koide N.; Han L., *Jap. J. Appl. Phys.*, **2006**, *45*, 638-640.

[150] Meyer G. J., *Nano. Lett.*, **2010**, *4*, 4337-4343.

[151] O'Regan B.; Grätzel M., *Nature*, **1991**, *353*, 737-740.

[152] Tatay S.; Haque S. A.; O'Regan B.; Durrant J. R.; Verhees W.; Kroon J. M.; Vidal-Ferran A.; Gaviña P.; Palomares E., *J. Mater. Chem.*, **2007**, *17*, 3037-3044.

[153] Zhang G.; Bala H.; Cheng Y.; Shi D.; Lv X.; Yu Q.; Wang P., *Chem. Commun.*, **2009**, *16*, 2198-2200.

[154] Grätzel M., *Acc. Chem. Res.*, **2009**, *42*, 1788-1798.

[155] Listorti A.; O'Regan B.; Durrant J. R., *Chem. Mater.*, **2011**, *23*, 3381-3399.

[156] Boschloo G.; Hagfeldt A., *Acc. Chem. Res.*, **2009**, *42*, 1819-1826.

[157] Hagfeldt A.; Boschloo G.; Sun L.; Kloo L.; Pettersson H., *Chem. Rev.*, **2010,** *110*, 6595-6663.

[158] Mishra A.; Fischer M. K. R.; Bäuerle P., *Angew. Chem. Int. Ed.*, **2009**, *48*, 2474-2499.

[159] Hara K.; Sato T.; Katoh R.; Furube A.; Yoshihara T.; Murai M.; Kurashige M.; Ito S.; Shinpo A.; Suga S.; Arakawa H., *Adv. Funct. Mater.*, **2005**, *15*, 246-252.

[160] Gao P.; Tsao H. N.; Grätzel M.; Nazeeruddin M. K., *Org. Lett.*, **2012**, *14*, 4330-4333.

[161] Kozma E.; Concina I.; Braga A.; Borgese L.; Depero L. E.; Vomiero A.; Sberveglieri G.; Catellani M., *J. Mater. Chem.*, **2011**, *21*, 13785-13788.

[162] Longhi E.; Bossi A.; Carlo G.; Maiorana S.; Angelis F. D.; Salvatori P.; Petrozza A.; Binda M.; Roiati V.; Mussini P. R.; Baldoli C.; Licandro E., *Eur. J. Org. Chem.* **2013**, *1*, 84-94.

[163] Cheng X.; Liang M.; Sun S.; Shi Y.; Ma Z.; Sun Z.; Xue S., *Tetrahedron*, **2012,** *68*, 5375-5385.

[164] Wang Z.; Koumura N.; Cui Y.; Takahashi M.; Sekiguchi H.; Mori A.; Kubo T.; Furube A.; Hara K., *Chem. Mater.*, **2008**, *20*, 3993-4003.

[165] Kanaparthi R. K.; Kandhadi J.; Giribabu L., *Tetrahedron*, **2012**, *68*, 8383-8393.

[166] Song J.; Amaladass P.; Wen S.; Pasunooti K. K.; Li A.; Yu Y.; Wang X.; Deng W.; Liu X., *New J. Chem.*, **2011**, *35*, 127-136.

[167] Kim S.; Lee J. K.; Kang S. O.; Ko J.; Yum J.; Fantacci S.; Angelis F. D.; Censo D. D.; Nazeeruddin M. K.; Grätzel M., *J. AM. Chem. Soc.*, **2006**, *128*, 16701-16707.

[168] Kim S.; Choi H.; Kim D.; Song K.; Kang S. O.; Ko J., *Tetrahedron*, **2007**, *63*, 9206-9212.

[169] Wang C.; Li J.; Cai S.; Ning Z.; Zhao D.; Zhang Q.; Su J., *Dyes Pigments*, **2012**, *94*, 40-48.

[170] Do K.; Kim D.; Cho N.; Paek S.; Song K.; Ko J., *Org. Lett.*, **2012**, *14*, 222-225.

[171] Susanto W.; Chu C.; Ang W. J.; Chou T.; Lo L.; Lam Y., *J. Org. Chem.*, **2012**, 77, 2729-2742.

[172] Zhang S.; Liu X.; Wang T., *Adv. Synth. Catal*., **2011**, *353*, 1463-1466.

[173] Ciszek J.W.; Tour J. M., *Tetrahedron. Lett.*, **2004**, *45*, 2801-2803.

[174] Lia P.; Fenwicka O.; Yilmazb S.; Breusovb D.; Caruanac D. J.; Allardb S.; Scherfb U.; Cacialli F., *J. Org. Chem.*, **2002**, *76*, 9073-9076.

[175] Kitamura C.; Tanaka S.; Yamashita Y., *J. Chem. Mater.*, **1996**, *8*, 570-578.

[176] Mangeney C.; Lacroix J.; Chane-Ching K. I.; Jouini M.; Villain F.; Ammar S.; Jouini N.; Lacaze P., *Chem. Eur. j.*, **2001**, *7*, 5029-5040.

[177] Kmínek I.; Výprachtický D.; Kříž J.; Dybal J.; Cimrová V., *J. Polym. Sci. A Polym. Chem.*, **2010**, *48*, 2743-2756.

[178] Nishida J.; Murakami S.; Tada H.; Yamashita Y., *Chem. Lett.*, **2006**, *35*, 1236-1237.

[179] Kim J.; Choi H.; Lee J.; Kang M.; Song K.; Kang S. O.; Ko J. , *J. Mater. Chem.*, **2008**, *18*, 5223-5229.

[180] Ge Y.; Smith D. K., *Anal. Chem.*, **2000**, *72*, 1860-1865.